

Theoretische Medizin und Biowissenschaften
der Medizinischen Fakultät
der Universität des Saarlandes, Homburg/Saar

Aus dem Bereich Biophysik

Ca²⁺ and reactive oxygen species as determinants of immune and
skin cell function -
A central role for Orai- and STIM-mediated
store-operated calcium entry

Dissertation zur Erlangung des Grades eines Doktors der Naturwissenschaften

der Medizinischen Fakultät
der UNIVERSITÄT DES SAARLANDES

2014

vorgelegt von: Stephanie Saul.
geb. am 24.11.1984 in Saarbrücken.

“Life is what happens while you’re busy making other plans.”

Uncredited

“My friends have made the story of my life. In a thousand ways they have turned my limitations into beautiful privileges and enabled me to walk serene and happy in the shadow cast by my desperation.”

Helen Keller

1 Contents

1	Contents.....	3
2	Glossary.....	7
3	Summary.....	9
3.1	Zusammenfassung.....	9
3.2	Summary.....	11
4	Scientific Acknowledgments.....	13
5	Private Acknowledgements.....	14
6	Introduction.....	15
6.1	Cellular Signaling.....	15
6.1.1	Calcium Signaling.....	15
6.1.2	Redox Signaling.....	17
6.1.3	Inflammatory and tumor environments.....	20
6.2	Monocytes.....	22
6.2.1	Monocytes in the scope of the immune system.....	22
6.2.2	Monocytes as professional phagocytes.....	24
6.2.3	Monocytes in chronic inflammatory diseases.....	26
6.3	Melanoma.....	28
6.3.1	Skin – Melanocytes – Melanoma.....	28
6.3.2	Melanoma progression.....	29
6.3.3	Major signaling pathways and molecular players in melanoma progression.....	31
6.3.4	Ca ²⁺ signaling in melanoma.....	32
6.4	Molecular aspects of calcium and redox signaling.....	33
6.4.1	Store-operated calcium entry <i>via</i> calcium-release activated channels.....	33
6.4.2	Underlying mechanisms of enzymatic ROS production.....	35
6.5	The interplay of Ca ²⁺ and redox signaling.....	37
6.5.1	CRAC Channels and Redox Signaling.....	37
6.5.2	Redox Regulation of CRAC Channels.....	38
6.6	Scientific Question.....	40
6.6.1	State of the art - The role of the individual Orai and STIM isoforms in the skin and innate immunity.....	40
6.6.2	Research focus.....	41
7	Materials and Methods.....	43
7.1	Materials.....	43
7.1.1	Chemicals.....	43

Contents

7.1.2	Kits and special laboratory equipment.....	44
7.1.3	Devices	45
7.1.4	Solutions and Media composition	46
7.1.5	Activators and Inhibitors	49
7.1.6	Objects of research (cell systems)	50
7.2	Methods	51
7.2.1	Cell isolation and cultivation	51
7.2.2	Expression analysis on mRNA level.....	52
7.2.3	Characterization of primary human monocytes by flow cytometry.....	55
7.2.4	Protein determination.....	56
7.2.5	Gene silencing using RNA interference (RNAi).....	58
7.2.6	Detection of reactive oxygen species	60
7.2.7	Calcium imaging	62
7.2.8	CellTiter-Blue viability and proliferation assay.....	63
7.2.9	Transwell-migration assay	65
7.2.10	Detection of cytokines using ELISA.....	65
7.2.11	Data Analysis and Statistics	66
8	Results	67
8.1	Characterization of investigated cell types	67
8.1.1	Orai and STIM expression profiles	67
8.1.2	The relative expression of Orai proteins regarding their redox properties	67
8.1.3	Validation of RNAi.....	69
8.1.4	Characterization of primary human monocyte phenotype.....	70
8.2	Store-operated calcium entry (SOCE) in human melanoma cell lines and	72
	monocytes	72
8.2.1	Activation and features of SOCE in human monocytes	72
8.2.2	Investigation of the contribution of CRAC channel components to SOCE	74
	in human monocytes.....	74
8.2.3	Investigation of SOCE in human melanoma cell lines SK-MEL-5 and	74
	WM3734.....	74
8.3	Production of reactive oxygen species in primary human monocytes	77
8.3.1	Source and subjection of the production of reactive oxygen species	77
8.3.2	Investigating the role of single Orai and STIM proteins in regulating	81
	NADPH oxidase activity.....	81
8.4	Redox regulation of store-operated calcium entry.....	85
8.4.1	Analysis of the redox-sensitivity of SOCE in human monocytes.....	85

8.4.2	The role of Orai3 in modulating redox-sensitivity of SOCE in human monocytes.....	86
8.4.3	The interplay of redox-sensitivity of SOCE and Ca ²⁺ - dependent ROS production	87
8.4.4	The role of the redox-resistant isoform Orai3 in Ca ²⁺ -dependent ROS production	89
8.4.5	A theoretical approach to estimate redox-sensitivity of SOCE in different cell systems.	90
8.5	The Ca ²⁺ and redox environment in regulating cellular functions – Preparative adjustment of experimental conditions.....	92
8.6	Ca ²⁺ environment and Ca ²⁺ signaling in melanoma progression: Proliferation vs. Migration	93
8.6.1	The regulation of melanoma proliferation by the extracellular Ca ²⁺ milieu and SOCE	93
8.6.2	The migratory potential of melanoma cells in dependency on SOCE	95
8.6.3	Molecular mechanisms involved in melanoma progression	96
8.7	Designation of monocyte survival by the extracellular Ca ²⁺ and redox environment.....	97
9	Discussion.....	100
9.1	STIM and Orai proteins differentially contribution to SOCE	100
9.1.1	Orai1/2 and STIM1/2 contribute to SOCE in monocytes, revealing an important role of the so far neglected isoforms Orai2 and STIM2.....	100
9.1.2	SOCE in melanoma cells lines is mediated by Orai1 and STIM2	101
9.1.3	Additional aspects – The differences and similarities regarding SOCE in different cell systems	102
9.2	ROS production in monocytes is dependent on Ca ²⁺ signaling with a particular role for Orai and STIM mediated SOCE	102
9.2.1	NOX2 is the source for enzymatic ROS production in monocytes	102
9.2.2	NOX2 activation is dependent on the elevation of Ca ²⁺ signals.....	103
9.2.3	Orai and STIM are differentially involved in regulating NOX2 activity.....	103
9.2.4	Additional aspects – Potential and limitation to the interpretation of ROS production by monocytes.....	105
9.3	Redox-regulation of CRAC channels.....	106
9.3.1	In Monocytes Orai3 is a redox-insensitive isoform, that serves as modulator of SOCE-dependent ROS production in monocytes	106
9.3.2	An equation describes the correlation between Orai3/Orai1 expression profiles and the redox sensitivity of SOCE	107
9.3.3	Can an equation be used to estimate redox-sensitivity of SOCE in different cell types?	109

Contents

9.3.4	H ₂ O ₂ induces an initial increase in Ca ²⁺ signals in human monocytes and melanoma cells with so far unknown function.....	109
9.3.5	Additional aspects – Orai3 and other players in redox regulation of SOCE.....	110
9.4	A phenotype switch in melanoma cell lines is dependent on Orai1 and STIM2.....	110
9.4.1	Orai1 and STIM2 in proliferation vs. migration	110
9.4.2	General vs. specific effects of the cellular environment and Ca ²⁺ signaling on proliferation and migration	111
9.4.3	Additional aspects – Orai1 and STIM2 in the context of melanoma onset and progression	111
9.5	Monocytes in an altered redox and Ca ²⁺ microenvironment	112
9.5.1	Monocytes react to changes in their environment, but are moderately insensitive to changes in the extracellular Ca ²⁺ concentration.....	112
9.5.2	Additional aspects – What additional parameters define redox sensitivity of monocytes?	113
9.6	Regulation of NOX and CRAC channel activity as therapeutical application in inflammatory and cancerous diseases: A clinical outlook	114
9.6.1	Regulation of CRAC channel activity as therapeutical application in melanoma treatment.....	114
9.6.2	Regulation of NOX and CRAC channel activity as therapeutical application in inflammatory diseases.....	114
9.6.3	Influencing cellular fate and survival by altering the extracellular environment.....	115
9.7	Concluding Remarks	116
10	Literature	117
11	Register of Figures.....	136
12	Register of Tables and Equations.....	138
13	Publications.....	139
14	Curriculum Vitae	140

2 Glossary

The glossary contains units and measurements used in the text of this work following the *International System of Units* (SI-System and Units) and abbreviations used and not explained in the text. All other abbreviations are explained in the text, at least once when first used.

Units and Measurements

μl	microlitre
μM	micromolar
g	gram
h	hour
kDa	kilo dalton
M	molar
min	minutes
ml	milliliter
mM	Milli molar
nM	nono molar
rpm	rounds per minute
s	seconds
xg	(x) fold earth acceleration
pmol	Pico molar
mT	Milli Tesla
mW	Milli Watt
mA	Milli Ampere
V	Volt

Miscellaneous abbreviations

Approx.	approximately
ATP	Adenosine triphosphate
BRAF	proto-oncogene B-Raf; serine/threonine-protein kinase
CC(R), CXC(R), CX ₃ C(R)	Classification of chemokine ligands and receptor (R) families
CD	Cluster of differentiation
CDK2	Cyclin-dependent kinase 2
cDNA	Copy DNA
CREB	cAMP response element-binding protein (transcription factor)
C-term/ N-term	Carboxy-terminus/ Amino-terminus of proteins
DEPC	Diethylpyrocarbonate (or diethyl dicarbonate)
DNA	Deoxyribonucleic acid
dNTPs	Desoxynucleotide-5'-triphosphates

Glossary

(dGTP, dATP, dTTP, dCTP)	Desoxyguanosine-, adenosine-, thymidine-, cytidine- 5'-triphosphate
EF-hand	Ca ²⁺ -binding domain
ER/SR	Endoplasmic/ sarcoplasmic reticulum
ERK (1/2)	Members of the extracellular signal-regulated kinase family
Ero1p	ER oxidoreductin 1
ERp57	Protein disulfide isomerase family A, member 3
FAD ⁺ /FADH + H ⁺	flavin adenine dinucleotide (reduced/ oxidized)
FC	Flow cytometer/ cytometry
Fcy	Fragment crystallizable receptor type γ (antibody binding receptor)
GAPDH	Glyceraldehyd-3-phosphat-dehydrogenase
HEK (cell line)	Human embryonic kidney (cell line)
HIF1- α	Hypoxia-inducible factor 1- α
HLA-DR	Human leukocyte antigen (type DR, MHC class II)
IgG	Immunoglobulin G (antibody)
IL	Interleukin
LBP	Lipopolysaccharide binding protein
LPS	Lipopolysaccharide
MEK	Dual specificity mitogen-activated protein kinase kinase 1
MHC II	Major histocompatibility complex class II molecule
NAD ⁺ /NADH + H ⁺	Nicotinamide adenine dinucleotide (reduced/oxidized)
NADP ⁺ /NADPH + H ⁺	Nicotinamide adenine dinucleotide phosphate (reduced/ oxidized)
NFAT	Nuclear factor of activated T cells
NfkB	Nuclear factor 'kappa-light-chain-enhancer' of activated B-cells
N-Ras	Member of the Ras superfamily of small GTPases
p16/ p21	Cell cycle regulators (cyclin-dependent kinase inhibitor 2A/ 1)
PCR	Polymerase chain reaction
Pdi1p	Protein disulfide isomerase
PI3K γ	Phosphatidylinositol-4,5-bisphosphate 3-kinase
RNA	Ribonucleic acid
RNAPol	RNA Polymerase
SDS	Sodium-dodecyl-sulfate
SEM	Standard error of the mean
TBP	TATA-Box binding protein
TLR-4	Toll-like receptor 4
TM	Trans-membrane region
TRP channel	Transient receptor potential channel
UV (radiation)	Ultraviolet (radiation)
Δ	Delta/ difference

3 Summary

3.1 Zusammenfassung

Die Funktion von Zellen wird maßgeblich durch das Zusammenspiel des extra- und intrazellulären Milieus bestimmt. Ca^{2+} Signalwegen kommt dabei eine wichtige Rolle zu. Die Haut und das Immunsystem stellen zwei Zellsysteme da, die unter physiologischen und pathologischen Bedingungen nicht nur durch Ca^{2+} , sondern auch durch das oxidative Milieu stark beeinflusst werden. Die Rolle und Regulation eines zentralen Ca^{2+} Signalwegs wurde in Melanom-Zelllinien und primären humanen Monozyten untersucht, da diese Zellen in der Tumor- und Entzündungsumgebung in der sie agieren, mit einem charakteristischem Ca^{2+} und oxidativen Milieu konfrontiert werden. Durch UV Strahlung kommt es in der Haut zur Freisetzung verschiedenster Hormone, die zu einer Produktion von reaktiven Sauerstoff Spezies (RSS) und der Aktivierung von Ca^{2+} Signalwegen führen können. Es konnte kürzlich gezeigt werden, dass Ca^{2+} Signalwege in Melanozyten essentielle Funktionen, wie z.B. die Pigment-Synthese, regulieren. Dagegen gab es wenige Informationen über die Rolle von Ca^{2+} Signalwegen in pathologischen Hautveränderungen, wie Melanomen. Wie in der Haut, konnte auch im erworbenen Immunsystem eine essentielle Funktion für Ca^{2+} Signalwege nachgewiesen werden, wie z.B. in Proliferation und Differenzierung von T-Zellen. Auch der angeborenen Immunantwort gegen schädliche Pathogene, konnte eine wichtige Rolle für die Produktion RSS, sowie Ca^{2+} Signalwegen zugeschrieben werden. Unter den verschiedenen Zellarten der angeborenen Immunität, gab es über die Rolle von Redox und Ca^{2+} Signalwegen in einer zentralen Zellart, den Monozyten, allerdings nur geringe Informationen.

Der in dieser Arbeit untersuchte Signalweg, ist der Speicher-gesteuerte Ca^{2+} -Einstrom (SGCE), der durch die *Calcium-release activated Ca^{2+}* (CRAC) Kanäle vermittelt wird. Zudem wurde die Rolle der molekularen Komponenten des SGCE, Orai und STIM untersucht. Diese Proteine sind für die Bildung des CRAC Kanals (Orai1-3), sowie seine Regulation verantwortlich (STIM1-2). Die Bestimmung des SGCE mittels fluoreszenz-basierter Messmethoden ermöglichte die Charakterisierung der intrazellulären Ca^{2+} Signale in den untersuchten Zelltypen. Die einzelnen Komponenten, die den CRAC Kanal bilden und steuern, wurden herunterreguliert um so ihre Beteiligung am SGCE zu ermitteln. Im Gegensatz zu anderen Phagozyten, zeigte sich in primären Monozyten nicht nur eine Beteiligung von Orai1 und STIM1 sondern auch Orai2 und STIM2 am SGCE. In Melanoma-Zelllinien hingegen, zeigte sich, dass der SGCE maßgeblich durch zwei der Isoformen vermittelt wird: Orai1 und STIM2.

RSS tragen nicht nur zur Abtötung von Pathogene bei, sondern wirken auch als Signalmoleküle indem sie Oxidationsreaktionen ermöglichen. Monozyten tragen in ihrer Funktion als Phagozyten zu einem oxidativen Milieu in entzündetem Gewebe bei, indem bei Pathogen-Kontakt eine Enzym-vermittelte RSS Produktion aktiviert wird. Die hauptverantwortlichen Enzyme sind die NADPH Oxidasen (NOX). NOX2 konnte in dieser Arbeit als das verantwortliche Enzym der RSS Produktion von Monozyten ermittelt werden. In einer vorhergehenden Studie konnte gezeigt werden, dass ein stark oxidatives Milieu, wie es durch Phagozyten im Rahmen einer Entzündung generiert wird, den SGCE in humanen CD4^+ T-Zellen inhibiert. Es zeigten sich zudem Unterschiede in der redox Sensitivität der einzelnen Kanal-bildenden Orai Proteine. Orai1 und Orai2 werden durch RSS inhibiert, wobei Orai3 sich als redox- insensitiv erwies. Es konnte zudem gezeigt werden, dass die Orai3 Expression im Laufe der T-Zell Differenzierung erhöht wird, um so Ca^{2+} Signale in T-Zellen auch in einem stark oxidativem Milieu aufrechterhalten zu können. Daher war es ein Hauptaspekt dieser

Arbeit, die Regulation der RSS Produktion durch ORAI und STIM vermittelten SGCE und wiederum die Wirkung der RSS auf die beteiligten CRAC Kanäle in einer Zellart zu untersuchen, die im Vergleich zu T-Zellen noch höheren Konzentrationen an RSS ausgesetzt ist. Monozyten eigneten sich aufgrund ihrer Funktion als RSS-Produzenten, daher besonders als Versuchsobjekt. Dazu wurde die extra- und intrazelluläre Produktion von $\bullet\text{O}_2^-$ und H_2O_2 anhand spektroskopischer und fluoreszenz-basierter Methoden bestimmt. Hierbei zeigte sich eine Abhängigkeit der NOX2-basierten RSS Produktion vom SGCE. Durch Herunterregulation der Orai und STIM Proteine konnte gezeigt werden, dass Orai1 und STIM1 und in besonderem Maß auch STIM2 für eine hinreichende RSS Produktion benötigt werden.

Der SGCE von Monozyten wies in Anwesenheit von H_2O_2 eine Dosis-abhängige Inhibierung auf. Eine Herunterregulation von Orai3 führte zu einer Verstärkung der Inhibition. Während Orai3 keine direkte Rolle an der Steuerung der Ca^{2+} -abhängigen RSS Produktion zukommt, moduliert das Protein die inhibierende Wirkung von H_2O_2 auf die RSS-Produktion. Unter Kontrollbedingungen führe eine H_2O_2 Behandlung nicht zu einer Inhibierung der RSS-Produktion, während eine verminderte Expression von Orai3 eine H_2O_2 -bedingte Inhibierung zur Folge hatte. Zusammenfassend belegen diese Ergebnisse die Existenz eines regulativen *Feedback-Loops* zwischen der Orai- und STIM-abhängigen RSS Produktion und der RSS-bedingten Inhibierung der CRAC Kanäle. Die festgestellte regulierende Wirkung des oxidativen Milieus unterstreicht die wichtige Rolle von RSS als Signalmoleküle im Immunsystem. Ein therapeutischer Eingriff in diesen regulatorischen *Loop* könnte eine Korrektur pathologischer RSS Level, wie sie z.B. bei rheumatoider Arthritis und Arteriosklerose vorliegen, ermöglichen. Obwohl dem SGCE eine große Bedeutung zukommt, zeigten Überlebensstudien, dass Monozyten eine hohe Resistenz selbst dramatischen Änderungen des Ca^{2+} Milieus gegenüber aufweisen.

In Melanomen kann ein spontaner Wechsel zwischen einem proliferativen und metastasierenden Phänotyp auftreten, der durch verschiedenste, teilweise unbekannt, Faktoren reguliert wird und über die Progression des Melanoms und das Ansprechen des Tumors auf konventionelle Therapien entscheidet. Um die Rolle des durch Orai und STIM vermittelten SGCE und die Rolle des extrazellulären Ca^{2+} Milieus für die Phänotyp Ausprägung zu bestimmen, wurde die Migration und die Proliferation von Melanom-Zelllinien untersucht. Verringerte extrazelluläre Ca^{2+} -Konzentrationen und durch Herunterregulation von Orai und STIM bedingte geringere Ca^{2+} -Signale führten zu einer verstärkten Proliferation der Zellen. Zudem zeigte sich eine erhöhte Expression des Microphthalmie-assoziierten Transkriptionsfaktors, ein bekannter Marker des proliferativen Phänotyps. Im Gegensatz dazu wurde das invasive Potenzial durch eine Herunterregulation von Orai1 und STIM2 vermindert. Dementsprechend zeigten Marker wie JARID1B und Brn2, die einen nicht-proliferierenden Phänotyp charakterisieren, eine verminderte Expression. Zusammenfassend unterstützen die Ergebnisse ein Model, in dem ein dynamischer Phänotypwechsel in Melanomen durch Orai1 und STIM2 kontrolliert wird. Eine pharmakologische Regulierung von Orai1 und STIM2 könnte die Metastasierung eines Melanoms verhindern und den Tumor empfänglicher für konventionelle Therapien machen, die vornehmlich stark proliferierende Zellen zum Ziel haben.

Weiter gedacht, können die in dieser Studie gewonnenen Erkenntnisse über die Regulation zellulärer Funktionen in monozyten und malnom Zellen durch CRAC Kanäle ein Zugewinn für die klinische Forschung sein. Die Ergebnisse zeigen, dass Orai and STIM potenzielle Angriffspunkte in der Behandlung entzündlicher Erkrankungen und in der Krebstherapie sein können. Den Isoformen Orai3 und STIM2 kommt dabei eine besonderer Rolle zu.

3.2 Summary

Cellular function is defined by the interplay between the extra- and intracellular milieu. In this regard, Ca^{2+} and redox signaling play a decisive role. The skin and the immune system are two examples where Ca^{2+} and redox signaling are known to control several physiological and pathological conditions. The presence and relevance of a major calcium signaling pathway was analyzed in human melanoma cell lines and primary human monocytes as they cope with a characteristic Ca^{2+} and redox milieu in their respective tumor and inflammatory environment. In the skin, UV exposure leads to the release of a plethora of hormones by keratinocytes and melanocytes and the subsequent activation of the production of reactive oxygen species (ROS), as well as calcium signaling cascades. Under physiological skin conditions calcium signaling was shown to regulate essential melanocyte functions as pigment synthesis, while there was little information available on its role in pathological conditions as melanoma. Calcium signals were likewise shown to play an essential role in adaptive immunity, such as regulating the proliferation and differentiation of T cells. Furthermore, ROS production and redox signaling, as well as calcium signaling play an important role in innate immune responses to invading pathogens. However, the role of calcium and redox signaling in a very central cell type of innate immunity, the monocytes, was so far only poorly investigated.

The signaling pathway investigated was the store-operated calcium entry (SOCE), mediated by the calcium release activated Ca^{2+} (CRAC) channels, as well as the specific roles of its molecular components Orai and STIM, responsible for channel formation and gating. Ca^{2+} signals of the investigated cell types were determined by fluorescence-based imaging methods. Specific siRNAs targeting the single channel components (Orai proteins) and their regulators (STIM proteins) were used to analyze their contribution to SOCE. In contrast to other phagocytes, not only Orai1 and STIM1, but also Orai2 and STIM2 contribute to SOCE in monocytes, whereas in melanoma cell lines, Orai1 and STIM2 are the dominant isoforms regulating SOCE.

Monocytes, as part of the first line of host defense, contribute to an oxidative milieu by enzyme-triggered ROS upon pathogen encounter. ROS are not only involved in pathogen clearance, but also act as signaling molecules by mediating oxidative regulation of proteins and enzymes. The NADPH oxidases (NOX) are responsible for enzymatic ROS production. The isoform NOX2 was identified as the major ROS-producing enzyme in human monocytes. A highly oxidizing environment, generated by ROS-producing phagocytes in an inflamed tissue, was shown to inhibit the essential SOCE in human CD4^+ T cells in a prior study. The channel forming Orai proteins display differences in their redox responses. Orai1 and 2 were shown to be inhibited by ROS, while Orai3 was shown to be redox-insensitive. Upon T cell differentiation, Orai3 is up regulated by CD4^+ T cells as mechanism to fine tune Ca^{2+} responses in an oxidizing milieu. Therefore, one of the major aspects of the here predated study was to investigate ROS production and SOCE, as well as the effect of produced ROS on CRAC channel activity, in a highly redox challenged cell type as monocytes. Using spectroscopic- and fluorescence-based techniques, the extra- and intracellular production of ROS was measured, revealing a dependency of NOX2 activity on SOCE. Orai1, STIM1 and STIM2 were revealed to equally contribute to SOCE-dependent ROS production. SOCE of monocytes was dose-dependent inhibited in the presence of H_2O_2 . This inhibitory effect was enhanced with the down-regulation of the redox-insensitive isoform Orai3. While there is no contribution to SOCE-dependent ROS production by Orai3, the isoform is responsible for the modulation of the inhibitory effect of H_2O_2 on SOCE: an H_2O_2 treatment does not alter SOCE-dependent ROS production under

control conditions, but in the absence of Orai3, ROS production is inhibited under H_2O_2 treatment. In summary, there are hints for a regulatory feedback loop between Orai and STIM-dependent ROS production and the ROS-dependent inhibition of the CRAC channels. The regulatory function of H_2O_2 emphasizes the role of ROS as signaling molecules. The feedback loop might serve as a therapeutic target to modulate pathological ROS levels as they are known to be part of the clinical pattern of different inflammatory diseases as rheumatoid arthritis or atherosclerosis.

Melanoma is one of the rarest, but most deadly form of skin cancer, progressing from melanocytes in the basal layer of the epidermis. The disease outcome, as well as the responsiveness to combination therapy is determined by spontaneous switching from proliferative to invasive phenotype. This phenotype switch and its underlying cellular features, proliferation and migration, are controlled by mainly unknown environmental factors. Therefore, the role of Orai and STIM-dependent Ca^{2+} signaling and the overall Ca^{2+} environment on melanoma phenotype was analyzed under lower extracellular Ca^{2+} conditions or following silencing of Orai1 and/or STIM2. In both cases, the experimental approaches resulted in a decrease in intracellular Ca^{2+} . This decrease correlated with enhanced proliferation and increased expression of microphthalmia-associated transcription factor, a marker for proliferative melanoma phenotype. As counterpart, the invasive and migratory potential of melanoma cells was tested upon silencing of Orai1 and/or STIM2. Invasion and migration of melanoma cells, as well as the according markers for a non-proliferative, tumor-maintaining phenotype such as JARID1B and Brn2 were decreased. In summary, the results support a dynamic phenotype switching model in melanoma controlled by Orai1 and STIM2. Pharmacological tuning of Orai1 and particularly STIM2 might thus prevent metastatic spread and render melanoma more susceptible to conventional combination therapy.

Regarding the role of extracellular environment for cellular functions, the impact of an altered calcium environment on cellular behavior was also tested. While SOCE shows a meaning in both investigated cell types, the extracellular Ca^{2+} milieu only bears a meaning in regulating melanoma proliferation. In contrast, monocytes display a strong resistance to changes in the Ca^{2+} milieu, even under challenging conditions.

In a broader scope, the findings on the role of the single Orai and STIM proteins in regulating cellular features of monocytes and melanoma, might provide new therapeutic applications for the treatment of skin cancer and innate immunity-associated diseases. In this regard, a distinctive role might come in for the STIM2 and Orai3 isoforms. Targeting this isoforms in a therapeutic approach could prevent harmful side effects on the respective signaling pathways, leaving Orai1 and STIM1 function unaltered, as the Orai1/STIM1 couple was shown to be essential in other cellular systems.

4 Scientific Acknowledgments

The experimental data of the here presented work was collected with the support of several scientific co-workers and collaborations that are stated here.

Reprints

Summary (English), Introduction (section 6.3) and Discussion (sections 9.4.2 and 9.4.3) are in part reprints or contain altered paragraphs from (Stanisz *et al.*, 2014).

Introduction (sections 6.1.3 and 6.6.1) and Discussion (sections 9.4, 9.5, 9.6) are in part reprints or contain altered paragraphs from (Saul *et al.*, 2013).

Scientific collaboration and access to cell lines and equipment

Acknowledgements to Dr. Alexander Rösch¹ and The Wistar Institute, Philadelphia, U.S.A, for providing the WM3734 melanoma cell line. Acknowledgments to Dr. Hedwig Staniz¹ and Prof. Thomas Vogt¹ for the productive collaboration with the Department of Dermatology and for providing the melanoma cell lines SK-MEL-5 and SK-MEL-28. Acknowledgments to Prof. Martina Sester and the Department of Virology (Saarland University, Homburg (Saar)) for granting access to the flow cytometer BD FACS Cantoll.

Scientific co-workers

Alexandra Stark¹, under the supervision of Dr. Hedwig Staniz¹ performed qRT-PCR experiments and Western-Blot analysis depicted in Figure 9 (B-D), Figure 11 (C and D) and Figure 28 and supported the cell culture of melanoma cell lines. The stated figures and panels were made and altered from data published in (Stanisz *et al.*, 2014).

Gertrud Schwär² performed and supported RNA-isolation, cDNA synthesis and qRT-PCR experiments providing the data depicted in Figure 9 (A) and Figure 17 (B).

David Conrad², under the supervision of Dr. Reinhard Kapp², performed the EPRS experiments depicted in Figure 16.

Dr. Reinhard Kapp² supported the analysis and statistic assessment of the data depicted in Figure 21 (D).

Cora Stephan supported the flow cytometry experiments depicted in Figure 12.

¹ Department of Dermatology, Universitätsklinikum des Saarlandes, Homburg (Saar), Germany

² Department of Biophysics, Saarland University, Homburg (Saar), Germany

5 Private Acknowledgements

Acknowledgments to Prof. Dr. Markus Hoth for his support and the opportunity to continue my research in the department of Biophysics. Markus was always a source of new input and ideas regarding my work and I am thankful for the trust he offered me.

My dearest thanks to my supervisor PD Dr. Ivan Bogeski. Ivan supported me not only in my professional but also private development and accompanied me through all ups and downs over the last four years. He gave me the opportunity to work independently and build and strengthen my confidence as a scientist.

In addition, I want to express my gratefulness to Prof. Dr. Barbara Niemeyer, Dr. Eva Schwarz and Dr. Reinhard Kappl, working with you was always exciting and informative. Barbara was always inspiring with her thought and ideas regarding my projects. I want to thank her for the ongoing support throughout my PhD time. I want to thank Eva for the intensive discussions and never making working with her boring. I also want to thank Reinhard for all the patience and time he invested in explaining whatever I was interested to know.

All my gratefulness to my dear friends and colleagues, who invested their time and energy in proofreading and editing the thesis. Thank you Dalia Alansary, Katja Kostelnik, Anna-Maria Miederer, Saskia Sperber, Judith Wahrheit and Katharina Zimmermann.

I would also like to express my acknowledgement to all the assistance I received during my time in the department of Biophysics. And I want thank Sandra Janku, Cora Hoxha, Gertrud Schwär, Petra Frieß, Andrea Armbrüster and Carmen Hessig for their technical assistance.

Thanks to all my colleagues at the department of Biophysics. You made the time of my PhD as exciting, interesting, instructive and fun as possible.

I hope that my family and friends are aware of my gratefulness for everything they give me every day.

6 Introduction

6.1 Cellular Signaling

Cell life is regulated by complex signaling and metabolic pathways. Cells therefore have to receive, recognize, coordinate and integrate a huge variety of signals. Besides their role as acceptors, cells take an active part in the signaling process. By production and release of signaling molecules (hormones, cytokines) that can bind to receptors on either the producing or neighboring cells, they trigger further cellular responses (referred to as autocrine or paracrine signaling). Cellular signaling also includes physical interaction of neighboring cells or with components of the extracellular matrix, for example during adhesion and migration. Besides hormone, cytokine and enzyme release also the coordination and orchestration of extracellular and intracellular ion concentrations shapes signaling events. Signaling *via* changes in ion concentrations encloses a seemingly unmanageable network that requires tight regulation of the involved components. A plethora of channels, pumps and transporters are active to coordinate mainly Ca^{2+} , Na^+ , K^+ and Cl^- concentrations for signaling purposes. The characteristics of two signaling molecules, namely Ca^{2+} and reactive oxygen species, that were investigated in the here presented study and their orchestration and relevance in a specific environment will be introduced in the following sections (6.1.1 - 6.1.3). This overview is followed by the presentation of the investigated cell types (6.2 and 6.3) and the molecular aspects underlying the analyzed signaling pathways with regard to the cellular context (6.4 and 6.5). Finally the detailed scientific questions addressed in this study are outlined with respect to the current knowledge regarding the investigated subject (6.6).

6.1.1 Calcium Signaling

Calcium ions (Ca^{2+}) fulfill multiple and highly differential functions on cellular levels by acting as second messenger in cell signaling. Ca^{2+} passes the plasma membrane (PM) of cells exploiting transporting systems, such as channels, pumps and exchangers. In contrast to other ions, the great ability of Ca^{2+} , to act as second messenger is based on its ubiquitous occurrence and the huge concentration gradients between the extracellular and intracellular space and subcellular compartments. The Ca^{2+} concentration ($[\text{Ca}^{2+}]$) of the extracellular space with 1-2 mM exceeds the concentration in the cytosol, with about 100 nM, to a 10.000 fold. Meanwhile, internal stores as the ER/SR hold 0.5 mM, again exceeding cytosolic concentration (Figure 1, A).

Ca^{2+} signal modulation

By changing cytosolic Ca^{2+} concentration ($[\text{Ca}^{2+}]_{i(\text{intracellular})}$), different cellular processes are regulated, among these cell differentiation and proliferation, gene expression, cytokine production, exocytosis, ion channel activation and inhibition (Berridge *et al.*, 2003; Clapham, 2007). Ca^{2+} signaling is even more elaborated as not only the rise in $[\text{Ca}^{2+}]_i$, but also time, shape, location and magnitude of the signal defines the process to be regulated. In immune cells such as T cells, Ca^{2+} signals were shown to define cell fate, by leading to proliferation, apoptosis or tolerance. The different outcome of a Ca^{2+} signal depends on the modulation of shape (transient or oscillatory) and magnitude (high or low) (Qu *et al.*, 2011). Within a Ca^{2+} signaling cascade, Ca^{2+} is bound by specialized Ca^{2+} -binding proteins, as calmodulin or the members of the S100 protein family (Clapham, 2007; Donato *et al.*, 2013). Ca^{2+} binding serves for either Ca^{2+} -buffering or the transduction of the Ca^{2+} signal, by activating downstream cascade components. A common way of signal transduction by elevating $[\text{Ca}^{2+}]_i$, is the

activation and translocation of transcription factors (TF), whereas different TFs require different signals. For example the abundantly present TFs NFAT and NF κ B, that are involved in regulating gene expression, promoting cell differentiation, proliferation, cytokine production and induction of immune responses (Pahl, 1999; Rao, 2009). NF κ B is activated by high, short-term signaling events, while NFAT activation requires a lower, but long-lasting rise in cytosolic Ca²⁺ (Rao *et al.*, 1997; Dolmetsch *et al.*, 1997; Berridge *et al.*, 1998; Crabtree, 1999).

Ca²⁺ homeostasis: the basis for Ca²⁺ signaling

A tightly regulated intermezzo of activation, inhibition and (co-) regulation of different kinds of Ca²⁺ permeating and transporting channels, pumps and exchangers is responsible for the maintenance of Ca²⁺ homeostasis and membrane potential. These two parameters are an essential prerequisite for proper signaling events across the plasma membrane. The plasma-membrane Ca²⁺ ATPase (PMCA) is an ATP-consuming ion pump transporting Ca²⁺ ions from the cytosol to the extracellular space providing a backhaul mechanism. This backhaul maintains the driving force, required for further signaling events, and prevents a harmful rise in [Ca²⁺]_i associated with apoptosis (Strehler & Treiman, 2004; Dong *et al.*, 2006; Pászty *et al.*, 2007). Another Ca²⁺ ATPase is located in the membrane of the ER, called sarcoplasmic /endoplasmic Ca²⁺ ATPase (SERCA). This enzyme is responsible for the (re-) filling of internal Ca²⁺ stores, after they were emptied upon signaling events and leakage, an important aspect in calcium homeostasis, but also specific calcium signaling pathways (Alonso *et al.*, 2012). A scheme describing the components involved in regulating Ca²⁺ homeostasis is given in Figure 1 (A).

Ca²⁺ channels

The variety of channels involved in regulating Ca²⁺ influx across the plasma membrane are sub-divided depending on their gating and activation mode into: receptor-operated channels, voltage-operated channels, second-messenger-operated channels and store-operated channels (SOC) (Parekh & Jr, 2005). SOC themselves are a highly versatile group of channels, but share a common activating pathway (see Figure 1, B and (Parekh & Jr, 2005)). The initial and central step in the activation cascade of SOC is the activation of phospholipase C (PLC) that results in cleavage of the membrane residing phosphatidylinositol (PIP₂) to diacylglycerol (DAG) and the release of inositol-(1,4,5)-trisphosphate (IP₃) to the cytosol. IP₃ binds to its cognate receptor (IP₃R) located in the ER membrane. IP₃R is a ligand-activated Ca²⁺ channel that releases Ca²⁺ from the internal stores to the cytosol upon activation. This rise is only transient due to the activity of PMCA, transporting Ca²⁺ to the extracellular space and SERCA, refilling the ER stores. Depletion of internal stores with transitional rise in [Ca²⁺]_i is the activating trigger for SOC in the plasma membrane (Figure 1, B). The Ca²⁺ influx by SOC is therefore referred to as store-operated Ca²⁺ entry (SOCE).

A member of the SOC family that is responsible for essential Ca²⁺ signaling events in many cell types is the calcium-release activated Ca²⁺ (CRAC) channel that mediates SOCE with a Ca²⁺ current (I_{CRAC}) displaying distinct biophysical features. I_{CRAC} was initially described in mast cells (Hoth & Penner, 1992; Zweifach & Lewis, 1993) and the molecular players of the CRAC channel remained unidentified for over 20 years. The CRAC channels and especially the role of their molecular components were the central point of this study and are described in detail below (6.4.1, 6.5 and 6.6.1).

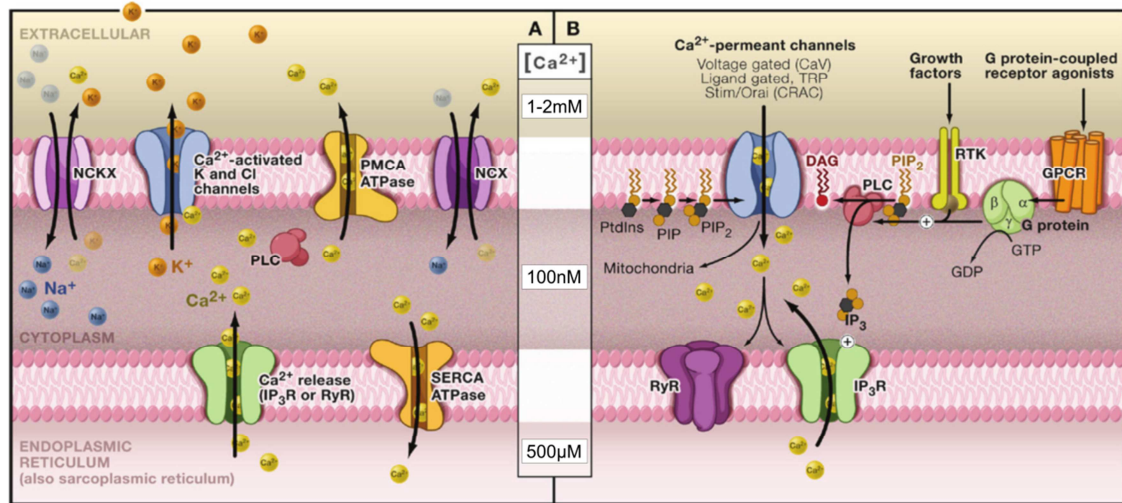


Figure 1 Calcium homeostasis and signaling

Adapted from (Clapham, 2007). (A) Involved channel and transporter activity in maintaining low cytosolic $[Ca^{2+}]$ at approx. 100 nM as requisite for Ca^{2+} signaling. Low cytosolic Ca^{2+} is maintained by extrusions of Ca^{2+} to the extracellular space by PMCA and to internal Ca^{2+} stores as the sacro-/endoplasmatic reticulum by SERCA. Ca^{2+} can be released from internal stores *via* Ca^{2+} -release receptors (IP_3R and RyR). Secondary regulators of Ca^{2+} concentrations as the NC(K)Xs are electrogenic and exchange cytosolic Ca^{2+} (and K^+) with sodium ions from the extracellular space. The activation of K^+ channels by Ca^{2+} and the subsequent efflux of K^+ enhance the driving force for Ca^{2+} as further prerequisite for Ca^{2+} signaling. (B) The signaling cascades activating store-operated Ca^{2+} entry. Activation of cell surface receptors as RTKs or GPCRs, lead to the activation of PLC and the generation of IP_3 and DAG from PIP_2 . IP_3 binds to its cognate receptor, releasing Ca^{2+} from internal stores. This store release leads to the activation of different plasma membrane residing Ca^{2+} channels. The Ca^{2+} influx *via* these activated channels to the cytosol is an important factor in regulating cellular functions. Abbreviations used: NC(K)X – Sodium (Na^+), calcium (Ca^{2+}), (potassium (K^+)) exchanger; PLC – Phospholipase C; PMCA – Plasmamembrane Ca^{2+} ATPase; IP_3R – Inositol-trisphosphate- receptor; RyR – Ryanodine receptor; SERCA – Sarco-/endoplasmic reticulum Ca^{2+} ATPase; PtdIns – Phosphatidylinositols; PIP – Phosphatidylinositol phosphate; PIP_2 – Phosphatidylinositol bisphosphate ; IP_3 – Inositol-(1,4,5)-trisphosphate; DAG – Diacylglycerol; RTK – Receptor tyrosine kinase; GPCR – G-Protein coupled receptor.

6.1.2 Redox Signaling

6.1.2.1 Reactive Oxygen Species: Types and features

Aside from Ca^{2+} as an important signaling molecule, more and more attention is paid to other small, organic molecules that act in signaling events. A prominent example are reactive oxygen species (ROS) that encompass a huge variety of approx. 20 small reactive molecules that initially derive from molecular oxygen (O_2). Among these are superoxide- ($O_2^{\cdot -}$), hydroxyl- (OH^{\cdot}), and peroxy- ($R-O_2^{\cdot}$) radicals, as well as hydrogen peroxide (H_2O_2) and hypochlorous acid (HOCl) (Dröge, 2002; Lambeth, 2004). The term ROS, although often misinterpreted only describing free radicals, comprises radical and non-radical species. These species differ in terms of their reactivity with organic molecules, their stability and life time and their spatial mobility. These features can be estimated by modelling approaches and based on chemical properties as the reduction potential or the determination of rate constants between different reaction partners. The occurrence of a redox reaction, depends on the abundance of the oxidants, the presence of antioxidants or decomposing enzymes and the presence of competing interaction partners (Winterbourn *et al.*, 2006; Winterbourn, 2008).

ROS production and formation includes conversion from different species into others, either spontaneously or by enzyme supported reactions, including dismutation, Fenton reactions (in presence of metal ions), peroxidase reactions (myeloperoxidase) and decomposition. An overview of major biological relevant ROS and the ways of (inter-) conversion is given in

Figure 2 (Lambeth, 2004).

The presence of these reactive molecules was considered as the companion of an aerobic life, because ROS can derive from electrons escaping the respiratory chain in mitochondria. These escaping electrons can react with molecular oxygen to generate the superoxide radical. In general, ROS can origin from either exogenous or endogenous sources. Exogenous triggers that give rise to ROS are irradiation, the uptake of environmental pollutants and different chemicals. Within cells, ROS can originate from specialized organelles as microsomes and peroxisomes and are generated by different enzymes, as NADP oxidases, cytochrome C oxidase and xanthine oxidase (Trachootham *et al.*, 2008). An uncontrolled increase in ROS is referred to as oxidative stress and usually related to unspecific oxidation of biomolecules with harmful consequences as tissue damage and DNA strand breaks. The term oxidative stress therefore has to be distinguished from redox signaling, describing a controlled, enzymatic regulated production of certain ROS with defined concentrations and targets (Valko *et al.*, 2007; Trachootham *et al.*, 2008). The enzymes responsible for regulated ROS production are called NADPH oxidase and are described in detail in a following section (6.1.2.3).

The importance of ROS was initially described in the immune system when upon pathogen encounter, a rapid increase in oxygen consumption and the release of huge amounts of ROS was observed in phagocytic cells (Babior, 1984a). This phenomenon is referred to as oxidative burst and was shown to be involved in pathogen clearance and initiation of further immune responses (Babior, 1984b; Reth, 2002). The involvement of ROS in regulating cellular function has expanded from the immune system to the brain, the skin and other organs. In a broader, more general scope, emerging evidence links ROS production and redox signaling to cancer (Waris & Ahsan, 2006; Liou & Storz, 2010).

6.1.2.2 ROS as signaling molecules

General aspects

To serve as signaling molecules and to avoid excessive ROS production reaching harmful levels, ROS concentrations, as well as Ca^{2+} concentrations, have to be tightly regulated. This is why ROS clearing enzymes and mechanisms are equally important as ROS production itself. Major ROS clearing enzymes and mechanisms comprise enzymatic and non-enzymatic components and systems, while several systems and components work together, overlap or depend on each other. Major enzymatic ROS clearing enzymes are the family of superoxide dismutase (SOD) or catalase, a heme-containing enzyme located in peroxisomes. SODs are involved in the dismutation of superoxide to H_2O_2 , while catalase degrades peroxides as H_2O_2 . The glutathione system together with glutathione peroxidase (GPx) and reductase (GR) is one example for a team up of enzymatic and non-enzymatic systems. GPx decomposes H_2O_2 to H_2O in a coupled reaction with the oxidation of reduced glutathione (G-SH) to form GS-SG. GR is involved in the recycling of oxidized GS-SG under NADPH consumption. Reduced G-SH is in addition involved in thiol-disulfide exchange reactions and is therefore dependent on GR recycling (Dröge, 2002; Bedard & Krause, 2007; Trachootham *et al.*, 2008).

Production of certain ROS is restricted to specialized compartments and the different specialized enzymes involved in ROS production and inter-conversion are likewise constrained

in expression or localization to certain tissues, cells or sub-cellular compartments. These strong restrictions emphasize the necessity of spatial and temporal control of ROS production. For example myeloperoxidases (MPO) that generate the highly reactive HOCl, important for pathogen clearance, are restricted to membrane enclosed endosomes, with also the product trapped in the compartment (van der Veen *et al.*, 2009; Winterbourn & Kettle, 2013). The key requirement for functional redox signaling is the maintenance of redox homeostasis, the balance between ROS production and scavenger activity. Imbalances are implicated in various diseases where either over- or underproduction of ROS without an adjustment of the scavenging machinery results in disease promotion (see 6.2.3 and 6.6.1 for details).

Modes of redox regulation

As signaling molecules ROS are involved in regulating cellular redox-mediated mechanisms that comprise transcriptional regulation or direct oxidative modification of proteins and enzymes. ROS can also be involved in regulating redox-sensitive interacting proteins, modifying enzymes and regulation of protein turnover (Trachootham *et al.*, 2008). A very common way of redox-regulation is the oxidative regulation of protein tyrosine kinases and phosphatases (PTKs and PTPs). In summary, oxidative events favor phosphorylation of PTK/PTP targets as oxidation activates PTKs and inactivates PTPs (Chiarugi, 2005). There are multiple ways how proteins can be modified by oxidation with consequential activation or inactivation of the target. In proteins, the major target for oxidative modifications are thiol groups or cysteine residues (Bourdon & Blache, 2001; Poole *et al.*, 2004; Groitl & Jakob, 2014). The different modes of oxidative modification comprise: reversible post-translational modifications such as S-gluthationylation, -prenylation and -farnesylations; the formation of disulfide bridges that are often involved in conformational changes of the target. The formation of reversible and irreversible sulphur acid derivatives such as sulfenic, sulfinic and sulfonic acid, are further ways to regulate protein function (Winterbourn & Hampton, 2008; Roos & Messens, 2011).

H₂O₂ as biologically relevant ROS

H₂O₂ is one of the biological most important ROS involved in regulation of cellular processes, because its properties fit key requirements of redox regulation. H₂O₂ has a limited target range and is mainly involved in the oxidation of cysteine residues, a key target in redox-regulated processes. In addition, oxidation of targets by H₂O₂ often requires activation energy although the reaction might be thermodynamically favored (Winterbourn, 2013). These strong restrictions prevent unspecific oxidation events. The damaging effects of H₂O₂ are limited and often caused by H₂O₂-derived species, rather than the oxidant itself, or only at very high concentrations. Compared to superoxide, H₂O₂ is very stable and is only decomposed in the presence of specialized enzymes as MPO generating HOCl, or catalase. The huge spatial motility of H₂O₂ that can be up to 1.5 mm and the fact that H₂O₂ can pass biological membranes is a key factor for the regulation of even distant intracellular or extracellular targets (Winterbourn, 2008). Still, it has to be considered that H₂O₂ gradient build up over membranes. H₂O₂, as well as other non-membrane-passing ROS, can be restricted to subcellular compartments due to the presence of reaction partners or antioxidative systems (Go & Jones, 2008; Jones & Go, 2010). Regarding the actual mode of H₂O₂-mediated redox regulation, there is still controversy whether direct or indirect oxidation of a target underlies the process. Direct oxidation of cysteine targets were described, but also different indirect models were suggested (Winterbourn, 2013). An indirect way for example would be the oxidative inactivation of a scavenging protein, interacting with the actual target, making the target accessible for oxidation.

6.1.2.3 ROS generating Enzymes: NADPH Oxidases

The main enzymatic sources for ROS are the seven members of the NADPH oxidase (NOX) and dual oxidase (Duox) family: NOX1-5 and Duox1 and Duox2. The first enzyme identified with the major function of generating ROS instead of producing it as a byproduct was the NADPH oxidase of phagocytes (neutrophils and macrophages), with its catalytic main subunit termed phox (phagocyte oxidase), also referred to as gp91^{phox}. In the family nomenclature the NOX of phagocyte that also serves as prototypic isoform, is termed NOX2.

NOX enzymes reside in the plasma membrane or the membrane of different endosomes and produce superoxide by transmitting electrons from NADPH to molecular oxygen. The different isoforms show distinct features and similarities in their core structure, the necessity and number of additional subunits and their activation mode. NOX1-4 share a basic core structure with a six-transmembrane-domain topology and cytosolic N- and C-termini. Two bound heme molecules in the core structure provide the electron transfer chain required for the electron transport. The electrons are carried by cyclic reduction and oxidation of iron-centers within the bound heme molecules. NOX5 differs from NOX1-4 in carrying an additional Ca²⁺ binding domain facing the cytosol. The core unit of the dual oxidases comprises an additional transmembrane-domain, a Ca²⁺ binding domain, as well as a peroxidase domain facing the extracellular or intra-endosomal space, which enables the oxidation of target proteins under H₂O₂ consumption in addition to superoxide production (Lambeth, 2004; Bedard & Krause, 2007).

NOX and Duox enzymes can be found in many cells and tissues, but still the expression of several isoforms is restricted to certain tissues, or cells preferentially express one isoform. As for example Duox 1 and 2 are mainly found in thyroid and phagocytes preferentially express NOX2 (Krause, 2004). Regarding the organ systems addressed in the here presented study, the differential expression of NOX isoforms in the immune system and melanoma is briefly summarized. So far, NOX1 and NOX4 were described to regulate tumor progression and also NOX2 was shown to be expressed and to promote growth of melanoma skin-grafts in rodents (Kelkka *et al.*, 2013). NOX1 activity was further related to enhanced invasion of melanoma cells (Liu *et al.*, 2012). NOX4 activity was also linked to regulate melanoma progression, by enhancement of melanoma growth (Brar *et al.*, 2002; Yamaura *et al.*, 2009) and by rendering melanoma growth from a radial to a vertical, hence more aggressive, phenotype (Govindarajan *et al.*, 2007). Although seeming to be mainly involved in enhancement of melanoma progression, NOX4-derived ROS was recently shown to induce an apoptotic pathway in melanoma cells (Liu *et al.*, 2014). In the immune system, NOX2 is the predominant expressed isoform, as it is responsible for ROS production of phagocytes and was shown to be expressed in neutrophils, macrophages and monocytes, and several immune-cell derived cell-lines (Bedard & Krause, 2007). Recently NOX4, in addition to NOX2, was also suggested to contribute to ROS production and cellular signaling in monocytes (Lee *et al.*, 2010a; Ullevig *et al.*, 2012).

6.1.3 Inflammatory and tumor environments

With Ca²⁺ and redox signaling as the major aspects of this study, two different cellular systems were the object of investigation: the skin and the immune system. The two seemingly very different systems share a high importance for Ca²⁺ and reactive oxygen species in regulating cellular (signaling) processes both, on a molecular level as second messenger and as a component of the cellular environment (see also 6.1.2.3 and 6.6.1).

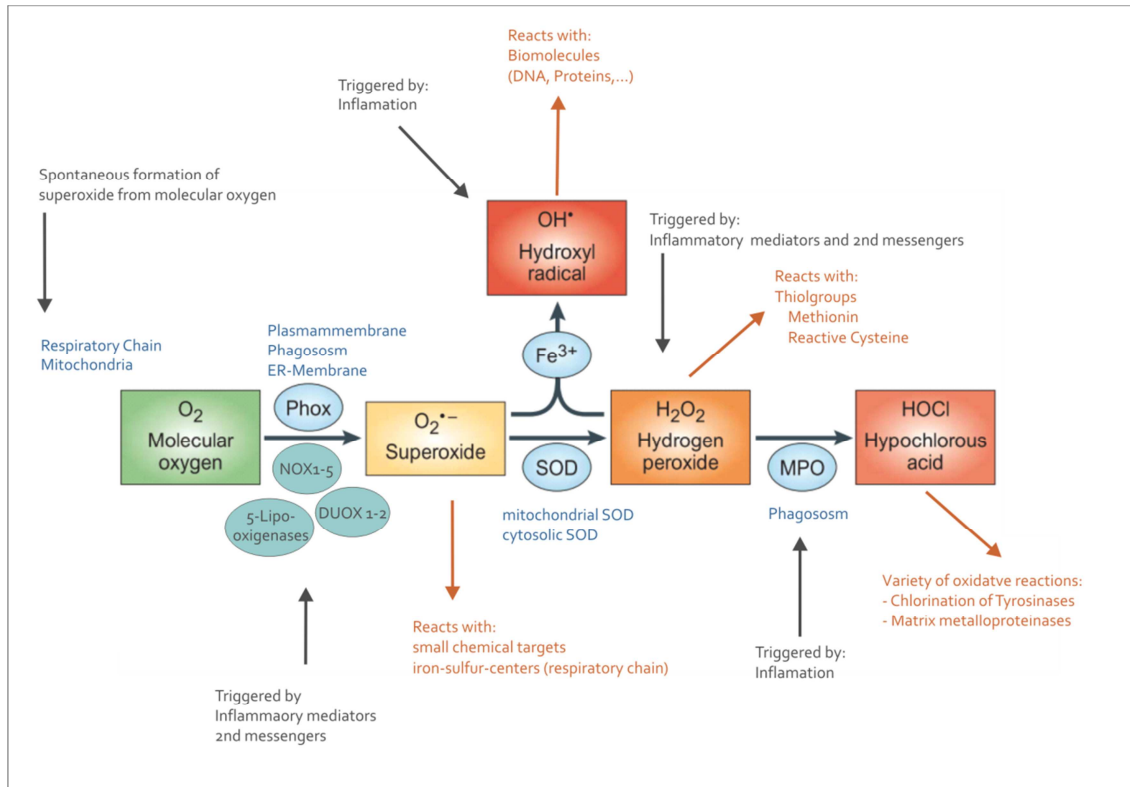


Figure 2 The basics of redox-signaling – Sources and inter-conversion of ROS

Generation of reactive oxygen species (ROS) in human immune cells (phagocytes), their inter-conversion (blue arrows), involved enzymes or cofactors (blue ellipses), the reactivity (red) of the specific ROS and events and molecules that trigger the production (grey arrows). Reactivity and harmfulness of ROS is indicated by the color shift from green (not harmful, little reactivity) to red (harmful, high and unspecific reactivity). Localization of involved enzymes is indicated in blue. Information about sources from (Bogeski *et al.*, 2011). Abbreviations used: Duox – Dual oxidase; NOX – NADPH oxidase; Phox – phagocyte NADPH oxidase (or NOX2); SOD – Superoxide dismutase, MPO - Myeloperoxidase. The figure is adapted and extended from (Lambeth, 2004).

Regarding the challenging conditions cells are facing under pathological skin and immune conditions, not only Ca^{2+} and redox-signaling processes, but also changes in the Ca^{2+} and redox-environment impact cellular functions. In this context, the two cell types regarded in this study are briefly introduced here in terms of the role of the environment for cellular function, while the signaling processes investigated in this study are already outlined above (see 6.1.1 and 6.1.2.). The two cell systems will further be described in the following sections (see 6.2 and 6.3).

6.1.3.1 Melanoma – an example for the role of a tumor environment

The skin is a solid example of how an environment impacts cellular fate and the overall function of an organ. The Ca^{2+} environment in the epidermis, the most outer region of this multilayer organ, was shown to define the function and development of the residing cells. The epidermis displays a Ca^{2+} gradient, with low concentrations in the basal area and increasing concentrations towards the outer rim (Elias *et al.*, 2002). This gradient was shown to determine the differentiation of keratinocytes, the major cell type in the epidermis, thereby ensuring barrier formation and sealing against the outer world (Hennings & Holbrook, 1983; Eckert *et al.*, 1997; Beck *et al.*, 2008). Under pathological skin conditions as malignant melanoma, the micro-environment was shown to hold a huge potential in regulating tumor progression. It was

reported, that malignant melanoma were reprogrammed to a benign phenotype when transferred to an embryonic cellular environment *in vitro* (Topczewska *et al.*, 2006; Díez-Torre *et al.*, 2009). Hypoxia, is a characteristic environmental condition involved in the induction of redox stress responses and is often observed in tumors as for example melanoma (Bedogni & Powell, 2009). Hypoxic conditions were shown to accelerate the malignant transformation of melanoma, demonstrating the important role of the micro-environment for cellular development (Bedogni *et al.*, 2005; Monsel *et al.*, 2010). Although the skin is indeed an individual organ, it is also considered as part of the innate immune system. While it serves as a physical barrier towards the outside world and harmful intruders it also homes cells of the immune system and is a site of inflammatory events. Within this context, inflammatory processes were shown to contribute to melanoma initiation. Cytokines and metabolites, such as ROS, released by inflamed endothelia or activated immune cells, can contribute to the inhibition of apoptosis, enhancement of proliferation, or cause DNA damage of benign cells, thereby promoting tumorigenic transformation.

6.1.3.2 Shaping monocyte and macrophage function – an example for the role of the inflammatory environment

Monocytes and macrophages are two cell types of the innate immune system that are allocated to inflammatory processes. These cells are responsible for the clearance of intruding pathogens and tissue repair, as well as the recruitment of other immune cells and their regulation by releasing specific pro-inflammatory cytokines and chemokines. Monocytes and macrophages are highly versatile cells that reside in different tissues and are exposed to specific, local environments. The cells fulfill a plethora of functions, such as pathogen clearance during inflammation or tissue repair and maintenance under steady-state and post-inflammatory conditions. Hence, different macrophage and monocyte subtypes develop and display specific characteristics depending on the local micro-environment (Nicholson *et al.*, 2009; Weidenbusch & Anders, 2012; Brüne *et al.*, 2013). In inflammation, monocytes and macrophages release ROS within the oxidative burst, thereby defining the local oxidative milieu themselves in addition to ROS release from other cells, as for example endothelia cells (Carta *et al.*, 2009). Due to the high potential of ROS to act as signaling molecules and the redox-sensitivity of various signaling pathways (see 6.1.2.2), the redox milieu not only contributes to shape cellular function of monocytes and macrophages themselves (Weidenbusch & Anders, 2012; Brüne *et al.*, 2013), but also other immune cells, as for example T cells (Trujillo *et al.*, 2014).

6.2 Monocytes

6.2.1 Monocytes in the scope of the immune system

Monocytes (MCs) are leukocytes that develop within the myeloid lineage of the hematopoietic system and are allocated to the innate immunity. The involved organs and cells of the innate immune system are the first line of host defense against intrusion of harmful pathogens and are mediators to adaptive immunity. Together with macrophages (MØ) and dendritic cells (DC), monocytes are further allocated as mononuclear phagocyte cells (MPCs). MPCs can be distinguished from other leukocytes as neutrophil granulocytes and natural killer cells, which are also part of cellular innate immunity. As mentioned above (6.1.3), monocytes are highly versatile cells that fulfill three major functions on a cellular and humoral level: 1) clearance of pathogens by phagocytosis and production of inflammatory cytokines, 2) immune modulation

by linking inflammatory processes to adaptive immunity and 3) presentation of antigens (Dale *et al.*, 2008; Auffray *et al.*, 2009; Geissmann *et al.*, 2010).

Monocyte features

Monocytes are non-proliferative cells that comprise 10% of human blood leukocytes and are found in the blood as well as in bone marrow and the spleen. They display characteristic morphological features as an irregular cell shape, an oval-shaped nucleus, cytoplasmic vesicles, a high cytoplasm-to-nucleus ratio and are very heterogeneous in size and shape. The life cycle of monocytes involves the development from bone marrow progenitors, circulation in the blood and invasion of peripheral tissues in response to chemoattractants and inflammation- or tumor-derived mediators (Partida-Sánchez *et al.*, 2004; Ingersoll *et al.*, 2011; Lee *et al.*, 2013).

Monocyte function

As effector cells, monocytes are professional phagocytes and are involved in pathogen clearance and tissue homeostasis as described in detail below (6.2.2). Monocytes fulfill immune-modulatory functions, as they give rise to macrophages and inflammatory dendritic cells. Macrophages, highly versatile cells themselves, are involved in tissue homeostasis and remodeling, clearance of invading pathogens and immune response enhancement by interaction with T cells and cytokine production (Suttles & Stout, 2009; Rees, 2010; Biswas & Mantovani, 2010). They can further differentiate into specialized cells to fulfill tissue specific functions. For example in the liver they are involved in lipid metabolism and toxin removal as kupffer cells or they contribute to neuronal patterning and fluid balance as microglia cells in the brain (Murray & Wynn, 2011; Wynn *et al.*, 2013). Dendritic cells are professional antigen presenting cells and serve in the transition from innate to adaptive immunity by linking inflammatory processes to T cell responses. Monocytes and macrophages hold the molecular machinery to process and present antigens, but compared to dendritic cells, their presenting capacity is much lower. Upon the uptake of an antigen (pathogen-derived material), DCs evade the tissue to enter the lymphatic system in order to present the processed antigen to naïve T cells in peripheral or central lymph nodes. Despite, or due to their versatile roles, monocytes and macrophages contribute, or are associated to pathological processes especially in inflammatory related diseases (as described below in 6.2.3).

Monocyte heterogeneity

In line with their high versatility, monocytes display at least three different phenotypes and are subdivided to: classical (or inflammatory), resident (or pro-inflammatory) and intermediate monocytes. An overview of the different phenotypes and their major features is given in Table 1. As effector cells monocytes are equipped with a huge variety of chemokine and adhesion receptors. These do not only mediate migration from blood to tissues during infection, submit responses to cytokines and are involved in cell activation, but are also used for classification of the subtypes (Gordon & Taylor, 2005; Robbins & Swirski, 2010; Tallone *et al.*, 2011). Examples of a choice of different surface molecules used for classification in general and two selected additional ones are presented in Table 2. The major characteristic of monocytes, that distinguishes this cell type from other leukocytes, is the expression of the CD molecule CD14. Meanwhile, the characteristic expression of the Fc γ receptors I (CD64) and III (CD16) is used to discriminate between the different monocyte subtypes. Others receptors used for this purpose are receptors of the chemokine family. Chemokines are important players in modulating and orchestrating innate and adaptive immune responses, as for example

monocyte recruitment to inflammatory sites and the migration from the blood vessel into the tissue. (Campbell *et al.*, 2003; Moser *et al.*, 2004; Ingersoll *et al.*, 2011; Shi & Pamer, 2011). The expression of the chemokine receptor CCR2 on inflammatory monocytes and the binding of its specific ligands, is important for the recruitment of this monocyte subtype (Weber *et al.*, 2000). CCR2 is consequentially only weakly expressed by the other subtypes. In contrast, the chemokine receptor CX₃CR1, promoting monocyte survival (Landsman *et al.*, 2009), is preferentially expressed by resident and intermediate monocytes.

It so to mention, that there are strong limitations to the classification and description of the different monocyte subtypes. The majority of studies investigating monocyte (and macrophage) subtypes are conducted in rodents and several molecules used for classification could not be identified in humans, as for example the surface molecule Lys6, to which no human counterpart could be identified so far (Gordon & Taylor, 2005; Ziegler-Heitbrock *et al.*, 2010). Classifications and nomenclatures are subject to constant changes and developments. A recent publication by Guilliams and colleagues, addressed the MCP system and suggested a new way of classification (Guilliams *et al.*, 2014). The authors proposed to subdivide the MPC system in two steps. The primary subdivision would be based on ontogenic parameters and in a second step, the cells would be classified based on their function and location. So far, the classification, as currently accepted and outlined above, is primarily based on function and location of the cells.

6.2.2 Monocytes as professional phagocytes

Phagocytosis

Together with neutrophils and macrophages, monocytes act as professional phagocytes. The major role of these cells is the clearance of pathogenic intruders and clearance of cell debris from necrotic and apoptotic cells. Phagocytosis leads to the degradation of the pathogen, meanwhile triggering further signaling events emphasizing the immune response. The clearance of pathogens involves the recognition of pathogenic patterns (pathogen associated molecular patterns, PAMPS) by surface molecules and receptors, the uptake (phagocytosis) of the pathogen and its degradation. Activation of the phagocyte is required for the initiation of phagocytosis and comprises a range of molecular stimulants. Among these, the binding of complement system components, that are involved in opsonization of the pathogen and facilitation of the uptake, or the binding of PAMPS to specialized receptors. Upon encounter with an intruder, binding of PAMPs or complement factors lead to the engulfment of the pathogen by the phagocyte. Thereby, the pathogen is trapped in a membrane enclosed endosome – the phagosome. This specialized endosome further fuses in the cytosol with lysosomes to form the phagolysosome, where pathogen killing takes place.

A classic example for PAMP recognition is the family of formylated peptide receptors (FPR). These G_i-protein-coupled receptors are specialized to bind formylated peptides, that derive from prokaryotic pathogens and mitochondria of host cells. Receptor binding triggers signaling cascades involved in chemotaxis and ROS production of phagocytes, as well as clearance of host cell debris (Reviewed for example by (Panaro *et al.*, 2006; Migeotte *et al.*, 2006)). Binding of FPR agonists results in GDP to GTP exchange on the α -subunit and the consequential dissociation of the $\beta\gamma$ -subunit. The $\beta\gamma$ -subunit activates PLC which is responsible for hydrolysis of PIP₂ to DAG and IP₃.

Table 1 Monocytes subsets in humans

Information on monocyte subset characteristics was selected and assorted from (Gordon & Taylor, 2005; Dale *et al.*, 2008; Shi & Pamer, 2011).

Monocyte Subset	Major characteristics	Features
Classical or Inflammatory	CD14 ^{high} CD16 ⁻ CD64 ⁺ CCR2 ^{high} CX3CR1 ^{low}	High phagocytic activity and cytokine production. CCL2 induced recruitment of MCs to inflammatory sites (lesions) is a critical step in monocyte recruitment
Resident or Pro-inflammatory	CD14 ⁺ CD16 ⁺ CD64 ⁻ CCR2 ^{low} CX3CR1 ^{high} CCR5	Resemble mature tissue macrophages and show preferential development to DCs (rather than classical monocytes).
Intermediate	CD14 ⁺ CD16 ⁺ CD64 ⁺ CCR2 ^{low} CX3CR1 ^{high}	Share high phagocytotic activity and cytokine expression with classical monocytes. Immune regulatory functions. Involved in anti-viral responses and patrolling. Intermediate phenotype in differentiation to DCs.

IP₃ binding to its cognate receptor in the ER-membrane leads to a release of Ca²⁺ from the ER-stores, an initial rise in cytosolic Ca²⁺ and the activation of SOC, followed by a sustained Ca²⁺ influx (see also 6.1, Figure 1 and Figure 6). This increase in cytosolic Ca²⁺ is one of the earliest responses of the cell to FPR activation and is associated to proper phagocyte function (Selvatici *et al.*, 2006). Ca²⁺ and DAG are important for the activation of PKC that is involved in several signaling pathways depending on phosphorylation events. The βγ-subunit also activates PI3ky that is responsible for the phosphorylation of PIP₂ to PIP₃ (Le *et al.*, 2002; Selvatici *et al.*, 2006). These membrane lipids serve as anchors in the plasma membrane and are involved in interactions with cytoskeleton components (actin filaments), thereby contributing to cytoskeleton rearrangements, which are important for phagocytosis and cell migration (Johnson & Rodgers, 2008; Chen & Iijima, 2012).

ROS production and pathogen degradation in phagocytosis

The phagolysosome comprises lytic substances and holds a pH of 7 in neutrophils and an estimated 5 - 5.5 in macrophages and monocytes (Lukacs *et al.*, 1990; Hackam *et al.*, 1997; Jankowski *et al.*, 2002; Nordenfelt & Tapper, 2011). In macrophages it was shown that the more acid pH contributes to the perfect milieu for pathogen degradation (Sturgill-Koszycki *et al.*, 1994). Phagocytosis is accompanied by the oxidative burst that provides a huge amount of ROS, essential to trigger further signaling events and degradation of the pathogen (see 6.1.2). As described above, the responsible enzymes involved in this ROS production are NOX producing \dot{O}_2^- . Further redox processes lead to the generation of H₂O₂ (triggered by SOD activity) and the production of HOCl by myeloperoxidases (see Figure 3 and 6.1.2). To the current view, pathogen clearance might be the results of parallel occurring events based on oxidation events and proteolytic degradation. Despite the intensive work invested in understanding and revealing the processes occurring in the phagosome, the hierarchy and meaning of the different aspects already identified is still under debate.

Table 2 Surface markers used for classification of monocytes subsets

Surface molecule	Other expression	Description and features
CD14		A component of the LPS-LBP-complex that binds LPS, a pathogen derived molecule, and is the co-receptor of TLR-4. The CD14-TRL4 couple is involved in the recognition and clearance of gram-negative bacteria.
CD16	FcγRIII	FcγRIII is the low affinity receptor for recognition and binding of IgG antibodies and is responsible for the facilitation of phagocytosis of IgG-bound antigens.
CD64	FcγRI	FcγRI is a high-affinity receptor for recognition and binding of IgG antibodies
HLA-DR		Part of the MHCII complex and involved in antigen-presentation. Peripheral blood monocytes are characterized by no or marginal expression of HLA-DR.
CCR2		Member of the CC-family of chemokine receptors. Binds CCL2 (= monocyte chemotactic protein-1, MCP-1) and is therefore involved in attracting and homing of leukocytes to sites of inflammation.
CX ₃ CR1		Only member of the CX ₃ C-family of chemokine receptors. Binds the ligand fractaline and is associated to survival of monocytes.
CD62L	Leukocyte L Selectin	A surface molecule involved in leukocyte rolling in the blood vessels. Rolling of the cells at the vessel wall is a prerequisite for transmigration into the tissue.

The complexity of ROS processes in the phagosome has been under continuing investigation for at least 30 years. Several groups, as for example Winterbourn and colleagues, provide precise insights into biochemical properties of ROS acting in the neutrophil phagosome (Winterbourn & Hampton, 2008; Winterbourn & Kettle, 2013). Another important factor in phagocytosis is the type of pathogen to be cleared. Ongoing research aims on identifying differences and similarities in innate immune responses to different types and subtypes of fungal, bacterial or viral infections (Serbina *et al.*, 2008; Shi & Pamer, 2011).

6.2.3 Monocytes in chronic inflammatory diseases

Although being of high importance in the immune response to bacterial, viral and fungal infections, monocytes also contribute to the pathogenesis of sterile inflammation or inflammatory diseases such as atherosclerosis and rheumatoid arthritis by production of inflammatory cytokines and ROS. Prolonged inflammatory processes with their corresponding side effects and the damage to host tissue promote the development of inflammatory diseases. However, familiar predisposition and genetic susceptibility towards the onset and manifestation of chronic inflammatory diseases has to be taken into consideration (Blandizzi *et al.*, n.d.; Incalcaterra *et al.*, 2013; Korczowska, 2014). The necessity to identify molecular players underlying monocyte (mal-) function gains importance, due to the high incident number of patients displaying chronic inflammatory diseases, and the consequential high social-economic burden (Jacobs *et al.*, 2011).

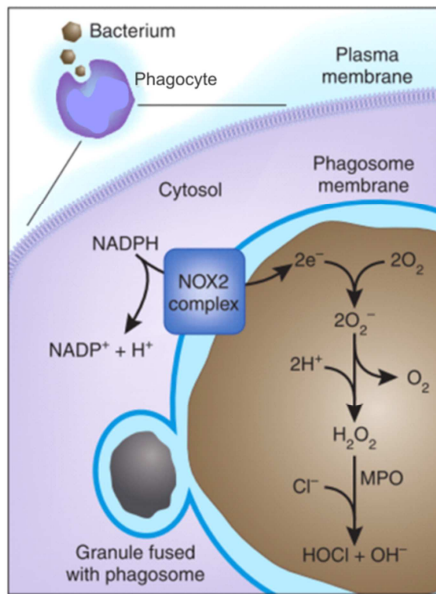


Figure 3 Generation of reactive oxidants by cellular NADPH oxidase systems

Oxidant generation in the phagosome following ingestion of a bacterium. NADPH oxidase (NOX2) is activated on the phagosomal membrane, and electrons are transported from NADPH across the membrane to oxygen to generate superoxide radicals, which dismutate to hydrogen peroxide. Degranulation releases myeloperoxidase (MPO), which generates hypochlorous acid (HOCl) involved in pathogen degradation and other decomposing acid enzymes and antimicrobial peptides. The figure and the text of the legend was adapted from (Winterbourn, 2008).

Atherosclerosis is a sterile inflammatory disease that is characterized by a chronic inflammation of the artery wall with the formation of atherosclerotic plaques. The recruitment of monocytes to atherosclerotic lesions is a hallmark in disease onset. Monocyte function and differentiation into macrophages and dendritic cells further contribute to the disease pattern (Galkina & Ley, 2009; Shi & Pamer, 2011; Fenyo & Gafencu, 2013). Especially the formation of foam cells that originate and mature upon the uptake of oxidized low-density lipoproteins by macrophages, as well as ROS production by monocytes and macrophages, were shown to accelerate the inflammatory process. These processes regulate monocyte and macrophage recruitment, differentiation, activation and autophagy, related to atherosclerotic symptoms and disease promotion (Cathcart, 2004; Galkina & Ley, 2009; Tavakoli & Asmis, 2012).

Another inflammatory disease displaying an involvement of innate immunity is rheumatoid arthritis (RA) (Gierut *et al.*, 2010; Ozbalkan *et al.*, 2010). RA is an autoimmune disorder with the key feature of imbalanced tissue homeostasis resulting in joint destruction, accompanied by pain, stiffness and swelling. Monocytes and monocyte-derived cells play a central role in disease progression. On the one hand, accumulation of macrophages and increased production of ROS is associated to tissue (cartilage) damage (Dröge, 2002; Hadjigogos, 2003). On the other hand, studies in rodents revealed, that arthritis severity is dependent on NOX activity, as activation of NOX2 and the subsequent ROS production were shown to reduce or protect from arthritis symptoms (Hultqvist *et al.*, 2006). In detail, the *ncf-1* gene, coding for a cytosolic NOX2 subunit (p47^{phox}), and mutations within the gene, were shown to regulate NOX2 activity and severity of arthritis (Olofsson *et al.*, 2003, 2007; Hultqvist *et al.*, 2011). NOX-derived and *ncf-1* regulated ROS were associated to regulate T cell activity and their impact on tissue damage and disease promotion (Gelderman *et al.*, 2006; Hultqvist *et al.*, 2006), emphasizing the protective role of ROS in autoimmune diseases (Hultqvist *et al.*, 2009; Pizzolla *et al.*, 2012).

6.3 Melanoma

6.3.1 Skin – Melanocytes – Melanoma

Structure of the skin and skin cancer origin

The skin is a highly complex organ, composed of different compartments and cell types. The major function of this organ is barrier formation against the outer world and the invasion of pathogens, prevention of water loss and protection against UV radiation (UVR). While the epidermis is composed of mostly two cell types, keratinocytes and melanocytes, the dermis hold different cell types and structures as fibroblasts, hair follicles, sweat glands, nerves and blood- and lymph-vessels. The dermis is bordered by the subcutaneous tissue that holds the major blood vessels for oxygen and nutrient supply of the skin. Figure 4 shows a schematic overview of the human skin.

Regarding pathological skin cancers, the outer layer, the epidermis, is of highest interest. The epidermis is build up from a basal layer of keratinocytes and melanocytes at the basement membrane that confines the epidermis from the dermis. The basal keratinocytes are covered by multiple layers of squamous keratinocytes that build up the different layers of the epidermis: stratum spinosum, stratum granulosum and stratum corneum. Basal keratinocytes are epidermal stem cells that continuously provide new cells and the layers display different stages of keratinocyte differentiation and barrier formation. Keratinocytes in the stratum corneum are completely differentiated (corneous cells) and are continuously shed off and replaced from the bottom layers. Melanoma is the most aggressive type of skin cancer that develops from the malignant transformation of melanocytes. During the malignant progression, melanoma cells spread into distant organs and thereby reduce the average survival of patients below 7 months (Balch *et al.*, 2009; Garbe *et al.*, 2011). Although, melanoma is the most aggressive malignant skin cancer it is the rarest one.

Melanocytes as origin for melanoma: their physiological function in skin pigmentation

Keratinocytes hold the pigment melanin that protects against UV radiation by absorbing radiation energy. Melanocytes are highly specialized cells that reside in the basal layer of the human epidermis. There they synthesize melanin, which is transported to the surrounding keratinocytes. Hence, these cells are responsible for skin pigmentation. Melanocytes display a long life span and are quite resistant to apoptosis (Quevedo *et al.*, 1969; Bowen *et al.*, 2003). This resistance is achieved by constitutive activity of anti-apoptotic mechanisms, such as the expression of the anti-apoptotic cell death regulator Bcl2. However, due to their long-life span, melanocytes are prone to the accumulation of mutations. In particular, defects in genes coding for cell cycle regulators are frequently found in early stages of melanoma (Greene, 1999; Marzuka-Alcalá *et al.*, 2014). Melanin synthesis is the major function of melanocytes and is restricted to specialized organelles: the melanosomes. Melanosomes hold the enzymes important for melanin synthesis as there are tyrosinase and tyrosinase related protein 1 and 2 (TYRP1,2) and are transferred to keratinocytes and thereby placed in the outer layers of the epidermis (Hearing, 2005). Pigmentation is highly differential between individuals, between and within different races. While the number of melanocytes is stable between individuals, the rate of melanin synthesis and the type of melanin produced defines the pigmentation status. The rate of melanin synthesis is further defined by the transcriptional regulation of the involved molecular components, such as TYRPs, transcription factors and growth factor receptors. In addition, there are two types of melanin synthesized, eumelanin and pheomelanin, with the

eumelanin amount as defining parameter of cutaneous pigmentation. Eumelanin displays a black or brown color and is therefore involved in UV radiation absorption in the skin, while pheomelanin displays a red color and is for example found in red haired individuals, lips, labia and the foreskin.

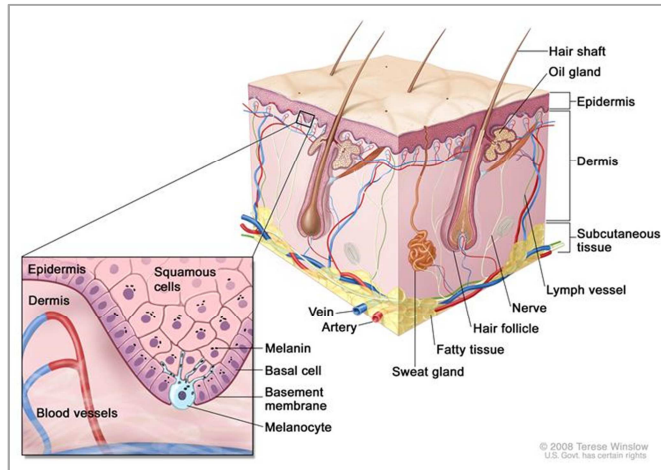


Figure 4 Schematic overview of the human skin and the comprising cell types

The human skin is comprised of three major layers with distinct functions: the subcutaneous tissue, the dermis and the epidermis. The subcutaneous tissue provides the major blood vessels for oxygen and nutrient supply. The dermis is the most complex layer, as it homes lymph- and blood vessels, hair follicles and sweat glands. The epidermis is mainly comprised of two cell types, melanocytes and keratinocytes. Melanocytes synthesize melanin for pigmentation and protection against UV radiation effects. Keratinocytes are responsible for the barrier formation to prevent water loss and the invasion of pathogenic intruders.³

6.3.2 Melanoma progression

The phases of melanoma progression

The progression of melanoma is described by the Clark model that subdivides tumorigenes and the accompanying and determining phenotypic and genotypic changes into five stages, as illustrated in Figure 5 (Clark *et al.*, 1984). Key factors in melanoma progression are altered migration and invasion, as well as aberrant proliferation and growth. Melanocytes undergo the malignant transformation to melanoma cells upon accumulation of mutation events and upon mutations in characteristic signaling pathways (see 6.3.3). In stage one benign nevi display an increased, though normal mode of proliferation and are the core nuclei for tumor development. The proliferation can be accompanied by an irregular growth of the residing melanocytes, and these aberrant, dysplastic nevi are further accounted to stage two. In this stage an increased number of characteristic mutations can be identified. Genetic defects are observed in genes coding for tumor suppressor genes and cell cycle regulators. Within progression, the tumor undergoes two differential growth phases. In stage three, the radial growth phase, melanoma cells gain the potential to outgrow the nevi and the basement membrane and invade the epidermis. The following vertical growth phase, stage four, describes the ability of the tumor cells to escape the epidermis and to trans pass the basement layer to invade the dermis. This change in growth phenotype is the result of an altered expression of cadherins and integrins that are important players in cell-cell, and cell-matrix interactions.

³ <http://www.cancer.gov/cancertopics/pdq/genetics/skin/HealthProfessional/>

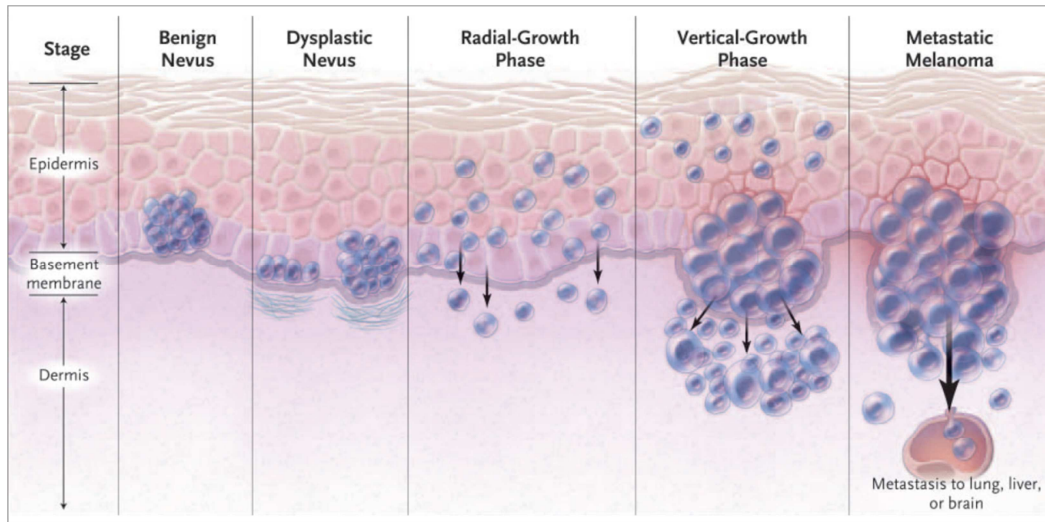


Figure 5 Melanoma Progression

The Clark model subdivides melanoma progression into five stages. These stages are characterized by specific morphological changes and the occurrence of molecular changes, as changed expression profiles of signaling cascades components involved in growth, survival, proliferation and invasion and metastasis. The figure was adapted from (Miller & Mihm, 2006).

Severe alterations in these cell adhesion mechanisms that usually regulate tissue homeostasis and remodeling can lead to the detachment of cells from the original tumor (Johnson, 1999). In this fifth stage, metastatic melanoma, cells successfully evade the dermis and enter blood and lymphatic vessels in the subcutaneous tissue and spread to distant sites of the body. Melanoma metastasis mainly establish in the liver, lungs and the brain, and survival rates significantly decline in this stage of tumor progression (reviewed and illustrated by (Miller & Mihm, 2006)). Several hypotheses have emerged to explain the escape of cells from the tumor as it occurs in stage four and five. Pani *et al.* for example, suggested that metastasis results from an escape mechanism of tumor cells, to avoid hypoxic conditions and an increased redox stress in the tumor (Pani *et al.*, 2010).

Phenotype switch: Proliferation vs. Migration

Regarding the issue of metastasis, it was observed that melanoma cells hold the ability and the potential to switch between different phenotypes to a rather more proliferative or more migratory type (Hoek *et al.*, 2008). This switch is essential to tumor cells to establish a metastasis, when proliferation and growth are required to form a solid tumor, following the migration from the original tumor site. Apparently, subpopulations of melanoma cells possess a considerable migratory capacity while still retaining the potential to switch into a highly proliferative phenotype after arriving at the metastatic niche (Pinner *et al.*, 2009). The mechanisms that control this phenotypic switch are largely unknown, but most likely involve extracellular signals from the tumor environment and complex intracellular signal transduction (Hoek *et al.*, 2006, 2008; Hoek & Goding, 2010). Factors that were shown to stimulate proliferation of cancer cells including melanoma by engagement of membrane bound receptors and subsequent activation of transcription factors, are for examples hormones and peptides *in vivo*, or fetal calf serum (FCS) *in vitro*. Ca^{2+} signaling was shown to regulate important downstream effects to these stimuli (Roderick & Cook, 2008). This supports the potential of differences in composition of a local environment to alter melanoma phenotype in terms of its proliferative features.

6.3.3 Major signaling pathways and molecular players in melanoma progression

Mitogen-activated protein kinase (MAPK) cascades

The family of mitogen-activated protein kinases (MAPK) build a network of signaling cascades that are involved in regulating gene expression, mitosis, metabolism, motility, survival, apoptosis, and differentiation (Pearson *et al.*, 2001; Cargnello & Roux, 2011). The signaling cascades are triggered by multiple activators binding to growth factor or G-protein-coupled receptors. Activation of MAPK cascades dependent on stepwise phosphorylation events of different MAPKs, resulting in phosphorylation and activation/inactivation of the final target substrate. In melanoma, the MAPK signaling cascade is a central pathway in regulating overall cellular functions. All MAPK signaling pathways consist of the following components: A MAPK kinase kinase (eg. B-Raf) that phosphorylates and activates the subsequent MAPK kinase (eg. MEK1) which is further responsible for the activation by phosphorylation of the final MAP kinase (eg. ERK1/2). Two important targets of the final MAP kinase ERK1/2 are the TFs CREB and MITF. The kinase activity of ERK1/2 leads to the phosphorylation of its target and its subsequent translocation to the nucleus. Ca^{2+} elevations upon cell stimulation are required for MAPKK kinase activation, as the initial activation of its family members, as for example B-Raf, is calcium/calmodulin-dependent (Salzano *et al.*, 2012). There are different MAPK pathways that share similar basic components, but differ in terms of their activation. One example is the activation by ligand binding to the MC1 receptor that is involved in adaptive tanning of the skin. In this case, the initial MAPKKK is B-Raf that is activated by the small GTPase N-Ras. The MAPK cascade has further interesting implications in melanoma treatment, because the genes coding for B-Raf and N-Ras are prominent oncogenes in cutaneous melanoma (Wang & Qi, 2013). *BRAF* shows point mutations in 40-65% of all cases and *NRAS* shows mutations in 10-20%. The most common *BRAF* mutation is the point mutation V600E, located in the kinase domain of the enzyme (Hocker & Tsao, 2007). The mutation leads to an over activation of the MAPK signaling cascades and it targets (as for example MITF). *BRAF*, as other melanoma oncogenes and signaling cascade components, have been considered as therapeutical target, because *BRAF* mutation often occur at the very beginning of melanoma onset (Pollock *et al.*, 2003; Dong *et al.*, 2003). B-Raf inhibitors have therefore evolved as important component of melanoma combination therapy (Wang & Qi, 2013).

Microphthalmalin-associated transcription factor (MITF)

The TF MITF is often referred to as master regulator of melanoma and melanocyte function (Levy *et al.*, 2006). This association is based on the plethora of target genes, regulated by MITF, that are involved in tumor-associated, but also basic cellular functions. In melanocytes, MITF is involved in the modulation of melanin synthesis, one of the major cellular functions, by regulating the expression of tyrosinase and TYRP1. An important aspect for melanoma progression is the survival and escape from cell cycle regulation of aberrant cells. Bcl-2, a central anti-apoptotic factor, as well as CDK2, p16 and p21, responsible for cell cycle regulation, are prominent targets of MITF. Furthermore, MITF is in charge of cellular stress responses by hypoxia-induced activation of HIF1-alpha. HIF1-alpha is a TF itself and activates the expression of genes, involved in responses to hypoxic stress, as for example growth factors essential for angiogenesis (MITF targets reviewed for example by (Cheli *et al.*, 2010)). MITF activity is not only regulated by upstream signaling cascades, but also on the DNA level. Brn2 is an important suppressor of MITF activity and is ubiquitously expressed in many cell lineages. Brn2 binds to the MITF gene, leading to suppression of MITF expression. In melanoma, activity

of Brn2 is therefore associated to the suppression of proliferation and differentiation and the enhancement of invasion and metastatic behavior (Goodall *et al.*, 2008).

Autocrine and paracrine signaling in the skin

Signaling in the skin and likewise in skin cancers such as melanoma is comprised of a complex network that is based on autocrine and paracrine signaling events. These events are responsible for the intercommunication between fibroblasts, keratinocytes and melanocytes and are mainly involved in the regulation of melanocyte function in UVR responses. A prominent example for simultaneous autocrine and paracrine signaling under physiological and likewise pathological conditions is the chemokine CXCL-8 (or IL-8) and its two cognate receptors CXCR1 and CXCR2. IL-8 was shown to play an important role in different cancers such as prostate-, breast- and skin cancer (Waugh & Wilson, 2008). The chemokine was credited to serve as important component of the tumor environment. IL-8 receptors are expressed not only on tumor cells, but also on endothelia cells, recruited neutrophils and tumor-associated macrophages. Therefore, IL-8 is involved in autocrine, as well as paracrine signaling in the tumor environment. Ligand-receptor interaction results in the activation of the coupled G-proteins and the subsequent activation of signaling cascades that result in the promotion of angiogenesis, enhanced proliferation and survival, as well as the promotion of migration and metastasis (Waugh & Wilson, 2008; Singh *et al.*, 2010). IL-8 secretion and binding to its receptors is involved in the regulation of a plethora of targets, as for example TFs involved in proliferation-associated genes (Wu *et al.*, 2012). The central MAPK-signaling cascade and its target were shown to be activated and regulated by IL-8. The cascade plays an important role in the enhancement of proliferation and survival of several tumors other than melanoma, such as ovarian and lung cancer (Venkatakrisnan *et al.*, 2000; Luppi *et al.*, 2007). Furthermore, IL-8 signaling holds an important role in melanoma progression and skin in general, due to its activation by UVR (Gebhardt *et al.*, 2007).

6.3.4 Ca²⁺ signaling in melanoma

Ca²⁺ is known to play an important role in skin function, displayed by the Ca²⁺ gradient in the epidermis. Lowest Ca²⁺ concentrations are found in the basal layer that increase towards the outer layer, the stratum corneum (Menon 1985). The gradient is involved in barrier formation and is in return regulated and maintained within the barrier. Disruption and reformation of the barrier after injury was shown to be accompanied by the loss and rebuild of the Ca²⁺ gradient (Elias *et al.*, 2002). Barrier formation is mainly provided by keratinocytes, and their proliferation and differentiation was shown to be defined by the epidermal Ca²⁺ gradient (see 6.1.3.1 and (Hennings & Holbrook, 1983; Eckert *et al.*, 1997; Beck *et al.*, 2008)).

In addition to the importance of extracellular Ca²⁺ levels, intracellular Ca²⁺ signaling regulates many processes in skin such as barrier formation, cell differentiation, melanogenesis and tumor progression. These signaling events are mediated by TRP and store-operated channels, as it is discussed below (6.6.1). Aberrant Ca²⁺ signaling was early credited to play an important role in cancer onset and progression. This association is based on the link of Ca²⁺ signaling to functions related to tumor development such as invasion, migration and proliferation of cancer cells (Capiod *et al.*, 2007; Monteith *et al.*, 2012; Schwarz *et al.*, 2013).

The strong relation of Ca²⁺ signaling to melanoma progression is based on the fact, that Ca²⁺ mobilization is one aspect in the activation of major signaling pathways, as for example MAPK. This central signaling cascade is regulated by Ca²⁺ itself, as well as it triggers the elevation of

Ca²⁺ signals (see above 6.3.3). Several transcription factors, down-stream targets of MAPK, such as MITF and NfκB are Ca²⁺-dependent in terms of their activation (see also 6.1.1). As it was pointed out above, NfκB is regulated by cytosolic Ca²⁺ mobilization and is involved in the transcriptional regulation of IL-8. Thereby Ca²⁺ signals are involved in regulation of a chemokine involved in several aspects of melanoma progression (6.3.3). Hence, Ca²⁺-mediating channels, that are responsible for cytosolic Ca²⁺ mobilization are important players in the regulation of melanoma progression and therefor an ongoing topic of research.

6.4 Molecular aspects of calcium and redox signaling

6.4.1 Store-operated calcium entry *via* calcium-release activated channels

The components ...

Although the current mediated by the CRAC channel was already identified in mast cells in the early nineties (Hoth & Penner, 1992; Zweifach & Lewis, 1993) it took a long and winding road till the STIM (Roos *et al.*, 2005; Liou *et al.*, 2005; Zhang *et al.*, 2005) and the Orai proteins (or CRAC modulators, CRACM) were identified as the molecular components of the CRAC channel (Feske *et al.*, 2006; Vig *et al.*, 2006b, 2006a; Zhang *et al.*, 2006; Prakriya *et al.*, 2006). STIM1 and 2 (or stromal-interacting molecule (STIM) 1 and 2) are monomeric proteins with a single trans-membrane domain. They were identified and proposed as tumor suppressor proteins (Manji *et al.*, 2000; Williams *et al.*, 2001), before they were later uncovered to gate the CRAC channels. As Ca²⁺-binding proteins, STIMs were identified as the missing link between the early observed presence of a Ca²⁺ entry mechanism and the release of Ca²⁺ from the ER (reviewed by (Johnstone *et al.*, 2010; López *et al.*, 2012; Soboloff *et al.*, 2012)). Orai1, Orai2 and Orai3 were identified as the pore-forming subunits of the CRAC channel (Prakriya *et al.*, 2006; Lis *et al.*, 2007; Gwack *et al.*, 2007), with four trans-membrane domains and cytosolic N- and C-Termini. From the five molecular players identified, the gating of Orai1 by STIM1 was the focus of early investigations, as it was shown to provide essential SOCE in T lymphocytes (reviewed by (Hogan *et al.*, 2010; Shaw & Feske, 2012a; Shaw *et al.*, 2013)).

... and the signaling cascade

A schematic overview of the signaling cascade is provided in Figure 6. The receptor triggered depletion of the ER Ca²⁺ stores (see 6.1 and Figure 6) is sensed by the ER-membrane residing STIM1 and STIM2 molecules. STIM1 and STIM2 are trans-membrane proteins, carrying EF-hands in the ER-luminal side. Under resting conditions and filled Ca²⁺ stores, Ca²⁺ is bound by the EF-hands. Upon depletion of the stores, Ca²⁺ dissociates from the molecule resulting in a conformational change leading to dimerization, translocation and cluster formation in areas close to the plasma-membrane; so-called puncta formation (Liou *et al.*, 2005; Barr *et al.*, 2009). Orai proteins are four-transmembrane proteins, forming homo- and heteromeric channels in the plasma-membrane. The so-called channel interacting domain (CAD) of STIM proteins was shown to be responsible for activation of the Orai proteins mediated by protein-protein-interaction with coiled-coiled domains in the C-term of Orai subunits (Frischauf *et al.*, 2009). STIM-Orai interaction is followed by change in channel conformation mediating an influx of Ca²⁺ from the extracellular space. The channel activity is regulated by two aspects: fast and slow Ca²⁺-dependent inactivation of the channel itself and the refilling of the ER-stores by SERCA. The Ca²⁺-dependent inactivation is overcome by Ca²⁺ uptake by mitochondria in close or further proximity to the channel, enabling a sustained Ca²⁺ influx that is for example responsible for activation of certain transcription factors (see 6.1).

Channel conformation ...

The biochemical properties of the Orai proteins to form homo- and heteromeric channels was investigated in detail, but the actual conformation of the CRAC channel is still under debate (Lis *et al.*, 2007; Gwack *et al.*, 2007; Peinelt *et al.*, 2008). Although the CRAC channel was described as tetrameric channel (Mignen *et al.*, 2008a; Penna *et al.*, 2008), a publication by Hou and colleagues in 2012 suggested a hexameric conformation, based on a crystallization model from *Drosophila* Orai protein (Hou *et al.*, 2012). Thompson and Shuttleworth described the hexameric channel to be a non-selective cation channel, conducting Ca^{2+} as well as Cs^+ and Na^+ , in contrast to the highly Ca^{2+} -selective tetrameric Orai channel, or the native CRAC channel itself (Thompson & Shuttleworth, 2013). Hence, further investigation is needed to solve the question of CRAC channel conformation.

Based on finding from heterologous expression studies, all Orai isoforms might form *bonafide* CRAC channels, since they all displayed CRAC channel characteristics (Mercer *et al.*, 2006; Lis *et al.*, 2007; DeHaven *et al.*, 2007). These characteristics encase activation by store depletion, Ca^{2+} over Na^+ selectivity and an inwardly rectifying current/voltage relationship of I_{CRAC} (Hoth & Penner, 1992; Zweifach & Lewis, 1993). In addition, all Orai proteins were shown to form homo- and heteromeric channels (Lis *et al.*, 2007; Gwack *et al.*, 2007; DeHaven *et al.*, 2007), but the stoichiometry of the single Orai-subunits in endogenous CRAC channel is controversial and under current investigation.

Orai2 was initially stated to either not function as a *bonafide* channel, as there was no effect on SOCE following down-regulation, or only in the presence of Orai1 (Feske *et al.*, 2006; Hoth & Niemeyer, 2013). The protein was also suggested to mediate remaining CRAC-like currents in immune cells from Orai1 knockout mice rather than Orai3 or another SOC (Vig *et al.*, 2008; Gwack *et al.*, 2008). The recent identification of a role for Orai2 (and STIM2) in mediating SOCE in neurons and dendritic cells implies that Orai2 forms an endogenous *bonafide* CRAC channel (Berna-Erro *et al.*, 2009; Bandyopadhyay *et al.*, 2011). Although Orai3 was described as *bonafide* CRAC channel *in vitro*, it might not be very likely that an Orai3 homo-multimer would form an endogenous channel. Orai3 is the lowest expressed isoform in most tissues with little exceptions. Thus and regarding that the CRAC channel might be a hexamer, an insertion of Orai3 in a hetero-multimer is more likely (Hoth & Niemeyer, 2013). As first example, the arachidonate-regulated Ca^{2+} channel (ARC channel), that displays a similar current/voltage relationship as I_{CRAC} , but is not store-operated, was shown to be formed by Orai1 and Orai3 (Mignen *et al.*, 2008b, 2009). The ARC channel was further described as pentameric Orai3/Orai1-multimer, although based on the results from Hou *et al.* (Hou *et al.*, 2012), a hexameric conformation of the I_{CRAC} -like ARC channel is also possible.

...and channel gating.

Concerning the gating mechanism, the current accepted model suggests an optimal Orai to STIM ratio of 1:2. Thus, within a tetrameric channel, an optimal or maximum Ca^{2+} influx results from binding of eight STIM molecules (Li *et al.*, 2011; Kilch *et al.*, 2013). The amount of publications regarding STIM1-gated Orai1 function exceeds the one regarding the other subunits. This imbalance is most likely based on the essential role of Orai1/STIM1 in T lymphocyte function (Feske *et al.*, 2006; Feske, 2010) and the strong immune phenotypes displayed by knockout mice (Oh-Hora *et al.*, 2008; Gwack *et al.*, 2008). STIM1 and STIM2 were both shown to activate Ca^{2+} currents mediated by Orai1, Orai2 and Orai3 (Parvez *et al.*, 2008;

Wang *et al.*, 2009; Schindl *et al.*, 2009). An emerging number of publications reveal equal importance in CRAC channel gating for both STIM isoforms (reviewed by (Johnstone *et al.*, 2010; López *et al.*, 2012; Soboloff *et al.*, 2012). Thus, the mode of STIM activation and the Orai isoform to which it binds might depend on expression profiles, cell functional needs and might even be related to the evolutionary ancestry and development of a cell type (Collins & Meyer, 2011).

Studies in cell types preferential expressing STIM2 rather than STIM1, actually revealed STIM2 as the dominant isoform regulating SOCE in cooperation with Orai2 (neurons and dendritic cells) and Orai1 (melanocytes) (Berna-Erro *et al.*, 2009; Bandyopadhyay *et al.*, 2011; Stanisiz *et al.*, 2012). Regarding cell functional needs, a study by Kar *et al.* revealed that activation of different types of receptors requires a differential contribution of STIM1 and STIM2 to trigger Ca^{2+} oscillations and transcription factor translocation (Kar *et al.*, 2012). STIM2 was early allocated to play a role in basal cytosolic Ca^{2+} homeostasis rather than Ca^{2+} signaling events (Brandman *et al.*, 2007), due to the lower Ca^{2+} -binding affinity of the STIM2 EF-hand compared to STIM1 (Zheng *et al.*, 2008). STIM2 was therefore related to trigger characteristic Ca^{2+} signals in response to the degree of store depletion, providing a mechanism to elevate different Ca^{2+} signals and cellular responses depending on the activation mode (Thiel *et al.*, 2013). Melanocytes and neurons both derive from pluripotent neuronal crest progenitor cells. The similarities in preferentially STIM2 over STIM1 expression might indicate a correlation of evolutionary development and dominance of a certain STIM isoform mediating SOCE.

6.4.2 Underlying mechanisms of enzymatic ROS production

The assembly process

Enzymatic production of ROS is strictly regulated as a requisite for ROS to serve as signaling molecules and to prevent harmful or pathological effects of imbalanced ROS levels (see also 6.1.2). The importance of a strict regulation is reflected by the activation mode that requires multiple coinciding processes, leading to the assembly of spatially separated subunits to form a functional holoenzyme. Due to its proven function in phagocytes as macrophages and neutrophils and its consequential importance for this work, the molecular aspects of the activation of enzymatic ROS production are illustrated for NOX2 (Figure 7).

The multi-component enzyme NOX2 is disassembled under resting conditions. Activation of a phagocyte upon pathogen encounter triggers coinciding activation pathways that result in the generation of the superoxide radical (O_2^-). The activated enzyme consists of a core unit, the flavocytochrome b588, a hetero-multimer of the catalytic subunit gp91^{phox} and the membrane protein p22^{phox}, three cytosolic subunits (p47^{phox}, p67^{phox} and p40^{phox}), the small GTPase RAC and two members of the S100 Protein family (Vignais, 2002; Kerkhoff *et al.*, 2005; Bedard & Krause, 2007; Bréchar *et al.*, 2013). The superscript (^{phox}) states the affiliation of the subunits to NOX2, the phagocyte oxidase (phox), while the given numbers of the proteins (p) reflect their molecular weight. In contrast to the components involved in SOCE, the proteins contributing to ROS production are not glycosylated, with exception of the glycoprotein gp91^{phox}. Under resting conditions, the subunits (with exception of the flavocytochrome) are disassembled and restricted to the cytosol. Gp91^{phox} holds the electron-transport chain responsible for the transfer of electrons from the electron donor NADPH to molecular oxygen, while p22^{phox} serves as a stabilizer for the enzyme and anchor for the cytosolic subunits. Upon stimulation four major cellular processes coincide to the assembly of the enzyme: 1) lipid metabolism, providing anchors for the recruitment of cytosolic subunits; 2) rise in cytosolic Ca^{2+} levels, leading to

translocation of Ca^{2+} sensing, complex stabilizing proteins and the activation of PKC; 3) phosphorylation of a cytosolic subunit initiating its translocation to the core unit and 4) nucleotide exchange on RAC, enabling the GTPase to bind to the complex and contribute to the activation. The three cytosolic protein subunits serve as organizer (p47^{phox}), activator (p67^{phox}) and modulator (p40^{phox}) within the assembly process and hold complex interactions among each other, with the core unit and membrane anchors (see Figure 31 for details).

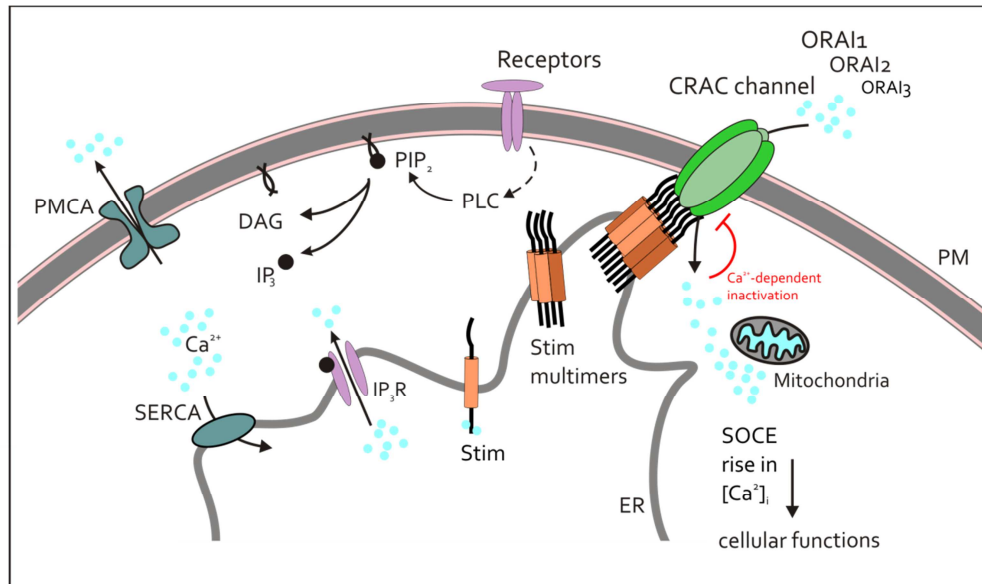


Figure 6 Store-operated Calcium Entry (SOCE)

Signaling cascade: Activation of cell-surface receptors triggers the activation of PLC and subsequent generation of IP_3 and DAG from PIP_2 . Soluble IP_3 binds to its cognate receptor in the ER-membrane (IP_3R). Upon binding, Ca^{2+} is released by IP_3R from internal Ca^{2+} stores. The drop in Ca^{2+} store content is accompanied by dissociation of Ca^{2+} from the EF-hands of so called STIM proteins residing in the ER- membrane (STIM1 and 2). Ca^{2+} unbound STIM proteins form dimers and relocate to ER junctions close to the plasma membrane to form puncta. STIM-clusters activate PM-residing CRAC channels that are buildup of hetero-tetramers of Orai family proteins (Orai1-3). Optimal activation of the channels occurs under the STIM-Orai stoichiometry of 2:1. Activated CRAC channels mediate the store-operated Ca^{2+} entry to the cytosol. Mitochondria in close vicinity to the channels buffer entering Ca^{2+} , thereby delaying fast and slow Ca^{2+} -dependent inactivation of the CRAC channels. SOCE mediated by CRAC channels fulfills a diverse set of functions in immune cells ranging from essential regulating to modest modulation of Ca^{2+} -dependent processes. Inactivation of the CRAC channels and refill of the Ca^{2+} stores by SERCA pumps in combination with extrusion of Ca^{2+} from the cytosol by PMCAs terminates SOCE meanwhile building up status quo for further signaling events. Abbreviations used: PLC – Phospholipase C ; PIP_2 - Phosphatidylinositol biphosphate; IP_3 – Inositol-(1,4,5)-trisphosphate; DAG – Diacylglycerol; IP_3R – Inositol-trisphosphate- receptor; STIM – Stromal interaction molecule; CRAC – Ca^{2+} -release activated Ca^{2+} channel; SOCE – Store-operated Ca^{2+} entry; SERCA – Sarco-/endoplasmic reticulum Ca^{2+} ATPase; PMCA – Plasma-membrane Ca^{2+} ATPase.

Focus on the role of Calcium in the assembly of NOX2:

A crucial step for the activation of NOX2 is the rise in cytosolic Ca^{2+} levels. Firstly, the activation of PKC is dependent on Ca^{2+} and the interaction with DAG to phosphorylate the cytosolic subunit p47^{phox} and $\text{gp91}^{\text{phox}}$ (Faust *et al.*, 1995; El Benna *et al.*, 1996; Raad *et al.*, 2009). This step is thereby not only dependent on Ca^{2+} signaling itself, but also the generation of DAG from PIP_2 as it takes place in the receptor mediated SOCE activation cascade (e.g. by activation of FPR receptors by bacterial products, see 6.2.2 and Figure 6). Besides phosphorylation of cytosolic subunits, phosphorylation of the core unit by PKC is involved in the activation

cascade. Secondly, the Ca^{2+} -binding proteins S100 A8/A9 that are expressed by phagocytes as neutrophils and monocytes, are recruited to the NOX2 complex upon Ca^{2+} -binding to their EF-hands, thereby contributing to NOX2 activation and stabilization (Kerkhoff *et al.*, 2005). These proteins are members of the Ca^{2+} -binding protein family S100 that fulfill multiple functions in inflammation, Ca^{2+} homeostasis, proliferation and migration (Donato *et al.*, 2013). S100 A8/A9 binds arachidonic acid (AA), which is also involved in stabilization of the NOX2 complex. The complex is recruited to the membrane by interaction with the subunit p67^{phox} and RAC (Kerkhoff *et al.*, 2005). It was shown that stimulation of different receptors triggers different signaling pathways that lead to the activation of PLC or PLD. In both cases, activation of kinases and the generation of specific second messengers lead to Ca^{2+} mobilization from internal stores and a Ca^{2+} influx *via* SOC (Nunes & Demaurex, 2010). Ca^{2+} signals are further involved in other factors that are important for phagocyte ROS production, as rearrangement of the cytoskeleton and fusion events of the phagosome with lysosomes or lytic granules (Nunes & Demaurex, 2010).

6.5 The interplay of Ca^{2+} and redox signaling

6.5.1 CRAC Channels and Redox Signaling

SOCE mediated by CRAC channels is accepted to play an important role in phagocytic ROS production, as it is involved in the assembly of NOX (Brécharde & Tschirhart, 2008; Nunes & Demaurex, 2010) (see also 6.4.2). The role of the single Orai and STIM isoforms in this context was so far only investigated in neutrophils and neutrophil-like cell lines, mainly focusing on the Orai1/STIM1 couple.

In neutrophil-like HL-60 cells, Orai1, in cooperation with TRPC channels 1 and 6, was suggested to mediate SOCE necessary for NOX activation and H_2O_2 production. Although the authors could not detect TRPC expression on protein level, the contribution was concluded from functional effects following siRNA treatment. Different stimuli were used and the physiological stimulus fMLF resulted in Ca^{2+} elevation and H_2O_2 production, while the SOCE activator Tg triggered Ca^{2+} signals but no production of H_2O_2 . In another study using the HL-60 cell line, phagosomal ROS production was shown to be dependent on Orai1 and STIM1 mediated SOCE. Although Orai2 and Orai3 mRNA expression levels were even higher than those of Orai1, RNAi mediated knockdown did not reveal a contribution to SOCE. Interestingly, STIM2 expression was neither investigated (mRNA expression level), nor targeted by RNAi. In addition to Orai1 and STIM1, the Ca^{2+} binding proteins S100A8/A9 were shown to serve as a Ca^{2+} sensor, linking Ca^{2+} influx to phagosomal ROS production (Steinckwich *et al.*, 2011). Regarding the role of STIM, Brécharde *et al.* identified and confirmed STIM1 as regulator of SOCE and to be involved in mediating the Ca^{2+} influx necessary for NOX-dependent ROS production in the HL-60 cell line. STIM2 expression was confirmed, but an siRNA-mediated knockdown did not reveal a contribution of this isoform to either SOCE, or Ca^{2+} -dependent ROS production (Brécharde *et al.*, 2009). Besides regulating SOCE and NOX activity, STIM1 was also shown to be involved in the recruitment of ER junctions to the phagosome. ER remodeling is often observed during phagocytosis and is involved in cytoskeleton rearrangement, an important mechanism for phagosomal maturation. STIM1 was revealed as key molecule in recruiting ER junctions and promoting phagosomal Ca^{2+} signals in mouse embryonic fibroblasts and the HL-60 cell line (Nunes *et al.*, 2012). So far, the participation of Orai1 and STIM1 in regulating SOCE-dependent activity of NOX enzymes was proven, leaving the role of Orai2, Orai3 and STIM2 within this process to be further elucidated.

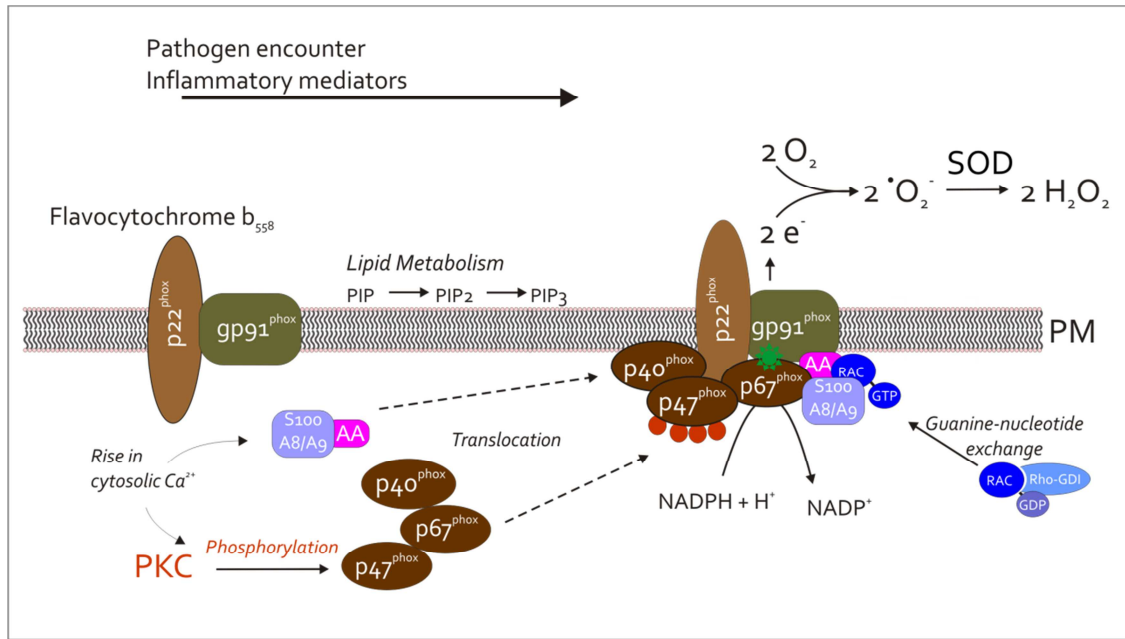


Figure 7 Components and assembly of NADPH oxidase 2

Assembly and activation of NOX2 upon inflammatory signals (adapted from (Lambeth, 2004)). The membrane-residing core unit flavocytochrome b_{588} is a hetero-multimer of the catalytic subunit $gp91^{phox}$ and the membrane protein $p22^{phox}$. Metabolism of PTPs in the membrane and interaction sites on $p22^{phox}$ provide lipid anchors for the recruitment of cytosolic components. Cell activation triggers a rise in cytosolic Ca^{2+} levels leading to the activation of PKC and the translocation of Ca^{2+} sensing S100 proteins to the PM (Steinckwich *et al.*, 2011; Br  chard *et al.*, 2013). The cytosolic subunits $p40^{phox}$ and $p67^{phox}$ are bound by the organizer subunit $p47^{phox}$. Phosphorylation of $p47^{phox}$ by PKC leads to exposure of interaction domains mediating the binding to $p22^{phox}$ and recruiting the bound subunits to the core unit. Translocation to the PM is facilitated by binding of $p47^{phox}$ to PIP_2 lipid anchors. Superoxide production is triggered by interaction of the activator domain of the activator subunit $p67^{phox}$ (green star) with $gp91^{phox}$. The small GTPase RAC is bound to the inhibitor RhoGDI under resting conditions. Upon cell activation, nucleotide exchange on GDP results in dissociation of the small GTPase RAC from its inhibitor and binding to the activator subunit $p67^{phox}$. The modulator subunit $p40^{phox}$ binds to membrane lipids and is involved in stabilization of the complex and enhancement of ROS production. The activated catalytic subunit generates the superoxide radical ($O_2^{\cdot-}$) by transferring two electrons from the electron-donor NADPH to molecular oxygen. Rapid dismutation of $O_2^{\cdot-}$ by SOD leads to the formation of H_2O_2 . *Abbreviations used:* p – protein, gp – glycoprotein, PIP – phosphatidylinositol phosphate; PIP_2 – phosphatidylinositol bisphosphate, PIP_3 – phosphatidylinositol trisphosphate, RhoGDI – Rho GDP-dissociation inhibitor, SOD – superoxide dismutase. Information taken from (Lambeth, 2004; Kerkhoff *et al.*, 2005; Bedard & Krause, 2007; El-Benna *et al.*, 2009).

6.5.2 Redox Regulation of CRAC Channels

Comparing the so far published reports of how ROS affects SOCE and CRAC channel activity revealed severe discrepancies. While on the one hand there seems to be an agreement on an inhibitory effect of ROS or oxidizing substances, others reported an elevation or enhancement of SOCE (reviewed by (Bogeski *et al.*, 2012; Nunes & Demareux, 2013)). While for example Bogeski *et al.* showed an H_2O_2 -induced inhibition of SOCE in T cells (Bogeski *et al.*, 2010), Grupe *et al.* reported a STIM1 mediated CRAC channel activation upon H_2O_2 treatment in HEK cells (Grupe *et al.*, 2010). The observed discrepancies can be allocated to either cell-type specific differences in the SOCE machinery and its regulation or to the differential functional outcome of the diverse types of thiol modifications (see 6.1.2 and (Nunes & Demareux, 2013)). It is therefore important to consider the species involved, the potential redox targets and the

biochemical type of modification to fully understand the underlying mechanism of redox regulation of SOCE in a certain cell type.

Nunes and colleagues recently summarized and evaluated to date work on redox regulation of SOCE (Nunes & Demaurex, 2013). They concluded two general mechanisms in the redox regulation of SOCE and CRAC channels with 1) the Ca^{2+} status of the ER regulated by ROS as modulator of CRAC channel activity and 2) STIM and Orai proteins as direct targets for redox modification. Early reports already demonstrated the elevation of cytosolic Ca^{2+} signals upon oxidative triggers. This Ca^{2+} elevations were mediated *via* activation of IP_3 and ryanodine receptors (Missiaen *et al.*, 1991; Hilly *et al.*, 1993; Poitras *et al.*, 1993), or the inhibition of SERCA (Xu *et al.*, 1997; Grover *et al.*, 1997; Barnes *et al.*, 2000), resulting in either an active or passive depletion of the ER Ca^{2+} stores. Thus, a redox-dependent regulatory mechanism of SOCE and the corresponding channels were revealed, prior to the identification of the molecular players of the CRAC channels (Parekh & Penner, 1995). In general ROS were suggested to be involved in regulating SOCE, by defining the amount of Orai and STIM proteins *via* transcriptional regulation (reviewed by (Trachootham *et al.*, 2008; Nunes & Demaurex, 2013)). A prominent example is the TF Nf κ B, involved in the transcription of Orai1 and STIM1 (Eylenstein *et al.*, 2012). Nf κ B activity is modulated by various signaling pathways upon receptor stimulation, among these also cellular redox homeostasis (Morgan & Liu, 2011). A shift to high oxidizing levels was shown to favor an inhibition of Nf κ B and subsequent down-regulation of Orai1 and STIM1 levels, while lower levels are related to an increased activity of the TF (Jing *et al.*, 2006; Wang *et al.*, 2012).

The STIM molecules appeared as interesting targets in the redox regulation of SOCE because they contain cysteine residues. Information from databases and primary structure analysis lists 5 cysteine residues for STIM1 and 15 for STIM2.⁴ They reside in an organelle strongly regulated by the local redox milieu: the ER. Among the two STIM isoforms most attention was so far paid to STIM1 and, though being an even more promising target, little information on STIM2 is so far available (reviewed by (Bogeski *et al.*, 2012)). Protein folding in the ER is redox-sensitive, as the protein Ero1p, involved in protein folding, is regulated by the oxidative state of the organelle. Ero1p catalyzes the reactivity of Pdi1P, a thioredoxin-like protein responsible for disulfide-bond formation. An increased oxidized ER status results in an inhibition of Ero1p and the subsequent reduced Pdi1p activity. STIM1 however was shown to bind to an oxidoreductase of the thioredoxin family (ERp57). This reductase acts together with the members of the isomerase PDI family, like Pdi1p. The binding of STIM1 by ERp57 depends on the redox state of the ER and regulates disulfide bond formation in STIM1, thereby influencing SOCE activity (Prins *et al.*, 2011).

Regarding the Orai proteins as potential redox targets, Bogeski and colleagues provided a detailed study on the redox sensitivity of the single Orai isoforms (Bogeski *et al.*, 2010). Orai1 and Orai2 were shown to carry three redox-sensitive cysteines; C126 and C143 in TM2 and C195 at the extracellular site of TM3. Orai3 instead lacks the cysteine 195 but holds two additional residues in an extracellular loop. Orai1 and Orai2 mediated SOCE was shown to be inhibited by pre-incubation with H_2O_2 , while Orai3 was redox-insensitive. Within the differentiation of naïve T cells to effector cells, Orai3 expression was up regulated with an increase in the relative Orai3 to Orai1 expression. This process was accompanied by an

⁴ See for example: http://www.ncbi.nlm.nih.gov/nuccore/NM_001169118.1 and <http://www.ncbi.nlm.nih.gov/nuccore/JX014264.1>

increase in redox resistance of SOCE. Mutagenesis studies revealed C195 as the residue defining redox sensitivity of Orai1 and Orai2. The up-regulation of Orai3 within differentiation was suggested as adaptive mechanism to tune redox sensitivity of SOCE to maintain sufficient Ca^{2+} signals in an oxidizing environment.

The results from Bogeski and colleagues raised the question whether the observed mechanism might be restricted and unique to T cells, or whether it is present in other cell types and organs coping with an oxidizing environment. Cells of the innate immunity as monocytes, encounter an oxidizing environment under physiological and pathological conditions, meanwhile contributing to a high redox state by production of ROS (see 6.2.2 and 6.2.3). In the scope of this study not only monocytes, but also the skin provides an excellent experimental background to study redox regulation of SOCE. Cells of the skin are redox challenged under UV radiation under physiological but also under cancerous conditions, such as melanoma (see 6.3.1).

6.6 Scientific Question

6.6.1 State of the art - The role of the individual Orai and STIM isoforms in the skin and innate immunity

With the essential role in T lymphocytes, the importance of Orai and STIM in adaptive immunity is indisputable, while there is only little known about the role of SOCE and the contribution of the single Orai and STIM subunits in innate immunity (Shaw & Feske, 2012b). As pointed out above (6.5.1), neutrophil granulocytes are the only intensively investigated cells of the innate immunity, displaying an essential role of Orai1 and STIM1 regulated SOCE during phagocytosis and ROS production (described in detail below) (Bréchar *et al.*, 2008, 2009; Steinckwich *et al.*, 2011). Monocytes take a central role in innate immunity as professional phagocytes and progenitors to dendritic cells and macrophages. Still, only few publications focused on the role of CRAC channels in mononuclear phagocyte cells and no information is available on the role of CRAC channels in monocytes themselves to the present day.

In rodent dendritic cells, Orai2 and STIM2 were shown to be the predominant CRAC channel components. In contrast to T lymphocytes, STIM2-gated and Orai2-mediated SOCE was identified as the major Ca^{2+} signaling process (Bandyopadhyay *et al.*, 2011). Further on, Félix and colleagues demonstrated an important role for STIM1 and Orai1 mediated SOCE in the maturation of human dendritic cells, while no expression, and hence no contribution, of STIM2 could be detected (Félix *et al.*, 2013). In murine macrophages, the Ca^{2+} response triggered by cell stimulation was found to be mediated by CRAC channels. This Ca^{2+} signals were linked to stimulation-induced ROS production, prior to the identification of the molecular components of the CRAC channels (Jin *et al.*, 2006). Gao *et al.* further suggested store-depletion and sustained Ca^{2+} signaling in human macrophages to be dependent on a close functional coupling of CRAC channels and potassium channels ($\text{K}_{(\text{Ca})3.1}$) (Gao *et al.*, 2010). In a broader scope, the role of CRAC channels was investigated in osteoclasts, a cell type important in bone remodeling and bone tissue homeostasis that derive from macrophages. Ca^{2+} signaling, important for osteoclast function, is mediated by CRAC channels and ryanodine receptors/channels (Robinson *et al.*, 2010). A down-regulation of the CRAC channel components was observed within osteoclast differentiation, however channel activity was shown to be important in late differentiation steps and overall cell function (Zhou *et al.*, 2011). In a recent report, a specific role of Orai1-mediated Ca^{2+} signaling was determined in osteoclast differentiation, by regulating the activity of the TF NFAT (Hwang & Putney, 2012).

As described above, Ca^{2+} is known to play an important role in skin function and intracellular Ca^{2+} signaling regulates many processes in the skin such as barrier formation, cell differentiation, melanogenesis and tumor progression (see also 6.3). These processes appear to be linked to the activity of several TRP channels rather than CRAC channels and only few publications pay attention to Orai and STIM mediated Ca^{2+} signals in the skin (Saul *et al.*, 2013). In keratinocytes, the presence of Orai and STIM is connected to basic Ca^{2+} signaling (Ross *et al.*, 2008), Ca^{2+} -switch mediated differentiation (Numaga-Tomita & Putney, 2013) and Ca^{2+} -dependent migration (Jans *et al.*, 2013). In melanocytes, Orai1 and STIM2 were finally proven to serve as the major Ca^{2+} influx pathway having an essential function for melanogenesis and adaptive tanning (Stanisz *et al.*, 2012). Thus, further investigation of Orai-, and STIM-regulated skin cell function, also under pathological conditions as melanoma, might reveal deeper insight into the role of CRAC channels in skin and tumor biology.

6.6.2 Research focus

The main aim of the here presented study was to identify the role of CRAC channels in general and the role of the single Orai and STIM isoforms in detail in primary human monocytes and melanoma cells. In both cases SOCE mediated by the CRAC channels was characterized and the major contributing Orai and STIM isoforms were further investigated in terms of their contribution to Ca^{2+} -dependent processes. The regulation of SOCE and the impact of the cellular environment on Ca^{2+} -signaling and overall cell function was an additional focus of the study. The specific and shared scientific questions of the two investigated cell systems are outlined below.

Monocytes. ROS production is an important function of monocytes during phagocytosis and was known to be dependent on Ca^{2+} signaling. Also, a role for Orai1 and STIM1 in this process was already identified in neutrophils. Monocytes, instead of neutrophils, were chosen as object of research because of two major aspects. On the one hand, the central position of monocytes in the MPC-system provides the potential to transfer experimental findings to the other members as dendritic cells and macrophages. On the other hand, the little information about the role of CRAC channels in this cell type provided the chance of entirely new insights. These aspects and the progressive emerging evidence for an important role of CRAC channel function and redox regulation of the channels were reason to develop and address the following questions:

What role do the SOCE and the mediating CRAC channels play in monocytes, and which Orai and STIM isoforms contribute to Ca^{2+} signaling?

Is ROS production in monocytes dependent on Orai and STIM-mediated Ca^{2+} signals?

How might ROS, produced by monocytes, impact Orai and STIM-dependent Ca^{2+} signaling?

Melanoma. Studies in human melanocytes revealed Orai-, and STIM-mediated SOCE as important Ca^{2+} signaling pathway. Orai and STIM mediated Ca^{2+} signaling was further already related to different malignant cancers. Based on the findings in human melanocytes and the prominent role of Ca^{2+} in regulating skin cell function, the following questions were addressed:

What role does the SOCE play in melanoma cells, and what Orai and STIM isoforms contribute to Ca^{2+} signaling?

Are the molecular players determining melanoma progression dependent on Orai and STIM presence and function?

ROS production in the skin upon environmental factors and characteristic ROS patterns in tumors pointed to the further question:

How might ROS influence Ca^{2+} signaling in cancer (melanoma) cells?

Monocytes and Melanoma. During the investigation of the general role of CRAC channels in the different cell systems, shared features and questions became obvious. Although the skin is indeed an individual organ, it is also considered as part of the innate immune system. The skin serves as a physical barrier towards the outside world and harmful intruders and therefore homes specialized immune cells. Regarding the challenging conditions cells are facing under pathological skin and immune conditions not only Ca^{2+} and redox signaling, but also changes in the Ca^{2+} and redox environment impact cellular functions. The analysis of the interdependency of ROS and Ca^{2+} signaling, as well as the impact of altered redox and Ca^{2+} conditions on cell function were therefore also addressed in the here presented study.

The ongoing association of CRAC channel function to not only physiological processes, but also pathological disease patterns, emphasizes the importance of gathering more information on the implication of the involved molecular players and to reveal and interpret their potential to serve as therapeutic targets.

7 Materials and Methods

7.1 Materials

7.1.1 Chemicals

Chemicals, dyes and reagents used for the presented study are listed in Table 3. General laboratory chemicals were purchased from Sigma-Aldrich and are not presented here.

Table 3 Chemicals

Chemical	Supplier	Product-/Order-number
2-Aminoethyl-diphenylborinate (2-APB)	Sigma	D9754
3-[1-[3-(Dimethylamino)propyl]-5-methoxy-1H-indol-3-yl]-4-(1H-indol-3-yl)-1H-pyrrole-2,5-dione (BisGö, Gö 6983)	Sigma	G1918
5-(and-6)-carboxy-2',7'-difluorodihydrofluorescein-diacetate (H ₂ -DCFDA)	Invitrogen	C 13293
Accutase	PAA	L11-007
Agarose Broad Range	Carl Roth GmbH	T846.3
Albumin (human)	Sigma	A9418
Ammonium chloride (NH ₄ Cl)	Sigma	A0171
Ammonium persulfate (APS)	Sigma	A3678
Amplex® UltraRed Reagent	Invitrogen™/Molecular Probes®	A36006
Albumin from bovine serum (BSA)	Sigma	A2153
Calcium chloride solution (CaCl ₂)	Fluka Analytical/ Sigma	21115
CellTiter-Blue®	Promega	G8081
Chloroform (99 %) 500 ml	Sigma	C-2432
Complete (Proteinase Inhibitor)	Roche	04 693 132 001
Diethylpyrocarbonat (DEPC)	Sigma	D5758
Dimethylsulfoxid (DMSO)	Sigma	D8418
Diphenyliodonium chloride (DPI)	Sigma	D2926
Ethanol 100 % absolute	Sigma	32205
Ethylenediaminetetraacetic acid (EDTA)	Sigma	E9884
Fetal bovine serum (Fetal calf serum (FCS))	Invitrogen/Gibco	10270-106
N-Formyl-Met-Leu-Phe (fMLF)	Sigma	F3506
Fura-2 AM	Invitrogen	F1221
Glucose	Merck	104933
Glycin	Applichem	A3707,1000

Materials and Methods

Chemical	Supplier	Product-/Order-number
Glycogen	Invitrogen	10814-010
H ₂ O ₂ (10M)	Sigma	31642
HEPES Sigma Ultra (50g)	Sigma	H7523
Insuline solution (human)	Sigma	I9278
Ionomycin (1mg)	Calbiochem	407950
Isopropanol	Fluka/Sigma	59304
Magnesium chloride solution (MgCl ₂)	JT Barker	0504
Methanol	Sigma	32213
N,N,N',N'-Tetramethylethyldiamin (TEMED)	Sigma	T7024
NP-40	Sigma	74385
Penicillin 10.000 U/ ml Streptomycin 10.000 µg/ ml	Invitrogen/Gibco	15140-122
Peroxidase from horseradish	Serva	31943
Phorbol 12-myristate 13-acetat (PMA), also known as 12-O-Tetradecanoylphorbol-13-acetate (TPA)	Sigma	P1585
Poly-L-ornithine hydrobromide	Sigma	P3655
Potassium bicarbonate (KHCO ₃)	Sigma	12602
Potassium chloride solution (KCl)	Merck	105833
Prestained Protein Ladder	Fermentas	26616
Rotiphoresegel 40	Roth	T802
Sodium chloride solution (NaCl)	Sigma	S9888
Sodium dodecyl sulphate (SDS)	Sigma	L3771
Superoxide Dismutase (SOD)	Sigma	S7511
4-Hydroxy-TEMPO (Tempol)	Sigma	176141
Thapsigargin (Tg)	Invitrogen	T7458
Tris HCL	Roth	9090.3
Trisbase	Sigma	T1503
Triton	Eurobio	018774
TRizol® Reagent	Invitrogen	15596-026
TWEEN® 20	Sigma	P1379

7.1.2 Kits and special laboratory equipment

General laboratory equipment that was used to conduct the described experiments, as cell culture supply, tubes, flasks, beaker, pipettes and other items, that are not listed in Table 4, were provided by Eppendorf, BDFalcon and Greiner Bio-One. Table 4 lists ready-to use kits and assay components used in transfections, qRT-PCR or Immunoblotting.

Materials and Methods

Table 4 Kits and special laboratory equipment

Item	Supplier	Product #
Amaxa NHEM-Neo Nucleofector Kit	Lonza AG	C-002-5C
Amaxa™ P3 Primary Cell 4D-Nucleofector™ X Kit L	Lonza AG	V4XP-3024
Amaxa™ Human Monocyte Nucleofector™ Kit	Lonza AG	VPA-1007
Amersham Hyperfilm ECL (High performance chemiluminescence film)	GE Healthcare	28906837
BCA Protein Assay Reagent (bicinchoninic acid)	Thermo Scientific	23225
Cell Culture Inserts (8 µm) pore size	Millipore	PIEP12R48
Costar Ultra Low Cluster Plate (24 well)	Corning Incorporated	3473
dNTPs (100 mM each)	Invitrogen	
dGTP Solution		10218-014
dTTP Solution		10219-012
dATP Solution		10216-018
dCTP Solution		10217-016
Dynabeads® Untouched™ Human Monocytes System	Invitrogen	113.50D
Oligo dT ₁₂₋₁₈ Primer	Invitrogen	18418-012
Pierce ECL Western Blotting Substrate	Thermo Scientific	32209
Protein LoBind Tubes	Eppendorf	022431081
QuantiGlo® Human IL-8 Chemiluminescent Immunoassay	R&D Systems	Q8000B
QuantiTect SYBR Green PCR Kit	Invitrogen	204145
RNase OUT™	Invitrogen	10777-019
Roti-PVDF (nitrocellulose membrane)	Roth	T8301
Superscript™ II Reverse Transcriptase Kit	Invitrogen	18064-014
96-Well Microplate (black/transparent)	BD Falcon™	353219

7.1.3 Devices

Major devices used for the performance of experiments are listed in Table 5 including their intended purpose. Specifications of application are presented in the according method sections.

Table 5 Devices and intended purpose

Item	Supplier	Purpose
4D-Nucleofector™ System: 4D-Nucleofector™ Core Unit 4D-Nucleofector™ X unit	Lonza	Transfection of primary cells

Materials and Methods

Item	Supplier	Purpose
Nucleofector™ II	Lonza	Transfection of Melanoma cell lines
Centrifuge 5415C	Eppendorf	Centrifugation of 1.5 ml reaction tubes
Centrifuge Universal 32R	Hettich	Centrifugation of 15/50 ml reaction tubes
MX3000 PCR Cycler MXPro Software	Stratagene	qRT-PCR
CFX96™ Real-Time System C1000™ Thermal Cycler	BioRad	qRT-PCR
Plate Reader Tecan Genios Pro	Tecan	Proliferation and survival of melanoma and monocytes
Plate Reader Tecan infinite M200 Pro	Tecan	Ca ²⁺ -dependent proliferation and survival of melanoma and monocytes
Electrophoresis System Mini-PROTEAN® System	BioRad	SDS-PAGE and Blotting
Electrophoresis System	BioRad	General purposes (Agarose gels)

7.1.4 Solutions and Media composition

Different solutions and media were used for cell isolation, cell culture, calcium imaging and ROS-measurements. Ready-to-use media and solutions are listed in Table 6. The composition of protein gels used for western blots, as well as the compositions of solutions and media with multiple components are presented in Table 7.

Table 6 Media and solutions for cell culture and experiments

Solution/Medium	Composition	Supplier	Product#
Dulbecco's Phosphate Buffered Saline (1x) (DPBS)	-	Invitrogen/Gibco	14190-094
Hank's BSS (1x) (HBSS)	-	PAA Laboratories	H15-009
L15 Leibovitz liquid-medium	-	Biochrom	F 21315
LSM 1077 Lymphocyte Separation Media (= Ficoll)	-	PAA Laboratories	J15-004
MCDB153 Keratinocyte medium	-	Biochrom	F8105
RPMI 1640 (1x) + L-Glutamin Medium	RPMI (500 ml) +10% FCS +1% Pen/Strep	Invitrogen/Gibco	21875-034

Materials and Methods

Table 7 Multi-component buffers, solutions and media

Solution/Medium	Composition
5x RIPA lysis buffer	50 mM Tris, pH 7,5 150 mM NaCl 2 mM EDTA 2 mM EGTA 0,2 % Triton 10% NP-40
Blotting buffer	10x SDS-Puffer (1 part) H ₂ O _{dest.} (7 parts) Methanol (2 parts)
Erythrocyte Lysis-buffer	100 ml (H ₂ O dest.) 0,829 g NH ₄ Cl 0,1 g KHCO ₃ 3,8 mg EDTA
Gel solution A (Rotiphoresegel 40)	40 % Acrylamid 1.04 % Bisacrylamid
Gel solution B	1.5 M Tris HCl (pH 8.8) 0.4 % SDS in H ₂ O _{dest.}
Gel solution C	0.5 % Tris HCl (pH 6.8) 0.4 % SDS in H ₂ O _{dest.}
PBS-T	0,1 % Tween in PBS
Protein separation gel (10 %)	2.5 ml gel solution A 2.5 ml gel solution B 5 ml H ₂ O _{dest.} 100 µl APS 8.3 µl TEMED
Protein separation gel (15 %)	3.75 ml gel solution A 2.5 ml gel solution B 3.75 ml H ₂ O _{dest.} 100 µl APS 8.3 µl TEMED
Protein stacking gel (5 %)	375 µl gel solution A 800 µl gel solution C 2.125 ml H ₂ O _{dest.} 33.3 µl APS 2.7 µl TEMED
Ringer-solution Physiological solution for Ca ²⁺ imaging and ROS measurements.	155 mM NaCl 4.5 mM KCl 10 mM Glucose

Materials and Methods

Solution/Medium	Composition
(0 mM Ca ²⁺)	5 mM HEPES 3 mM MgCl ₂ 1 mM EGTA In H ₂ O _{dest.}
Ringer-solution (0.25 mM Ca ²⁺)	155 mM NaCl 4.5 mM KCl 10 mM Glucose 5 mM HEPES 2.75 mM MgCl ₂ 0.25 mM CaCl ₂ In H ₂ O _{dest.}
Ringer-solution (0.5 mM Ca ²⁺)	155 mM NaCl 4.5 mM KCl 10 mM Glucose 5 mM HEPES 2.5 mM MgCl ₂ 0.5 mM CaCl ₂ In H ₂ O _{dest.}
Ringer-solution (1 mM Ca ²⁺)	155 mM NaCl 4.5 mM KCl 10 mM Glucose 5 mM HEPES 2 mM MgCl ₂ 1 mM CaCl ₂ In H ₂ O _{dest.}
Ringer-solution (20 mM Ca ²⁺)	155 mM NaCl 4.5 mM KCl 10 mM Glucose 5 mM HEPES 2 mM MgCl ₂ 20 mM CaCl ₂ In H ₂ O _{dest.}
SDS (1x from 10x in H ₂ O _{dest.})	10 x SDS-buffer: 250 mM Tris Base 1,92M Glycin 1 % SDS
Stripping buffer	100 mM Glycin in H ₂ O _{dest.} (pH 2,8)
Tumor-medium (2 % TU-medium)	MCDB153 (4 parts) L15- Medium (1 part) 2 % FCS 1,68 mM CaCl ₂ 2.5 ng/ml Insulin

7.1.5 Activators and Inhibitors

Several activators or inhibitors of cellular components or pathways were used in the presented study to investigate the role of Orai and STIM mediated Ca^{2+} -signaling in monocyte and melanoma function.

Table 8 lists the chemicals and describes their function within the experiments whereas information on chemical supply is presented in Table 3.

Table 8 Activators and inhibitors of Ca^{2+} and redox signaling pathways

Chemical	Specifications and features	Application
Gö6983 (BisGö)	Inhibitors of protein kinase C (PKC) Isoforms PKC α , PKC β , PKC σ and PKC ζ . ⁵	Used as inhibitor of ROS production, by blocking all of the different PKC isoforms, which are responsible for phosphorylation of cytosolic NOX2 subunits. Inhibition of the assembly of the holo-enzyme (indirect inhibition).
DPI	Unspecific inhibitor of nitric oxide synthase (NOS) and NADPH oxidases (NOX). ⁶ Upon interaction with an electron-transporter, DPI forms a radical that further inhibits the transporter through covalent binding. DPI inhibits members of the NOX family by interaction with the heme- or flavin group of the catalytic subunit. DPI also inhibits xanthine oxidase, mitochondrial complex I and cytochrome P450 reductase (Bedard & Krause, 2007).	Used as inhibitor of ROS production, by targeting the responsible enzyme NOX2 (direct inhibition).
fMLF	Formylated tri-peptide (methionine, leucine and phenylalanine), bacterial product that is bound by specialized receptors (formylated peptide receptors = FPR) that are G-protein coupled and trigger an immune response in monocytes (and other phagocytes) (Le <i>et al.</i> , 2002; Lee <i>et al.</i> , 2010b).	Trigger of SOCE for calcium imaging and ROS measurements. Used as a rather physiological activator of SOCE (compared to Tg), <i>via</i> receptor activated depletion of internal Ca^{2+} stores, resulting in the activation of CRAC channels.
Ionomycin	Ion carrier, specific to bind and transport Ca^{2+} through biological membranes. ⁷	Used for calibrations for calcium imaging to gain a sufficient Ca^{2+} depletion from all internal Ca^{2+} stores (ER, mitochondria, vesicles). Used in combination with Thapsigargin.
PMA	Artificial, but potent activator of PKCs that mimics the molecular structure of physiological PKC activator DAG (Castagna <i>et al.</i> , 1982).	Used as potent activator of NOX2 (ROS production) by interacting with PKC, an essential step to activate the assembly of the NOX enzyme. Serves as positive control, due to its reliable and strong response.

⁵ <http://www.sigmaaldrich.com/catalog/product/sigma/g1918?lang=de®ion=DE>

⁶ <http://www.sigmaaldrich.com/catalog/product/sigma/d2926?lang=de®ion=DE>

⁷ <http://www.merckmillipore.com/germany/life-science-research/ionomycin-free-acid-streptomyces-conglobatus>

Chemical	Specifications and features	Application
Thapsigargin	Artificial SERCA blocker, indirect activator of SOCE (Lytton <i>et al.</i> , 1991). Tg blocks SERCA, thereby preventing backhaul of Ca ²⁺ to the ER stores. ER stores are thereby emptied due to lack of compensation of constant Ca ²⁺ leakage to the cytosol. This leads to multimerization of STIM and further activation of CRAC channels.	Passive activation of CRAC channels and SOCE in calcium imaging and ROS measurements.

7.1.6 Objects of research (cell systems)

Research on primary human cells and cell lines has been approved by the local ethics committee. Figure 8 shows representative images of the melanoma cell lines and primary human monocytes, used for experiments.

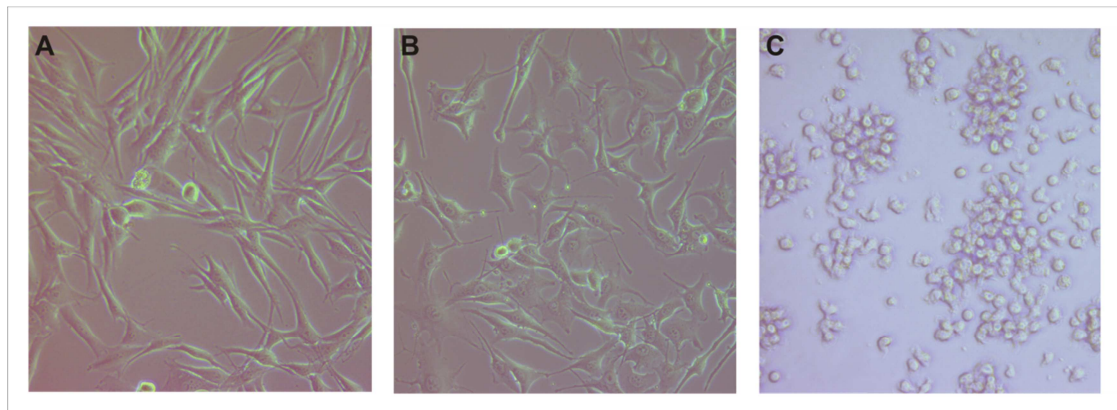


Figure 8 Primary human monocytes and SK-MEL-5 and WM3734 melanoma cell lines

Representative images of human melanoma cell lines WM3734 (A), SK-MEL-5 (B), and primary human monocytes (C). Images were recorded using an inverted Zeiss microscope with a 40x magnification.

7.1.6.1 SK-Mel-5 and SK-MEL-28

SK-Mel-5 and SK-MEL-28 are commercially available melanoma cell lines and were provided by the Institute of Dermatology (Dr. Hedwig Stanis, Prof. Dr. Thomas Vogt), originally purchased from the CLS Cell Lines Service GmbH, Germany⁸. SK-Mel-5 cell line originates from an axillary lymph node metastasis of a caucasian female, aged 24 years. SK-MEL-28 derived from a primary skin melanoma of a 51 year old male patient of unknown ethnic. The two cell lines were (together with others) first isolated by Carey *et al.* (Carey *et al.*, 1976). These cell lines carry a characteristic mutation of the BRAF gene, that codes for the B-raf protein, a serine-tyrosine kinase and a member of the MAPK/ERK signaling pathway. Due to the regulatory nature of this pathway and its components in cell differentiation and growth, mutations often lead to cancer progression.⁹ BRAF is therefore also referred to as proto-

⁸ http://www.cell-lines-service.de/content/index_ger.html

⁹ Summarized information on BRAF mutation was found on: http://www.neuropathologie.med.uni-muenchen.de/genetik/braf-v600_mutationsstatus/index.html

oncogene and the BRAF V600E mutation is very often found in tumor cells (Davies *et al.*, 2002). SK-Mel-5 and SK-MEL-28 were cultured in standard RPMI medium, supplemented with 10% FCS and were splitted biweekly with a ratio of 1:3.

7.1.6.2 WM3734

The WM3734 cell line was kindly provided by the Wistar Institute, Philadelphia, PA USA (Dr. Thomas Roesch, Prof. Dr. M. Herlyn) and is not commercially available. The WM (Wistar Melanoma) 3734 cell line originates from a human melanoma brain metastasis. The cells were cultured in 2% TU medium (see Table 6 and (Satyamoorthy *et al.*, 1997; Roesch *et al.*, 2010)) and splitted with a ratio of 1:2 to 1:3 twice a week.

7.1.6.3 Primary human monocytes

Primary monocytes were isolated from human blood samples (see 7.2.1), provided by the Institute of Haemostaseology, Universitätsklinikum Saarland (Prof. Dr. Eichler). Monocytes originate from the myeloid lineage in the differentiation of leukocytes and can be characterized by their CD expression pattern. Three monocyte subtypes are present in humans and can be identified by their distinct CD expression (see above in 6.2.1). The inflammatory phenotype (that covers 95% of circulating blood monocytes) shows a characteristic CD pattern with CD14^{high}, CD64^{high}, CCR2, CD62L and the absences of CD16 (Gordon & Taylor, 2005). Monocytes were cultured in RPMI medium supplemented with 10% FCS and, if required, 0.1% penicillin/streptomycin. Cells were kept in a cell culture incubator at all times at 37 °C with 5% CO₂ in the atmosphere. These culture conditions are further referred to as standard culture conditions and standard culture medium (with or without antibiotics) or RPMI (+10% FCS).

7.2 Methods

7.2.1 Cell isolation and cultivation

Primary human monocytes were isolated from peripheral blood mononuclear cells (PBMCs). PBMCs were obtained from leukocyte-reducing-system (LRS) chambers, provided by the local blood bank (Department of Haemostaseology, Universitätsklinikum Saarland). The cells were separated from the rest of blood content by Ficoll density gradient centrifugation. The Ficoll was placed in a 50 ml Falcon tube and centrifuged shortly (RT, 1000 x g, 30 s). The tubes contain filters at the bottom of the tube to facilitate the formation of the density gradient. Further on, the blood from LRS-chambers was rinsed onto the Ficoll and the density gradient was established by centrifugation (RT, 450 x g, 30 min, no brake). The separated leukocyte phase was transferred to a new reaction tube and washed once by centrifugation with HBSS (RT, 250 x g, 15 min). Remaining erythrocytes and thrombocytes in the leukocyte pellet were abolished by erythrocytes lysis (2 ml Erythrocyte-lysis-buffer, Table 6), followed by gentle centrifugation (RT, 130 x g, 10 min).

Monocytes were isolated from PBMCs (in PBS + 0.5% BSA) either by negative isolation or by adhesion. Negative isolation was performed using the Dynabeads® Untouched™ Human Monocytes System following the manufacturer's instructions. In a first step, PBLs were mixed with a blocking reagent against Fc-receptors to prevent a cross-reaction or activation of the monocytes *via* CD64 within the procedure. Next an antibody mixture was added, that targets for specific markers of T cells, NK-cells and other PBMC (despite monocytes). These cells were further bound by secondary antibodies that target for the Fc-region of the first set of antibodies. The secondary antibodies were conjugated to magnetic beads, which allowed separation of the

monocyte fraction from the rest of the PBMCs (antibody- and bead-bound) using a magnet. The monocytes in suspension were further cultured in standard culture medium at standard conditions (see 7.1.6.3). 1.5×10^8 PBLs were used per isolation with a yield of 14% on average.

For isolation by adhesion, $1.5\text{-}2.5 \times 10^8$ PBMCs were transferred into culture flasks (175 cm^2) containing 30 ml standard culture medium (plus antibiotics) and kept under standard culture conditions for 2 h to allow adherence of the monocytes to the flask surface. Next, growth medium was exchange and cells were harvested after additional 24h of incubation in fresh medium (plus antibiotics). Cells were washed with PBS (supplemented with 0.5% BSA), scratched from the surface to detach using cell scrapers and suspended in standard culture medium (no antibiotics). After isolation, cells were cultured in RPMI (10% FCS) in 24-well plates (ultra-low attachment surface, see Table 4), with a density of $1\text{-}4 \times 10^6$ cells/ ml and well. Purification and cell quality was determined by flow cytometry (see 7.2.3).

7.2.2 Expression analysis on mRNA level

In general, the status of protein biosynthesis, and hence the expression levels of genes, can be tested by determination of either mRNA or protein level. The protein biosynthesis includes two major steps: transcription and translation. In transcription, a complementary RNA sequence (= template) of a gene is synthesized. The template, generated in the nucleus and further transported and processed to the cytosol, serves as outline for translation. Due to its transmitting character from DNA to protein sequence the template is referred to as messenger RNA (mRNA). Total (m)RNA can be isolated from cells and transcribed to cDNA (reverse transcription). Based on cDNA a PCR can be performed providing quantitative and temporal representation of the expression status of the cells. Here, the method was used to test the general expression status and to confirm the success of knockdown experiments.

7.2.2.1 RNA-Isolation and cDNA synthesis

Isolation of total RNA from the cells is based on the so-called “single-step” method, initially introduced by Chomczynski and Sacchi (Chomczynski, 1987). Monocytes ($1\text{-}3 \times 10^6$) and melanoma cells ($0.5\text{-}1 \times 10^6$) were collected per sample and suspended in 800 μl of Trizol reagent (contains Guanidiniumthiocyanate und Phenol). Samples were stored at $-80 \text{ }^\circ\text{C}$ prior to further handling. Cells were thawed at RT and centrifuged to separate solved components from cell debris ($12000 \times \text{g}$, 10 min, at $4 \text{ }^\circ\text{C}$). Guanidiniumthiocyanate in solution is responsible for lysis of the cells and digestion of endogenous RNAses that would otherwise disintegrate the sample. The supernatant was further incubated at RT for 5 min and 160 μl chloroform were added. By thoroughly shaking three liquid phases build up due to the chemicals in suspension: RNA is solved in the upper water phase, while the intermediate phase contained DNA and the lower phenol phase solved proteins. The water phase was transferred to a new reaction tube. RNA was pulled down by addition of 1 μl glycogen and 400 μl isopropanol and incubation at RT for 10 min. After centrifugation ($12000 \times \text{g}$, 10 min, at $4 \text{ }^\circ\text{C}$) and removal of the supernatant, RNA was washed in ethanol (800 μl 75% in DEPC-treated $\text{H}_2\text{O}_{\text{dest.}}$ from 100% ethanol) by further centrifugation ($12000 \times \text{g}$, 10 min, at $4 \text{ }^\circ\text{C}$). RNA pellet was dried, suspended in 10 μl DEPC-treated $\text{H}_2\text{O}_{\text{dest.}}$ (RNase free) and controlled by running a 2% agarose gel. Photometric determination of concentration was performed using a 1:50 dilution of the RNA in a standard photometer calculated with Equation 1.

Equation 1 $\text{RNA (ug/ml)} = \text{OD}_{260} \times 40 \text{ (Absorption coefficient)} \times \text{Dilution factor}$

Synthesis of cDNA was performed using a standard PCR-cycler with 0.8 µg (0.5 µg in cases with low yield) with a total volume of 10 µl and 1 µl oligo-dT-primers (0.5 µg/µl) and 1 µl dNTPs (mixture of dNTPS for strand synthesis). After 5 min heating to 65 °C, 4 µl 5x first strand buffer, 1 µl DTT (0.1 M) and 1 µl RNase OUT (components from the RNase out Kit) were added and heated to 42 °C for another 2 min. As final step 1 µl SuperscriptII Reverse Transcriptase was added and further incubated at 42 °C for 50 min. In this step the strand synthesis was finally performed by the enzyme, whereas the recent steps were responsible for annealing of the necessary components to the template. The procedure ended with a final temperature rise to 72 °C for 15 min and a cool down to 4 °C.

7.2.2.2 Quantitative (real-time) polymerase chain reaction (qRT-PCR)

The cDNA obtained from reverse transcription served as template for quantitative PCR. In this variation of the PCR technique DNA fragments (cDNA) are amplified by the use of specific primer pairs for the genes of interest. In this study specific primers for the detection of *Orai1-3*, *STIM1-2* and *NOX* family members were used. The PCR conditions used are presented in Table 9 and were chosen to fit the primer and sample needs. Primer Sequences and specifications are listed in Table 10 and Table 11.

The double-stranded cDNA template is denaturated and separated into single strands by an initial rise in temperature to 94 °C. This is followed by repeated temperature cycles for annealing of the primers to the single strands, elongation of the complementary strand by the enzyme DNA-polymerase and again denaturation to generate new single strands for the next step. The temperatures in the elongation steps were chosen depending on the primer sequence to ensure optimal annealing to the single DNA strands.

Table 9 PCR conditions for quantitative real-time PCRs

Melanoma cell lines			Monocytes		
15 min	94 °C		15 min	94 °C	
30 s	94 °C		30 s	94 °C	
45 s	58 °C	45 cycles	45 s	55 °C	45 cycles
30 s	72 °C		30 s	72 °C	
60 s	95 °C		60 s	95 °C	
30 s	55 °C		30 s	55 °C	
30 s	95 °C		30 s	95 °C	
			30 s	25 °C	

This temperatures can be defined in a simplified way by calculating the amount of GC (4 °C for each nucleotide) and of AT (2 °C for every nucleotide). To quantify the level of gene expression a fluorescent dye – *SYBRGreen* – was used, that intercalates within the double strand helix of the DNA. Upon excitation, the resulting emission can be measured when the dye is intercalated. The intensity of the fluorescent signal reflects the amount of cDNA of the gene of interest and thereby reflects the expression level of the mRNA in the analyzed sample. The expression was normalized to the reference gene TATA-box binding protein (TBP), always in the presence of a second reference gene RNAPolymerase (RNAPol) to verify the reliability of the first one. These reference genes are used, since the expression of the gene of interest has to be evaluated in the context of total gene expression of the sample cells. All templates were tested in duplicates. The QuantiTect SYBR Green PCR Kit provided all necessary components

for the amplification (salts, nucleotides, dye). Each template was tested with 0.5µg cDNA and 1 µl of the according primer pair. For each primer pair a negative control (water instead of cDNA template) was used. Two different PCR-cycler, as listed in Table 5 and the corresponding software were used. to perform the experiments. The analysis of the PCR results is based on the $2^{-\Delta\Delta C_T}$ method (Livak & Schmittgen, 2001; Huggett *et al.*, 2005; Bustin *et al.*, 2009). The software determines the so-called quantification cycle (C_q value, former C_T value with T for threshold), that reflects the cycle number in the PCR when the intensity threshold of the system for the SYBRGreen signal is first exceeded. The signal intensity is measured at the end of each elongation step when DNA is in a double-stranded form and the dye can intercalate into the helix. The lower the C_q value, the higher the expression of the gene of interest in the sample. All PCR conditions were tested in duplicates. Resulting C_q values were therefore averaged (referred to as ΔC_q). ΔC_q values were further normalized to the expression of the reference genes by the calculation of the $\Delta\Delta C_q$ value (ΔC_q value target gene – ΔC_q value reference gene) and are presented as $2^{-(\Delta\Delta C_q)}$. This parameter was used to evaluate and discuss the expression levels of the genes of interest.

7.2.2.3 Expression analysis of Orai and STIM isoforms

The expression levels of the CRAC channel components Orai1-3 and STIM1 and 2 in primary cells, cell lines and cells transfected with siRNA against the respective targets were determined using the Primer sets presented in Table 10 to evaluate general expression levels and to confirm the success of RNAi. Templates for the expression analysis were obtained as described above (0) and PCR conditions are presented in Table 9.

Table 10 Primer sequences for quantitative RT-PCR of Orai and STIM

Primer	Sequence	Annealing Temperature [°C]	Expected product size [bp]
Orai1_forward	5' ATGAGCCTCAACGAGCACT 3'	58	190
Orai1_reverse	5' GTGGGTAGTCGTGGTCAG 3'	58	
Orai2_forward	5' TGGAACTGGTCACCTCTAAC 3'	60	165
Orai2_reverse	5' GGGTACTGGTACTGCGTCT 3'	60	
Orai3_forward	5'GTACCGGGAGTTCGTGCA 3'	58	192
Orai3_reverse	5'GGTACTCGTGGTCACTCT 3'	56	
TBP_forward	5' CGGAGAGTTCTGGGATTGT 3'	58	160
TBP_reverse	5' GGTTCTGGCTCTTATC 3'	58	
RNAPol_forward	5' GGAGATTGAGTCCAAGTTCA 3'	58	133
RNAPol_reverse	5'GCAGACACACCAGCATAGT 3'	58	
STIM1_forward	5' CAGAGTCTGCATGACCTTCA 3'	60	124
STIM1_reverse	5' GCTTCTGCTTAGCAAGGTT 3'	60	
STIM2_forward	5' GTCTCCATTCCACCTATCC 3'	62	113
STIM2_reverse	5' GGCTAATGATCCAGGAGGTT 3'	60	

7.2.2.4 Expression analysis of NOX family isoforms

The presence of the NOX family isoforms (Nox1, Nox2, Nox3, Nox4, Nox5, Duox1 and Duox2) was analyzed by quantitative real-time PCR based on cDNA from primary human monocytes as described above (0). Primers were designed using the free-available software Primer3¹⁰. The specificity of the used primers was verified on positive controls prior to the experiments. Positive controls were generated by 1) performing standard PCR using the chosen primers and 2) cloning the obtained products into the pJet vector. The cDNA templates for positive control generation were: HCT116 for Nox1; primary human monocytes for TBP, RNA polymerase, Nox2 and Duox2; HEK wild type cells for Nox3 and 4; HL-60 cells for Nox5 and DU145 for Duox2. Sequence analysis of the constructs carrying the positive controls, confirmed the specific gene detection using the primers shown in Table 11. For qRT-PCR the same temperature and time settings were used as for analysis of Orai and STIM expression (see Table 9).

Table 11 Primer sequences for quantitative RT-PCR of NOX family members

Primer	Sequence	Annealing Temperature [°C]	Expected product size [bp]
Nox1_forward	5' AATCCTTGGGTCAACATTGG 3'	58	109
Nox1_reverse	5' CCTCAGGAAGGACAGCAGAT 3'		
Nox2_forward	5' TCACTTCCTCCACCAAAACC 3'	58	211
Nox2_reverse	5' GGGATTGGGCATTCTTTAT 3'		
Nox3_forward	5' GCCCAACTGGAACAATGAGT 3'	58	147
Nox3_reverse	5' ATGAACACCTCTGGGGTCAG 3'		
Nox4_forward	5' CTGGTGAATGCCCTCAACTT 3'	58	115
Nox4_reverse	5' GGCCAGGAACAGTTGTGAAG 3'		
Nox5_forward	5' ATCTGCTCCAGTTCCTGCAT 3'	58	142
Nox5_reverse	5' ACAAGATTCCAGGCACCAG 3'		
Duox1_forward	5' CCACCAGGAGTGGCATAAGT 3'	58	212
Duox1_reverse	5' TGGTCATTCTCCTCCACCTC 3'		
Duox2_forward	5' GGCTCCCCAGAGGATAAGTC 3'	58	199
Duox2_reverse	5'GTCAGCTCCTCCTTGTCCTG 3'		

7.2.3 Characterization of primary human monocytes by flow cytometry

Flow cytometry (FC) was used to characterize the monocyte subtype at hand and the purity of the isolation steps. FC is a technique that is suitable to collect statistical data from a huge population of cells, by simultaneous analysis of multiple characteristics. The parameters that can be analyzed are cell size and number, cell complexity (internal and external granularity), surface marker expression (phenotype determination) or the health status of the cells. For the purpose of this study the flow cytometer Canto II from BD and the corresponding FACSDiva software were used. In order to characterize the monocyte subset, the expression of chosen surface proteins (= markers, CD-molecules) was analyzed using specific antibodies that were conjugated to fluorophores.

¹⁰ <http://www.ncbi.nlm.nih.gov/tools/primer-blast/>

Monocytes appear in three different subsets (Gordon & Taylor, 2005), with the inflammatory or classical subset showing the highest proportion (95 %) of circulating blood monocytes. Based on the publication from Tallone and colleagues (Tallone *et al.*, 2011), five CD markers were chosen to characterize the present monocyte subset: CD14, CD16, HLA-DR, CD62L and CD64. Three stainings were performed with 1) CD14, CD16, HLA-DR and CD62L; 2) CD14, CD16, HLA-DR and CD64 and 3) the corresponding isotype controls to test for unspecific antibody binding. Table 12 shows the antibodies, their conjugated fluorophore and isotype controls including their properties, used for characterization. 1×10^6 monocytes (day three after isolation) were washed once and re-suspended in 100 μ l PBS (+0.5 % BSA). 5 μ l of the desired antibody solution or isotype control was added and incubated for 15 min at RT or 30 min at 4 °C. Labeled cells were washed twice in PBS (+0.5 % BSA) and re-suspended in a final volume of 200 μ l PBS (+0.5 % BSA) and measured within 2-4 h.

Table 12 Antibodies and isotype controls used for flow cytometry

Indication (Target)	Fluorophore	Antibody subtype	Supplier	Catalogue #
PE anti-human CD14 Antibody (CD14)	PE	IgG1	biolegend	325606
Anti-Human CD16 FITC (CD16)	FITC	IgG1	eBioscience	11-0168-42
Pacific Blue™ anti-human HLA-DR Antibody (HLA-DR)	Pacific Blue	IgG2b	biolegend	327016
APC anti-human CD62L Antibody (CD62L)	APC	IgG1	biolegend	304810
PE/Cy7 anti-human CD64 Antibody (CD64)	PE-Cy7	IgG1	biolegend	305021
Pacific Blue™ Mouse IgG2b, κ Isotype Ctrl Antibody	Pacific Blue	IgG2b	biolegend	400331
PE Mouse IgG1, κ Isotype Control Antibody	PE	IgG1	biolegend	400111
Mouse IgG1 K Isotype Control Alexa Fluor® 488	FITC (Alexa488)	IgG1	ebioscience	53-4714-42
APC Mouse IgG1, κ Isotype Control Antibody	APC (Alexa647)	IgG1	biolegend	400119
PE/Cy7 Mouse IgG1, κ Isotype Control Antibody	PE-Cy7	IgG1	biolegend	400125

7.2.4 Protein determination

Western blot (Immunoblotting) technique was used to determine Orai and STIM isoform protein expression and to verify the success of RNAi mediated knockdowns. In addition, the technique was used to determine the expression of the TF MITF, Jarid1B and the pro-apoptotic factor Brn2 in melanoma cell lines. In the following section the experimental outline is described, combining general aspects of the technique and the specifications used for this study. The determination of protein content of a sample is achieved by the combination of different steps. In a first step, the protein is made available by lysis of the cells and further denaturated. In a second step, the proteins are separated according to their size using a SDS-polyacrylamid-gel electrophoresis (SDS-PAGE).

Following the separation, the proteins are transfer from the gel to a nitrocellulose membrane. In a final step, the membrane is probed with specific antibodies to detect the desired proteins. Antibodies used in the here presented study are listed in Table 13.

Table 13 Antibodies used for western blot

Antibody	Dilution	Supplier	Order#	Secondary AB
Brn2	1:100	Sigma	AV31218	rabbit
GAPDH	1:8000	Santa Cruz	sc-25778	rabbit
Goat anti mouse	1:10000	Sigma	A-3682	= secondary AB
Goat anti rabbit	1:10000	Jackson ImmunoResearch	111-035-046	= secondary AB
JARID1B	1:100	Novus	NB100-97821	rabbit
MITF	1:250	Sigma	HPA003259	rabbit
Orai1	1:2000	Sigma	O8264	mouse
STIM2	1:2000	Sigma Anaspec	S8572 PRS4125	rabbit

Cells were harvested and shock frozen in liquid nitrogen as preparation for protein extraction. Samples were re-suspension in 1xRIPA lysis-buffer and incubation on ice for 30 min. The lysis-buffer contained proteinase inhibitors as essential component to prevent digestion of the samples by endogenous proteinases. Shear forces were used to facilitate protein extraction by passing the cell suspension through hallow needles repeatedly. Protein concentration of the lysate was determined using the bicinchoninic acid (BCA) protein assay following the manufactures instructions.¹¹ Protein content of the sample is calculated from a standard curve, based on defined protein concentrations, determined for each single experiment. 20 µg of protein, mixed with 5 µl page ruler, were separated by 15 % or 10 % SDS-PAGE (130 V, 60 mA, 2 h) in 1xSDS-running buffer. The highly negatively charged chemical SDS binds protein, creating a negatively charged complex, thereby enabling an efficient separation during electrophoresis. The composition of buffers and gels used for this study are presented in Table 6 with single components listed in Table 3. Separated protein was blotted from gels onto nitrocellulose membranes (70 V, 20 mA, 16 h) in blotting buffer. The transfer is a necessary step to detect the desired proteins, since the epitopes of the proteins are not available for antibody detection when bound in the gel, but become accessible after transfer onto a membrane. The membranes were blocked in 5 % milk in PBS-T for one hour to prevent unspecific antibody binding in the following steps. Primary antibodies were incubated with the membrane overnight at 4 °C. The membranes were washed three times with PBS-T and were subsequently incubated with the appropriate secondary antibody for one hour at RT. The membranes were washed again three times with PBS-T and detected with Pierce ECL western blotting Substrate on Amersham Hyperfilm ECL. Different exposure times (1-30 min) were used depending on the primary antibody. To evaluate protein amount and equal loading, blots were stripped and probed against GAPDH as loading control. Due to its abundantly high expression, GAPDH is commonly used as reference to normalize target protein expression.

¹¹ <http://www.piercenet.com/browse.cfm?fldID = 02020101>

7.2.5 Gene silencing using RNA interference (RNAi)

7.2.5.1 Method

There are in general two different approaches to regulate gene expression, either by altering or deleting the DNA-sequence or by interfering in protein biosynthesis at a post-transcriptional level. Gene silencing, by alteration of DNA sequence (mutation), or a gene knock-out, by deleting a DNA sequence, are different approaches to target a gene on DNA level. Another option is the RNA interference (RNAi) on mRNA level using so-called small-interfering RNAs (siRNA). That way, the gene sequence stays untouched and can be transcribed into mRNA, but further translation is prevented. Gene-silencing by siRNAs or other regulatory small RNA constructs like microRNAs are also endogenous processes to regulate gene expression.

SiRNAs are short (21-23 bp), double-stranded RNA sequences. Such siRNAs can be processed *in vitro* and transfected into cells. Double-stranded siRNAs are recognized and separated into single strands by the RNA-induced silencing complex (RISC), a multi-component enzyme. The sense strand of the construct is identical to the target mRNA, thus the antisense strand binds the target mRNA after being processed within the cell. The resulting double-strand RNA complex is again recognized by RISC, degraded and the target mRNA is no longer available as template for protein translation. This knockdown of gene function is only transient, because mRNA is constantly processed. In addition the siRNA itself is prone to degradation.

7.2.5.2 Nucleofection of siRNA

Nucleofection is a type of electroporation that is used to transfer siRNAs (or DNA constructs) into cells. Pooling the cells and the construct to be transferred in a salt free solution and subjecting it to an electric pulse, enables the construct to traverse the membrane. The manufacturer claims to guarantee a directed trafficking of the construct into the nucleus, thereby increasing the efficiency of transfection. This method was designed for transfection of primary cells and difficult-to-transfect cell lines. Moreover, it serves as a method to transfect non-proliferating cells and as an alternative method to the usage of lentiviral transfection. The devices used for electroporation of melanoma cell lines and monocytes are presented in Table 5. 1×10^6 melanoma cells and 7.5×10^6 monocytes were used per transfection and gently centrifuged (200 x g, 6 min for melanoma and 1500 x g, 6 min for monocytes). The cell pellet was re-suspended in 100 μ l of the respective nucleofector solutions (at RT) including 2-4 μ l of the desired siRNAs or control non-silencing RNA (approx. 20-30 pmol). The suspension was placed in a cuvette and subjected to electroporation using the specific protocols (intensity and time of the pulse, cell specific pre-sets provided by the supplier).¹² 500 μ l of pre-warmed medium was added immediately after pulsing and the whole mixture was transferred into the specific culture plates containing pre-warmed medium.

In all cases despite STIM2 and Orai2, a mixture of 2 different siRNAs was used (see Table 14). The sequences of the siRNAs for knockdown of Orai1, Orai2, Orai3 and STIM1 genes were chemically modified to ensure stability over 48 h. The modifications were initially introduced in the lab to stabilize siRNA for transfection of primary T cells. The insertion of chemical modifications was shown to support stability of siRNA by several research groups and information about the used modifications was taken from (De Paula *et al.*, 2007; Mantei *et al.*,

¹²http://bio.lonza.com/fileadmin/groups/marketing/Downloads/Protocols/Generated/Optimized_Protocol_302.pdf

2008). Besides lack of stability, the induction of an immune response by siRNAs, has to be taken into consideration (Judge *et al.*, 2005; Whitehead *et al.*, 2011). Based on findings that modifications at the C2' ribose provoke a reduced immune response and increase the stability of the siRNA, these modifications were chosen for the here described experiments (De Paula *et al.*, 2007; Mantei *et al.*, 2008). The used siRNAs to target the different CRAC channels components are listed in Table 14. To rule out side effects of the transfection method or the presence of small RNAs in general, non-targeting RNAs were used in separated control transfections. Depending on the used siRNAs modified or unmodified RNAs were used as corresponding controls, as listed in Table 15.

Table 14 Sequences of siRNAs used for specific gene knockdowns

The modifications introduced to the siRNA sequence are indicated as follows: OMe, O-methylation at C2' of the ribose; d, deoxygenation at C2' of the ribose. The sense strands display a TT overhang at the 3'end of the sequence, a typical feature of siRNAs.

Target mRNAs and sequences of used siRNAs

<i>Target mRNA</i>	<i>Orai1 (NM_032790)</i>
Orai1.1	O1.1 sense 5' OMeC-OMeG-GCCUGAUCUUUAUCG-d(UCU)-d(OMeT-OMeT) 3'
	O1.1 antisense 5' dA-AGACGAUAAAGAUCAGGC-OMeC-OMeG 3'
Orai1.2	O1.2 sense 5' OMeC-OMeA-ACAUCGAGGCGGUGA-d(GCA)-d(OMeA-OMeT-OMeT) 3'
	O1.2 antisense 5' d(U)-UGCUCACCGCCUCGAUGU-OMeT-OMeG - 3'
<i>Target mRNA</i>	<i>Orai2 (NM_032831)</i>
Orai2	O2 sense 5' OMeC-OMeA-ACAUGAGUGCUGAGC-dU-dU-dA-dOMeA-dOMeT-dOMeT 3'
	O2 antisense 5' dU-UAAGCUCAGCACUCAUGU-OMeT-OMeT 3'
<i>Target mRNA</i>	<i>Orai3 (NM_152288)</i>
Orai3.1	O3.1 sense 5' OMeC-OMeA-CCAGUGGCUACCUCC-d(CUU)-d(OMeA-OMeT-OMeT)3'
	O3.1 antisense 5' d(U)-AAGGGAGGUAGCCACUGG-OMeT-OMeG 3'
Orai3.2	O3.2 sense 5' OMeT-OMeC-CUUAGCCCUUGAAAU-d(ACA)-d(OMeA-OMET-OMeT)3'
	O3.2 antisense 5' d(U)-(UGUAUUUCAAGGGCUAAG)-OMeG-OMeA 3'
<i>Target mRNA</i>	<i>STIM1 (NM_003156)</i>
STIM1.1	S1.1 sense 5' OMeU-OMeG-AGGUGGAGGUGCAAU-d(AUU)-OMeA-OMeT-OMeT 3'
	S1.1 antisense

Target mRNAs and sequences of used siRNAs

	5' dU-AAUUAUUGCACCUCCACCU-OMeC-OMeA 3'
STIM1.2	S1.2 sense 5' OMeC-OMeU-GGUGGUGUCUAUCGU-d(UAU)-OMeU-OMeT-OMeT 3' S1.2 antisense 5' dA-AUA 3'ACGAUAGACACCACC-OMeA-OMeG 3'
<i>Target mRNA</i> STIM2	<i>STIM2 (NM_001169117.1)</i> S2 sense 5' UAAGCAGCAUCCCACAUGA-d(TT) 3' S2 antisense 5' d(TT)-UCAUGUGGGAUGCUGCUUA 3'

Table 15 Sequences of non-targeting RNAs used as controls for specific gene knock-downs

The modifications introduced to the siRNA sequence are indicated as follows: OMe, O-methylation at C2' of the ribose; d, deoxygenation at C2' of the ribose. The sense strands display a TT overhang at the 3'end of the sequence, a typical features of siRNAs.

Sequences of used non-targeting control RNAs

Control (1) Unmodified by Microsynth	Sense 5' AAAGGUAGUGUAAUCGCCUUGTT 3' Antisense 5' CAAGGCGAUUACACUACCU 3'
Control (2) Modified by Microsynth	Sense 5' OMeA-OMeA-AGGUAGUGUAAUCGC-d(CUU)-OMeG-OmeT-OMeT 3' Antisense 5' dC-AAGGCGAUUACACUACCU 3'
Control (3) Modified by Qiagen	Sense 5' OMeA-OMeA-UUCUCCGAACGUGUC-d(ACG)-OMeU-OMET-OMeT-OMeT 3' Antisense 5' d(A)-CGUGACACGUUCGGAGAA-OMeT-OMeT 3'

7.2.6 Detection of reactive oxygen species

7.2.6.1 Electron Paramagnetic Resonance Spectroscopy (EPRS)

EPRS technique was applied to characterize the source and the role of SOCE for ROS production by primary human monocytes and was performed by Reinhard Kappl and David Conrad (Institute of Biophysics, Saarland University). The EPR experiments were performed with a Bruker spectrometer (ESP300e) equipped with a standard 4102ST cavity which holds the capillary support quartz glass finger. The finger is temperature controlled and set to 37 °C for experiments with cells (temperature controller BiIII-TGC, Noxygen). The modulation amplitude was generally 0.1 mT and the microwave power was set to 20 mW as standard condition for all experiments. Spectra were recorded with scan times of 60 s and stored consecutively to monitor the kinetic behavior of the signal. 2.5-5 x 10⁵ monocytes were used per experiment and stimulated with the according additives. Tg was used to passively activate

CRAC channels and Bisgö and DPI to inhibit NOX2. 300 μM of the redox activated cyclic hydroxylamine spin trap CMH (1-hydroxy-3-methoxycarbonyl-2,2,5,5-tetramethylpyrrolidine) was used for all experiments to monitor superoxide production. CMH was added last, the sample was filled in a 50 μl glass capillary and immediately transferred into the capillary holder. The experiments were performed in Ringer's solution at 37 $^{\circ}\text{C}$ (Ca^{2+} free or containing 1mM [Ca^{2+}]). The oxygen concentration in solution was about 200 μM . All control experiments with single components of the assays and CMH were tested for unwanted radical production. In addition, superoxide radical as the reacting species was identified by suppression of the CMH signal by SOD (100 U/ml) acting as scavenger. The EPR spectra of the CM radical were evaluated with the custom-made program Medeia which measures the peak-to-peak intensity and width of one (or several) lines of a radical visible in a time series. In absence of line width changes and saturation effects, the intensity information can be translated to radical concentration by calculating the integral of the monitored line and considering the multiplicity of the radical signal. This value is compared to a reference sample of known concentration (usually 100 μM Tempol) recorded under identical conditions for quantitative measures.

7.2.6.2 Fluorescent Dyes

H_2O_2 production by monocytes was measured extracellular using the H_2O_2 sensitive and specific fluorescent dye Amplex[®]UltraRed (AUR). AUR reacts with H_2O_2 to its fluorescent product Resorufin in a 1:1 relation, catalyzed by horseradish peroxidase (HRP). NOX2-dependent H_2O_2 production by monocytes was measured after activation of SOCE by Tg or fMLF and the PKC activator PMA as positive control (1 μM each). Experiments were performed in 96-well plates (black casket/ transparent bottom). All experiments were conducted in Ringer's solution with 1 mM [Ca^{2+}] or Ca^{2+} free (0 mM [Ca^{2+}]). 25.000 cells/ well were used in duplicates or triplicates per condition. The total desired cell number for one experiment was centrifuged, re-suspended in Ringer's solution with a concentration of 25.000 cells/ 10 μl and seeded into the 96-well plate. Assay components and concentrations were: AUR (50 μM), HRP (0.5 U/ml) and SOD (10 U/ml) in 180 μl / well. SOD was added to the reaction to ensure a sufficient conversion of the initially produced superoxide to H_2O_2 . PMA, Tg and fMLF concentration was set to 20 μM and used with a volume of 10 μl /well to achieve a final concentration of 1 μM . For negative controls Ringer's solution containing 2 % DMSO was added with 10 μl /well to achieve a final concentration of 0.1 % . 2-APB and DPI were used yielding to a final concentration of 50 μM and 10 μM , therefore preset to 2 mM and 1 mM. H_2O_2 production by measurement of the resulting Resorufin intensity (as RFU), with excitation at 535 nm and emission at 590 nm, was performed using the Tecan GENios Pro Reader with a bottom reading setting. ROS production was recorded for 50-90 min with a cycle time of 2 min. Different concentrations of H_2O_2 were measured in three independent experiments with AUR to create a standard curve, with a regression value of 0.999. The standard curve was further used to calculate [H_2O_2] based on RFUs (see Equation 2 and result section).

$$\text{Equation 2} \quad \text{H}_2\text{O}_2 \text{ (nM)} = (\text{RFU}/2.56) - 47.32$$

Internal ROS was determined on single cell level by the fluorescent dye H_2 -DCFDA displaying an excitation maximum at 485 nm and an emission maximum at 535 nm. H_2 -DCFDA is a rather non-specific sensor of internal ROS. The dye is a fluorescein-derivate (chemically reduced), that carries an ester bound diacetate-group, rendering it cell membrane permeable. The dye is trapped in cells due to cleavage of the diacetate-group by endogenous esterases. It was chosen, to test a H_2O_2 feedback on ROS production, instead of the more reliable AUR, because of the required pre-treatment of the cells with H_2O_2 for the intended purpose. Cells

were loaded with Thapsigargin and H₂-DCFDA (1 μM each) for 30 min at RT for both, control and H₂O₂ conditions. Prior to loading a pre-treatment with 300 μM H₂O₂ for 15 min at dark (RT) was performed to determine the effect of oxidants on Tg-triggered ROS production. Loading and pre-treatment, as well as the measurements were performed in 1 mM [Ca²⁺]_i Ringer's solution. Cell handling and recordings were done using the same hard- and software components as for fluorescent-based calcium imaging (see 7.2.7). Recorded RFUs were calculated and presented as percent of un-stimulated, H₂-DCFDA loaded control cells.

7.2.7 Calcium imaging

7.2.7.1 Method

The here described method, referred to as calcium imaging, was used to measure intracellular Ca²⁺ concentrations [Ca²⁺]_i of monocytes and melanoma cell lines (SK-MEL-5 and WM3734) on single cell level. Cells were loaded with the dye Fura-2AM which comprises a polyaminocarboxylate fluorophore, that binds divalent ions such as Ca²⁺ and is conjugated to a acetoxymethylester-group (AM). The AM-group enables the dye to permeate into cells and is further cleaved off by endogenous esterases in the cytosol, trapping the dye in the cell. Fura-2AM is a ratiometric dye that exhibits two absorption maxima with excitation at 340 nm and 380 nm and one emission maximum at 510 nm. The binding of Ca²⁺ results in an increased emission under excitation at 340 nm and a decreased emission under excitation at 380 nm. The emission ratio 340 nm/ 380 nm reflects changes in [Ca²⁺]_i and is indicated as relative fluorescent unit (RFU). This relative indicator can be converted to a Ca²⁺ concentration ([Ca²⁺]_i) after calibration of the system to evaluate the minimal and maximal achievable values of the investigated cell types under defined measuring conditions. This method of estimating [Ca²⁺]_i was initially proposed by Grynkiewicz and colleagues (Grynkiewicz *et al.*, 1985) and the provided equation was used to convert fluorescent units to calcium concentration (Equation 3). Parameter definitions of the Grynkiewicz equation are as follows: Kd: dissociation constant, sf1 (signal free dye): signal of unbound dye at 340 nm; sf2: signal of unbound dye at 380 nm; sb1(signal bound dye): signal of Ca²⁺ bound dye at 340 nm excitation; sb2: signal of Ca²⁺ bound dye at 380 nm excitation. The parameter R_{min} is calculated from (sf1/sf2), and reflects the lowest possible Ca²⁺ concentration and R_{max}, calculated from (sb1/sb2), defines the highest possible values. The advantages of a ratiometric determination are the abolishment of usual occurring problems like imbalanced loading and bleaching events.

$$\text{Equation 3 Calcium (nM)} = Kd (\text{Fura}) \times ((\text{RFU}-R_{\min})/(R_{\max}-\text{RFU})) \times (\text{sf2}/\text{sb2})$$

7.2.7.2 Experimental handling

The data was recorded on a set-up comprising an inverted microscope (Olympus IX70) using a 20x objective (UApo/340, N.A. 0.75), a xenon-lamp with control unit (Polychrome V monochromator), an infrared lamp and a CCD camera (all items provided by T.I.L.L. Photonics GmbH), using the tillvison software. For measurement of monocytes, experiments were performed with 1-5 x 10⁵ cells per measurement. Cells were loaded with 1 μM Fura-2AM (25 min, RT) in standard culture medium containing 100 mM HEPES to stabilize pH. Loaded cells were placed on coverslips coated with poly-l-ornithine (0.1 mg/ml in H₂O_{dest}) to prevent movement of the cells during the measurements. Coverslips were placed into a measuring chamber, connected to a perfusion system. For measurement of melanoma cell lines, cells were seeded on coverslips two days before the experiments and were loaded with 1 μM Fura-2AM in their specific culture medium (20 min, 37 °C, 5% CO₂).

The standard measuring protocol involved perfusion steps of Ringer's solutions with different calcium concentrations (see Table 6), supplemented with Thapsigargin (Tg, 1 μ M) or fMLF (1 μ M) to activate CRAC channel signaling. These steps were: 0.5 mM [Ca^{2+}] to estimate basal concentrations, 0 mM [Ca^{2+}] to abolish extracellular Ca^{2+} , 0 mM [Ca^{2+}] containing a stimulus to activate the signaling cascade by depleting the intracellular Ca^{2+} stores, re-addition of 0.5 mM [Ca^{2+}] to estimate Ca^{2+} influx *via* activated channels, followed by 0 mM [Ca^{2+}] to stop the influx. This protocol is further referred to as store-depletion protocol. As described above the calculation of [Ca^{2+}] based on RFU values requires a calibration of the system. Calibrations were performed on non-transfected monocytes and SK-MEL-5 cells (as representative for melanoma cell lines). Calculation of [Ca^{2+}] was based on the measured RFUs, with the parameters given in Equation 4 for monocytes and Equation 5 for melanoma.

$$\text{Equation 4 } \text{Calcium (nM)} = \text{Kd (224nM)} \times ((\text{RFU}-0.183)/(5.736)) \times 5.149$$

$$\text{Equation 5 } \text{Calcium (nM)} = \text{Kd (224nM)} \times ((\text{RFU}-0.158)/(4.798)) \times 6.421$$

The calibration protocol involved perfusion steps of Ringer's solution with different Ca^{2+} concentrations and chemicals to elevate Ca^{2+} from all subcellular compartments. These steps were: 0.5 mM [Ca^{2+}] to estimate basal concentrations; 0 mM [Ca^{2+}] plus ionomycin (4 μ M) and Tg (1 μ M) to remove Ca^{2+} from all cellular compartments and the cytosol; followed by re-addition of 20 mM [Ca^{2+}] to achieve the highest possible [Ca^{2+}]_i.

7.2.8 CellTiter-Blue viability and proliferation assay

The CellTiterBlue viability assay was used to analyze cell survival and proliferation of monocytes, SK-MEL-5 and WM3734. Survival and proliferation was tested according to specific culture environments or following RNAi to determine involvement of CRAC channels in these processes. The assay is based on the conversion of the indicator dye Resazurin to its fluorescent form Resorufin by metabolically active cells. The dye displays an excitation maximum at 574 nm and an emission maximum at 590 nm. For measurements an excitation wavelength of 535 nm was applied to prevent interference with the used culture medium. For non-proliferating monocytes this assay was used to determine the number of surviving cells in an oxidizing environment and/or when exposed to different extracellular Ca^{2+} concentrations. For melanoma cells the assay was used to determine proliferation when exposed to different Ca^{2+} concentrations in the medium or following a knockdown of Orai1 or STIM2. All experiments were performed in 96-well plates (black casket/transparent bottom), with triplicates per condition, using 25,000 cells/well for monocytes and 4000 or 3000 cells/well for SK-MEL-5 and WM3734 respectively. Fluorescence was detected using the Tecan GENios Pro Readers with bottom reading setting. The specific measurement parameters are listed in Table 16.

In order to determine monocyte survival in an oxidizing environment cells were seeded in 200 μ l standard culture medium per well, containing increasing concentrations of H_2O_2 ranging from 1 μ M to 10 mM (concentration in medium). Cells were cultured under these conditions for 24 h. 20 μ l of CellTiterBlue was added per well and incubated for 3h before fluorescence was detected. IC_{50} of cell viability was calculated from RFUs of H_2O_2 treated cells, normalized to untreated control cells. The Origin software and an exponential decay fitting was applied to determine the IC_{50} .

To analyze the effect of ion changes in the extracellular compartment on cell survival and proliferation, different Ca^{2+} concentrations in medium were achieved by supplementation with the Ca^{2+} -chelator EGTA.

Table 16 Experimental settings of CellTiterBlue Assays

Measurement Purpose	Device used	Parameters/Settings
Survival of monocytes in an oxidizing environment (H ₂ O ₂)	Tecan GENios Pro Reader	Number of flashes/Well: 5 Manual gain: 42 Integration time: 40 µs Multiple Reads/Well: 3X3
Survival of monocytes in an oxidizing environment (H ₂ O ₂) depending on the extracellular Ca ²⁺ milieu	Tecan infinite M200 Pro Reader	Number of flashes/Well: 5 Manual gain: 75 Integration time: 40 µs Multiple Reads/Well: none
Proliferation of SK-MEL-5 cells with knockdown of Orai1 and Stim2	Tecan GENios Pro Reader	Number of flashes/Well: 3 Manual gain: 35 Integration time: 40 µs Multiple Reads/Well: 3X1 (line)
Proliferation of SK-MEL-5 cells depending on the extracellular Ca ²⁺ milieu	Tecan infinite M200 Pro Reader	Number of flashes/Well: 5 Manual gain: 75 Integration time: 40 µs Multiple Reads/Well: 3X3

The resulting free Ca²⁺ concentration ($[Ca^{2+}]_{free}$) was measured using two different techniques: The Calcium Gen.2 Assay (Roche Diagnostic)¹³ performed by the Central Clinical Laboratory, University of Saarland and the Combination Calcium Electrode perfectION™ (Mettler Toledo)¹⁴. A stock-solution of 100 mM EGTA in H₂O_{dest.} was used to adjust $[Ca^{2+}]_{free}$ in the medium. The Calcium Gen.2 Assay, in general, is used for quantification of $[Ca^{2+}]_{free}$ in serum, plasma or medium samples. Within the assay performance, free Ca²⁺ binds to a chromofor NM-BABTA in a 1:1 relation which results in a color shift of the solution. In a second step EDTA is added. This calcium chelator has a higher binding affinity to Ca²⁺ than BABTA, resulting in the formation of an EDTA-Ca²⁺ complex and free BABTA in solution. The concurrent color back-shift of the solution is measured using excitation at 340 nm and is proportional to the free (bondable) Ca²⁺ concentration in the sample. Measurement of $[Ca^{2+}]_{free}$ using the calcium electrode were performed following the manufacturer's instructions.¹⁵ The electrode was calibrated using three defined Ca²⁺ concentrations (2.5 x10⁻⁵ mM, 2.5 x10⁻⁴ mM, 2.5 x10⁻³ mM) in H₂O_{dest.}. 10 ml of RPMI +/- 10% FCS and +/- EGTA (0.1-0.9 mM) were prepared and subjected to the different techniques. For each EGTA concentration in both medium types three independent measurements were performed.

¹³ Description of test performance by Roche Diagnostic see: http://www.roche-diagnostics.de/diagnostics/testsundparameter/immundiagnostik/calcium/Documents/FactSheet_Calcium2.pdf

¹⁴

http://de.mt.com/de/de/home/supportive_content/product_documentation/operating_instructions/_GB_Fluoride/jcr:content/download/file/file.res/perfectION_Guidebook_Fluoride_de.pdf

¹⁵

http://de.mt.com/de/de/home/supportive_content/product_documentation/operating_instructions/_GB_Fluoride/jcr:content/download/file/file.res/perfectION_Guidebook_Fluoride_de.pdf

For Proliferation and survival experiments of monocytes and melanoma cells in different Ca^{2+} milieus, EGTA supplemented medium was prepared 2-fold concentrated and equilibrated at 37 °C, 5% CO_2 for minimum 2 h. The equilibration step was necessary, due to a high influence of EGTA supplementation on medium pH. Cells were seeded in 100 μl medium/ well (no EGTA-supplementation) and 100 μl /well of the prepared medium. Cells were incubated under these condition for 48 h/ 72 h (melanoma) or 48 h with or without 24 h of additional treatment with H_2O_2 (monocytes). 20 μl of CellTiterBlue was added per well after 48 h and incubated for another 3 h before fluorescence was detected.

7.2.9 Transwell-migration assay

Migration properties of melanoma cell line WM3734 was determined in a transwell-migration assay. Within this assay, cells were allowed to adhere to and migrate through a membrane with a specific pore size. The membrane is part of a cell culture insert that was placed in a well of a 24-well plate, thereby creating two compartments: the upper compartment containing cells in their respective medium and a lower compartment (the culture plate well), also containing medium. For this study the role of CRAC channels for migration of melanoma cells was investigated by knockdown of Orai1 and STIM2 using RNAi (see 7.2.5).

WM3734 transwell-migration was determined using cell culture inserts with 8 μm pore size, following the manufacturer's instructions. 24 h after transfection, 1×10^5 Orai1, STIM2 and control siRNA treated cells were loaded with the fluorescent dye Calcein-AM (1 μM) for 25 min at 37 °C. Calcein-AM is a cell permeable dye and is trapped in the cell after cleavage of the AM-group by endogenous esterases in the cytosol. Cell were washed after loading, re-suspended in standard culture medium with 1×10^5 cells/ 200 μl , seeded with 200 μl / insert and placed in 24-well plates. Cells were allowed to adhere to the membrane of the insert and migrate for 24 h (37 °C, 5 % CO_2). Inserts were then placed into wells containing 1 ml accutase, for detachment of the cells from the downside of the membrane for 20 min (37 °C, 5 % CO_2). Amount of migrated cells was detected by measuring Calcein fluorescence using the Tecan infinite M200 Pro Plate Reader with a 470/525 nm excitation/emission and a bottom reading setting. Accurate cell number was calculated from Equation 6, based on a calibration curve ($R^2 = 0.985$), determined from three independent measurements using Calcein-loaded cells with defined cell numbers ranging from 1×10^2 – 1×10^5 .

Equation 6 Cell number = $\text{RFU}/0.037$

7.2.10 Detection of cytokines using ELISA

IL-8 production by SK-MEL-5 cells was measured using the QuantiGlo[®] Human IL-8 Chemiluminescent Immunoassay. QuantiGlo works as a sandwich enzyme linked immunosorbent assay (ELISA). To bind IL-8 from a sample a monoclonal IL-8 antibody is immobilized on a microplate. Within the assay, IL-8 from the sample binds to the antibody and non-bound sample components are removed in a wash step. Next, a polyclonal IL-8 antibody is added to bind the Fc region of IL-8. Since IL-8 from the sample is bound from two sides, this way of detection is referred to as "sandwich assay". The polyclonal antibody is conjugated to a functional peroxidase. This enzyme reacts with the luminol substrate added in the last step, producing light.

This way of chemiluminescence detection (light generation by enzyme activity) eliminates background interferences and is more sensitive than other methods. The intensity of emitted light is proportional to the amount of bound IL-8.¹⁶

In order to measure IL-8 production by SK-MEL-5 cells, samples were taken from supernatants of proliferation experiments with a total volume of 120 μl (pooled from according triplicates) and diluted with $\text{H}_2\text{O}_{\text{dest.}}$ (1:2). Samples were treated following the manufacturer's instructions. 50 μl of diluted sample were placed in the prepared antibody coated wells of the provided 96-well plate, mixed with the provided assay diluent and incubated for 2 h (RT, shaking) to enable IL-8 in the sample to bind to the immobilized antibodies. Wells were washed three times and 200 μl of provided IL-8 conjugate (containing the polyclonal IL-8 antibodies) were added to each well. After an incubation period of 3 h (RT, shaking), the wells were carefully washed as described before. 100 μl of freshly prepared luminol substrate (mixture of enhanced stabilized luminol and stabilized hydrogen peroxide, 1:2) were added to each well, incubated for 20 min. Developed luminescence was measured using the Tecan GeniosPro reader with 1000 ms lag-time and 500 ms read-time. All conditions were measured in duplicates. IL-8 concentration was calculated using a calibration curve (Equation 7, with $R^2 = 0.987$), that was drawn from one of two independent collected standard curves based on a provided IL-8 standard.

$$\text{Equation 7 IL-8 (pg/ml)} = ((\text{Mean RLU} - S_0 (\text{zero value of standard curve})) / 733.92)$$

7.2.11 Data Analysis and Statistics

Figures and graphs. Data analysis was performed using the software Microsoft Office Excel and Origin Pro 6.1 if not otherwise indicated. All line and bar graphs were plotted with Microsoft Excel, with exception of the box-plot-whisker-diagrams and diagrams for IC_{50} determination that were plotted with Origin Pro. All figures and schemes presented in this dissertation were edited using CorelDraw X4.

Statistics. Data is presented as mean or median with error bars indicating the standard error of the mean (SEM). For determination of statistical significance of the obtained results, the standard student T-Test (paired or un-paired) was applied. The T-Test was also applied under non-optimal conditions, when sample size was < 30 and when data sets did not follow a gaussian distribution. Significant changes are indicated with * for $p < 0.05$, ** for $p < 0.01$ and *** for $p < 0.001$. All data sets were tested for outliers using the free-available outlier calculator (graph pad) and outliers with a significance level of 0.01 were excluded from calculations.¹⁷

¹⁶ <http://www.rndsystems.com/pdf/q8000b.pdf>

¹⁷ <http://www.graphpad.com/quickcalcs/Grubbs1.cfm>

8 Results

8.1 Characterization of investigated cell types

8.1.1 Orai and STIM expression profiles

An essential part of the characterization of SOCE and the analysis of the individual CRAC channel components required investigation of their expression patterns. The expression levels of Orai and STIM family members in primary human monocytes (day 1-3 after isolation) and three different melanoma cell lines (SK-MEL-5, SK-MEL-28 and WM3734) were compared to reference genes, using qRT-PCR. The three melanoma cell lines were chosen due to their difference in origins. SK-Mel 28 derived from a primary melanoma, while SK-MEL-5 and WM3734 derived from metastatic melanoma (see 7.1.6 for details). The results of qRT-PCR, presented in Figure 9 (A and B), revealed a distinct expression of the single isoforms in the different cell types. In monocytes Orai1 and Orai2 as well as STIM1 and STIM2 showed comparable expression levels (Figure 9, A). On the other hand, melanoma cell lines show a significantly higher expression of Orai1 and STIM2 compared to Orai2 and Orai3 and STIM1, respectively (Figure 9, B). In all tested cell lines Orai1 expression exceeded Orai2 with $2^{-\Delta\Delta Cq}$ values being 6-, 12- and 7- fold higher for SK-MEL-5 (2.21 to 0.18, Orai1/Orai2), SK-MEL-28 (1.96 to 0.31, Orai1/Orai2) and WM3734 (1.57 to 0.22, Orai1/Orai2), respectively. Similarly, STIM2 expression level was higher than that of STIM1 in all tested cell types. The expression level was increased 5-fold for SK-MEL-28 and WM3734 (1.43 or 1.56 to 0.28 or 0.32, STIM1/STIM2) and 4-fold in the case of SK-MEL-5 (1.12 to 0.29, STIM1/STIM2). In all cases (monocytes and melanoma) expression levels of target genes were normalized to the reference gene TBP. In monocytes, Orai3 was the least expressed isoform with an absolute expression value of 0.13 ($2^{-\Delta\Delta Cq}$). Melanoma cell lines showed a higher Orai3 expression with 0.43 and 0.34 for SK-MEL-28 and SK-MEL-5, respectively. WM3743 Orai3 expression with a $2^{-\Delta\Delta Cq}$ value of 0.11 was lower than that of other melanoma cell lines, but comparable to expression levels in monocytes. Among the Orai isoforms, Orai2 was the least expressed in melanoma cell lines.

In order to verify whether the differences observed in mRNA expression levels also exist on protein levels, western blot analysis was performed for melanoma cell lines. The expression of Orai1 and STIM2 was compared to GAPDH, which served as reference and loading control. Representative blots are shown in Figure 9 (C and D). In the investigated cell lines, Orai1 and STIM2 showed variable protein levels (reflected by differences in band size and run point), which can be explained by different post-translational modifications. Orai1 protein runs as two distinguishable bands due to differences in post-translational glycosylation. The non-glycosylated protein runs at the expected 34 kDa, while the complex glycosylated protein runs at 55 kDa. (Figure 9, C). STIM2, that has an estimated molecular weight of 100 kDa, depicted a major band between 95 and 110 kDa and several smaller bands between 80 and 95 kDa (Figure 9, D).

8.1.2 The relative expression of Orai proteins regarding their redox properties

The relative expression of the different isoforms of Orai and STIM proteins, rather than the absolute expression, are more likely to shape SOCE in different cell types. Orai3 is the least expressed isoform in monocytes and relatively low expressed in melanoma cell lines (Figure 9). Its relative expression though showed interesting differences. Orai3 has distinguishable biophysical and pharmacological properties when compared to Orai1 and Orai2, which bear

Results

relatively comparable properties (see 6.4.1). The current study focused on differences in redox-properties and the relative expression of the isoforms. Thus, the relative expression of the redox-insensitive isoform Orai3 to the sensitive isoform Orai1 (Orai3/Orai1) was determined for primary human monocytes and melanoma cell lines using the corresponding $2^{-\Delta\Delta Cq}$ values (Figure 10).

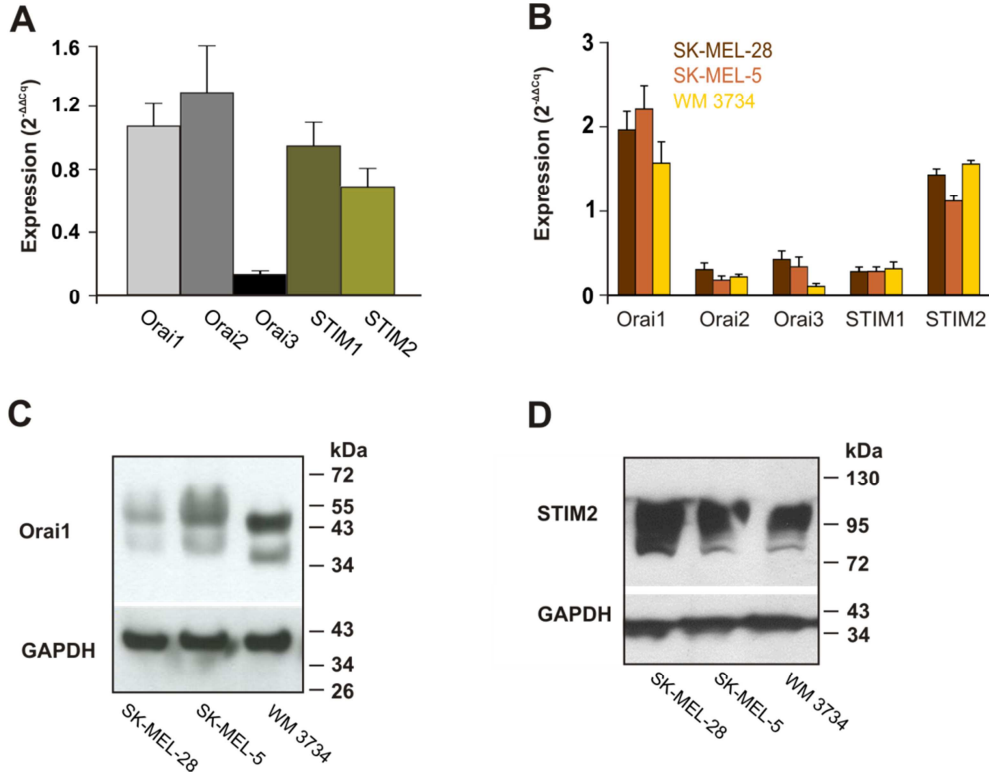


Figure 9 Expression of Orai and STIM isoforms in primary human monocytes and melanoma cell lines.

Expression pattern of Orai and STIM isoforms in investigated cell types was determined by qRT-PCR and western blot. (A) mRNA levels determined for primary human monocytes. (B) mRNA levels determined for human melanoma cell lines SK-MEL-28 (brown), SK-MEL-5 (orange) and WM3734 (yellow). (C-D) Representative western blots of Orai1 (C) and STIM2 (D) expression in human melanoma cell lines normalized to the reference gene GAPDH (loading control). Expression of mRNA indicated as $2^{-\Delta\Delta Cq}$ values averaged from $n = 8$ (monocytes) and $n = 3$ (melanoma cell lines) experiments, normalized to the reference gene TBP. Error bars indicate SEM.

In a recent study (Bogeski *et al.*, 2010), relative Orai3 expression was determined for CD4⁺ T helper cells (naïve and effector). These values are presented in Figure 10 (grey shades) for comparison with permission of the authors. With a ratio value of 0.04 effector T cells showed 2-fold higher relative Orai3 to Orai1 expression than naïve cells. Monocytes (blue) showed a ratio value of 0.15, reflecting a 3.5-fold higher relative Orai3 expression compared to effector T cells. The melanoma cell lines were variable, with SK-MEL-5 (orange) being comparable to monocytes while SK-MEL-28 displayed a significantly higher ratio of 0.21 (brown). WM3734 displayed a significantly lower ratio of 0.07 (yellow). These ratio values and their functional influence were important for different aspects of this study and are further discussed below.

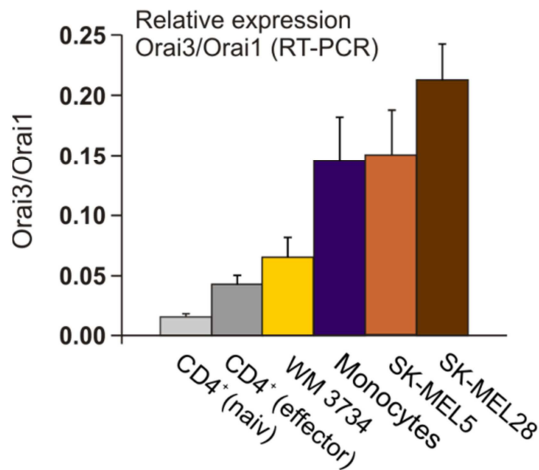


Figure 10 Relative Orai3 expression levels.

Relative Orai3 to Orai1 expression ratio calculated from $2^{-\Delta\Delta Cq}$ values from qRT-PCR data with $n = 5$ (CD4⁺ T cells), $n = 7$ (monocytes), $n = 3$ (melanoma cell lines) independent experiments. Data for CD4⁺ T cells (naïve and effector) was taken with permission from Bogeski *et al.* (Bogeski *et al.*, 2010) and is depicted here for comparison with monocyte and melanoma data.

8.1.3 Validation of RNAi

Down-regulation on mRNA level of the single Orai and STIM isoforms was achieved by application of RNAi technology. Cells were transfected with specific siRNAs, followed by intracellular Ca²⁺ imaging experiments to decipher the importance of the missing protein on SOCE. For monocytes, the results are presented in Figure 11 (A) as averages of at least three independent experiments. Expression values were determined both for control non-targeting RNA (NT RNA) transfected cells (CTRL, black) and cells transfected with specific siRNA targeting the single Orai or STIM isoform (siRNA, red). The efficiency of RNAi was determined as the percentage of change in relative expression values (Figure 11, B), displaying high variation depending on the different siRNA. Percentages were calculated from $2^{-(\Delta\Delta Cq)}$ values for the single isoforms to the respective controls. Knockdown of Orai1 and Orai3 mRNA was nearly complete with 93% and 88%, respectively (light grey and black). The knockdown of Orai2 and STIM1 was less effective with 74% and 71% (grey and dark green). In the case of STIM2 the used siRNA deleted 47% (light green) of the respective mRNA.

Efficiency of knockdown of siRNAs targeting Orai1 and STIM2 was also monitored on protein level by Western blot analysis for SK-Mel5 melanoma cells. Lysates obtained from NT RNA (CTRL) or Orai1 or STIM2 siRNA transfected SK-MEL-5 cells were probed with the respective Orai1, STIM2 or control (GAPDH) antibodies. The representative blots in Figure 11 (C and D), show that Orai1 and STIM2 proteins were successfully down-regulated. Cross reactivity of STIM siRNA was excluded by probing for STIM2 in STIM1 down-regulated cells. The resulting blot (Figure 11, D) showed an unaltered STIM2 expression level compared to the control.

The same siRNAs were used for RNAi in monocytes and melanoma cell lines. Orai1, Orai3 and STIM1 siRNAs were previously tested for specificity and efficiency and regularly used in the laboratory at the beginning of this study. Orai2 and STIM2 siRNAs were tested during this study and two sequences were selected to perform the presented experiments. In order to rule out possible cross reactivity of the individual siRNAs on other Orai or STIM isoforms, the expression of all 5 isoforms (Orai1-3 and Stim1-2) was monitored by qRT-PCR in each knockdown experiment. The tested siRNAs showed isoform specificity with the exception of Orai3 siRNA. The down-regulation of Orai3 was accompanied by down-regulation of Orai1 mRNA levels by 20% on average ($n = 6$, data not shown). Other siRNAs did not show any interference with the expression of other isoforms.

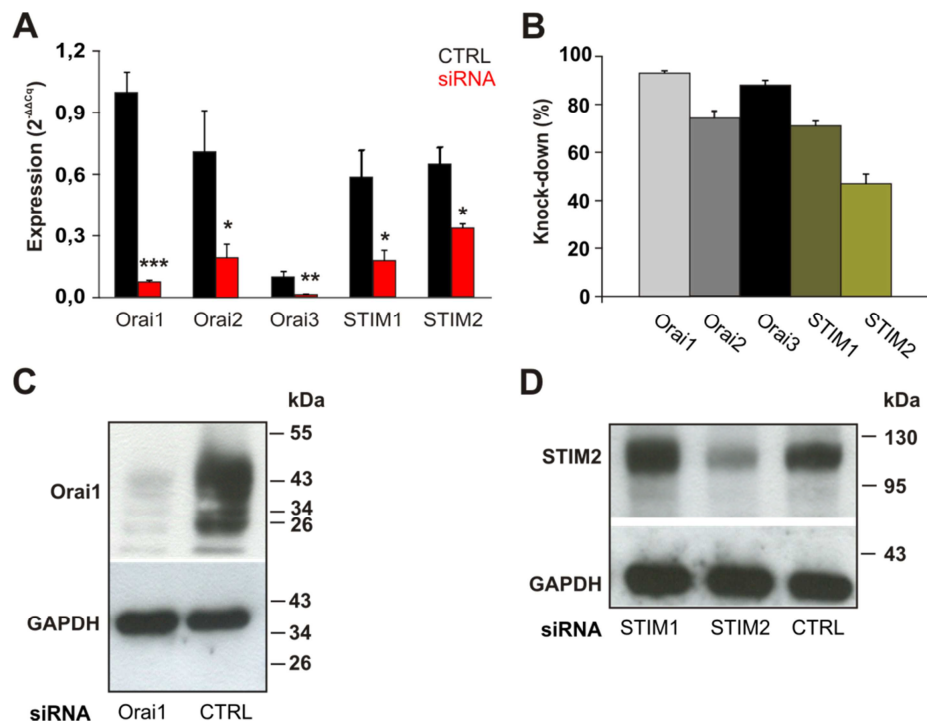


Figure 11 Confirmation of RNAi induced down-regulation of Orai and STIM isoforms in human monocytes and melanoma cell lines.

(A-D) Samples from primary human monocytes and SK-MEL-5 cells, transfected with siRNA targeting the single CRAC channel subunits, were collected 48h after transfection, transcribed to cDNA and subjected to qRT-PCR or used for western blot analysis. Results of qRT-PCR presented as $2^{-\Delta\Delta Cq}$ values. (A) mRNA levels determined for NT RNA transfected (black) and Orai1-3 and STIM1 and STIM2 siRNA transfected cells (red). (B) Success of down-regulation presented as percent of control. Means were calculated from $n = 6$ (Orai1), $n = 4$ (Orai2), $n = 8$ (Orai3), $n = 4$ (STIM1) and $n = 4$ (STIM2) independent experiments. (C-D) Representative western blots of samples from NT RNA and Orai1 and STIM2 siRNA transfected SK-MEL-5 cells. Error bars indicate SEM and significance of knockdown is indicated with *, $p < 0.05$, **, $p < 0.01$ and ***, $p < 0.001$, determined by the paired standard student's t-test.

8.1.4 Characterization of primary human monocyte phenotype

The isolation of primary human monocytes from PBMCs was achieved either by bead-isolation or adhesion. While bead isolation provided a nearly 100% pure monocyte population, the adhesion method was more prone to contain a fraction of lymphocytes from the PBMCs. Not only purity, but also the phenotype of the monocyte subset was of interest for further experiments. The phenotype of isolated monocytes and the purity of the isolation protocol were therefore confirmed in three in-dependent flow cytometry experiments.

Figure 12 (A) shows a representative dot plot of a monocyte fraction at day three after isolation by adhesion. In a first step, the lymphocyte-monocyte fraction was gated based on size and granularity (marked in blue, first plot in A). Smaller (and more granular) cells were identified as apoptotic cells or cell debris (lower left corner, A). In a second step, the monocyte fraction was gated (marked in blue, second plot in A). The overall percentage of lymphocytes in the monocyte fraction was 19.65 %, revealing a purity of 80.35% for monocytes using the adhesion-method for isolation (Figure 12, B). The identification of the monocyte subset was preliminary based on the determination of the expression of the surface markers CD14, CD16 and HLA-DR (see 7.2.3 for argumentation for choice of markers).

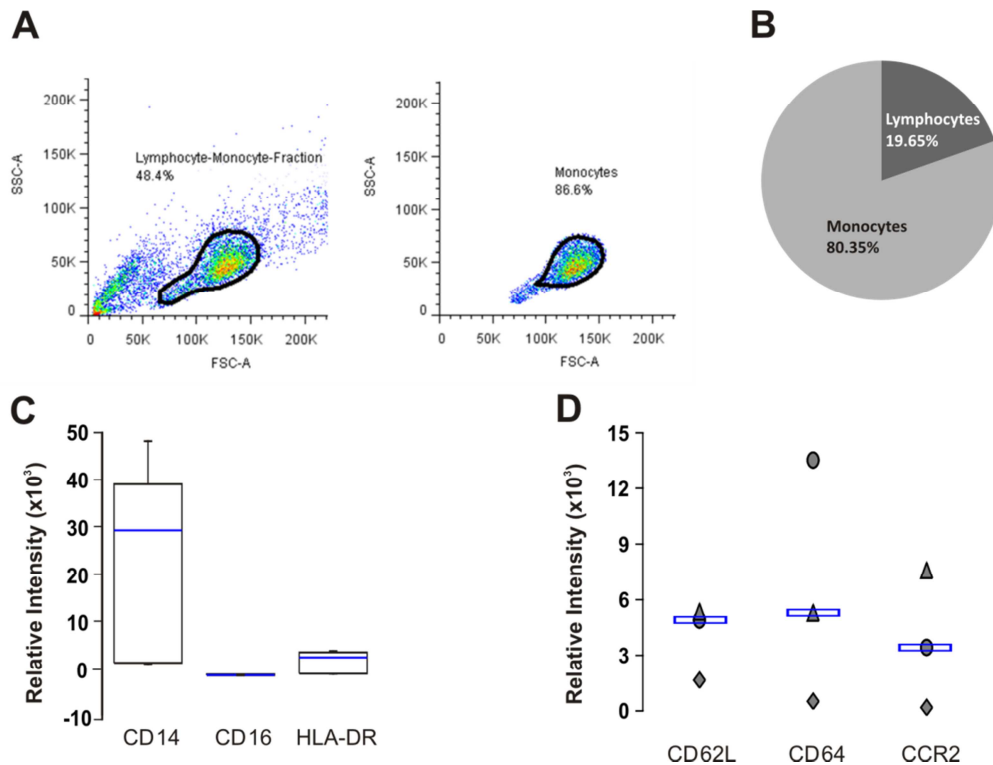


Figure 12 Characterization of monocyte subset using flow cytometry

The purity of isolation of primary human monocytes by adhesion and the definition of the monocytes subset was analyzed by flow cytometry. (A) Representative dot plots of flow cytometry measurements of a monocyte population. Side scatter (SSC) reflects the granularity of cells, while the forward scatter (FSC) indicates the size of the cells. Lymphocyte-monocyte-fraction gated based on size and granularity (blue, first plot) and the monocyte fraction was further gated within the first population (blue, second plot). (B) Purity of monocyte fraction was determined with 80.35%. (C) Expression of surface markers was determined on relative fluorescent intensities of fluorophore-conjugated antibodies targeting CD14, CD16 and HLA-DR. Presented as box-plot-whisker-diagrams, indicating the median (blue), minimal and maximal values and boxes enclosing 25% -75% of the data points. Purity and expression levels of CD14, CD16 and HLA-DR were based on $N = 3$, number of isolations and $n = 22$, number of performed measurements. (D) Expression of additional surface markers CD62L, CD64 and CCR2 determined from, $N = 3$ independent isolations and $n = 3$ independently performed measurements per isolation. Data is presented as single data points (one geometrical figure presents one data set) and median fluorescent intensity is indicated in blue.

The expression was determined within the gated monocyte fraction (A) as relative fluorescent intensities measured from fluorophore-conjugated antibodies targeting the different surface markers. Results are presented as box-plot-whisker-diagrams indicating the median levels (blue). The presented monocyte subset was identified as $CD14^{\text{high}}$ (30.31×10^3), $CD16^-$, with intermediary expression of HLA-DR (3.59×10^3) (Figure 12, C). Expression of additional surface markers was determined for a more detailed characterization (Figure 12, D). CD62L, a leukocyte antigen responsible for rolling and adhesion of monocytes in blood vessels showed an intermediary expression with a median fluorescent intensity of 4.89×10^3 . CD64, the Fc γ RIII receptor and CCR2, a chemokine receptor responsible for chemoattraction of the cells to sites of infections likewise showed an intermediary expression with median fluorescent intensities of 5.28×10^3 and 3.42×10^3 . Intensities for CD62L, CD64 and CCR2 are presented as single data points with the median indicated in blue (Figure 12, D).

8.2 Store-operated calcium entry (SOCE) in human melanoma cell lines and monocytes

8.2.1 Activation and features of SOCE in human monocytes

The characterization of SOCE in the investigated cell types was based on Ca^{2+} imaging experiments. The SERCA blocker Thapsigargin (Tg) was used as activator of SOCE following a store-depletion protocol. This protocol triggers SOCE and allows measurement of changes in cytosolic $[\text{Ca}^{2+}]_i$, thereby separating the depletion of the internal calcium stores and the influx *via* activated CRAC channels. The protocol is described below (and in 7.2.7.2). and was used for all following calcium imaging experiments, unless otherwise indicated.

Cells were perfused with Ringer solution containing 0.5 mM Ca^{2+} to generate a base line. After 250s cells were perfused with buffered Ringer's solution (0 mM Ca^{2+}) to distinguish pre-activated cells. The stimulus (Tg or fMLF) was added in buffered 0 mM Ca^{2+} Ringer's solution 750s after start of recording, to empty the internal Ca^{2+} stores by blockage of SERCA (see introduction and Materials for details). The emptying of the stores, leads to an increase in intracellular, cytosolic calcium ($[\text{Ca}^{2+}]_i$) termed, Tg- Ca^{2+} release. After another 750 s, Ca^{2+} was re-added to the extracellular solution by perfusion with Ringer's solution, containing 0.5 mM Ca^{2+} together with the corresponding stimulus. The following rise in $[\text{Ca}^{2+}]_i$ was mediated by the prior activated CRAC channels. This protocol was used to determine the effect of Orai and STIM knockdowns on SOCE and hence their contribution to calcium signaling. Initially the activation of SOCE was tested in primary human monocytes on day 1-3 after isolation using two different stimuli: Tg and fMLF. Tg served as artificial, but well tested and acknowledged trigger of SOCE. In contrast, fMLF served as physiological stimulus; by triggering SOCE *via* binding to a PAMP recognition receptor specific to detect formylated peptides deriving from bacteria (see also Table 8 for details). The two different stimuli triggered Ca^{2+} responses with distinct features (Figure 13, A). The depletion of internal stores following fMLF stimulation resulted in a high, but transient rise in $[\text{Ca}^{2+}]_i$ with a Ca^{2+} influx rate of 7.7 nM/s. A lower, but prolonged rise in $[\text{Ca}^{2+}]_i$ with an influx rate of 0.3 nM/s was observed following a Tg stimulation (Figure 13, B, Release). The Ca^{2+} influx *via* CRAC channels, following the re-addition of extracellular Ca^{2+} showed a rate of 5 and 2.5 nM/s for Tg and fMLF, respectively (Figure 13, B, Entry). The Tg stimulation resulted in an increase in $[\text{Ca}^{2+}]_i$ with a peak Ca^{2+} of 496.9 nM and the development of a plateau phase with 163.3 nM Ca^{2+} (Figure 12, C). The plateau phase was calculated as $\Delta\text{Calcium}$ between $[\text{Ca}^{2+}]_i$ at 1500 s (beginning of re-addition phase) and $[\text{Ca}^{2+}]_i$ at 2250 s (end of re-addition phase). fMLF stimulation displayed a smaller peak Ca^{2+} and plateau with 198.4 nM and 23 nM (see quantification in Figure 13, C).

In addition, the elevation of SOCE using Tg or fMLF was analyzed regarding the response to the SOC inhibitor 2-APB. SOCE was measured using Tg or fMLF in Ringer's solution containing 1 mM $[\text{Ca}^{2+}]_i$ (Figure 13, D and E, black traces). Stimulation with Tg and fMLF in the presence of 2-APB (Figure 13, D and E, green traces) resulted in the significant decrease in peak calcium. $[\text{Ca}^{2+}]_i$ decreased from 930.6 nM to 130.8 nM under Tg stimulation and from 1028.7 nM to 410.6 nM under fMLF stimulation (Figure 13, F).

Regarding the important parameters for characterization of SOCE (peak calcium and $\Delta\text{Calcium}$), Tg stimulation revealed a higher and prolonged signal compared to fMLF stimulation (Figure 13 A-C). Based on these results, Tg was the stimulus of choice for further calcium imaging experiments (see also 9.1.3 for a detailed discussion of stimuli choice).

Results

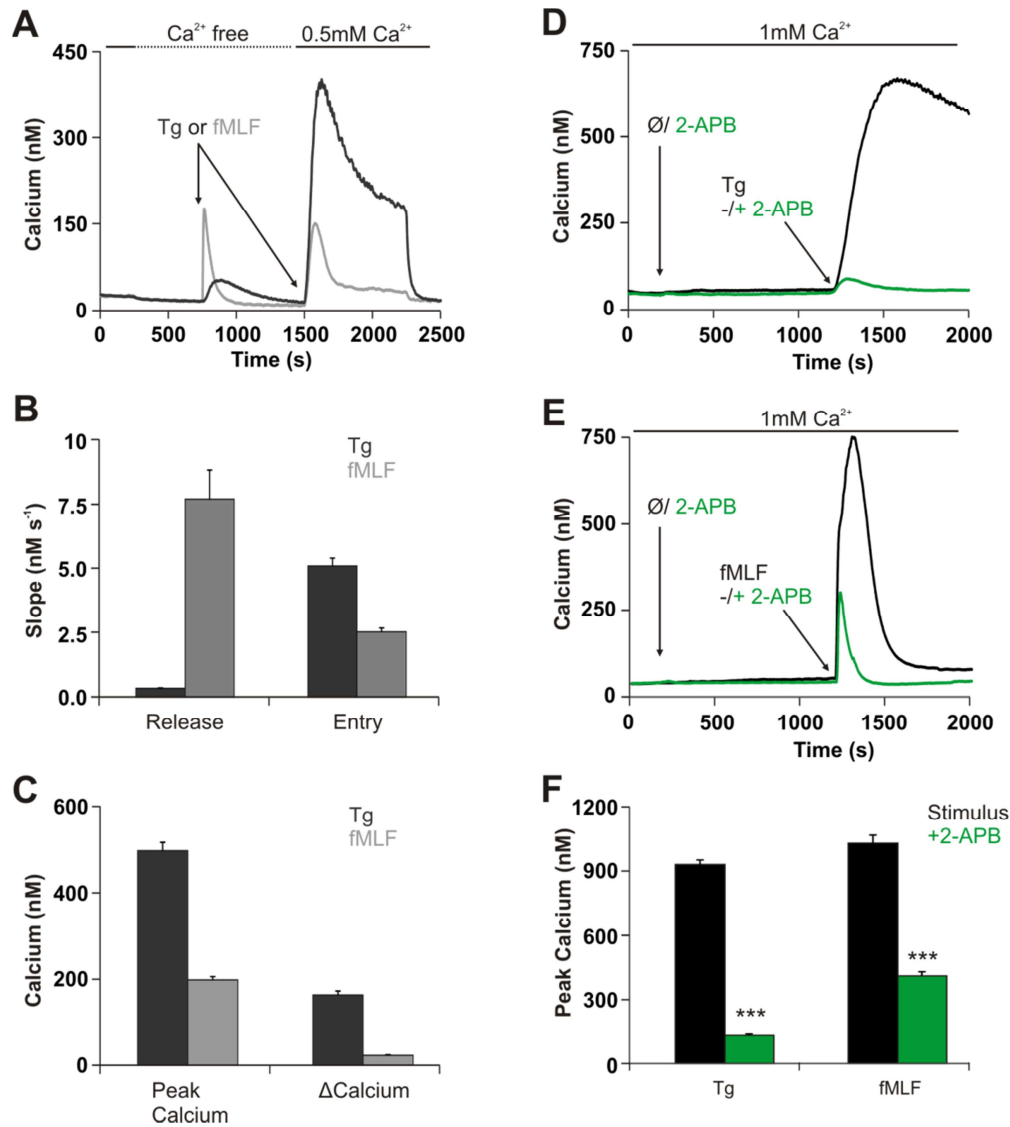


Figure 13 Activation and inhibition of SOCE in monocytes using two different stimuli.

Fluorescence based calcium imaging experiments to characterize SOCE in primary human monocytes. (A-C) Thapsigargin (Tg) and fMLF triggered SOCE in human monocytes. (A) Comparison of SOCE, triggered by Tg (black) or fMLF (grey). Stimuli were applied in Ca^{2+} -free solution (black arrow) to deplete internal Ca^{2+} stores (1st rise in $[\text{Ca}^{2+}]_i$) and activate CRAC channels. Re-addition of Ca^{2+} (0.5 mM) allowed SOCE through activated channels (2nd rise in $[\text{Ca}^{2+}]_i$). (B) Quantification of Ca^{2+} influx rates (slope) of store release (stimulus in Ca^{2+} -free Ringer's solution) and Ca^{2+} entry *via* activated channels (stimulus in 0.5 mM Ca^{2+} Ringer's solution). (C) Quantification of maximal Ca^{2+} values (Peak Calcium) and height of plateau phase after Ca^{2+} re-addition ($\Delta\text{Calcium}$). (D) Tg-triggered SOCE in 1 mM Ca^{2+} Ringer's solution in absence (black trace) and in presences (green trace) of the store-operated channel inhibitor 2-APB (50 μM). (E) fMLF-triggered SOCE in 1 mM Ca^{2+} Ringer's solution in absence (black trace) and in presences (green trace) of the SOC inhibitor 2-APB (50 μM). (D and E) Cells were incubated with buffer (\emptyset) or 2-APB for 10min before activation of SOCE. (F) Quantification of peak Ca^{2+} in control conditions (black bars) and in presence of 2-APB (green bars). Results are presented as means calculated from at least 3 independent experiments with total number of analyzed cells (n): n = 690 (Tg), n = 602 (fMLF), n = 606/292 (Tg -/+ 2-APB) and n = 803/714 (fMLF -/+ 2-APB). Error bars indicate SEM with significance of change in peak calcium by 2-APB treatment indicated as ***, p < 0.001, determined using the unpaired student's t-test.

8.2.2 Investigation of the contribution of CRAC channel components to SOCE in human monocytes.

The contribution of the single CRAC channel components (Orai) and the regulator proteins (STIM) to Ca^{2+} signaling in monocytes was analyzed by Ca^{2+} imaging. RNAi knockdown of the single isoforms Orai1-3 and STIM1-2 using specific siRNAs facilitated the investigation of the role of the individual channel and regulator molecules in detail. Primary human monocytes were isolated from PBMCs, transfected immediately after isolation and measured after 48 h. Transfection with NT RNA was performed in all conditions (referred to as control or CTRL RNA). The previously described store-depletion protocol (8.2.1) was applied to analyze changes in intracellular (cytosolic) Ca^{2+} concentration ($[\text{Ca}^{2+}]_i$). The depletion of the internal ER-store release by Tg was not-affected by the knockdown of the single Orai and STIM isoforms (Figure 14, A-E).

The siRNA mediated knockdown of Orai1, Orai2, STIM1 and STIM2 (blue traces in Figure 14) resulted in a significant decrease in SOCE compared to the corresponding controls (black traces in Figure 14). Conversely, the knockdown of Orai3 resulted in a small, though not significant, increase in SOCE (Figure 14, C). SOCE was quantified as $\Delta[\text{Ca}^{2+}]_i$ between the end of the plateau phase and before re-addition of 0.5 mM Ca^{2+} . The control transfected cells showed highly variable Ca^{2+} responses ranging from 248 nM to 473 nM. Therefore, the effects of the knockdown of the different isoforms were presented as percentages of the corresponding control measurements (Figure 14, G), providing a more reliable parameter. The knockdown of STIM1 resulted in the strongest reduction of SOCE by 54%, while knockdown of STIM2 or Orai1 lead to a milder and comparable reduction of 38% and 36%, respectively. The smallest reduction was observed with knockdown of Orai2, which resulted in a 25% decrease in SOCE. On the other hand, Orai3 down-regulation resulted in a 9% increase in SOCE.

8.2.3 Investigation of SOCE in human melanoma cell lines SK-MEL-5 and WM3734

Orai1 and STIM2 were identified as major expressed isoforms in the investigated melanoma cell lines (Figure 9, panel B). Therefore, the contribution of these two isoforms in SOCE was further investigated using calcium imaging. SOCE was measured in SK-MEL-5 and WM3734 cell lines not only to characterize Ca^{2+} signals, but also to determine possible differences due to the origins of the cell lines (primary tumor vs. secondary brain metastasis, see 7.1.6). The store-depletion protocol was slightly modified compared to monocyte experiments. The initial perfusion with Ca^{2+} containing Ringer's solution was omitted and 0.25 mM instead of 0.5 mM Ca^{2+} was used for Ca^{2+} re-addition. The chosen Ca^{2+} concentrations for re-addition were optimal to detect changes in SOCE in the respective cell types (experimental observation). In general, a lower Ca^{2+} concentration is suitable to detect even small effects of a knockdown. In the case of monocytes, 0.5 mM Ca^{2+} was the lowest concentration applicable, regarding overall cell responses.

Thapsigargin stimulation elevated Ca^{2+} signals in SK-MEL-5 and WM3734 cell lines (Figure 15, A and C), that showed a quick run-down after Ca^{2+} re-addition; hence a plateau phase was not definable. Changes in SOCE resulting from knockdown of the different genes were therefore estimated from the change in the influx rates (slope) in siRNA treated cells, compared to the respective controls (black bar graphs in Figure 15 (B and D)).

The SK-MEL-5 and WM3734 melanoma cell lines displayed differing Ca^{2+} signals, with obvious differences in ER- Ca^{2+} content and Ca^{2+} -influx rates under control conditions.

Results

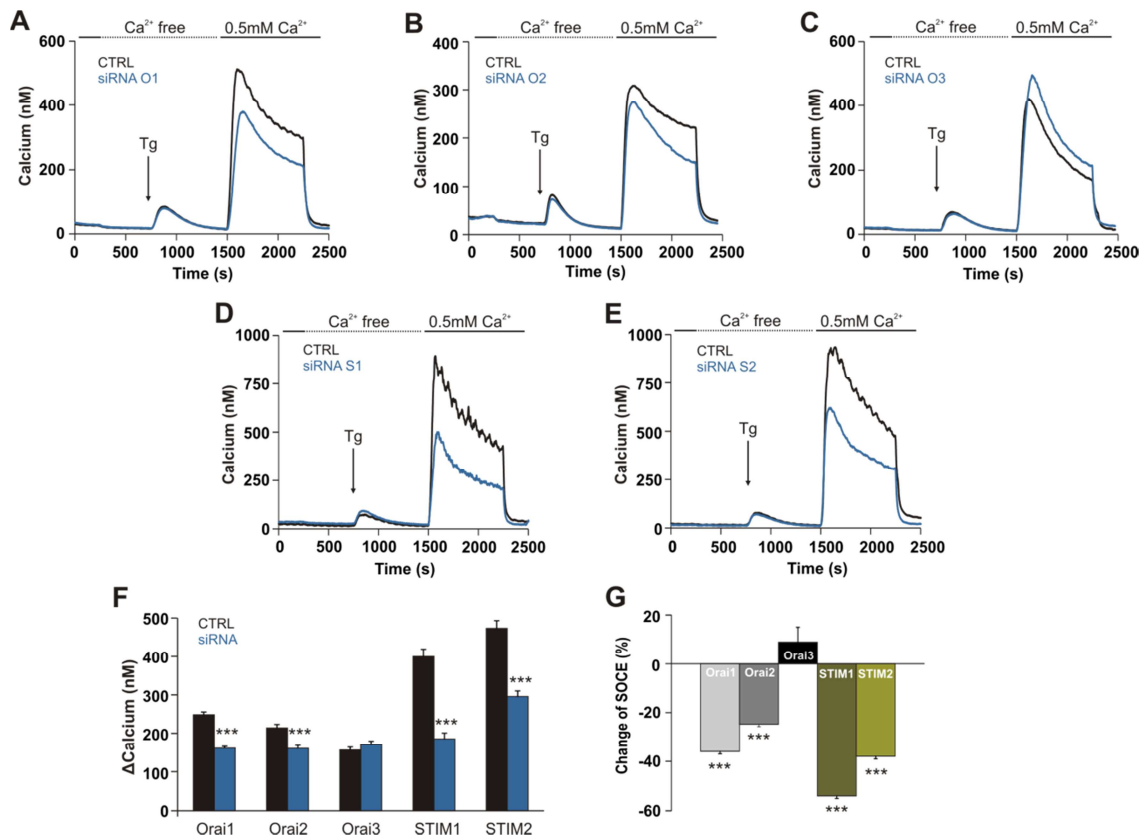


Figure 14 Contribution of single Orai and STIM isoforms to Store-operated Ca²⁺ Entry (SOCE) in primary human monocytes.

Fluorescence-based calcium imaging to characterize the contribution of single CRAC channel components Orai1-3 and STIM-2 to SOCE in primary human monocytes. (A-E) Thapsigargin (Tg) was applied in Ca²⁺ -free solution (black arrow) to deplete internal Ca²⁺ stores (1st rise in [Ca²⁺]_i) and activate CRAC channels. Re-addition of Ca²⁺ (0.5 mM) allowed SOCE through activated channels (1st rise in [Ca²⁺]_i). Averaged Ca²⁺ traces for control transfected cells (CTRL, black) and siRNA transfected cells (blue) for knockdown of Orai1 (A), Orai2 (B), Orai3 (C), STIM1 (D) and STIM2 (E) measured 48 h after transfection. (F) Quantification of SOCE by determination of ΔCalcium on single traces (averaged in A-E), calculated from [Ca²⁺]_i at the end of the plateau phase and [Ca²⁺]_i before Ca²⁺ re-addition. (G) Determination of percent of change (%) due to knockdown of the single isoforms compared to controls. Traces were averaged from at least three independent experiments with number of analyzed cells (n) n = 1132/1178 (CTRL/Orai1), n = 836/740 (CTRL/Orai2), n = 510/618 (CTRL/Orai3), n = 573/580 (CTRL/STIM1) and n = 685/711 (CTRL/STIM2). Error bars indicate SEM and significance of change in SOCE by knockdown of Orai and STIM is indicated with ***, p < 0.001, using the unpaired student's t-test.

In SK-MEL-5 cells, the increase of cytosolic Ca²⁺ following external Ca²⁺ re-addition reached a similar level as that observed after store depletion (first and second peak, black trace in Figure 15, A). In contrast, the activation of CRAC channels in WM3734 cells lead to a significantly higher Ca²⁺ influx compared to the Tg-induced store depletion (first and second peak, black trace in Figure 15, B). The influx rates following Ca²⁺ re-addition were higher in WM3734 than in SK-MEL-5 cell lines (3.47 vs. 1.19 nM/s, black traces and bar graphs, Figure 15). The control traces present a global average of all control transfected cells, while for the bar graphs averages of the single knockdowns are presented with their corresponding controls.

In contrast to the Ca²⁺ signals under control conditions, the effect of single and concomitant knockdown of Orai1 and STIM2 was comparable between the two cell lines. In SK-MEL-5 cells, the down-regulation of Orai1 slowed the calcium influx rate from 1.64 nM/s to 0.18 nM/s, while

Results

the knockdown of STIM2 had a less severe impact with a slowdown from 1.04 to 0.55 nM/s. The double knockdown of Orai1 and STIM2 showed an intermediary effect by decreasing the influx rate to 0.20 nM/s compared to the control value of 1.04 nM/s (Figure 15, B). In the case of WM3734, controls were measured in parallel to the three different knockdowns, providing the same influx rate of 3.47 nM/s for all conditions. This rate was reduced by down-regulation of Orai1 to 0.49 nM/s, of STIM2 to 1.18 nM/s and by the double knockdown to the greatest extent to 0.18 nM/s (Figure 15, D).

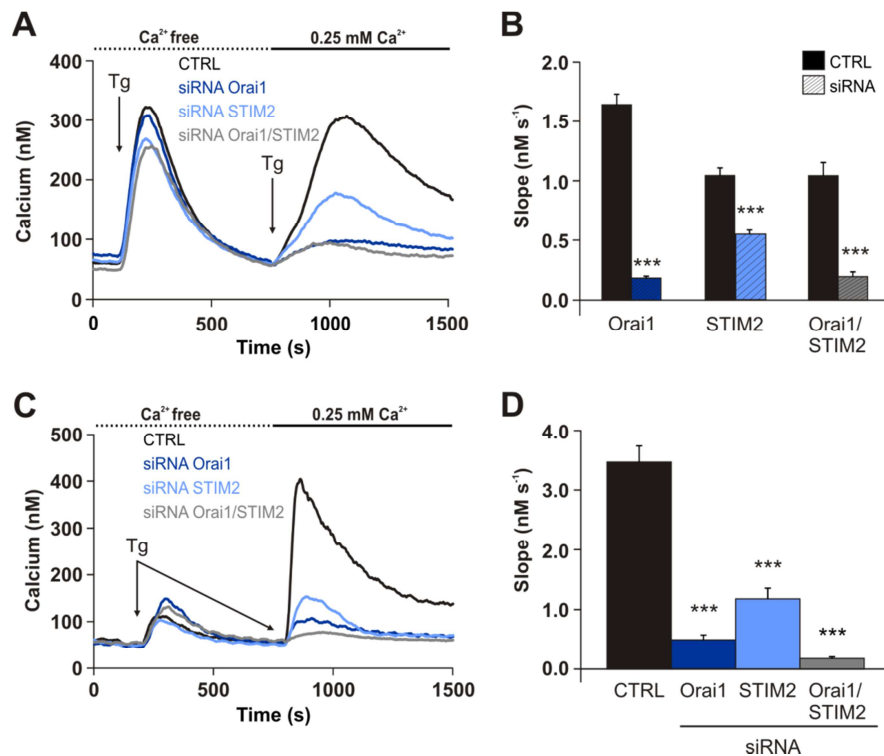


Figure 15 Contribution of Orai1 and STIM2 to Store-operated Ca²⁺ Entry (SOCE) in human melanoma cell lines SK-MEL-5 and WM3734.

Fluorescence based calcium imaging to characterize the contribution of single CRAC channel components Orai1-3 and STIM1-2 to SOCE human melanoma cell lines SK-MEL-5 and WM3734. Thapsigargin (Tg) was applied in Ca²⁺-free solution (black arrows in A and C) to deplete internal Ca²⁺ stores (1st rise in [Ca²⁺]_i) and activate CRAC channels. Re-addition of Ca²⁺ (0.25 mM) allowed SOCE through activated channels (2nd rise in [Ca²⁺]_i). (A and C) Averaged Ca²⁺ traces for control transfected cells (CTRL, black) and siRNA transfected cells for knockdown of Orai1 (blue), STIM2 (light blue) and Orai1/STIM2 (grey) in SKMel-5 (A) and WM3734 (C) cells. (B and D) SOCE was quantified by calculation of calcium influx rates (slope) after Ca²⁺ re-addition for SK-MEL-5 (B) and WM3734 (D). Traces and slopes were averaged from at least three independent experiments with total number of cells (n) analyzed: n = 79/94 (CTRL/siRNA Orai1), n = 157/189 (CTRL/siRNA STIM2) and n = 78/86 (CTRL/siRNA Orai1+STIM2). Error bars indicate SEM and significance of change in influx rates by knockdown of Orai and STIM is indicated with ***, p < 0.001, determined using the unpaired student's t-test.

8.3 Production of reactive oxygen species in primary human monocytes

As professional phagocytes, monocytes are involved in the elimination of intruding pathogens. The production of reactive oxygen species (ROS) is an important factor in the immune response against the intruders. In addition, certain ROS as H_2O_2 serve as second messengers in cellular signaling. SOCE mediated by CRAC channels is accepted to play an important role in phagocytic ROS production, as it is involved in the assembly of NOX. The role of the single Orai and STIM isoforms in this context was so far only investigated in neutrophils and neutrophil-like cell lines, mainly focusing on the Orai1/STIM1 couple (see 6.5.1 for details). Therefore, the ROS production by monocytes regarding the involvement of Ca^{2+} signaling and particularly the role of CRAC channels was analyzed using two different approaches: spectroscopic- and fluorescence-based techniques.

8.3.1 Source and subjection of the production of reactive oxygen species

8.3.1.1 Measurement of superoxide production using electron paramagnetic resonance spectroscopy (EPRS)

EPRS is a well-established and reliable technique to detect reactive radical species as superoxide (O_2^-), that is the main initially produced ROS by NOX and mitochondria. Therefore, EPRS was applied as first technique to determine the source of ROS production in monocytes, as well as the contribution of Ca^{2+} in general. Tg was used as stimulus to trigger activation of SOCE via CRAC channels. The measurement of ROS using EPRS is based on the reaction of O_2^- with a spin trap. This molecule is oxidized upon encountering a radical, thereby forming a stable radical itself, displaying a unique spectroscopic signal. Changes in ROS levels are reflected by changes in the intensity of the spectroscopic signal and were converted to O_2^- concentrations ($[\text{O}_2^-]$), based on a calibration of the system (7.2.6.1). Freshly isolated monocytes were subjected to EPRS measurements and production of O_2^- upon stimulation was recorded for 21 min. The changes in ROS levels were plotted over time (Figure 16, A). The amount of produced ROS was calculated as difference in $[\text{O}_2^-]$ between start (1 min) and end (21 min) of the measurements and is presented as ΔO_2^- (Figure 16, B).

Tg stimulation triggered ROS production displaying a sigmoidal kinetic (Figure 16, A, brown trace) with significant increase in the amount of O_2^- produced from $4\ \mu\text{M}$ to $26.9\ \mu\text{M}$ compared to unstimulated cells (Figure 16, A and B, brown and black traces and bars). Two inhibitors of known components of enzymatic ROS production were applied to confirm the source of measured ROS production. BisGö is an inhibitor of PKC that is involved in phosphorylation of the cytosolic NOX2 subunit p47^{phox} and hence the assembly process (see 6.1.2.3 for details). DPI targets the NOX core complex and is, in comparison to BisGö, a direct inhibitor of the ROS producing enzyme. Inhibition of PKC by application of BisGö (orange trace and bar in Figure 16 A and B), resulted in a significant decrease in Tg triggered ROS production to base line to $4.7\ \mu\text{M}$ (after 21 min). Likewise, following application of DPI, O_2^- production was significantly decreased to $8.04\ \mu\text{M}$ (olive trace and bar in Figure 16 A and B). Elimination of extracellular Ca^{2+} similarly resulted in a significant decrease in ROS production to $2.8\ \mu\text{M}\ \text{O}_2^-$ (blue-green trace and bar in Figure 16, A and B).

The effect of the altered extracellular Ca^{2+} concentrations and NOX inhibitors on Tg-triggered ROS production occurred immediately after application. In the inset in Figure 16 (A), providing an expanded view of the first 10 min of the measurements, it is shown that kinetics of the

treated cells deviate from those of control cells already within 2.5-3 min. The finding that several factors can interfere with the ROS production at an early time point within recording time was the motivation to analyze kinetics of ROS production in more detail (see below 8.3.1.3 and 8.3.2).

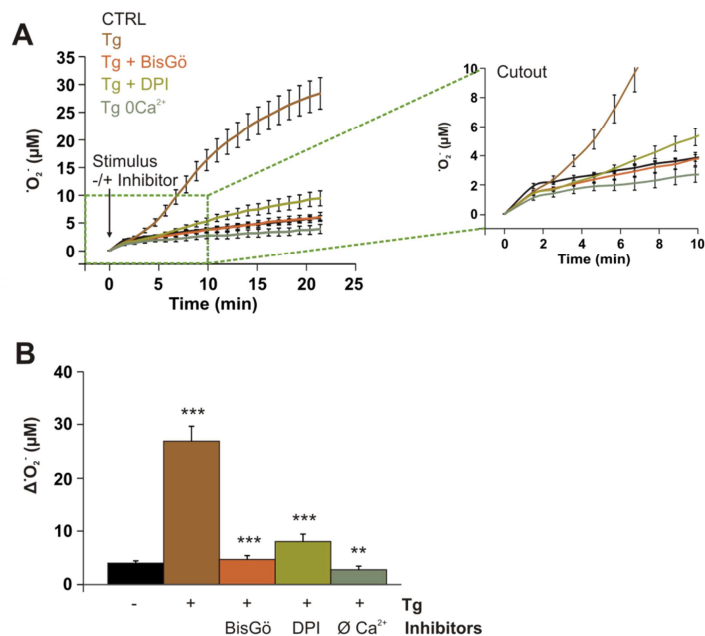


Figure 16 Dependency of superoxide production by primary human monocytes on SOCE

Electron paramagnetic resonance spectroscopy (EPRS) recordings using the CMH spin trap, to characterize the source and the dependency on SOCE of Tg-triggered superoxide production. Monocytes were isolated from PBMCs and subjected to EPRS at day 0 and 1 after isolation. (A) Kinetics of O_2^- production triggered by Tg (brown), with untreated cells as control (CTRL, black), in the presence of the PKC inhibitor BisGö (orange) and the NOX2 inhibitor DPI (olive) and under abolishment of external Ca^{2+} (Ca^{2+} -free Ringer's solution, \emptyset , green). All experiments were performed in 1 mM Ca^{2+} Ringer's solution, despite Ca^{2+} -free condition with $n = 14$ (CTRL), $n = 6$ (Tg) and $n = 4$ (BisGö, DPI and Ca^{2+} -free) independent experiments. Cutout of panel A depicts kinetics in the first 10 min for better visualization. (B) Quantification of superoxide production as ΔO_2^- , calculated as difference in $[O_2^-]$ at the beginning (1 min) and at the end (21 min) of the measurements. For all conditions, 250.00-500.000 cells were used per measurement and superoxide production was normalized to a cell number of 10.000. Error bars indicate SEM and significance is indicated with **, $p < 0.01$ and ***, $p < 0.001$, determined using the unpaired student t-test.

8.3.1.2 Experimental groundwork for measuring H_2O_2 production using the H_2O_2 -sensitive dye AmplexUltraRed

Besides EPRS, a redox-sensitive fluorescent dye was used as second approach to measure ROS production and its Ca^{2+} dependency in more detail. The H_2O_2 -sensitive fluorescent dye AmplexUltraRed (AUR) was used to determine the amount of produced ROS when triggered by different stimuli in the presence and absence of inhibitors of either Ca^{2+} signaling or ROS producing enzymes (Figure 18). Calibration measurements were performed to convert the measured fluorescence intensity into H_2O_2 concentrations ($[H_2O_2]$). Three independent experiments were performed, determining the fluorescence intensity of AUR in Ringer's solution in absence of cells and in presence of H_2O_2 concentrations ranging from 1 nM to 1 μ M. Measured relative fluorescence intensities were plotted as relative fluorescent units (RFU) against the applied $[H_2O_2]$. The resulting data showed linear correlation with a regression factor of 0.999 (Figure 17, A). The equation describing the linear fit was used to convert obtained RFUs from measurements to $[H_2O_2]$.

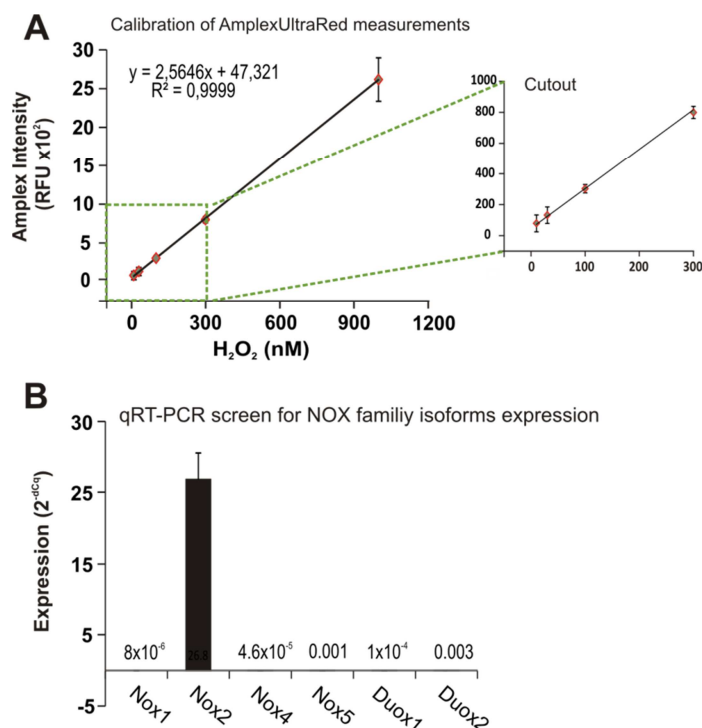


Figure 17 Preparatory experiments for fluorescence-based detection of H_2O_2 and interpretation.

(A) Calibration of fluorescence based AmplexUltraRed (AUR) measurements to quantify H_2O_2 concentrations. Linear curve fit of fluorescence intensity of AUR in dependency of different concentrations of H_2O_2 from three independent experiments with a regression factor of 0.99. The curve equation was further used to quantify experiments. Cutout of (A) shows curve linearity in the low concentration range. (B) Expression profile of NADPH oxidase (NOX) 1-5 and Dual oxidase (Duox) 1 and 2 in primary human monocytes. Expression was determined by qRT-PCR, normalized to the reference gene TBP and is presented as $2^{-\Delta\Delta Cq}$ values, averaged from five donors. Error bars indicate SEM.

In EPRS measurements, the unspecific inhibitor of NADPH oxidases, DPI significantly decreased Ca^{2+} -dependent ROS production. A qRT-PCR screen was performed to estimate the expression level of all seven NOX family members in monocytes and to identify the responsible isoform(s), relevant to the measured ROS (7.2.2.4). The expression was estimated from the obtained $2^{-\Delta\Delta Cq}$ values, normalized to the reference gene TBP (Figure 17, B). NOX2 showed the highest expression level in primary human monocytes with a $2^{-\Delta\Delta Cq}$ value of 26.8. Other NOX and Dual oxidase (Duox) isoforms were expressed at much lower levels ($2^{-\Delta\Delta Cq} \leq 0,003$), while NOX3 expression was below the detection limit.

8.3.1.3 Ca^{2+} dependency of H_2O_2 production

In order to further analyze the Ca^{2+} dependency of ROS production and in more detail, the contribution of the single Orai and STIM isoforms in this process, an additional technique was applied. The H_2O_2 sensitive fluorescent dye AmplexUltraRed (AUR) was chosen due to two aspects: First, although superoxide is the initial produced ROS by NOX2, H_2O_2 is the biological most-relevant species (see 6.1.2.2 for details). Secondly, the effect of ROS, and specifically H_2O_2 as signaling molecule, on SOCE was an aspect of the here presented study. It was therefore reasonable to choose a species-specific detection method. Measurements using AUR were performed on primary human monocytes at day two and three after isolation by adhesion. Resulting fluorescence intensities were converted to $[\text{H}_2\text{O}_2]$ using Equation 2 (see 7.2.6.2 and Figure 17).

As in EPRS experiments Tg was used as non-physiological stimulus to activate SOCE. In addition, fMLF was used as physiological stimulus that was shown before to activate the investigated Ca^{2+} signaling pathway (Figure 13). In order to confirm a Ca^{2+} -dependency of ROS production, measurements were performed in Ca^{2+} -free Ringer's solution (0 mM $[\text{Ca}^{2+}]$) or solution containing 1 mM $[\text{Ca}^{2+}]$. Averaged traces from $n = 4$ (Tg) and $n = 8$ (fMLF) independent measurements are presented in Figure 18 (A and B). In the presence of Ca^{2+} , Tg and fMLF application triggered a production of H_2O_2 with a mean concentration of 0.344 μM for Tg and 0.401 μM for fMLF stimulation after 90 min (Figure 18, C). H_2O_2 concentrations after 90 min were obtained by normalization of the change in RFUs to intensities of non-stimulated cells in the same conditions. RFUs were further converted to $[\text{H}_2\text{O}_2]$ using Equation 2. The results are presented as $\Delta\text{H}_2\text{O}_2$, calculated from averaged $[\text{H}_2\text{O}_2]$ between the end (last five data points) and the beginning (first three data points) of each measurement. Kinetics from Tg stimulation in 1 mM $[\text{Ca}^{2+}]$ Ringer's solution showed a sigmoidal shape, while kinetics from fMLF stimulation displayed a logarithmic shape with a rapid increase and a prolonged saturation phase (Figure 18, A and B, black traces). In absence of external Ca^{2+} , Tg-induced ROS production was completely abolished. ROS production triggered by fMLF stimulation was still measurable with a similar kinetic as the control condition, but significantly reduced to 0.260 μM H_2O_2 at the end of the recording (Figure 18, B and C, orange trace and bars). The artificial stimulus PMA is widely used to trigger ROS production in phagocytes, *via* activation of PKC. PMA stimulation (kinetics not shown) was therefore used as positive control revealing a high ROS production in absence or presence of external Ca^{2+} with concentrations reaching 9 μM and 9.72 μM respectively (Figure 18, C). The Ca^{2+} dependency of the different stimuli was more apparent when the percent reduction in ROS production in the absence of external Ca^{2+} was calculated (Figure 18, E). PMA-triggered ROS production was only slightly reduced by 7% due to elimination of external Ca^{2+} . FMLF-triggered ROS production was reduced by 44%, while Tg-triggered ROS production was completely abolished (100% reduction).

In addition to presentation of the data as mean values, box-plot-whisker-diagrams were used to present the data allowing a direct assessment of the variability of $\Delta\text{H}_2\text{O}_2$ within independent experiments (Figure 18, D). A box plot encloses 25% to 75% of the data points around the median in blue with the whiskers indicating minimal and maximal values. The median values deviated from mean values by about 40% in the case of Tg stimulation (1 mM $[\text{Ca}^{2+}]$). The mean $[\text{H}_2\text{O}_2]$ was 0.344 μM , while the median H_2O_2 concentration was 0.204 μM . With fMLF stimulation the median and mean values were more comparable (0.324 μM vs. 0.401 μM) displaying a deviation of 20%. In agreement with the above shown results from EPRS experiment (Figure 16), AUR measurements showed a reduction of Tg- and fMLF-induced ROS production in the presence of DPI (Figure 18, F). Here, inhibition of NOX enzymes resulted in a complete abolishment of Tg-triggered ROS production. FMLF-induced ROS production was significantly decreased from 331.3 nM H_2O_2 to 48.29 nM representing a reduction of 88%.

Results

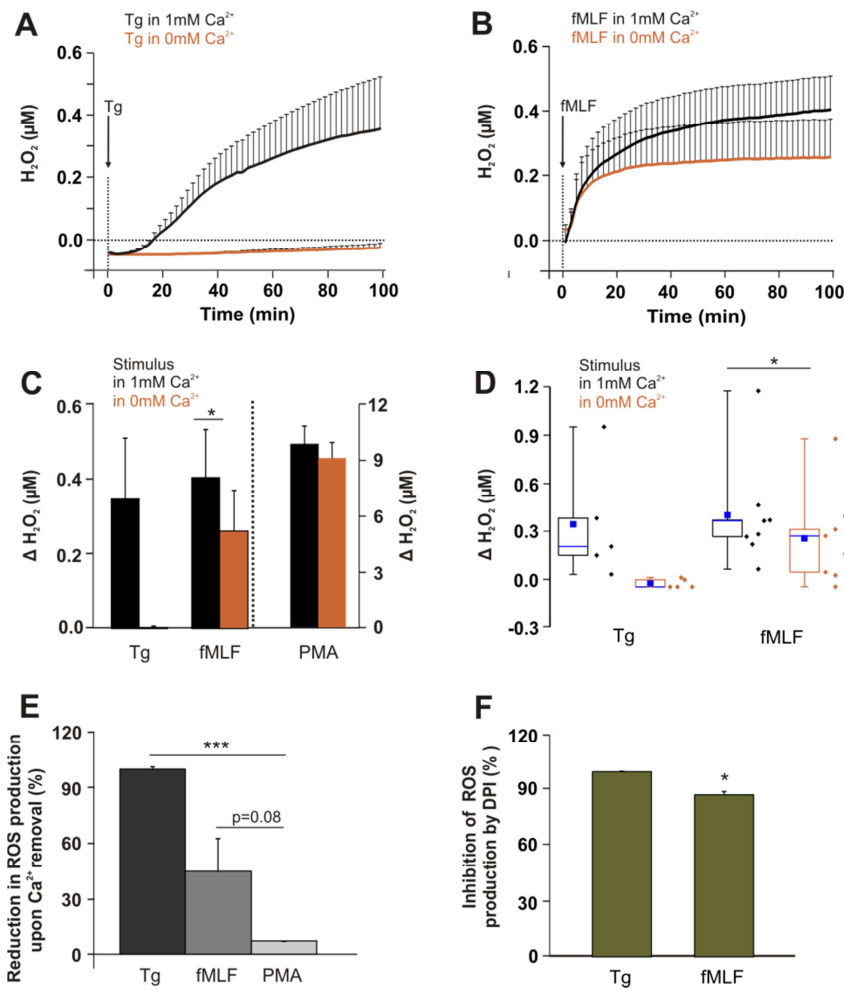


Figure 18 Analysis of Ca^{2+} -dependent ROS production by human monocytes.

Measurement of H_2O_2 production by primary human monocytes using the fluorescent dye AmplexUltraRed (AUR). (A-B) Kinetics of measurements in 1 mM Ca^{2+} Ringer's solution (black traces) and in Ca^{2+} free Ringer's solution (0 mM Ca^{2+} , orange traces) using Tg (A) and fMLF (B) as stimuli (1 μ M each). Stimuli were applied before starting the measurements (black arrows). (C) Quantification of H_2O_2 production after 90 min (ΔH_2O_2) as means from $n = 4$ (Tg) and $n = 8$ (fMLF) independent experiments. PMA was used as positive control in $n = 5$ independent experiments. (D) Box-plot-diagrams depict values from Tg and fMLF experiments indicating the median (50%, blue line), the mean (blue square), minimal and maximal values (dashes), with boxes enclosing 25% -75% of the data points around the median. (E) Reduction in ROS production upon removal of external Ca^{2+} (0 mM Ca^{2+}) as percentage (%) of Ca^{2+} containing conditions. (F) Quantification of measurement of Tg and fMLF induced ROS production in presence of NOX2 inhibitor DPI (10 μ M) quantified as ΔH_2O_2 from $n = 7$ (Tg) and $n = 6$ (fMLF) experiments. Error bars indicate SEM and significance of effects of treatments is indicated with *, $p < 0.05$ and ***, $p < 0.01$, determined using the paired and unpaired (E) standard student's t-test.

8.3.2 Investigating the role of single Orai and STIM proteins in regulating NADPH oxidase activity

Subsequent to the analysis of the Ca^{2+} dependency of ROS production by monocytes, the particular contribution of the CRAC channels (Orai1 and Orai2) and their regulators (STIM1 and STIM2) in regulating ROS production was investigated. Primary human monocytes were isolated from PBMCs by adhesion and transfected immediately after isolation with NT RNA (CTRL) or Orai1, Orai2, STIM1 or STIM2 siRNA. Fluorescence based ROS measurements

were performed 48 h following transfection. Experiments were performed as described in 7.2.6.2 using Tg as stimulus. FMLF was used as second stimulus in parallel in all measurements and served as an internal control (data not shown). Kinetics of ROS production were obtained as described above and in 7.2.6.2. The results of Tg induced ROS production in siRNA and NT RNA (CTRL) transfected cells are presented in Figure 19.

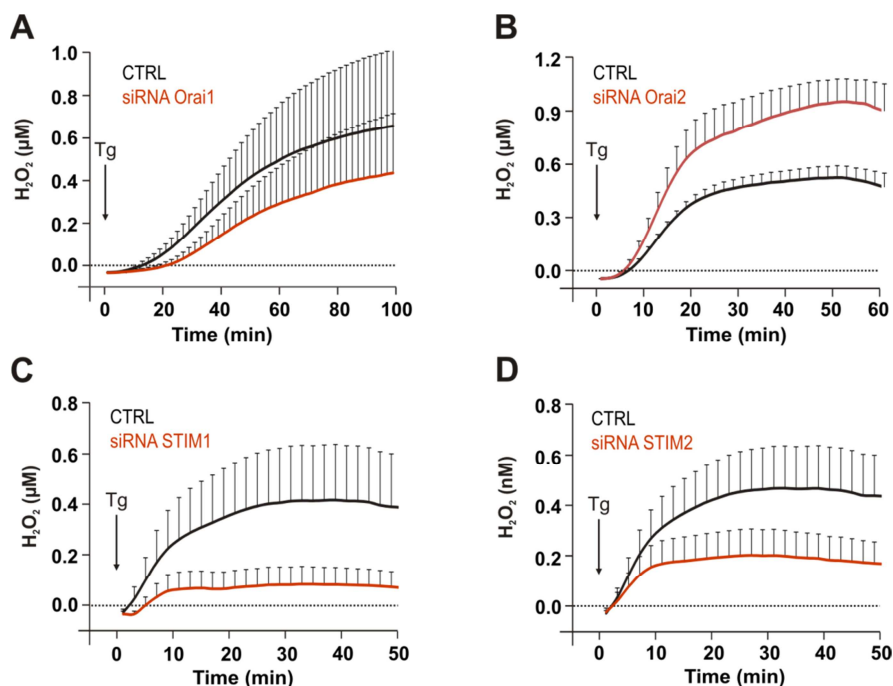


Figure 19 H_2O_2 measurements to determine the contribution of the single CRAC channel components to NOX2 activity.

Fluorescence based detection of external H_2O_2 production in primary human monocytes to determine the contribution of the single Orai and STIM isoforms. Cells were transfected with NT RNA (CTRL, black) and Orai1, Orai2, STIM1 or STIM2 siRNA (red). AmplexUltraRed was used to determine kinetics of H_2O_2 production. Obtained RFU values were converted to H_2O_2 concentrations based on a calibration curve ($y = 2.5646x + 47.321$). Experiments were performed in 1 mM Ca^{2+} Ringer's solution, Tg was used as stimulus to trigger ROS production (black arrow) and depicted kinetics are corrected by their specific controls (kinetics of untreated cells). Averaged kinetics were calculated from $n = 7$ (CTRL/siRNA Orai1), $n = 5$ (CTRL/siRNA Orai2) $n = 5$ (CTRL/siRNA STIM1) $n = 6$ (CTRL/siRNA STIM2) independent experiments. Averaged traces of the single knock-downs (red) of Orai1 (A), Orai2 (B), STIM1 (C) and STIM2 (D) are presented together with their respective controls (black). Error bars indicate SEM.

Three parameters were considered in the analysis of the results: 1) the time course of H_2O_2 production, 2) the rate of production and 3) the amount of H_2O_2 that was produced. Alterations in time course and productions rates were described based on the averaged kinetics (Figure 19) and not on single kinetics. This limited descriptive analysis was inevitable, due to a high variability within and in between the single measurements and conditions and is related to a high donor variability (further discussed below 9.2.4). The kinetics presented in Figure 19 are described in the text below and the determined overall effects resulting from siRNA treatment are summarized in Table 17.

Time course. The overall time course of H_2O_2 production under control conditions (black traces in Figure 19, A-D), showed a sigmoidal shape displaying a lag phase with a very slow increase in H_2O_2 , followed by a faster main production phase with a steep slope and a prolonged steady production phase, ending with saturation in most cases (B-D). This typical shape was most

obvious in Orai1 and Orai2 knockdown experiments (A and B). The duration of the lag phase varied from a few minutes (STIM1, C) up to 20 min (Orai1, A). The same variability was observed for the duration of ROS production till saturation was reached. An increase in ROS could be observed from the beginning of the experiments. However, the onset of net H_2O_2 production, when the H_2O_2 concentration exceeded the baseline of not-stimulated cells (DMSO treated, dotted lines in A-D), could take several minutes. The onset of net ROS production was significantly shifted when Orai1 mRNA was down-regulated (red trace in A). Under control conditions, H_2O_2 levels exceeded the basal level after 13 min (Orai1 control, A), while it took 23 min (Orai1 siRNA, A) on average under knockdown conditions. Orai2 down-regulation resulted in faster onset of net ROS production to start immediately with the recording, while it took 7 min under control conditions (B). STIM1 down-regulation resulted in a slight shift from 3 min to 7 min (C). There was no shift detectable in the case of STIM2 with an onset after 3 min in both, knockdown and control condition (D).

Main production phase. The plotted kinetics revealed a phase with a maximal increase in H_2O_2 production which is referred to as main production phase. The rate of H_2O_2 production in this phase was determined by calculating the slope (nM H_2O_2 /min) of the averaged traces (Table 17). The onsets of the main production phase coincide with the onset of net ROS production in all experimental sets. When Orai1, STIM1 or STIM2 mRNA was down-regulated, the production rate decreased compared to respective controls (compare red to black traces in Figure 19, A, C and D) with kinetics from knockdown cells running below their respective controls. The production rate was 4.86-fold decreased when STIM1 mRNA was down-regulated from 26.43 to 5.44 nM/min. Changes in production rate were less prominent in case of Orai1 down-regulation with a 1.42-fold decrease from 11.55 to 8.16 nM/min and least effected when STIM2 was down-regulated, only showing a 0.57-fold decrease from 39.29 to 22.46 nM/min. In contrast to the other isoforms, Orai2 down-regulation resulted in a 4.9-fold increase of the production rate from 28.86 nM/min to 110.08 nM/min (Figure 19, B). With exception of the Orai1 data set, where a steep increase in H_2O_2 production could be observed for over 30 min, the main production phase did not last longer than 15 min in the other cases. Until saturation was reached (see below). A further increase in H_2O_2 was detectable, but with an obviously reduced rate.

Saturation. Although the main production phase was quite restricted over relatively short time (see above), H_2O_2 was still produced in a prolonged phase for up to 50 min, before saturation was reached. In the case of Orai1 saturation was not even reached within 100 min of recording (Figure 19, A). A saturation of H_2O_2 productions was reached after 55 min in the experimental set regarding the role of Orai2, both in control and knockdown conditions. Kinetics of STIM1 and STIM2 knockdowns (red traces in Figure 19, C and D) reached saturation, eight min before their respective controls.

Net production of H_2O_2 . The amount of H_2O_2 produced upon Tg stimulation under the different observed conditions (Figure 20, CTRL – black, siRNA – red) was determined after 90 min of recording, from single H_2O_2 kinetics. The last five values from each kinetic were averaged and are presented as single data points in Figure 20. In addition, the results are presented in box-plot-whisker-diagrams to demonstrate the distribution of the values. Diagrams indicate the median (blue lines) and average (blue squares) value, minimal and maximal values (whiskers), and boxes enclose 25-75% of the data set around the median.

Results

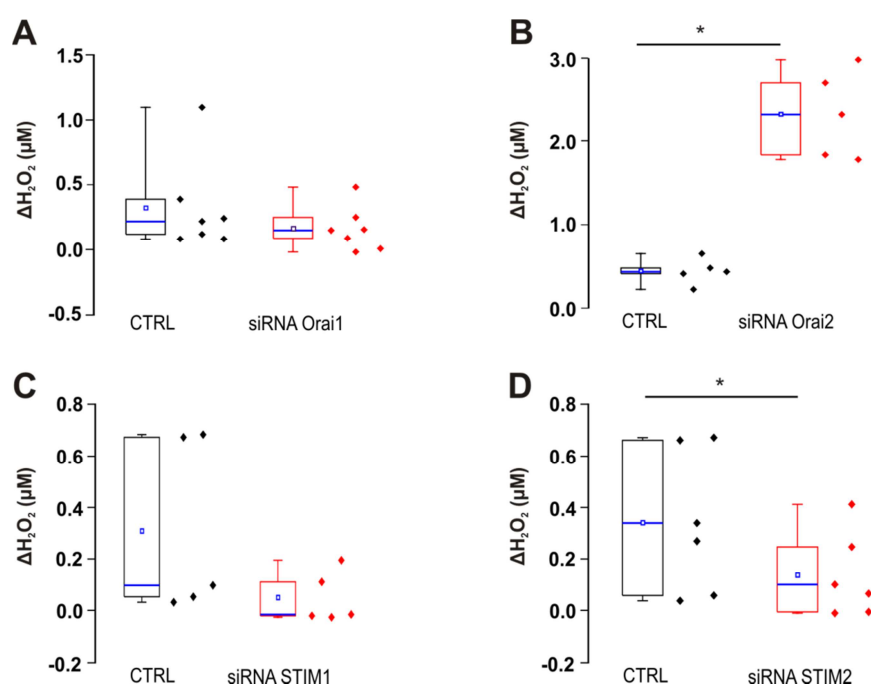


Figure 20 Quantification of H₂O₂ measurements using AmplexUltraRed based on kinetics.

Quantification of external H₂O₂ concentrations determined for control transfected cells (CTRL, black) and cells transfected with siRNAs (siRNA, red) targeting Orai1 (A), Orai2 (B), STIM1 (C) and STIM2 (D). Quantification of H₂O₂ production from single traces after 90 min (Δ H₂O₂), depicted as box-plot-whisker-diagrams next to single data points. Diagrams indicate the median (50 % , blue), minimal and maximal values (whiskers) with boxes enclosing 25 % -75% of the data points around the median. Quantification is based on kinetics displayed in Figure 19, from n = 7 (Orai1 CTRL/siRNA), n = 5 (Orai2 CTRL/siRNA) n = 5 (STIM1 CTRL/siRNA) n = 6 (STIM2 CTRL/siRNA) independent experiments. Significance is indicated with *, p < 0.05, determined using the paired standard student's t-test.

Table 17 Parameters characterizing kinetics of H₂O₂ production (presented in Figure 19)

Presented parameters were collected from averaged kinetics displayed in Figure 19. Main production phase was defined as time span in which the steepest increase in H₂O₂ (min⁻¹) was detectable. Onset of saturation phase was defined as time point when values from kinetics declined the first time, or showed not further increase. Production rate was determined from linear fits of data points in the main production phase.

	Time point exceeding base line (min)	Main production phase (min)	Production rate (nM/ min)	Onset of saturation (min)
CTRL	13	23-60	11.55	-
Orai1	23		8.16	-
CTRL	7	5-20	28.86	55
Orai2	0		110.08	55
CTRL	3	<15	26.43	43
STIM1	7		5.44	35
CTRL	3	< 15	39.29	39
STIM2	3		22.46	31

Down-regulation of either STIM2 or Orai2 mRNA, resulted in significant, but opposed changes in the amount of H₂O₂ produced after 90 min (Figure 20, B and D). Median H₂O₂ was significantly decreased 3.9-fold from 305.59nM to 77.68nM in the case of STIM2, but was increased 5.4-fold from 431.92nM to 2.32 μM in the case of Orai2. Like for STIM2, down-regulation of STIM1 resulted in an obvious, but statistically non-significant, decrease in H₂O₂ levels (Figure 20, C). Median H₂O₂ was decreased 6-fold from 96.04 to 0 (below base line). Noteworthy, compared to the other data sets, the STIM1 set was the only one displaying control values below 200nM. The effect of ORAI1 mRNA down-regulation was the least, with a 1.45-fold decrease in H₂O₂ from 217.44 to 150.06nM (median values, Figure 20, A).

8.4 Redox regulation of store-operated calcium entry

SOCE and the contribution of Orai and STIM to Ca²⁺-dependent ROS production by monocytes were analyzed in separate approaches. The consequential experiments aiming at the analysis of the mutual effects of the two processes are presented in this section. The impact of produced ROS (H₂O₂) on SOCE and subsequently on Ca²⁺-dependent ROS production was analyzed. In addition, an equation was introduced to apply the regulatory redox mediated mechanism to other cell systems investigated in this study, namely melanoma cell lines.

8.4.1 Analysis of the redox-sensitivity of SOCE in human monocytes

Initially, the effect of H₂O₂ on SOCE in human monocytes was investigated in calcium imaging experiments as described in 7.2.7. For this data set and also the following data sets presented in section 8.4.2, monocytes were isolated using the bead-isolation instead of the adhesion method (7.2.1). Method change was the result of changes in overall laboratory organization and in terms of time management and efficiency. Monocytes were incubated for 10 min in Ringer's solution containing different concentrations of H₂O₂ (1 μM, 10 μM, 100 μM, 300 μM, 1 mM, 3 mM and 10 mM), before Tg addition and activation of SOCE. Averaged traces (except for the 10 mM condition) are presented in Figure 21 (A-C). The control trace (black), with no H₂O₂ applied prior to Tg stimulation, displayed a rise in [Ca²⁺]_i in response to external [Ca²⁺] re-addition, as already presented in Figure 13 (D).

Application of H₂O₂ resulted in a dose-dependent rise in [Ca²⁺]_i prior to application of Tg (Figure 21, A). This effect was transient in the case of 10 μM H₂O₂, but was stable for concentrations ≥100 μM H₂O₂ (green and grey traces in Figure 21, B-C). The rise of [Ca²⁺]_i following store depletion correlated inversely with H₂O₂ evoked rise in [Ca²⁺]_i. This correlation was most obvious in case of 1 mM and 3 mM H₂O₂ (Figure 21, C). To quantify the effect of H₂O₂ on Tg-triggered SOCE, ΔCalcium was calculated from the single calcium traces as described before (8.2.1) and as depicted in Figure 21 (C).

The obtained ΔCalcium values were plotted against H₂O₂ concentrations to determine the half-maximal inhibitory concentration (IC₅₀) of H₂O₂ (Figure 21, D). The resulting dose-response curve displayed two phases and was therefore best described with a second order exponential decay equation, instead of the commonly used Hill-equation. Phase 1 showed a nearly linear decay of ΔCalcium values in response to treatment with 0-100 μM H₂O₂, while phase 2 showed an exponential decay of ΔCalcium values in response to treatment with 300 μM-10 mM H₂O₂. The IC₅₀ was determined as 155 μM H₂O₂.

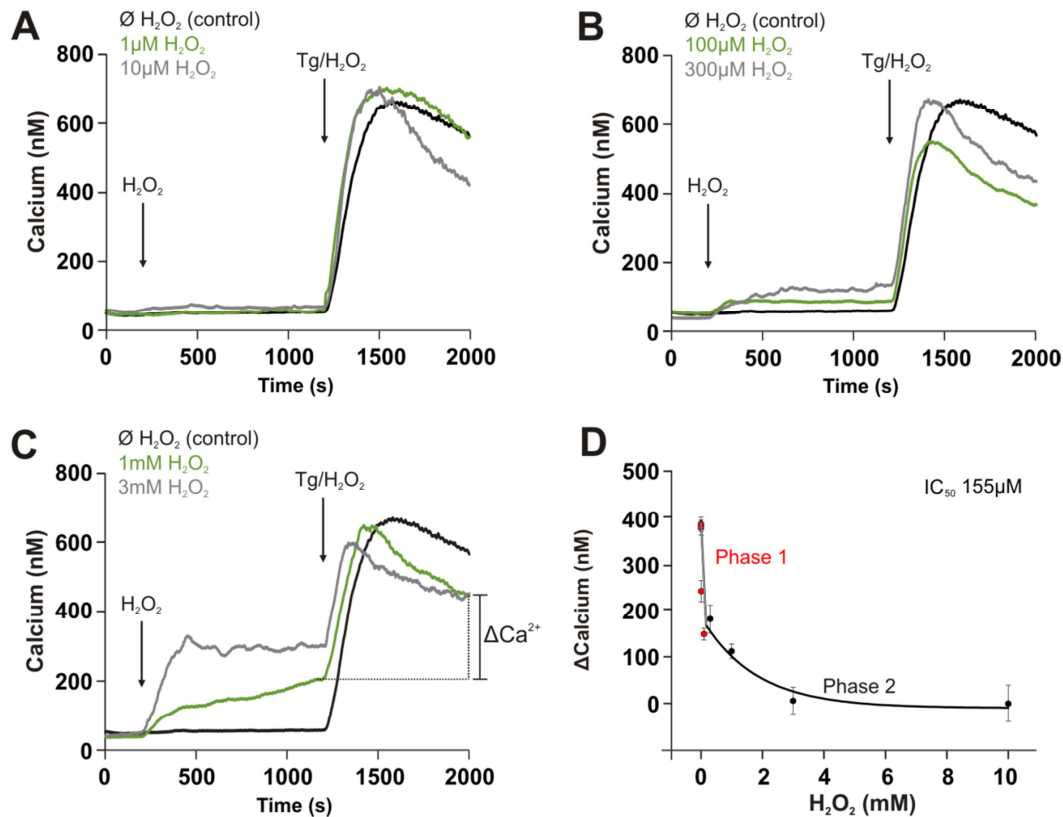


Figure 21 Inhibition of store-operated Ca²⁺ entry in human monocytes by H₂O₂

Analysis of the inhibitory effect of H₂O₂ on SOCE in primary human monocytes using fluorescence-based calcium imaging. (A-C) Cells were incubated with different H₂O₂ concentrations or buffer (∅) (first arrow) before activation of SOCE by Tg application (second arrow). Tg was applied in presence of buffer or the respective H₂O₂ concentration to prevent wash-out effects. (A) Averaged traces from measurements in the absence (control, ∅H₂O₂) or presence of 1 μM (green) or 10 μM (grey) H₂O₂. (B) Averaged traces from measurements in the absence (control, ∅H₂O₂) or presence of 100 μM (green) or 300 μM (grey) H₂O₂. (C) Averaged traces from measurements in the absence (control, ∅H₂O₂) or presence of 1 mM (green) or 3 mM (grey) H₂O₂. (D) Quantification of SOCE as ΔCalcium calculated from [Ca²⁺]_i at the end of the plateau phase and [Ca²⁺]_i before Tg stimulation. ΔCalcium values plotted against respective H₂O₂ concentrations to determine IC₅₀ from a second order exponential decay fit. Kinetics and quantifications were averaged from at least three independent measurements with (n) as total number of cell analyzed: n = 606 (control), n = 832 (1 μM), n = 382 (10 μM), n = 420 (100 μM), n = 101 (300 μM), n = 499 (1 mM), n = 111 (3 mM) and n = 394 (10 mM). Error bars indicated SEM.

8.4.2 The role of Orai3 in modulating redox-sensitivity of SOCE in human monocytes

As shown above, SOCE was inhibited by H₂O₂ with an IC₅₀ of 155 μM (Figure 21, D). The relatively high expression of the redox-insensitive isoform Orai3 (Figure 9 and Figure 10) already indicated a potential role in influencing the observed redox-sensitivity of SOCE.

The role of Orai3 in redox-regulation of SOCE was analyzed in Ca²⁺ imaging experiments as described above (Figure 21). SOCE was measured with and without pre-treatment with H₂O₂ in NT RNA transfected cells (CTRL) and Orai3 siRNA transfected cells (siRNA Orai3) (Figure 22). Monocytes were transfected immediately after bead-isolation. Measurements were performed as described in the above section 48 h after transfection. Under control condition, without pre-treatment with H₂O₂, down-regulation of Orai3 mRNA resulted in a significant increase in SOCE compared to control cells (compare black traces in A and B, Figure 22). Pre-treatment with

100 μM H_2O_2 for 10 min, prior to SOCE activation using Tg (green traces in Figure 22, A and B), significantly inhibited SOCE. $\Delta\text{Calcium}$ was decreased in presence of H_2O_2 from 540.53 to 343.50 nM in NT RNA transfected cells and from 635.35 to 292.84nM in siRNA transfected cells (green bars in C, Figure 22). Thus, the inhibitory effect of H_2O_2 on SOCE was significantly enhanced in Orai3 silenced cells. SOCE was inhibited by 54%, compared to 38% inhibition in control transfected cells (Figure 22, D).

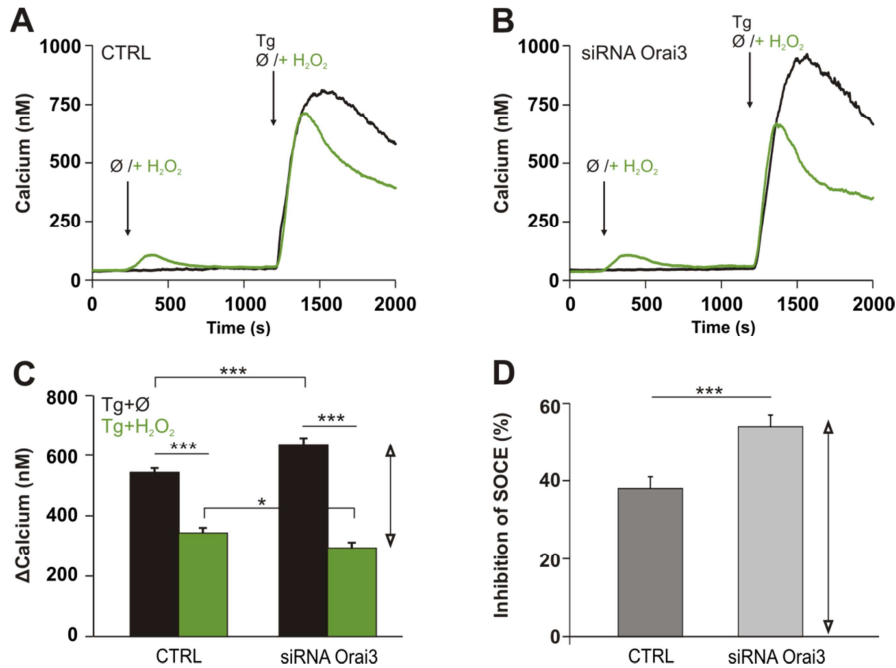


Figure 22 The role of Orai3 in modulating the redox-sensitivity of store-operated Ca^{2+} entry

Analysis of the role of Orai3 in redox-sensitivity of SOCE in primary human monocytes using fluorescence based calcium imaging experiments. (A and B) Cells were incubated with 100 μM H_2O_2 or buffer (\emptyset) (first arrow) before activation of SOCE by Tg application (second arrow). Tg was applied in presence of buffer or H_2O_2 to prevent wash-out effects. (A) Averaged calcium traces from control transfected cells in absence (black) or presence (green) of 100 μM H_2O_2 . (B) Averaged traces from cells transfected with Orai3 siRNA in absence (black) or presence (green) of 100 μM H_2O_2 . (C) Quantification of SOCE as $\Delta\text{Calcium}$ calculated from $[\text{Ca}^{2+}]_i$ at the end of the plateau phase and $[\text{Ca}^{2+}]_i$ before Tg stimulation. (D) Inhibition (as %) of SOCE by 100 μM H_2O_2 in control and siRNA treated cells (indicated with grey arrows in C and D). Kinetics and quantifications were averaged from at least three independent measurements with (n) as total number of cell analyzed: n = 455 (CTRL), n = 496 (CTRL, H_2O_2), n = 589 (siRNA) and n = 441 (siRNA, H_2O_2). Error bars indicate SEM and significance is indicated with ***, p < 0.001, determined using the unpaired standard student's t-test.

8.4.3 The interplay of redox-sensitivity of SOCE and Ca^{2+} - dependent ROS production

The above described work demonstrates that SOCE in primary human monocytes is inhibited by H_2O_2 with an IC_{50} of 155 μM (Figure 21). An effect that was significantly enhanced when Orai3 mRNA levels were down-regulated using RNAi (Figure 22). In respect to these findings and work previously shown by Bogeski and colleagues (Bogeski *et al.*, 2010), redox sensitivity of SOCE was analysed in regard of the relative expression of Orai3 and Orai1. Therefore, redox-sensitivity of SOCE, indicated by the IC_{50} , was plotted against the relative Orai3/Orai1 mRNA ratio for naïve and effector T cells and monocytes. The plot revealed a strong correlation between the two parameters (Figure 23, A). The resulting plot could be fit to a logarithmic curve function with a regression value of 0.998 (Figure 23, A).

Results

The curve function is given in Equation 8 and was further used to estimate redox sensitivity of SOCE from qRT-PCR data (see below and 8.4.5).

$$\text{Equation 8 } y = 63.59 \ln(x) + 279.42$$

In regard of the correlation between the redox-sensitivity and relative Orai3 expression levels (Figure 23, A), the effect of H₂O₂ on SOCE -dependent ROS production in correlation with Orai3 expression was next investigated. Internal ROS production in primary human monocytes was measured in imaging experiments using the redox-sensitive dye H2-DCFDA as described in 7.2.6.2. A scheme of the experimental procedure is given in Figure 23 (C). Monocytes, either transfected with NT RNA or Orai3 siRNA were incubated with 300 μM H₂O₂, prior to stimulus application. Tg was applied to determine the role of Orai3 in Ca²⁺-/SOCE-dependent ROS production. Changes in ROS production were calculated from H₂O₂ treated cells as percent of non-treated (no H₂O₂), Tg stimulated cells (Figure 23, B). Treatment of control transfected cells with H₂O₂ did not reveal a change in Tg-triggered ROS production (CTRL). In contrast, Tg-triggered ROS production was significantly inhibited by 19% upon H₂O₂ treatment in Orai3 knockdown cells (Orai3). These results point to a role for Orai3 not only in modulating SOCE under oxidative stress, but also in mediating downstream effect on SOCE-dependent ROS production.

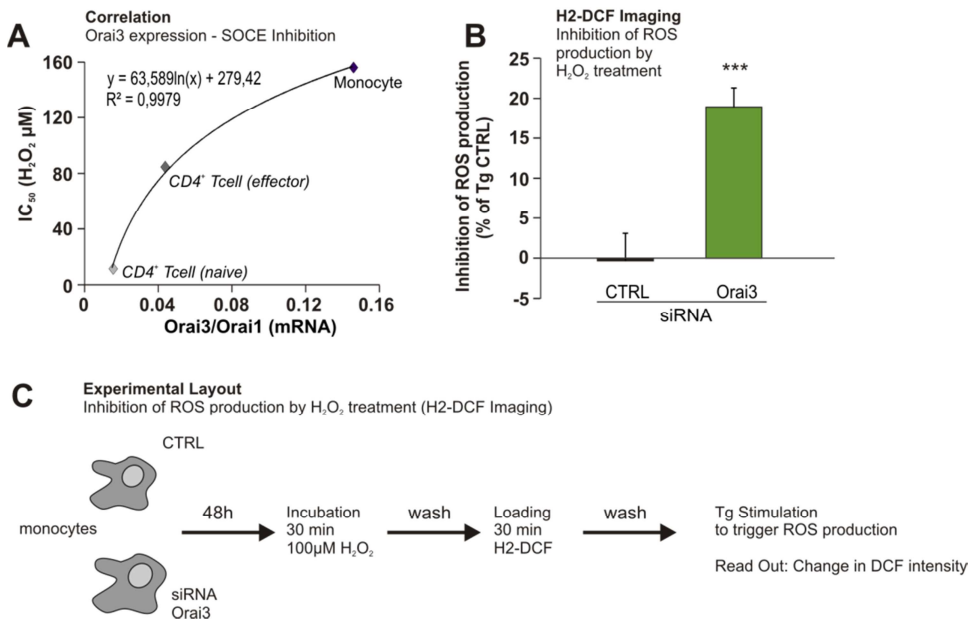


Figure 23 Concurrence of Orai3 expression and redox-sensitivity of SOCE and Ca²⁺-dependent ROS production in human monocytes.

(A) Correlation between IC₅₀ of H₂O₂ on SOCE and the relative Orai3/Orai1 mRNA expression ratios in primary human CD4⁺ naïve and effector T cells and primary human monocytes. Parameter correlation fitted by a logarithmic function with a regression value of 0.998. Values for CD4⁺ cells were already published by (Bogeski *et al.*, 2010) and are presented here with permission after re-calculation, for comparison with monocyte data. (B) Analysis of the impact of H₂O₂ on SOCE-dependent ROS production in reliance of Orai3 expression levels. Internal ROS production was measured using the redox-sensitive dye H2-DCFDA following H₂O₂ treatment (300 μM) and Tg stimulation. Inhibition of ROS production by H₂O₂ is calculated as percent (%) of Tg stimulated controls for control transfected cells (CTRL, black bar) and cells transfected with Orai3 siRNA (Orai3, dark green bar). Values are presented as means from at least 3 independent experiments with (n) as total number of analyzed cells: n = 842 (CTRL siRNA, H₂O₂ treatment) and n = 760 (Orai3 siRNA, H₂O₂ treatment). (C) Scheme of experimental procedure for results presented in (B). Error bars indicated SEM, significance is indicated with ***, p < 0.001, determined using the paired standard student's t-test.

8.4.4 The role of the redox-resistant isoform Orai3 in Ca^{2+} -dependent ROS production

In preceding experiments, the role of Orai3 for redox-mediated inhibition of SOCE was analyzed, as presented in the above sections. The Ca^{2+} -dependent ROS production implied further investigation of the contribution of Orai3 in regulating ROS production itself, as already analyzed for the other Orai and STIM isoforms.

AmplexUltraRed was used to measure the produced H_2O_2 from cells transfected either with NT RNA or Orai3 siRNA. Experiments were performed as described in section 8.3.2. Again, the three major parameters 1) time course of H_2O_2 production, 2) the rate of production and 3) the amount of H_2O_2 produced, were considered to further evaluate the role of Orai3 in Ca^{2+} -dependent ROS production. Results were quantified based on the average kinetics, with exception of the net ROS production that was analyzed for single measurements, due to a high variability within and in between the single measurements and conditions. These parameters are summarized in Table 18, while average kinetic traces and the quantification of net H_2O_2 production are presented in Figure 24.

Time course. The average time course of H_2O_2 production determined for NT RNA or Orai3 siRNA transfected monocytes (black and red in Figure 24, A), did not display a sigmoidal shape similar to that observed in Figure 19 (A). The produced H_2O_2 exceeded baseline within 3 or 5 min (CTRL and siRNA, respectively), immediately merging into the main production phase without running through a further lag phase. From 20 min on, H_2O_2 produced by cells treated with Orai3 siRNA reached a higher level than that produced by control transfected cells. This effect was only seen on the averaged trace. Single traces were comparable to control traces, with exception of a single event that led to a higher curve run on average. This effect is also reflected by the results from calculation of net ROS production (see below and Figure 24, B). Both curves did not reach saturation within recording time.

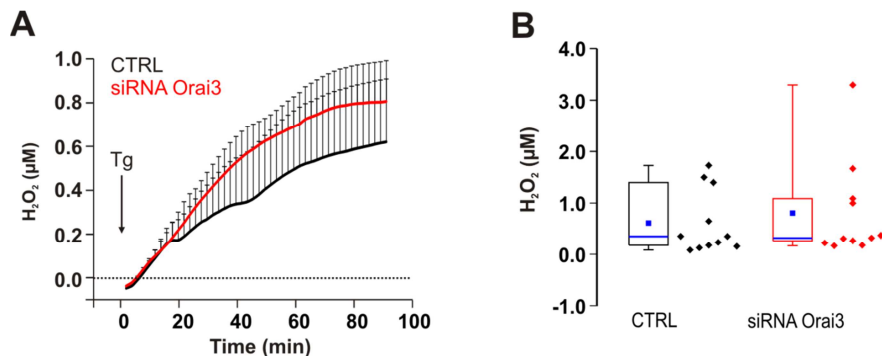


Figure 24 The role of Orai3 in Ca^{2+} -dependent ROS production.

Fluorescence-based detection of external H_2O_2 production by monocytes to analyze the role of Orai3 in Ca^{2+} -dependent ROS production. AmplexUltraRed was used to determine kinetics of ROS production. Experiments were performed in 1 mM Ca^{2+} Ringer's solution. Tg was used to trigger ROS production (black arrow) and depicted kinetics are corrected by their respective controls (kinetics of untreated cells). (A) Averaged traces of H_2O_2 production following Tg stimulation (arrow) from NT RNA (CTRL, black trace) and Orai3 siRNA (red trace) transfected cells. H_2O_2 was calculated from RFUs with $y = 2.5646x + 47.321$ (calibration curve, Figure 17, B). Quantification of net H_2O_2 production after 90min, depicted as single data points and as box-plot-whisker-diagrams, indicating the median (50%, blue lines) and average (blue squares) values, minimal and maximal values (whiskers), with boxes enclosing 25-75% of the data set. Kinetics and net H_2O_2 was calculated from $n=11$ (CTRL/siRNA Orai3) independent experiments. Error bars in (A) indicate SEM.

Main production phase. The main production phase lasted from 5 to 20 min for both control and siRNA transfected cells. In this phase, the net H₂O₂ production was slightly increased (1.16-fold) in response to Orai3 down-regulation from 14.90 to 12.85 (nM/ min⁻¹). The main production phase merged into a prolonged production phase with a decreased slope compared to the main phase, without reaching saturation within recording time.

In contrast, Orai3 down-regulated cells showed continuous production of H₂O₂ with a high production rate for another 22 min before merging into the prolonged phase. However, saturation was also not reached in case of Orai3 knock-down.

Net H₂O₂ production. The amount of H₂O₂ produced upon Tg stimulation under the different observed conditions (CTRL - black, siRNA - red) was determined after 90 min of recording, from single H₂O₂ kinetics and is presented in Figure 24 (B). Regarding the kinetics and average values (blue squares in B), down-regulation of Orai3 seemed to result in an increase in Tg-triggered H₂O₂ production from 613.76 to 807.10nM. As already observed in other data sets (Figure 20), the single data points showed a broad distribution as illustrated by the box-plot-whisker diagrams. A single data set (max data point in Figure 24, B (red)) lead to the impression of an increased ROS production upon Orai3 down-regulation on average. In the majority of the data sets, net ROS production in Orai3 knockdown cells was unaltered or even reduced compared to controls.

Table 18 Parameters characterizing kinetics of H₂O₂ production (presented in Figure 24)

Presented parameters were collected from averaged kinetics displayed in Figure 24. Main production phase was defined as time span in which the steepest increase in H₂O₂ (min⁻¹) was detectable. Onset of saturation phase was defined as time point when values from kinetics declined the first time, or showed not further increase. Production rate was determined from linear fits of data points in the main production phase.

	Time point trespassing zero base line (min)	Main production phase (min)	Production rate (nM/ min)	Onset of saturation (min)
CTRL	5	5-20	12.85	-
Orai3	3		14.90	-

8.4.5 A theoretical approach to estimate redox-sensitivity of SOCE in different cell systems.

The relative Orai3 to Orai1 expression levels and IC₅₀ values for ROS-mediated inhibition of SOCE showed a strong correlation as presented in Figure 23 and Equation 8. This correlation was thought to serve as prediction model of redox-sensitivity of SOCE from qRT-PCR data, in so far untested cell types. Equation 8 was therefore used to calculate an IC₅₀ value from the measured Orai3/Orai1 mRNA ratios determined for melanoma cells lines (presented in Figure 10).

As presented in Figure 25, IC₅₀ could be calculated from Orai3/Orai1 ratio values giving an estimated IC₅₀ of 154.39 μM H₂O₂ for SK-MEL-5 and 179.66 μM H₂O₂ for SK-MEL-28. This suggested a redox-sensitivity or resistance of SOCE comparable to that of monocytes. The calculated IC₅₀ for WM3734 cells was lower than that of the SK-MEL cell lines and with 101.28 μM H₂O₂ more comparable to the redox-sensitivity of effector T cells than monocytes. In all cases, H₂O₂ incubation resulted in the previously observed increase in [Ca²⁺]_i, prior to the

Results

activation of SOCE (see also Figure 21). SK-MEL-5 displayed a high Ca^{2+} influx following the addition of H_2O_2 . In contrast, SK-MEL-28 only showed a moderate increase and WM3734 cells only displayed a very small and transient rise (green trace, first rise in Ca^{2+} in Figure 25, A, C and D). SOCE was triggered using Tg (black traces in Figure 25, A, C and E) and all measurements were performed in 0.25 mM Ca^{2+} Ringer's solution.

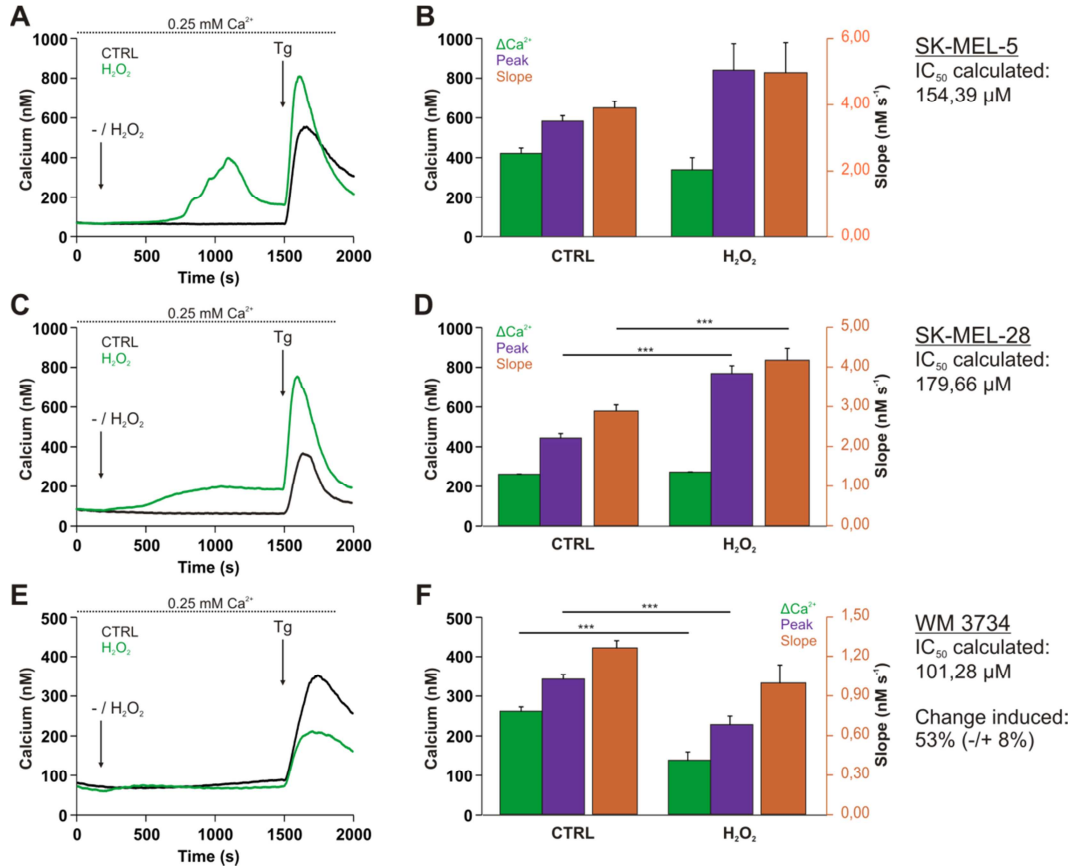


Figure 25 Theoretical estimation and experimental determination of redox-sensitivity of SOCE in melanoma cell lines based on Ora3/Orai1 mRNA ratios.

Analysis of redox sensitivity of SOCE in melanoma cell lines using fluorescence-based calcium imaging with Fura-2AM loaded cells to determine intracellular Ca^{2+} concentrations $[\text{Ca}^{2+}]_i$. (A,C,E) Averaged traces from cells in the absence (black), or presence (green) of H_2O_2 . Cells were incubated with buffer (-) or H_2O_2 (1st arrow) before activation of SOCE by Tg application (2nd arrow). H_2O_2 concentrations used were assumed as IC_{50} concentration for the respective cell line, calculated from an equation, correlating Orai3/Orai1 mRNA expression ratios to redox-sensitivity of SOCE. H_2O_2 concentrations were calculated from Equation 8 ($y = 63.59 \ln(x) + 279.42$) with 154.39 μM for SK-MEL-5 (A and B), 179.66 μM for SK-MEL-28 (C and D) and 101.28 μM for WM3734 (E and F). (B,D,F) Quantification of peak calcium (purple) and slope (orange) of Ca^{2+} entry following Tg application. ΔCa^{2+} (green) calculated from $[\text{Ca}^{2+}]_i$ at the end of the plateau phase (WM373), or after 1750 s of recording (SK-MEL-5 and 28), and $[\text{Ca}^{2+}]_i$ before Tg application. Kinetics and quantification were averaged from 2 independent measurements with total number of analyzed cells (n): n = 34/23 (-/ H_2O_2) for SK-MEL-5, n = 42/37 (-/ H_2O_2) for SK-MEL-28 and n = 24/19 (-/ H_2O_2). Error bars indicated SEM, significance of effects is indicated with ***, $p < 0.001$ determine using the paired standard student T-Test.

The treatment of the different melanoma cell lines with the calculated $[\text{H}_2\text{O}_2]$ resulted in opposite effects on Tg-triggered SOCE. There was no inhibition of SOCE observed in the case of SK-MEL-5 and SK-MEL-28. In both cases the calculated parameters to describe SOCE

following Tg stimulation were increased rather than decreased. In SK-MEL-5 cells, there was a tendency of a reduction in ΔCa^{2+} from 421.59 to 339.56 nM. However, the incubation with 150 μM H_2O_2 resulted in an obvious, though not significant, increase in peak calcium values (583.81 to 841.22 nM) and the corresponding influx rate (3.90 to 4.97 nM/s) (Figure 25, A and B). In the case of SK-MEL-28 the promoting effect of H_2O_2 on SOCE was even stronger.

Incubation with 180 μM H_2O_2 resulted in a significant increase of peak calcium (purple) from 442.20 to 767.35 nM, and from 2.88 to 4.17 nM/s in the corresponding Ca^{2+} influx rate (orange), while ΔCa^{2+} (green), calculated at 1750s, was only slightly altered by the incubation with H_2O_2 (260.56 to 271.29 nM) (Figure 25, C and D). In contrast, WM3734 cells showed a significant reduction of ΔCa^{2+} (green) from 259.97 to 137.04 nM, and peak calcium (purple) from 340.91 to 226.76 nM (Figure 25, E and F). The influx rate (orange) also showed an obvious, though not significant decrease from 1.26 to 0.99 nM/s upon H_2O_2 treatment (Figure 25, F).

8.5 The Ca^{2+} and redox environment in regulating cellular functions – Preparative adjustment of experimental conditions

Intracellular processes are not only regulated by the cellular signaling machinery and its regulation (here Ca^{2+} channels), but also by the influence of the extracellular environment. The tumor- and inflammatory environment display highly specialized features regarding a plethora of factors, as pointed out in the introduction (6.1.3). Therefore, it was also an aim of this work to shed light on how the Ca^{2+} and redox environment regulate monocyte and melanoma function. The here described experimental adjustments were used to determine to effects of a changed environment on aspects as cell survival and cell proliferation (see below, 8.6 and 8.7).

To analyze the impact of a changed Ca^{2+} environment *in vitro*, the standard culture conditions were altered by including the Ca^{2+} chelator EGTA to adjust the extracellular Ca^{2+} concentration in the medium (referred to as free $[\text{Ca}^{2+}]$ or $[\text{Ca}^{2+}]_{\text{ext}}$). The resulting free $[\text{Ca}^{2+}]_{\text{ext}}$ was determined using two different methods, as described in 7.2.8. The Ca^{2+} concentrations were determined in three independent measurements per condition and are summarized in Table 19. For analysis of the role of other medium supplements (serum proteins) the Ca^{2+} concentrations in serum free (RPMI) and serum containing medium (RPMI + 10% FCS) were determined. Serum supplementation of RPMI medium shifted the free $[\text{Ca}^{2+}]$ from 221 μM to 377 μM Ca^{2+} , an increase of 59% (see Table 19, 0mM EGTA). Ca^{2+} concentrations depicted in the graphs of Figure 26 and Figure 30 represent the numbers given in Table 19.

Changes in redox environment were achieved by adding different concentrations of H_2O_2 to the standard culture medium. H_2O_2 was used to mimic a redox environment due to its biological relevance and its role as signaling molecule. Final H_2O_2 concentrations in the medium were not further verified. In contrast to Ca^{2+} , H_2O_2 concentrations were not assumed to be stable over time. Although H_2O_2 is one of the more stable ROS, e.g. compared to superoxide, it is reactive with proteins and a decrease of the adjusted concentrations was assumed to inevitably occur within a short time. Therefore, the results of the respective experiments reflect the long-term effects of an acute exposure.

Table 19 Ca^{2+} concentration in RPMI medium supplemented with Ca^{2+} chelator EGTA.

Ca^{2+} concentrations of EGTA supplemented RPMI medium (-/+10% FCS) were determined in three independent experiments per condition. The Calcium Gen.2 Assay (Roche Diagnostic, performed by the Central Clinical Laboratory at Universitätsklinikum Saarland), and the Combination Calcium Electrode perfection™ (Mettler Toledo) were used to determine free Ca^{2+} concentrations.

EGTA (mM)	0	0.1	0.2	0.3	0.4	0.5	0.6	0.7	0.8	0.9
$[\text{Ca}^{2+}]_{\text{RPMI}}$ +10% FCS (μM)	377	338	292	224	179	152	93.2	72.7	36.5	0.89
SEM	28.7	35.5	35.2	39.0	45.4	31.0	38.6	27.4	31.8	0.45
$[\text{Ca}^{2+}]_{\text{RPMI}}$ (μM)	221	165	113	67.5	27.4	6.3	0.51	0.37	0.31	0.27
SEM	29.6	9.54	6.67	6.75	4.45	1.61	0.03	0.03	0.04	0.03

8.6 Ca^{2+} environment and Ca^{2+} signaling in melanoma progression: Proliferation vs. Migration

8.6.1 The regulation of melanoma proliferation by the extracellular Ca^{2+} milieu and SOCE

Extracellular Ca^{2+} concentration plays a critical role in skin barrier formation and differentiation of skin cells. This contribution to cell function pointed to a possible role of the Ca^{2+} environment in rendering melanoma progression, by influencing tumor associated features as proliferation and migration (see 6.3.2). Several components of the local environment hold the potential to alter cellular features. Among these also hormones and peptides, that can bind to receptors and subsequent activate intracellular signaling pathways (see 6.3.2). Therefore, the dependence of FCS-induced proliferation on extracellular Ca^{2+} of SK-MEL-5 melanoma cells was analyzed in the following section using the CellTiterBlue assay (see 7.2.8). Extracellular Ca^{2+} concentrations were adjusted as described above (8.5) and cells were cultivated for 48 h. The influence of serum proteins on proliferation was analyzed by serum (FCS) starvation of the cells.

Proliferation of SK-MEL-5 cells was altered by changes in $[\text{Ca}^{2+}]_{\text{ext}}$ displaying a unique dependency (Figure 26, A and B). In the presence of FCS, SK-MEL-5 cells showed an inversely $[\text{Ca}^{2+}]_{\text{ext}}$ -dependent proliferation. Optimal (or maximal) proliferation was observed at a relatively low $[\text{Ca}^{2+}]_{\text{ext}}$ concentration of 0.15 mM (marked in red in Figure 26, B). Lowering $[\text{Ca}^{2+}]_{\text{ext}}$ below this critical concentration caused dramatic decline in melanoma proliferation and also a further increase above 0.15 mM had a, though milder, tendency to decrease proliferation. The decrease of $[\text{Ca}^{2+}]_{\text{ext}}$ from 0.37 mM (Ca^{2+} concentration under standard culture condition) to 0.15 mM resulted in an increase in proliferation of 39% (red marks and bars in Figure 26, B and C). Proliferation of cells subjected to FCS starvation was unaffected by varying $[\text{Ca}^{2+}]_{\text{ext}}$ over the range from 0.221 mM down to the critical concentration of 27,4 μM (Figure 26, A). Below this critical concentration, SK-MEL-5 cells showed a similar dramatic decline in proliferation compared to serum supplied cells. FCS deprivation led to a similar, though less pronounced, alteration in proliferation in response to changing $[\text{Ca}^{2+}]_{\text{ext}}$. However, the absolute proliferation level of serum deprived cells was lower than that of serum supplied

Results

cells. In standard culture conditions with 0.22 mM $[Ca^{2+}]_{ext}$, proliferation was increased by 57% upon addition of FCS to the culture medium for 48 h (grey boxes and bar in Figure 26, A-C).

Observations on Ca^{2+} dependence of melanoma proliferation implied that a partial reduction of SOCE by silencing of Orai1 or STIM2 should increase proliferation. Figure 26 (D) shows that Orai1 and STIM2 siRNA-treated SK-MEL-5 cells, indeed, grew faster than control cells (in RPMI + 10% FCS, 0.37 mM free Ca^{2+}). These results supported the findings shown in Figure 26 (B). The increase in cell proliferation 48h after transfection was 43% and 25% compared to control transfected cells (CTRL, black), following Orai1 (gold) or STIM2 (brown) siRNA treatment (Figure 26, D). This effect was even more pronounced 72 h after siRNA-transfection, with an increase in proliferation of 64% when Orai1 mRNA was down-regulated and a respective increase of 56% when STIM2 was targeted (Figure 26 E)

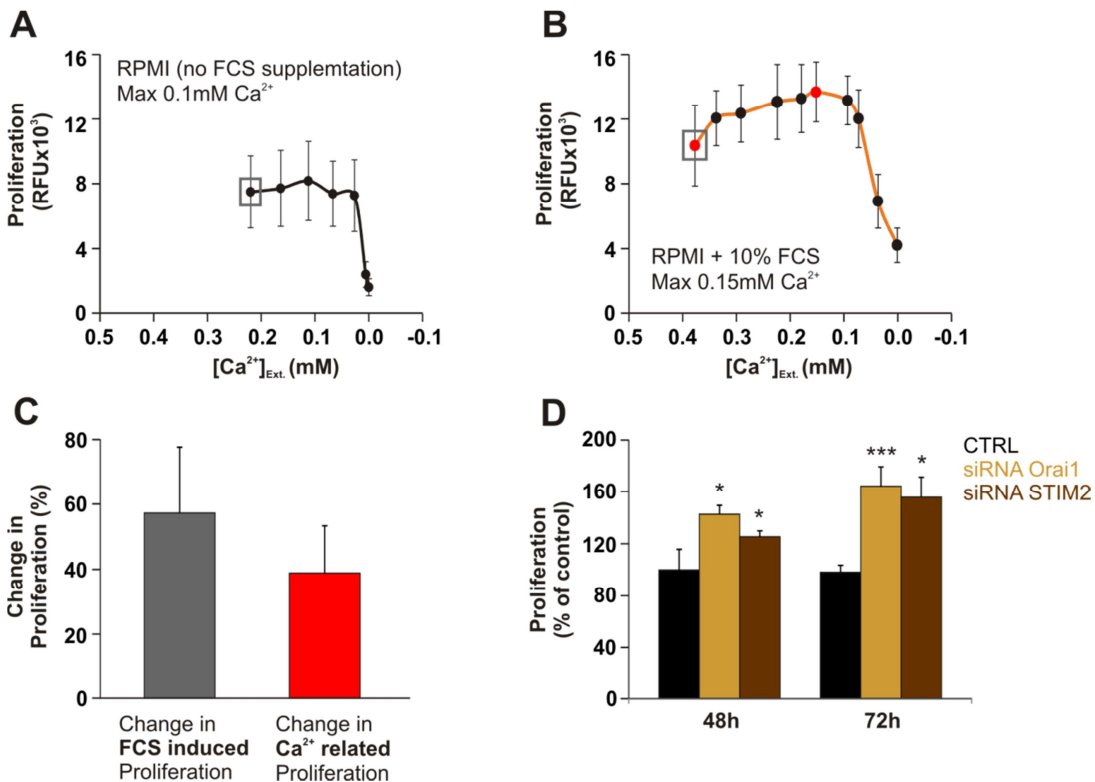


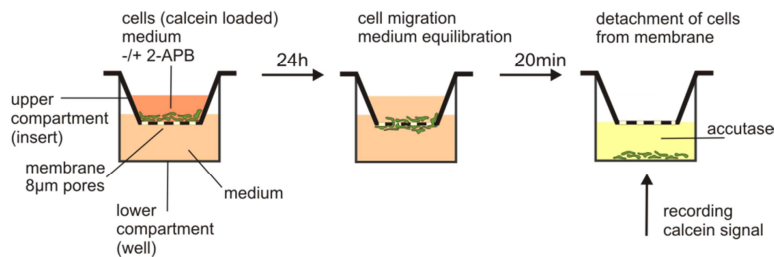
Figure 26 Ca^{2+} -dependency of melanoma proliferation.

Analysis of the proliferative capacity of SK-MEL-5 cells in dependency of the extracellular Ca^{2+} milieu and in dependency of CRAC channel components Orai1 and STIM2, using the CellTiterBlue Viability Assay. Different $[Ca^{2+}]_{ext}$ were adjusted by adding the Ca^{2+} chelator EGTA (Table 19) to the respective culture media. The role of Orai1 and STIM2 was determined in control or siRNA transfected cells. (A-B) Proliferation of SK-MEL-5 cells 48 h after transfection in standard culture medium in the absence (A, black trace) or presence (B, orange trace) of FCS supplementation in dependency of $[Ca^{2+}]_{ext}$. (C) Quantification of change in proliferation in dependency of FCS supplementation calculated at 0.2 mM Ca^{2+} (grey in A-C) and quantification of change in proliferation in dependency of $[Ca^{2+}]_{ext}$ (in the presence of FCS) calculated between 0.15 mM and 0.377 mM $[Ca^{2+}]_{ext}$ (red in A-C). Results in A-C are presented as means from $n = 3$ independent experiments. (D) Proliferation of SK-MEL-5 cells, transfected with control RNA (CTRL, black) and Orai1 siRNA (gold) and STIM2 siRNA (brown) in standard RPMI medium + 10% FCS (0.377 mM $[Ca^{2+}]_{ext}$). Proliferation was measured after cultivation for 48 h and 72 h, reflecting 72 h and 96 h after transfection. Results in D are presented as means from $n = 10/9$ (CTRL, 48/72 h), $n = 10/9$ (Orai1, 48/72 h) and $n = 4/4$ (STIM2, 48/72 h) independent experiments. Error bars indicate SEM and significance is indicated with *, $p < 0.05$ and ***, $p < 0.001$, determined using the paired standard student's t-test.

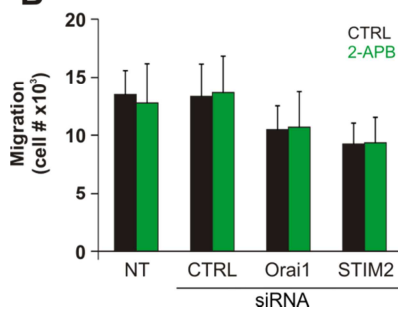
8.6.2 The migratory potential of melanoma cells in dependency on SOCE

Migration of melanoma cells in dependency of CRAC channel mediated SOCE was tested using the transwell-migration assay as described in 7.2.9 and illustrated in Figure 27 (A). WM3734 was the cell line of choice for this set of experiments due to their high migratory potential. Non-transfected cells (NT), as well as cells treated with non-targeting RNA (CTRL) and cells treated with Orai1 or STIM2 siRNA, were allowed to migrate through the provided membranes under standard culture conditions for 24 h. The number of cells migrated was determined using a calibration curve obtained from defined cell numbers (see 7.2.9 for details). Besides the contribution of Orai1 and STIM2 to regulation of melanoma cell migration, the importance of Ca^{2+} signaling in general was further analyzed using the Ca^{2+} channel inhibitor 2-APB. The inhibitor was applied to non-transfected cells, as well as non-targeting RNA and siRNA treated cells (green bars in Figure 27, B). Under control conditions the number of cells that migrated within 24 h was comparable with 13.400 of 100.000 seeded cells (NT and CTRL, black bars in Figure 27, B). On the one hand, down-regulation of Orai1 and STIM2 mRNA resulted in a significant decrease in the number of migrated cells to 10.466 and 9236 respectively. On the other hand, blocking channel activity using 50 μ M 2-APB did not influence the migratory potential (compare black to green bars in Figure 27, B). When normalized to control transfected cells, Orai1 and STIM2 down-regulation resulted in a significant reduction of migration with 21% and 29% respectively (Figure 27, C).

A



B



C

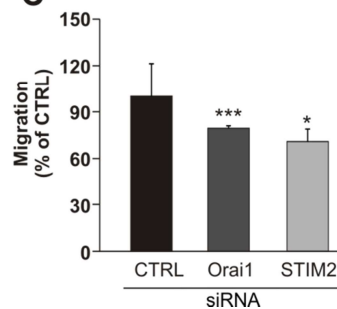


Figure 27 CRAC channel -dependent migration of the WM3734 melanoma cell line.

Determination of the migratory capacity of melanoma cell line WM3734 in dependency on Ca^{2+} -signaling in general and CRAC channel components Orai1 and STIM2, using a transwell-migration assay. (A) Schematic overview of experimental set-up and performance. (B) WM3734 cells transfected with control RNA and Orai1 and STIM2 siRNA were used 24 h after transfection and were allowed to migrate for another 24 h. The number of migrated cells in absence (black) and presence (green) of SOC inhibitor 2-APB was calculated from a standard curve based on fluorescence signals of defined cell numbers. (C) Quantification of effect of Orai1 and STIM2 down-regulation on migration calculated as percentage of control transfected cells. Quantification is based on at least three independent experiments. Error bars indicate SEM and significance is indicated with *, $p < 0.05$ and ***, $p < 0.001$, determined using the paired standard student's t-test.

8.6.3 Molecular mechanisms involved in melanoma progression

To gain insight into the molecular mechanisms enabling Orai1 and STIM2 to regulate the melanoma phenotype, the expression of markers involved in regulating gene expression related to proliferation or migration was analyzed by western blot (as described in 7.2.4). Lysates were obtained from cells treated with NT siRNA or Orai1 or STIM2 siRNA. In addition, cells were transfected with siRNA targeting STIM1 to test for isotype specific effects.

Microphthalmia-associated transcription factor (MITF) is a Ca^{2+} -dependent master regulator of proliferative genes in melanoma. The expression of MITF in cells treated with Orai1, STIM2 and STIM1 siRNA was determined to analyze down-stream effects of altered Ca^{2+} signaling. A representative western blot is shown in Figure 28 (A).

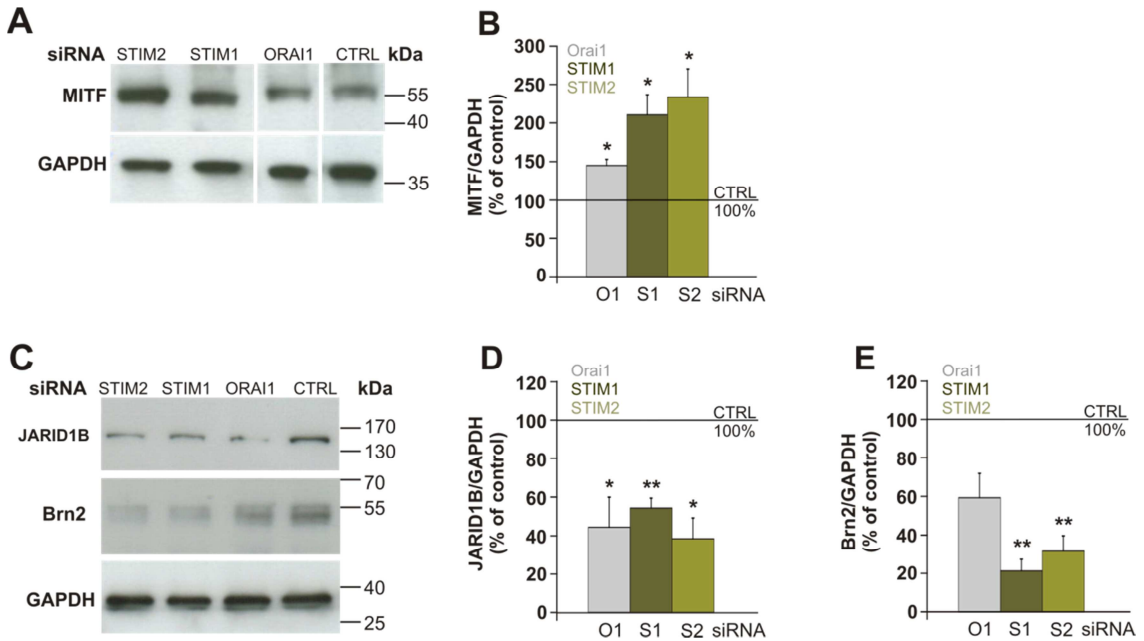


Figure 28 Expression analysis of phenotype markers in human melanoma cell line SK-MEL-5.

Expression of molecular markers was determined by western blot analysis to define a migratory or proliferative phenotype. Expression of phenotype markers MITF (TF), JARID1B (histon-demethylase) and Brn2 (TF) was determined in SK-MEL-5 cells, transfected with control siRNA (CTRL) and siRNA targeting Orai1, STIM1 and STIM2. (A and C) Representative western blots of the detection of expression of MITF (A) and JARID1B and Brn2 (C). (A-E) Protein samples were collected from four independent experiments on day 2 after transfection. Expression was quantified in relation to loading control GAPDH. Quantification of change in marker expression upon Orai1 and STIM knock-downs presented as % of expression in control transfected cells (set to 100 %, black lines) for MITF (B), JARDI 1B (D) and Brn2 (E). Quantification is based on n= 4 (MITF), n = 4 (JARID1B) and n= 3 (Brn2) independent experiments (western blots). Error bars indicated SEM and significance is indicated with *, p < 0.05 and **, p < 0.01, determined using the paired standard student's t-test.

MITF protein was up-regulated 2.7-, 2.5- and 1.6-fold in SK-MEL-5 cells upon knockdown of STIM2, STIM1 and Orai1. This up-regulation is concurrent to an increased proliferation (Figure 28, B and Figure 26, D). In addition, the effects of down-regulation of Orai1 and STIM2 on markers which are typically seen in slow-cycling, pro-metastatic melanoma cell phenotypes were analyzed. These markers were the histone demethylase JARID1B (J1B) and the transcription factor Brn2. As presented in Figure 28 (D), JARID1B protein was significantly reduced by 62%, 46% and 56% in STIM2, STIM1 and Orai1 down-regulated SK-MEL-5 cells.

For Brn2 the respective values were 79%, 68% and 41% (Figure 28, E). A representative western blot is shown in Figure 28 (C).

The cytokine IL-8, a member of the CXC-chemokine family, promotes cell proliferation and serves as an autocrine growth factor in melanoma progression (see 6.3.3 for details). With regard to markers involved in regulating gene expression related to either a more proliferative or migratory phenotype (see above), the secretion of IL-8 was determined to further verify the role of Orai1 and STIM2 in defining the respective phenotype. IL-8 was measured in an ELISA from cell culture supernatants as described in 7.2.10. Supernatants were collected from cells either treated with NT RNA or Orai1 and STIM2 siRNA.

The knockdown of Orai1 mRNA resulted in a significant increase in secreted IL-8 from 3.12 ng/ml under control conditions (CTRL) to 5.04 ng/ml (Figure 29, A), reflecting an increase of 64% (Figure 29, B). The influence of STIM2 mRNA down-regulation was determined in a separate data set, with measured IL-8 levels of 0.54 ng/ml under control and 1.53 ng/ml under knockdown conditions (Figure 29, A). Although the absolute IL-8 concentration was much lower in the STIM2 data set compared to Orai1, the effect of the knockdown was far more distinct, reflecting a 190% increase in IL-8 secretion.

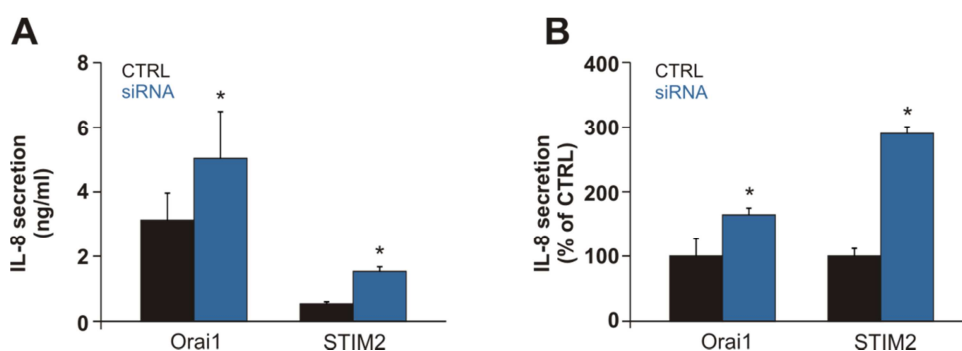


Figure 29 IL-8 secretion by SK-MEL-5 melanoma cell line.

IL-8 production by SK-MEL-5 cells was determined by ELISA to characterize the role of Orai- and STIM-mediated Ca^{2+} signaling on cytokine production. (A and B) IL-8 secretion by cells, transfected with control siRNA or Orai1 and STIM2 siRNA. Data was averaged from $n = 8$ (control/siOrai1) and $n = 4$ (control/siSTIM2) independent experiments. (A) Amount of IL-8 secretion upon siRNA treatment, presented as ng/ml. (B) Quantification of effect of STIM2 and Orai1 down-regulation on cytokine secretion calculated as % of control transfected cells. Error bars indicate SEM, significance is indicated with *, $p < 0.05$, determined using the paired standard student's t-test.

8.7 Designation of monocyte survival by the extracellular Ca^{2+} and redox environment

In contrast to melanoma cells, monocytes are non-proliferative cells. It was observed throughout the study, that the number of surviving monocytes declined rapidly after isolation under standard culture conditions with a loss up to 50% at day 3 (data not shown). Data obtained so far concerning the effect of altered Ca^{2+} concentration on cell proliferation implied a potential role of the extracellular Ca^{2+} milieu for long-term survival effects. In terms of the extracellular environment, monocytes contribute to an oxidizing environment by production of ROS (see 6.1.3.2 and 6.2.2). Hence, the effects of an altered extracellular milieu on cellular survival was analyzed *in vitro* by changing Ca^{2+} concentration of the culture medium RPMI or increasing the redox stress with supplementation of H_2O_2 (described above in 8.5). Regarding

the results obtained from melanoma experiments, the influence of hormones and serum proteins in regulating cell survival was investigated by serum supply or deprivation of the culture medium. Survival of non-stimulated monocytes was tested under different conditions using the CellTiterBlue viability assay as described in 7.2.8 with summarized results presented in Figure 30.

Redox stress. The presence of increasing concentrations of H_2O_2 decreased the number of viable monocytes with an IC_{50} of 150 μM , after 24 h in culture (Figure 30, A). The IC_{50} was determined by plotting the resulting intensities from viable cells with the corresponding H_2O_2 concentration.

The data points were fitted with a first order exponential decay fit and the IC_{50} was graphically determined, as already explained in 8.4.2. The determined concentration of 150 μM H_2O_2 was used in further experiments to evaluate the reaction of cells to an external applied redox stress.

Ca^{2+} dependency of monocyte survival. While experiments in melanoma cells revealed a high impact of the $[\text{Ca}^{2+}]_{\text{ext}}$ on cell proliferation, monocyte survival was nearly unaffected by a decrease in Ca^{2+} levels under standard culture conditions (orange trace in Figure 30, B and C). FCS deprivation rendered the cells, however, sensitive to changes in the $[\text{Ca}^{2+}]_{\text{ext}}$ (black traces in Figure 30, B and C). After 24 h, cell survival rapidly declined when the $[\text{Ca}^{2+}]_{\text{ext}}$ reached levels below 0.07 mM. This effect increased when the duration of cultivation under serum-deprivation was prolonged to 48 h. In that case, Ca^{2+} levels below 0.11 mM led to a decline in cell survival (black trace in Figure 30, D). At an intermediate $[\text{Ca}^{2+}]_{\text{ext}}$ of 0.22 mM (grey box in Figure 30, B), FCS starvation had no further influence. When $[\text{Ca}^{2+}]_{\text{ext}}$ was reduced to a level < 0.001 mM (red box in Figure 30, B), monocytes survival under starvation was significantly reduced by 61%. This effect was even more obvious after 48h of cultivation, where a significant reduction of survival of 84% was detected (quantified in Figure 30, E). In presence of Ca^{2+} (0.22 mM), only a moderate reduction of 8% was detectable. Taken together, in presences of FCS, monocyte survival was unaffected by even severe changes in $[\text{Ca}^{2+}]_{\text{ext}}$ (orange traces in Figure 30, B and C). Monocytes also displayed a non-significant tendency to a higher survival at decreased Ca^{2+} levels (0.11 mM, Figure 30, C).

Concurrence of Ca^{2+} and redox challenges in monocyte survival. Cells were cultured for 24 h under variable Ca^{2+} concentrations and in the absence or presence of FCS, prior to the incubation with the beforehand determined IC_{50} of 150 μM H_2O_2 for another 24 h. On the one hand, cultivation for 48 h under altered Ca^{2+} levels, did not reveal an additional effect to the inhibitory effect to the H_2O_2 treatment over the investigated Ca^{2+} range (green trace in Figure 30, C). On the other hand, upon FCS starvation and unaltered $[\text{Ca}^{2+}]_{\text{ext}}$ of 0.22 mM, monocyte survival was decreased about 94% in the presences of H_2O_2 . In the presence of FCS, cell survival was only decreased about 39%, revealing a significant difference in the response to H_2O_2 depending on the presence of FCS. A comparable, yet not significant, relation was given under reduced Ca^{2+} levels (< 0.001 mM) with 74% inhibition of cell survival under starvation and only 44% inhibition in the presence of FCS (Figure 30, F).

Results

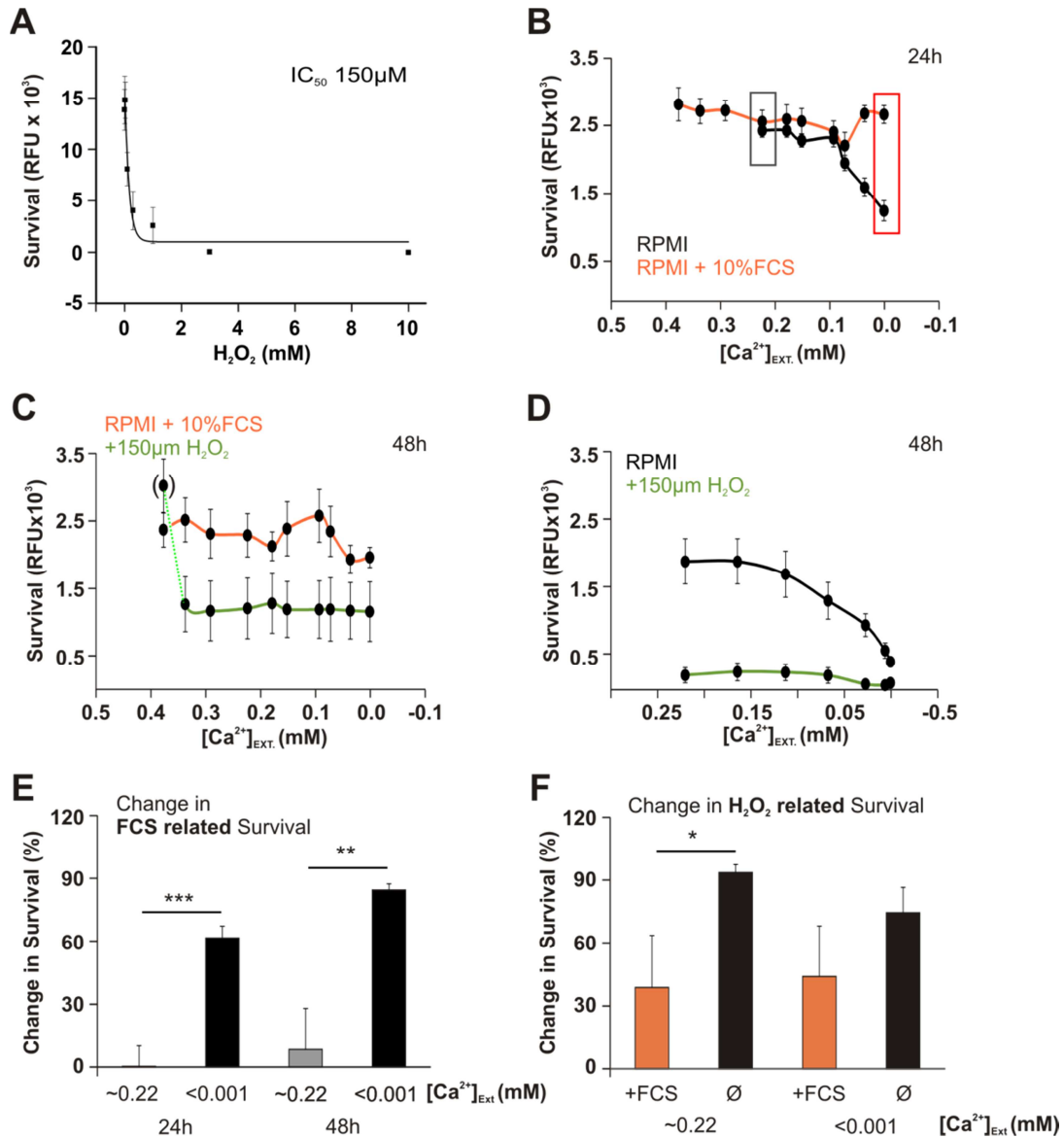


Figure 30 Monocyte survival in dependency of the Ca²⁺ and redox environment.

Analysis of the survival of primary human monocytes in different redox and Ca²⁺ milieu, using the CellTiterBlue Viability Assay. Different [Ca²⁺]_{ext} were adjusted by adding the Ca²⁺ chelator EGTA to the standard culture media (Table 19). (A) Survival of monocytes in dependency of increasing [H₂O₂]_{ext} (1 μM-10 mM) depicted as means, averaged from at least n = 3 independent measurements per H₂O₂ concentration. Determination of IC₅₀ by a first order exponential decay fitting of the data set. (B) Survival of monocytes after 24 h in presence (orange) or absence (black) of serum proteins (FCS) in dependency of [Ca²⁺]_{ext}. (C-D) Survival of monocytes after 48 h in presence (C, orange trace) or absence (D, black trace) of serum proteins (FCS) in dependency on [Ca²⁺]_{ext} and in presence (green) or absence (orange and black) of 150 μM H₂O₂. (E) Quantification of change in survival related to FCS supplementation calculated at 0.22 mM and <0.001 mM [Ca²⁺]_{ext}. (F) Quantification of change in survival related to H₂O₂ treatment calculated at 0.22 mM and <0.001 mM [Ca²⁺]_{ext} in presence (orange) and absence (black) of FCS. For Ca²⁺-related survival studies (B-F), n = 2 independent experiments with n = 6 data points/measurement were performed. First data point in brackets in C identified as significant outlier. Error bars indicate SEM and significance is indicated with *, p < 0.05, **, p < 0.01 and ***, p < 0.001, determined by the paired standard student's t-test.

9 Discussion

Intra- and intercellular signaling regulating cellular functions involves and is influenced by the extracellular environment. Cellular signaling is not only influenced by the extracellular milieu, but also alters and defines the extracellular space by release of signaling molecules and enzymes. The immune system and the skin are both considered as organ systems displaying a high importance for Ca^{2+} and reactive oxygen species in regulating cellular (signaling) processes. Ca^{2+} and ROS act on a molecular level as second messengers and as components of the cellular environment. The investigation of the regulation of a certain Ca^{2+} signaling pathway, the store-operated Ca^{2+} entry (SOCE), in the context of the skin and the immune system was focus of the here presented study.

9.1 STIM and Orai proteins differentially contribution to SOCE

9.1.1 Orai1/2 and STIM1/2 contribute to SOCE in monocytes, revealing an important role of the so far neglected isoforms Orai2 and STIM2.

Calcium imaging experiment revealed a contribution of all Orai and STIM isoforms to SOCE, though to a different degree. Down-regulation of STIM1 and STIM2 revealed the strongest impact and reduction of SOCE. Although the success of down-regulation using siRNA was rather limited, especially in the case of STIM2, where only 47% of the respective mRNA was targeted. It is likely to assume that full diminishing of STIM1 and/ or STIM2 mRNA will lead to an almost complete abolishment of the protein and subsequent SOCE. The strong contribution of STIM2 in SOCE, demonstrate the differences in SOCE regulation and gating among different cell types. So far, STIM1 was reported to be the dominant isoform in most studied immune cells, and for dendritic cells, STIM2 alone was suggested to be the dominant player (see 6.6.1 for details). In monocytes the two STIM isoforms have an equal contribution to SOCE and, as pointed out below, also in Ca^{2+} -dependent ROS production. Orai1 is the dominant Orai isoform contributing to SOCE, a finding concomitant with results from other phagocytes (see above, 6.6.1). The limited contribution of Orai2 to SOCE was surprising, regarding a report from 2011 presenting Orai2 to be the dominant isoform in dendritic cells that, as monocytes, show a high expression level of Orai2 (Bandyopadhyay *et al.*, 2011). The high Orai2 expression though pointed to a potential high contribution to SOCE in monocytes, although the insufficient down-regulation by siRNA (74%) has to be taken into consideration. Orai3 down-regulation resulted in the expected rise in SOCE, which can be related to its lower Ca^{2+} conducting capacity compared to Orai1 and Orai2. Based on the results obtained from this study, the expression level of Orais and STIMs can be related to their degree of contribution to SOCE, with exception of Orai2. To describe this relation, the absolute and relative expression has of the proteins have to be considered: Firstly, a high absolute expressed isoform also showed a high contribution to SOCE and *vice versa*. Secondly, and even more important, the relative expression of Orai and STIM molecules as determinants. In general, SOCE was shown to have an optimal channel to gatekeeper ratio with 1:2 Orai(1) to STIM(1) (Li *et al.*, 2011). As it was shown in this study for monocytes and prior for T cells (Bogeski *et al.*, 2010), the relative Orai3 to Orai1 expression is an important parameter in the modulation of redox sensitivity of SOCE. In addition, the ration of Orai3 to Orai1 (and Orai2) will impact overall SOCE due to the differences in Ca^{2+} conductance. As it was observed in monocytes, SOCE increases under control conditions in the absence of Orai3 (see. Figure 14 Figure 22). The observed increase though was not always

significant. In order to analyze the impact of altered Orai3 expression on Ca^{2+} influx in more detail, patch-clamp analysis on Orai3 knockdown cells compared to control cells would be the method of choice. Such experiments might provide an insight into altered I_{CRAC} depending on the Orai isoform composition. The analysis of the SOCE using calcium imaging only provides information on global Ca^{2+} signals. Since the analysis of I_{CRAC} was not an aim of this study and due to difficulties in the performance of patch-clamp on primary human monocytes, the analysis was restricted to SOCE.

The general importance of the SOCE in monocytes is difficult to judge due to lack of full down-regulation of the components and the lack of information on a monocyte phenotype from knockdown mice. The obvious importance for STIM in regulating SOCE implies a potential role in regulating other Ca^{2+} channels also expressed by monocytes. A siRNA screen of TRP channel expression in primary human monocytes (one cDNA sample, full data not presented here) showed that TRPV2, TRPV6, TRPM2 and TRPM7 are expressed on a comparable, or even higher level than Orai and STIM isoforms with $2^{-\Delta\Delta\text{Cq}}$ values of 3.85 (V2), 1.00 (V6), 0.32 (M2) and 0.51 (M7). Especially TRPV6 as Ca^{2+} -selective channel might be an important player in monocyte Ca^{2+} signaling. Furthermore, TRPC and Orai proteins have been suggested to associate to mediate SOCE in different cell types and systems (Bréchar *et al.*, 2008; Saul *et al.*, 2013). This option might not be the case for monocytes, because TRPC mRNA detection was either not possible (TRPC3) or only on marginal levels (TRPC1, $2^{-\Delta\Delta\text{Cq}} < 0.002$). Further analysis of TRP expression in these cells and studies on monocytes from STIM (and Orai) knockout mice are likely to fill in the gaps in understanding the precise role of the single isoforms in this cell type.

9.1.2 SOCE in melanoma cells lines is mediated by Orai1 and STIM2

In the two investigated melanoma cell lines, Orai1 and STIM2 were the dominant expressed isoforms. Down-regulation of Orai1 and STIM2 resulted in an almost complete reduction of SOCE, and the simultaneous knockdown of Orai1 and STIM2 almost completely abolished SOCE. Orai1 and STIM2 therefore can be considered as essential components in the SOCE signaling cascade of melanoma cells. As for monocytes the expression profile reflects the contribution to SOCE. The results from melanoma cell lines are further in line with the findings from primary melanocytes, where Orai1 and STIM2 were previously shown to be the dominant isoforms (Stanisz *et al.*, 2012). Despite the fact, that Orai1 and STIM2 regulate SOCE in the two different cell lines investigated in this study, they also displayed obvious differences. In SK-MEL-5 cells the Ca^{2+} elevations following store release were as high as the Ca^{2+} influx mediated by activated CRAC channels, while the store release from WM3734 cells was much smaller compared to SK-MEL-5 and smaller than the Ca^{2+} influx. These results suggest substantial differences in size and capacity of the internal Ca^{2+} stores. Also the influx rates differed between the cell lines, where WM3734 showed a fast and steep influx after Ca^{2+} re-addition, while the rates in SK-MEL-5 cells displayed lower influx rates. These overall differences in Ca^{2+} signal shape might be of importance in the regulation of downstream Ca^{2+} -dependent functions, or might be an adaptation to their respective environment. Regarding the regulation of down-stream effects, there were intensive investigations on how distinct Ca^{2+} signal modulations trigger different Ca^{2+} -dependent responses in cells, as for example the regulation of different transcription factors or activation of signaling cascades (eg. MAPK) (see 6.1.1 and 6.3.3 for details).

9.1.3 Additional aspects – The differences and similarities regarding SOCE in different cell systems

Dominance of Orai and STIM isoforms. This study emphasized the importance of STIM2 in respect to the so far more thorough investigated isoform STIM1. In the investigated cell types STIM2 was shown to be either the main expressed isoform (melanoma) or it was shown to act together with STIM1 and contribute to SOCE to the same degree (monocytes). Orai2 was not targeted in melanoma cell lines in this study. Its relative low expression (compared to Orai1 and Orai3) might be an indicator for only a marginal contribution to SOCE, or it might contribute to specialized functions. The little contribution of Orai2 to SOCE in monocytes and the clear dominant role of Orai1 in all investigated cell types of this study, confirms the dominance of Orai1 in regulating SOCE in many cell types, such as immune and skin cells.

Physiological versus non-physiological stimulation. In a recent study analyzing the role of SOCE in melanocyte function (Stanisz *et al.*, 2012), endothelin-1 (ET-1) was used as physiological stimulus to trigger SOCE *via* binding to its cognate receptor. However, ET-1 stimulation of melanoma cell lines failed to activate SOCE. Thus, the widely accepted drug Tg was used to trigger the activation of the CRAC channel signaling cascade. Although the presence of SOCE in melanoma cells is indisputable, the identification of a physiological stimulus will be the next step to take, in order to further analyze the role of SOCE in tumor progression and to target the signaling cascade for therapeutic means. An example would be ligands of the metabotropic glutamate receptor, that are expressed in melanoma and were shown to trigger IP₃ release and ER Ca²⁺ store depletion (Lee *et al.*, 2008). The physiological ligand, glutamate, could be used as physiological stimulus to trigger SOCE, but also other signaling cascades in melanoma. In monocytes Tg was used to carefully analyze the effects of Orai and STIM down-regulation on SOCE and Ca²⁺-dependent ROS production. In addition, the physiological stimulus fMLF was applied, since it was shown to successfully activate CRAC channels by binding to its receptor FPR1 (Li *et al.*, 2008; Bréchar *et al.*, 2008). The existence of SOCE following Tg and fMLF stimulation could be shown by its abolishment in the presence of the SOCE inhibitor 2-APB. As representative shown for the analysis of Ca²⁺ dependency of SOCE in monocytes (Figure 18), the observed effects under Tg stimulation were also detectable under fMLF stimulation, but were usually less pronounced and subject to even higher fluctuations. Regarding this, and the differences in Ca²⁺ signal shape under fMLF and Tg stimulation in store-depletion protocols (see Figure 13), Tg was the more suitable stimulant to carefully detect an impact of Orai and STIM down-regulation on Ca²⁺ signals and Ca²⁺-dependent ROS production (see also 9.2.2).

9.2 ROS production in monocytes is dependent on Ca²⁺ signaling with a particular role for Orai and STIM mediated SOCE

9.2.1 NOX2 is the source for enzymatic ROS production in monocytes

In the immune system, NOX2 is the predominant expressed isoform, as it is responsible for ROS production by phagocytes and was shown to be expressed in neutrophils, macrophages, monocytes, and several immune-cell derived cell-lines (see 6.1.2.3 and 6.6.1). The recent suggestion that NOX4 is an additional source of ROS (especially H₂O₂) (Lee *et al.*, 2010a; Ullevig *et al.*, 2012), could not be verified or confirmed by the here presented study. Although the experimental set up in this study could clearly show NOX as the source of ROS in response to stimulation, the inhibitors used were rather unspecific. DPI is a known inhibitor of NADPH

oxidases, but cannot be used to distinguish between different NOX isoforms. The PKC inhibitor Bis/Gö instead is more specific, since it activates PKC, a key step in the assembly process of the NOX2 (see also Table 8). Activation of NOX4 does not require the activation of PKC, because NOX4 activity is not dependent on the recruitment of cytosolic subunits. A step regulated by phosphorylation of the mentioned subunits by PKC in the case of NOX2. The most convincing evidence for the sole presence of NOX2 in monocytes was the qRT-PCR screen of NOX and DUOX family members that did not show the presence of NOX4 mRNA (Figure 17). The functionality of the used NOX4 primers was confirmed by internal positive controls, and was in addition successfully used to detect NOX4 expression in melanoma cell lines (data not shown).

9.2.2 NOX2 activation is dependent on the elevation of Ca²⁺ signals

The applied methods used to determine ROS production upon activation of SOCE both confirmed the dependency of ROS production (superoxide and H₂O₂) on the influx of Ca²⁺ from the extracellular space. Independent on the measuring technique, the removal of extracellular Ca²⁺ caused complete abolishment of ROS production under Tg stimulation. However, under fMLF stimulation the production of H₂O₂ was only reduced to 50 %, leaving the initial rise in H₂O₂ following stimulus application unaltered (see panel B in Figure 18). An explanation of the different effect of Ca²⁺ removal depending on the stimulus is the difference in the activation of NOX2 using Tg or fMLF. As pointed out in the introduction and above, Ca²⁺ elevation is an important step in the assembly process of NOX2 (6.4.2). Under the use of Tg this Ca²⁺ elevation is the only activation step in the otherwise complex process. With the physiological stimulant fMLF, Ca²⁺ elevation is only one aspect of the signaling cascade, as the receptor engagement also leads to the activation of PKC not only by Ca²⁺, but also by the generation of DAG (6.2.2). The Ca²⁺ released from internal stores, usually fails to activate NOX2 alone. In the case of fMLF the concomitant activation of PKC by DAG seems to be sufficient to activate NOX2 in the absence of external Ca²⁺, though in a limited manner.

9.2.3 Orai and STIM are differentially involved in regulating NOX2 activity

9.2.3.1 *Orai1, STIM1 and STIM2 provide a Ca²⁺ influx necessary for ROS production*

The influx of extracellular Ca²⁺ to the cytosol required for proper ROS production was shown to be mediated mainly by Orai1, STIM1 and STIM2. The reduction of the amount of H₂O₂ produced following Tg stimulation in Orai1, STIM1 and STIM2 siRNA treated cells, could be correlated to the degree of reduction of SOCE. The contribution of Orai1 and STIM1 in phagocyte ROS production has already been demonstrated for neutrophils (see 6.6.1) and could be confirmed for monocytes in this study.

Regarding the role of STIM molecules in phagocyte ROS production, a contribution of STIM2 was so far either ruled out or not the topic of investigations (see 6.6.1). The comparable expression levels and the equal effect of STIM1 and STIM2 down-regulation on SOCE implied a contribution of not only STIM1 but also STIM2 in monocyte ROS production. Regarding the impact of down-regulation one can assume that STIM2 might even play a dominant role. STIM1 down-regulation, though more efficient than STIM2, did not result in a stronger reduction in H₂O₂ production compared to STIM2. In line with the effects on SOCE, it is likely that a full down-regulation of STIM2 (and STIM1) will lead to a complete abolishment of H₂O₂ production. On the basis of this study, the gating of the CRAC channels, rather than the channel components itself seem to be the major players in regulating Ca²⁺-dependent ROS production.

In a broader scope, additional functions of STIM molecules are possible, as for example in regulating other Ca^{2+} channels, thereby influencing ROS production (compare to 9.1.1). A Ca^{2+} -independent context is likewise possible, as it will be discussed below in the additional aspect section (see 9.2.4).

9.2.3.2 Kinetic analysis

The kinetics of H_2O_2 production displayed high donor and experimental variability regarding overall shape and production rates. In most cases two phases could be observed: a main production phase, where a constant increase in net H_2O_2 production could be observed, and a prolonged or saturation phase, in which no additional H_2O_2 was produced, or with a clearly reduced rate. Due to high donor dependent variations, the overall kinetic analysis was limited to be descriptive (see Table 17 and Table 18). Differences in production rates were obvious, though a standardized definition of a phase and its production rate would have been highly subjective and was therefore not further analyzed.

Anyway, the tendencies observed might be a first indication for implications and further analysis. For example, the differences in reaching saturation might depend on the inactivation of the CRAC channels. Therefore, different composition of Orai and STIM isoforms in the machinery and the mode of inactivation are likely determinants of the period of ROS production. The same accounts for changes in production rates, in response to down-regulation of Orai and STIM (see Table 17). Time scale and production rates are possible modulators of redox signaling, that could result in different cellular responses, as it was shown for the modulation of Ca^{2+} signals (see 6.1.1). Overcoming the issue of high donor dependency using an appropriate cell line, might be a possibility to analyze ROS production kinetics in a more objective manner.

9.2.3.3 Something new: Orai2

Regarding the strong evidence for Orai1 and STIM1/2 mediating the necessary Ca^{2+} influx for ROS production, the results of Orai2 down-regulation on H_2O_2 production were surprising. Although Orai2 down-regulation resulted in reduced SOCE, H_2O_2 production was severely increased instead of decreased. This contrary effect was also the most stable one, compared to the effect of Orai1 or STIM1/2 down-regulation. While the data sets of Orai1 and STIM1/2 displayed a huge variety and donor dependent fluctuations, the increase in H_2O_2 production in Orai2 knockdown cells was stable and nearly free of instabilities. With the intensive studies conducted in neutrophils and respective cell lines and the results of this study, there is no doubt for the dependency of ROS production on Ca^{2+} signaling and a contribution of SOCE (see 6.5. for details). This and the fact that the impact of Orai2 down-regulation on SOCE was mild compared to the impact on H_2O_2 production implies a Ca^{2+} -independent mechanism underlying the observed events.

Based on the obtained results it is possible to hypothesize that Orai2 is an inhibitory modulator of NOX2 activity with the purpose to prevent overshooting responses. As presented in the scheme below (Figure 31) the assembly process of the different subunits of NOX2 depends on various protein-protein and protein-lipid interactions between the different cytosolic subunits and the membrane residing core unit as well as the plasma membrane. To act as modulator, Orai2 might be a competitor in binding of NOX2 subunits, thereby limiting the number of fully assembled holoenzymes and the amount of ROS produced by the cells. However, two factors restrict the hypothesis. Firstly, the binding of NOX2 subunits has to take place *via* a unique binding site not present in Orai1 and Orai3 or underlying a specific binding affinity to be limited

to Orai2. This binding site is in addition supposed to be an PRR or an SH3 domain to properly bind NOX2 subunits in competition to the cytosolic subunits. Based on the ongoing research to identify the exact structural basis of the SOCE machinery, one could suggest a potential NOX-binding site in the cytosolic regions of Orai2. This region are the C- and N-terminal regions as well as the cytosolic loop between the trans-membrane domains 2 and 3 (Stathopoulos & Ikura, n.d.). However, there is no valid information so far available, that would explain a unique binding of Orai2 (instead of Orai1 or Orai3). Secondly, the observed effect, though strong and stable, is limited to Tg stimulation. While in all other investigated cases, fMLF stimulation displayed the same tendency as Tg, fMLF-induced ROS production is not altered in Orai2 knockdown cells. Therefore, a verification of the suggested hypothesis requires intensive molecular analysis of the binding properties of all Orai proteins with the potential NOX2 targets and a careful analysis of the activation pathway and the chosen stimulant.

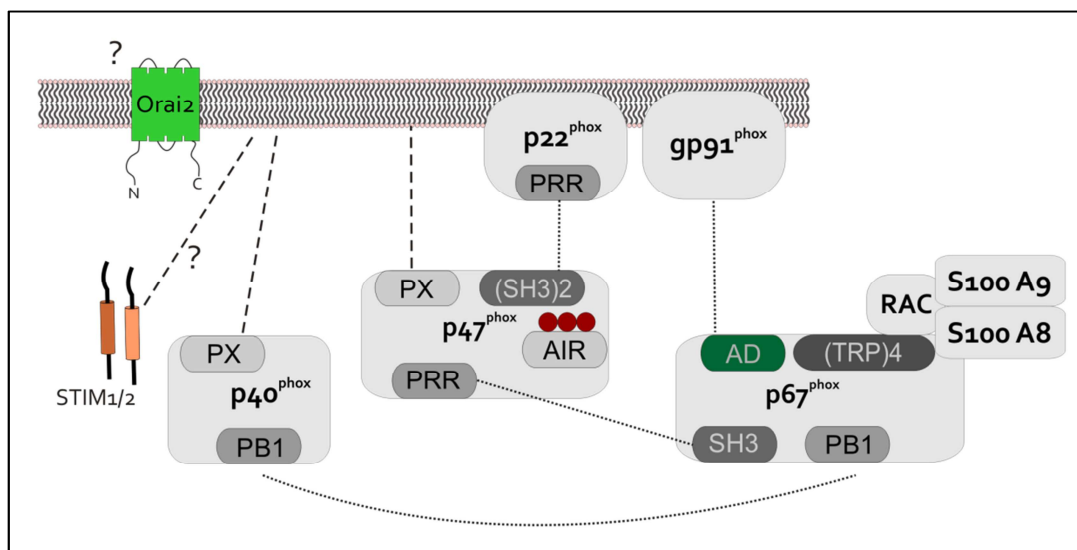


Figure 31 Interaction and binding within the assembly process of NADPH oxidase 2

Scheme of protein-protein interactions among the different subunits in the assembly of NOX2 and a potential involvement of Orai2 binding sites. Dotted lines indicate protein-protein interactions and dashed lines indicate interaction of proteins with membrane lipids. The AIR of p47^{phox} is bound to (SH3)₂ when not phosphorylated. Phosphorylation (red dots) exposes SH3 domains for binding to p22^{phox}. Domain nomenclature and explanations: PX – Phox homology domain, SH3 – SRC Homology 3 Domain, SRC – Proto-oncogene tyrosine-protein kinase Src (sarcoma), AIR – auto-inhibitory region, PRR - proline-rich region, PB1 – Phox and Bem1p protein domain (involved in protein-protein-interactions), TRP - tricodecapeptide repeat (TPR) domains, AD – activation domain. Information taken from (Lambeth, 2004; Kerkhoff *et al.*, 2005; Bedard & Krause, 2007; El-Benna *et al.*, 2009).

9.2.4 Additional aspects – Potential and limitation to the interpretation of ROS production by monocytes

Potential for interpretation: Orai and STIM molecules in the NOX2 assembly process. As suggested for Orai2 above, also STIM proteins hold potential to be involved in regulation of NOX2 assembly in a Ca²⁺-independent context. STIM1 and STIM2 were shown to bind phosphatidylinositol phosphates (PIPs). PIPs are important anchors in the plasma membrane to bind the modulator and organizer subunits p40^{phox} and p47^{phox}, thereby stabilizing the NOX2 complex (see Figure 31). STIM2 binds the PIP metabolites PIP₂ and PIP₃, while STIM1 is limited to PIP₃ binding (Ercan *et al.*, 2009). STIM1 and STIM2 could therefore be involved in stabilizing the NOX complex, or could be involved in the physical and functional coupling of

NOX and Orai channels to provide local Ca^{2+} signals, as shown for STIM1 in neutrophils (Nunes *et al.*, 2012).

Limitations to interpretation: Fluctuations in monocyte ROS production. Limitations in cell numbers restricted knockdown experiments to fluorescent methods and the analysis of the amount of ROS produced under different conditions revealed high fluctuations, even between control conditions (see black data points in Figure 20). The high fluctuations can partially be explained by general donor dependency usually observed using primary cells and by fluctuations in the expression of NOX2 (see high SEMs in Figure 17). Due to the high fluctuations the results were presented showing both the mean and the median values (Figure 20). In optimal distributed data sets, median and mean values show no or only limited deviation as for example in the Orai2 and STIM2 data sets. In a more diverse picture as the data sets for Orai1 and STIM1, there is a high deviation between the two parameters. Although in all cases the tendency of the result of the knockdown was obvious, statistical analysis only showed significance in the case of Orai2 and STIM2.

9.3 Redox-regulation of CRAC channels

9.3.1 In Monocytes Orai3 is a redox-insensitive isoform, that serves as modulator of SOCE-dependent ROS production in monocytes

Orai3 defines redox-sensitivity of SOCE. H_2O_2 inhibits SOCE in monocytes with an IC_{50} of 155 μM , displaying a higher redox-resistance than other mammalian cells. Naïve and effector T cells were shown to be more redox-sensitive, with an IC_{50} of 10 and 83 μM respectively (altered calculations from (Bogeski *et al.*, 2010)). The importance of Orai3 in regulating the redox-sensitivity of CRAC channels in T cell differentiation was demonstrated by Bogeski and colleagues (Bogeski *et al.*, 2010) and pointed towards a role of Orai3 in redox-challenged cells such as phagocytes. These findings could be confirmed by this study, as down-regulation of Orai3 resulted in an increased inhibition of SOCE. This study showed that the modulatory role of Orai3 is not a T cell specific, but rather a general mechanism of immune cells to protect their Ca^{2+} signaling pathway by up-regulation or general high expression levels of Orai3. RNAi mediated down-regulation of Orai3 did not reveal an active contribution to NOX2 activity (8.4.4). However, the redox-insensitive isoform indeed holds an important function as modulator of redox-sensitivity of SOCE in monocytes. The presence of Orai3 defines the redox-sensitivity of CRAC channels, while the other isoforms mediate and regulate SOCE thereby defining the amount of ROS produced. The analysis of overall redox-sensitivity of SOCE revealed a biphasic effect of H_2O_2 (see two phases in Figure 21, D). This might be an indication for differences in the mode of redox-regulation of the CRAC channel. It is possible, that different concentrations of the oxidant results in different oxidation modes (indirect vs. direct), or different oxidation states of the target cysteine residues (see 6.1.2.2 for details).

A regulatory feedback loop. In monocytes Orai3 is not only a modulator of redox sensitivity of SOCE, but is also part of a feedback loop in the interplay between CRAC channels and NOX2 activity. The suggested feedback loop (Figure 32, A) describes the restriction of overshooting ROS production by NOX2 *via* a feedback of the produced H_2O_2 on the CRAC channels that provide the required Ca^{2+} signal. By partial inhibition of the SOCE, NOX2 activity is reduced but prolonged. Calcium imaging and ROS measurements provided evidence for dependency of NOX2 activity on Orai and STIM mediated Ca^{2+} signals and on the inhibitory effect of H_2O_2 on SOCE (8.3.2 and 8.4.1). Further experiments aimed to analyze the impact of Orai3 down-

regulation on Tg triggered, hence Ca^{2+} -dependent, ROS production (see Figure 23, B). The experiments revealed an inhibition of Tg-triggered ROS production only in the absence of Orai3. Taken together, these experiments were the basis for the suggested feedback loop. A regulatory feedback loop is of physiological relevance due to the importance of restriction and regulation of ROS production. This regulation is a necessity and prerequisite to prevent pathological effects of ROS and to serve as signaling molecules (see also 6.1.2).

Channel constitution and its effect on redox sensitivity and SOCE. As pointed out in the introduction the actual confirmation state of activated CRAC channel is not fully elucidated (see 6.4.1). Based on the results from T cell studies and the results from monocytes, an increasing number of channels containing Orai3 subunits, can be linked to overall decreased Ca^{2+} permeability, hence smaller SOCE. In parallel, higher Orai3 expression leads to a gain in redox-resistance (Figure 32, B). The overall channel confirmation will also depend on the expression level of the single Orai subunits. As illustrated in the upper part of Figure 32 (B) one can assume how the channel confirmation might occur depending on the abundance of the single isoforms in different immune cell types. In T cells, Orai1 is the dominant expressed isoform, while in monocytes Orai2 is expressed at comparable levels. It is therefore to assume, that Orai1 and Orai2 subunits are equally abundant in the CRAC channels of monocytes. Unpublished data from Dr. Dalia Alansary (Niemeyer/Hoth group, Biophysics, Homburg), revealed that one Orai3 subunit per channel is sufficient to gain redox-resistance while further insertion of Orai3 does not enhance this effect. One can conclude that it is the number of channels containing an Orai3 subunit that defines the overall sensitivity of SOCE, rather than the number of Orai3 subunits per channel. These observations also imply the favor of heteromeric channels rather than homomeric ones.

9.3.2 An equation describes the correlation between Orai3/Orai1 expression profiles and the redox sensitivity of SOCE

Regarding the expression of Orai3 it is important to note that not the absolute Orai3 expression, but rather the relative Orai3 to Orai1 ratio defines redox sensitivity of SOCE. These relative ratios were determined for all investigated cell types in this study revealing similarities and differences between monocytes and melanoma and in between melanoma cell lines. WM3734 showed the lowest Orai3/Orai1 expression ratio of the tested cell lines. This might be ascribed to the different origin of this cell line that derives from brain metastasis compared to cell lines deriving from primary melanoma (see 7.1.6).

As differences in Ca^{2+} signaling, differences in gene expression can be considered as result of adaption to a certain specialized environment. High Orai3 levels can be ascribed to adaption to a redox-challenging environment as effector T cells or phagocytes encounter in inflammation. In the case of melanoma the high absolute Orai3 expression levels as well as the high Orai3/Orai1 ratios might be an adaption to both, high UV-induced redox stress in the skin and a cancerous environment. The role of Orai3 in tumor progression was so far intensively investigated in the context of breast cancer and recently also prostate cancer (Motiani *et al.*, 2010, 2013; Faouzi *et al.*, 2011; Holzmann *et al.*, 2013). Increased levels of Orai3 were observed in breast cancer cell lines, supporting the idea of Orai3 adapting to a cancerous environment. In contrast, Holzmann and colleagues reported decreased Orai3 levels in cancerous tissue compared to healthy controls (Holzmann *et al.*, 2013). The difference in Orai3 expression ratio in melanoma and healthy tissue was not analyzed in a direct comparison in the here presented study. The contradictory observations regarding Orai3 levels in cancer

emphasize the importance to regard relative, rather than absolute expression values, when comparing different cell types.

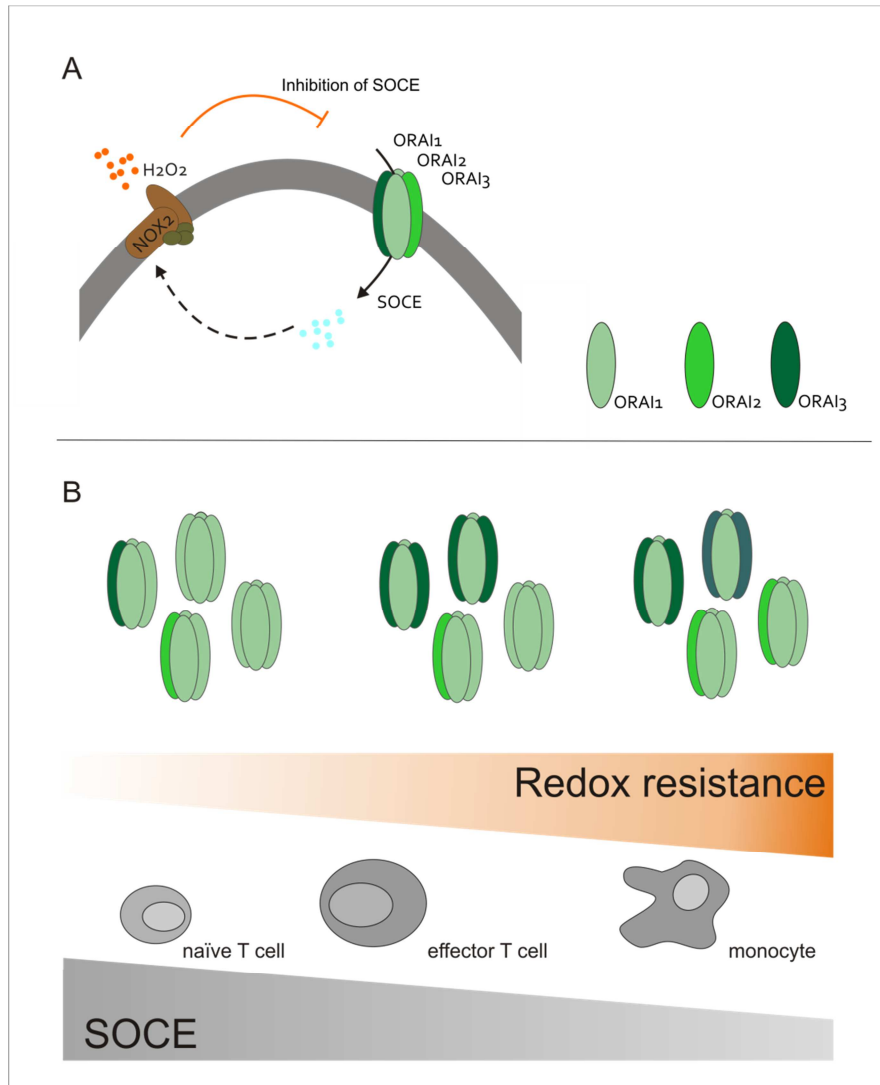


Figure 32 Orai3 as modulator in the interdependency of SOCE and ROS production

(A) Scheme describing the regulatory feedback loop between Ca²⁺-dependent ROS production and the activity of CRAC channels. NOX2 activity requires Ca²⁺ signals mediated by CRAC channels. H₂O₂ produced by NOX2 feeds back on the CRAC channels by inhibiting Orai1 and Orai2, but not Orai3. This loop might prevent overshooting ROS production, by dampening Ca²⁺ elevations. (B) Suggested channel configuration of T cells and monocytes in regard to SOCE and the redox resistance of CRAC channels, defined and modulated by the amount of channels holding an Orai3 subunit. This scheme is based on findings from this study and from Bogeski and colleagues (Bogeski *et al.*, 2010).

The observed correlation between the relative Orai3/Orai1 expression ratio and redox sensitivity of SOCE was determined by relating the Orai3/Orai1 ratios to IC₅₀ values of H₂O₂ induced inhibition of SOCE. The logarithmic dependency from redox sensitivity on the relative Orai3 level was in line with the mechanism of Orai3 insertion to CRAC channels as described above. In a linear correlation, additional Orai3 units would result in a constant increase of redox sensitivity. The logarithmic correlation instead implies a limitation to insertion, when additional Orai3 units will not result in further increased redox sensitivity. Instead, the relative abundance of Orai1 and Orai2 channels in the case of monocytes, containing one Orai3 subunit is likely to define the overall redox sensitivity.

9.3.3 Can an equation be used to estimate redox-sensitivity of SOCE in different cell types?

The equation described, correlating redox sensitivity of SOCE to the relative Orai3/Orai1 expression ratio, was thought to serve as prediction method to estimate the redox sensitivity for a cell type from qRT-PCR data. The benefit of such a prediction method, if applicable, would be to avoid the time consuming experiments to determine an IC_{50} , by accessing the easier and faster obtainable PCR data. Using the model biased IC_{50} concentrations in calcium imaging experiments for the three investigated melanoma cell lines, limitations and advantages of such a prediction method became obvious (see Figure 25). In the case of WM3734 the calculated IC_{50} concentration of 100 μM H_2O_2 indeed resulted in 53% reduction of SOCE in imaging experiments. This close fit of estimated and measured values seemed to be a proof of principle for the suggested method. However, in the case of the SK-Mel cell lines the method showed its limitations. In both cell lines, with more pronounced characteristics observed in SK-MEL-28, the calculated H_2O_2 concentration did not result in a reduction of SOCE. In contrast, all determined parameters: ΔCa^{2+} (reflecting SOCE), peak Ca^{2+} values and the influx rates after channel activation (slope) were increased. These results showed that although the equation seems to apply to certain cell types and Orai3 is indeed a modulator of Ca^{2+} sensitivity in T cells and monocytes, it is not the only defining parameter. The interpretation of the complete lack of an inhibition of SOCE by H_2O_2 and the opposed augmentation of the Ca^{2+} signal, requires further analysis. The redox regulation of SOCE, thus a clear picture in so far analyzed immune cells, is different in melanoma cell lines, probably underlying different or additional regulatory components. It is also to be considered, that other groups reported an elevation of SOCE in the presence of H_2O_2 (Grupe *et al.*, 2010). The repeatedly observed difference between WM and SK-Mel cell lines again, might be explained by adaption to the specific environment of their origin.

9.3.4 H_2O_2 induces an initial increase in Ca^{2+} signals in human monocytes and melanoma cells with so far unknown function

The treatment of cells with different concentrations of H_2O_2 resulted in an initial rise in Ca^{2+} in all investigated cell types. This effect, here referred to as initial effect, has early been reported by others (Bogeski *et al.*, 2010). The elevation of Ca^{2+} can partially be explained by activation of the IP_3 receptor and the release from internal stores. It was shown, that thiol modification of the IP_3R lead to Ca^{2+} store depletion (Hilly *et al.*, 1993; Parekh & Penner, 1995). More recently, Zheng and colleagues showed H_2O_2 to be an activator of the IP_3 receptor (Zheng & Shen, 2005). The initial effect is subject to modulation and is measurable *via* patch clamp suggesting a channel underlying the observed effect (observation, unpublished data, (Bogeski *et al.*, 2010)). Some groups have suggested TRPM2 as the channel in charge (Kolisek *et al.*, 2005; Ishii *et al.*, 2006; Grupe *et al.*, 2010). Though not representative, the qRT-PCR screen performed to analyze the expression of TRP channels in monocytes was also performed on a cDNA sample from the monocyte/macrophage cell line THP-1 (see 9.1.1). In both cases, TRPM2 mRNA was expressed with the same $2^{-\Delta\Delta Cq}$ values, but THP-1 cells lack the initial effect in calcium imaging experiments even under high H_2O_2 concentrations (observation, data not shown). These observations do not support TRPM2 as potential channel mediating the initial effect. The unaltered presence of the initial effect in Orai3 knockdown cells also rules out the protein as potential target. Still, based on the experiments conducted in this study and without further precise analysis, it is not possible to conclude on a molecular mechanism of the observed initial effect.

9.3.5 Additional aspects – Orai3 and other players in redox regulation of SOCE

The data obtained from monocytes and melanoma cell lines, with respect to data from T cell studies, pointed towards two statements regarding redox regulation of CRAC channels: 1.) Orai3 acts as modulator of redox sensitivity in so far analyzed immune cells, but this mechanism is not fully transferable to other cell systems such as melanoma cell lines. 2.) Opposed results from different melanoma cell lines regarding redox regulation of CRAC channels implies other and additional components involved in the response of Ca^{2+} signals to oxidative signals or stress.

A potential player other than Orai3 involved in redox regulation of CRAC channels is STIM2. Cysteine residues are the major target in proteins for H_2O_2 induced redox modification. STIM2 with 15 determined cysteine residues holds a high potential of being regulated by H_2O_2 (see 6.1.2.2). Especially in systems displaying a high STIM2 expression such as melanoma, H_2O_2 induced cysteine modification might influence protein function, thereby regulating or influencing CRAC channel activity.

9.4 A phenotype switch in melanoma cell lines is dependent on Orai1 and STIM2

9.4.1 Orai1 and STIM2 in proliferation vs. migration

Orai1 and STIM2 were shown to be the molecular players underlying the regulation of the Ca^{2+} -dependent switch in melanoma from a migratory/invasive to a rather proliferative phenotype. High Orai1 and STIM2 expression levels were shown to favor an invasive phenotype, while a down-regulation of the two isoforms resulted in increased proliferation and a decreased migratory capacity (Figure 26 and Figure 27). The modulatory function of Orai1 and STIM2 was not only proven by the chosen read outs, migration and proliferation analysis, but was also supported on a molecular level. The change in expression of transcription factors following the down-regulation of Orai1 and STIM2, confirmed the switch from a migratory to proliferative phenotype (see Figure 28). The master regulator of melanoma function MITF was shown to promote cell proliferation (see 6.3.3 and (Levy *et al.*, 2006)) and displayed a significant up-regulation in Orai1 and STIM2 down-regulated cells. Brn2 is involved in the transcriptional regulation of melanoma progression and fulfills various functions in regulating basic gene expression (see 6.3.3 and (Goodall *et al.*, 2008)). The TF binds to promoter regions close to binding sites of MITF, thereby repressing its function. This repression of MITF is diminished under low Brn2 expression levels, as observed in Orai1 or STIM2 siRNA treated cells, again supporting a more proliferative phenotype by increasing MITF activity. The histone-demethylase Jarid1B was initially described to be up regulated in slow-cycling melanoma subpopulations (Roesch *et al.*, 2010). The significant down-regulation of Jarid1B under Orai1 and STIM2 siRNA treatment supports the switch to a fast-cycling, speaking highly proliferative, phenotype.

As it was pointed out in the introduction, major signaling pathways as MAPK signaling cascades are highly Ca^{2+} -dependent. Targets of MAPK as MITF, Brn2 or NF κ B are involved in regulation of proliferation in melanoma (see 6.3.3). The activity of the TFs (see above) and the expression of their target genes (see below) is therefore highly Ca^{2+} -dependent, providing a high potential for Orai1 and STIM2 in their regulation. For example, the expression of IL-8, the marker cytokine of melanoma, involved in the promotion of proliferation and tumor progression

is mainly regulated by the Ca^{2+} -dependent TF NF κ B. This cytokine is therefore potentially regulated by Orai1/STIM2 mediated Ca^{2+} signaling. IL-8 secretion was increased upon the down-regulation of Orai1 and STIM2 (see Figure 29). Hence, IL-8 levels served as additional proof of the stated phenotype switch. Though it is to consider, that increased expression and secretion of IL-8 and its cognate receptors CXCR1 and CXCR2 have been associated not only to an enhancement of proliferation and cell growth of melanoma, but also a promotion of vertical growth and metastasis (reviewed by (Singh *et al.*, 2010)). IL-8 results upon down-regulation of Orai1 and STIM2 therefore have to be interpreted in the context of the results from transwell-migration experiments presented in this study (8.6.2) and results from spheroid assays presented in (Stanisz *et al.*, 2014). Since both types of experiments revealed an attenuation of the migratory potential and invasion, the increased IL-8 secretion can be accounted as indicator for an enhanced proliferation and the stated phenotype switch. One can assume, that the observed IL-8 increase is not sufficient to cause pro-invasive effects in melanoma and is outweighed by the influence on proliferation. In addition, the complex activity of IL-8 in melanoma progression was usually observed in the background of changes in the expression of CXCR1/2 (Venkatakrisnan *et al.*, 2000; Waugh & Wilson, 2008). Orai1 and STIM2 down-regulation might not affect the expression of the respective receptors, resulting in a sole consequence of enhanced proliferation. In order to verify this assumption and to further elucidate the role of Orai1/STIM2-mediated Ca^{2+} signaling for cytokine expression, additional experiments on CXCR expression are required. In contrast to melanoma, down-regulation of Orai1 or STIM2 in primary melanocytes, the origin of malignant melanoma, resulted in reduced proliferation (Stanisz *et al.*, 2012). This opposed results might speak for a tumor specific mechanism of Orai1 and STIM2 shaping the melanoma phenotype.

9.4.2 General vs. specific effects of the cellular environment and Ca^{2+} signaling on proliferation and migration

Regarding proliferation of melanoma, both the extracellular Ca^{2+} environment and Orai1- and STIM2-mediated signaling were shown to regulate cellular functions, thereby determining the cell phenotype. A reduced Ca^{2+} availability, either by lowering $[\text{Ca}^{2+}]_{\text{ext.}}$ or by reducing Orai1/STIM2-mediated SOCE, resulted in an enhanced proliferation. In contrast to proliferation, migration seems to be specifically regulated by Orai1 and STIM2 and not by Ca^{2+} signals in general. The use of the unspecific Ca^{2+} channel blocker 2-APB did not result in a reduced migration in untreated and control transfected cells (Figure 27, A). However, the knockdown of Orai1 or STIM2 significantly reduced the migratory capacity. Hormones and peptides *in vivo*, or fetal calf serum (FCS) *in vitro*, stimulate the proliferation of cancer cells including melanoma by the engagement of membrane-bound receptors. The subsequent activation of transcription factors involves Ca^{2+} signaling as important player in this process (Roderick & Cook, 2008; Prevarskaya *et al.*, 2011). The reduced proliferation observed under serum deprivation supports the important general role of the local environment in shaping the melanoma phenotype.

9.4.3 Additional aspects – Orai1 and STIM2 in the context of melanoma onset and progression

Orai1 and STIM2. The general role of Ca^{2+} for melanoma proliferation might be related to the regulatory function of the Ca^{2+} gradient in the epidermis that has already been shown to be involved in keratinocyte differentiation and skin barrier formation (see 6.3.1). Melanocytes can cope with very low $[\text{Ca}^{2+}]_{\text{ext.}}$, as they reside in the basal epidermal layer, displaying the lowest

Ca^{2+} concentration within the gradient. The experimentally determined low Ca^{2+} concentrations for optimal melanoma proliferation, suggests that melanoma cells reside in an optimal environment for proliferation in the basal epidermal layer. The enhanced proliferation following Orai1 or STIM2 down-regulation might lead to intracellular Ca^{2+} levels that promote proliferation. This levels might also match the actual Ca^{2+} levels melanocytes and melanoma cells hold in an environment with a low $[\text{Ca}^{2+}]$.

It is still not fully understood how melanoma cells acquire their enormous metastatic potential. Apparently, subpopulations of melanoma cells possess a considerable migratory capacity while still retaining the potential to switch into a highly proliferative phenotype after arriving at the metastatic niche (Pinner *et al.*, 2009). The mechanisms that control this phenotypic switch are largely unknown but most likely involve extracellular signals from the tumor environment and complex intracellular signal transduction (Hoek *et al.*, 2006, 2008; Hoek & Goding, 2010). Based on the identification of Orai1 and STIM2 in the regulation of the phenotype it is likely to assume that changes in Orai1 and STIM2 expression in response to environmental or local triggers define tumor invasion and spreading. A future project might focus on the identification and analysis of potential triggers responsible for changes in Orai1 and STIM2 expression. The determination of different Ca^{2+} concentrations in metastatic niches will give further insight into the role of the environment for phenotype shaping. It is further worth to analyze whether melanoma subpopulations show differences in Orai and STIM expression, and whether the balance between these subpopulations defines the overall tumor phenotype, as it was shown for Jarid1B (Roesch *et al.*, 2010).

A possible function for STIM1 in melanoma. Initially, STIM1 was tested in several experiments to serve as isoform control. Although STIM2 is indeed the higher expressed STIM isoform, STIM1 down-regulation also showed an impact on the expression of molecular markers (see Figure 28). Therefore, STIM1 might also contribute to SOCE and other cellular functions. However, since a concomitant down-regulation of Orai1 and STIM2 already resulted in an almost complete abolishment of SOCE, an essential role for STIM1 is not likely.

9.5 Monocytes in an altered redox and Ca^{2+} microenvironment

9.5.1 Monocytes react to changes in their environment, but are moderately insensitive to changes in the extracellular Ca^{2+} concentration

In comparison to T cells, monocytes display a stronger resistance towards the impact of an oxidative milieu in both, Ca^{2+} signaling and overall survival. Still, an oxidative milieu, with H_2O_2 as observed parameter, results in a reduced survival rate of monocytes with an IC_{50} of 150 μM . The redox resistance and stability in an oxidizing environment of the cells became more obvious under further challenging conditions, when the impact of the IC_{50} concentration of 150 μM was stable with no regard to the external Ca^{2+} concentration. The presented data in Figure 30 (C) shows one data point not coherent with the remaining results. Although the measured survival under 150 μM H_2O_2 did not show a decrease in survival, compared to the non-treated condition, it was not further considered because it was identified as significant outlier (indicated by brackets and dotted line). In all other cases, a concentration of 150 μM indeed resulted in an obvious decrease of survival (see also Figure 30, A). Monocytes do not proliferate under standard culture conditions and are considered as non-proliferative cells. The effect of a changing environment was therefore analyzed based on the survival of the cells over time.

As well as melanoma cell lines, serum protein deprivation resulted in severe changes in cell survival rates. Although the effect of H₂O₂ was stable in the absence or presence of serum proteins, the cells reacted to alteration in the Ca²⁺ environment after serum deprivation for 24 and 48 h. Taken together, although monocytes as highly versatile cells are in general strongly influenced by their environment, they displayed a strong resistance to Ca²⁺ and redox challenges.

9.5.2 Additional aspects – What additional parameters define redox sensitivity of monocytes?

In order to fully understand and reveal the mechanisms underlying the strong redox resistance of Ca²⁺ signaling and overall survival of monocytes, it is important to understand the contribution and adaptation of the antioxidant systems. The presence of antioxidant systems is detectable either by mRNA or protein analysis. It is far more complicated to analyze the activity of the different systems or enzymes. The standard assays require a destruction of the cells and simply detect the activity of the enzyme in a cell lysate. These approaches are limited in their informative value, because they do not monitor enzyme activity in intact cells. An initial approach was therefore to determine mRNA levels of two players of the most abundant antioxidant enzymes/systems dealing with H₂O₂: namely catalase and glutathione reductase (GR) (data not shown but briefly described here). The analysis of mRNA levels in untreated monocytes and monocytes challenged with fMLF revealed minor, though unstable and non-significant, changes to acute induction of increased redox levels. Possible changes in the context of Orai and STIM down-regulation were also analyzed. It became obvious, that catalase and GR expression displayed a general strong donor dependency and were prone to fluctuations as observed for NOX2 expression. Catalase mRNA levels showed a tendency of reduction in Orai3 knockdown cells, while they were increased following the knockdown of Orai1. GR mRNA levels were meanwhile increased under STIM1 down-regulation. Further analysis of expression levels of other enzymes as SOD, in parallel to additional methods, is required to interpret the regulation of anti-oxidative systems by Orai and STIM mediated Ca²⁺ signaling.

A physiological approach to determine the actions and reactions of the antioxidant system to changes in the Orai/STIM machinery or the environment is the use of genetically encoded redox sensors. Examples are redox-sensitive GFP constructs (roGFP) or the H₂O₂-sensitive sensor HyPer. These constructs can be targeted to different subcellular compartments and are used to analyze real-time, single cell biased oxidative processes in intact living cells (Belousov *et al.*, 2006; Gutscher *et al.*, 2008). Different roGFP derivatives have been established and are applied in revealing oxidative processes of the immune and the cardiovascular system (Pal *et al.*, 2013; Ezeriņa *et al.*, 2014). In the here presented study, the limitations of the analysis of real-time ROS production on single cell level was based on two issues. On the one hand, the overexpression rates of the constructs at hand were either limited (HyPer, 5-10%) or nearly not detectable (roGFP). On the other hand, the expression of GFP constructs in monocytes turned out to be inapplicable, due to the high autofluorescence of the cells at 470nm excitation. Using optimized constructs, further analysis might give insight into the function of antioxidant systems of primary phagocytes and their adaptation to altered Ca²⁺ and redox signaling processes. A recent improved HyPer-Red construct is currently under investigation, and will be suitable to analyze intracellular H₂O₂ concentrations in cells such as monocytes (work by Belousov *et al.* unpublished to date).

9.6 Regulation of NOX and CRAC channel activity as therapeutical application in inflammatory and cancerous diseases: A clinical outlook

9.6.1 Regulation of CRAC channel activity as therapeutical application in melanoma treatment

Aberrant Ca^{2+} signals have early been correlated to cancer (Monteith *et al.*, 2012; Schwarz *et al.*, 2013), due to their multiple roles in regulating cellular functions, as proliferation and migration that are related to cancer development (Qu *et al.*, 2011). Several Ca^{2+} mediating channels have therefore been a target of investigation, among these the CRAC channels and their components. So far, several reports correlated aberrant Orai and STIM expression levels to cancerous diseases (reviewed by (Hoth & Niemeyer, 2013)). There are contradictory results and observations regarding the correlation of, for example, increased or decreased STIM2 expression levels to disease outcome. This implies a rather specific than general role of STIM molecules in cancerogenesis and progression. McAndrew and colleagues reported the STIM1/STIM2 expression ratio as critical parameter in breast cancer prognosis with the poorest survival rate of patients displaying a STIM1(high) to STIM2(low) expression (McAndrew *et al.*, 2011). Also in prostate cancer, a low STIM2 expression was related to an increased Gleason grade, hence a poor therapeutical prognosis (Ashida *et al.*, 2012). In glioblastoma, high STIM2 expression was determined and designated as potential target (Ruano *et al.*, 2006). With the results from the here presented study, it is obvious, that the effects of aberrant STIM2 levels are highly specific to the type of cancer and have to be interpreted in the context of other parameters. For example, while in melanoma a high STIM2 level is related to an invasive and migratory phenotype, Aytes and colleagues reported high STIM2 levels to favor a less invasive phenotype and an augmented cell growth in colorectal cancer (Aytes *et al.*, 2012).

Although STIMs were initially identified as tumor suppressor genes (see 6.4.1), STIM2 (and Orai1) can be partially considered as tumor promoters in melanoma, due to their contribution to migration and invasion. The use of siRNAs targeting Orai1 and STIM2 expression in melanoma could be a therapeutical approach to render the tumor to a proliferative status to increase the susceptibility to conventional radiation and chemotherapy. Given that STIM2 has been shown to have no or minor effects in cells with predominant expression of STIM1 (Peel *et al.*, 2006; Potier *et al.*, 2009; Mancarella *et al.*, 2013), the possibility arises to target SOCE by modulators of STIM2. The potentially big advantage of such a STIM2-targeted therapy is based on the fact that immune cells depend more on STIM1 and may thus not be significantly affected by interfering with STIM2 function. Hence, manipulations of STIM2 function will very likely have minor effects on the antitumor immune response, that mainly relies on T cell and NK cell activity (Stanisz *et al.*, 2014).

9.6.2 Regulation of NOX and CRAC channel activity as therapeutical application in inflammatory diseases

Targeting NADPH oxidases and monocyte function. NOX enzymes are active in signaling pathways and immune responses and their aberrant activity can be a cause for different disease patterns or are related to them. Their implication in inflammatory and cancerous diseases made them a potential therapeutical target (Bonner & Arbiser, 2012; Weyemi *et al.*, 2012). Several molecules were identified as NOX inhibitors over the years and also found their

way into clinical application (reviewed by (Jaquet *et al.*, 2009)), but the search for new NOX inhibitors and new approaches to diminish NOX activity is ongoing (Di Marco *et al.*, 2014). Regarding the different NOX isoforms, NOX2 is the most prominent target, although most inhibitors lack isotype specificity (Cifuentes-Pagano *et al.*, 2014). Results from the here presented study questions the role of NOX4 in monocytes. Nevertheless, it is to mentioned that Tavakoli and colleagues also discussed and suggested NOX4 derived ROS as new and potential target in the treatment of atherosclerosis (Tavakoli & Asmis, 2012). As pointed out before, not only overshooting but also insufficient ROS levels and mutations in NOX subunits impairing a sufficient enzyme assembly can be the cause of inflammatory and autoimmune diseases (see 6.1.2.2). Hultqvist and colleagues have previously demonstrated the protective role of ROS in autoimmune diseases (Hultqvist *et al.*, 2009). Very recently the group approached the identification and analysis of NOX2 activators, instead of inhibitors, in the treatment of inflammatory and autoimmune diseases (Hultqvist *et al.*, 2014).

Targeting specific CRAC channel components as novel approach in the treatment of inflammatory diseases. The results from this study highlight the interdependency of CRAC channels and NOX2 activity. This points to an indirect regulation of ROS signaling in monocytes in inflammatory diseases, by targeting CRAC channels. In this approach, STIM2 and Orai3 are the most promising targets to modulate NOX2 activity, meanwhile limiting unwanted side effects. By targeting the modulatory subunit Orai3, NOX2 activity can be altered, without complete loss of physiological relevant ROS production. As it was shown in this study, targeting Orai3 will in addition only have minor effects on overall Ca^{2+} signaling in monocytes and on other immune cells. The same argumentation accounts for STIM2 as potential target. The equal contribution of STIM1 and STIM2 will allow augmenting ROS levels by partially decreasing SOCE, without affecting Ca^{2+} signaling in neighboring immune cells as T cells (see also 9.6.1).

9.6.3 Influencing cellular fate and survival by altering the extracellular environment

Regarding the influence of the environment to the here investigated cell types, artificial induced changes of the Ca^{2+} and redox environment hold a high potential to influence cell function instead of a direct targeting of CRAC channels and NOX enzymes. Chance of success of the mentioned approach might be higher in melanoma rather than in a monocyte related diseases. Changing the extracellular matrix composition is challenging, but likewise effective to render melanoma more proliferative and hence more susceptible to conventional treatments. In addition, the high dependency of melanoma proliferation on $[\text{Ca}^{2+}]_{\text{ext.}}$ in comparison to the remarkable resistance of monocytes, points to melanoma as most promising system. Interfering in the local environment of the skin provides the advantage of a less invasive method and the reduction of systemic side effects. In contrast to skin, altering the local redox environment at sites of inflammation bears the high risk of systemic side effects and seems to be more challenging. However, instead of a direct targeting of the inflammatory environment, new approaches consider monocytes and macrophages as potential tool to alter the local environment *via* a cellular back door. Addressing this issue, monocytes and macrophages have evolved as such cellular tools in the treatment of atherosclerosis. Lee and colleagues recently described an elegant way of targeting overshooting ROS levels in atherosclerotic lesions, providing a new approach in regulating a local redox environment. Monocyte recruitment, as characteristic step in lesion formation, was exploited as shuttle to traffic stabilized catalase, usually prone to degradation, to the site of inflammation, thereby reducing local ROS levels (Lee, 2014).

9.7 Concluding Remarks

The analysis of SOCE and the role of the single CRAC channel components was conducted in primary human monocytes and melanoma cell lines and revealed several major findings. Ca^{2+} signaling plays an important role in the immune system. It was shown to regulate essential T cell functions and is an important factor in innate immune responses. It was shown, that monocytes, in contrast to other phagocytes as neutrophils, express all five Orai and STIM isoforms that contribute to SOCE. In addition, both STIM proteins equally contribute to SOCE and Ca^{2+} -dependent ROS production in human monocytes. These results emphasized an active contribution for STIM2 in different cellular functions that seem to be a unique monocytes feature compared to other phagocytes. NOX2 was the only noteworthy expressed NOX isoform in primary human monocytes. NOX2 activity was shown to be dependent on CRAC channel activity to generate sufficient amounts of ROS. The redox-insensitive isoform Orai3 is a modulator in the interdependence of CRAC channels and NOX2 activity and defines redox sensitivity of SOCE in monocytes. These results showed that the strategy of high Orai3 expression as protective mechanism in an oxidative milieu is not only present in CD4^+ T helper cells, but also monocytes. The skin, is another organ where Ca^{2+} and redox signaling hold a high potential to regulate cellular functions. In a prior study, Orai and STIM were shown to regulate melanocyte function. It could be shown in the here presented study, that also under pathological skin conditions, as melanoma, SOCE and its molecular components regulate cellular features that define the tumor phenotype. Orai1- and STIM2-dependent calcium entry was shown to inversely regulate melanoma proliferation and migration in the observed phenotype switch. Cellular functions are not only defined by intracellular signaling pathways but also by specific environments. The Ca^{2+} and redox environment was shown to differentially regulate SOCE and cell behavior of monocytes and melanoma cells. In a broader scope, the findings on the role of the single Orai and STIM proteins in regulating cellular features of monocytes and melanoma, might provide new therapeutical applications for the treatment of skin cancer and innate immunity-associated inflammatory diseases. In this regard, a distinctive role might come in for the isoforms STIM2 and Orai3.

10 Literature

- Alonso MT, Manjarrés IM & García-Sancho J (2012). Privileged coupling between Ca(2+) entry through plasma membrane store-operated Ca(2+) channels and the endoplasmic reticulum Ca(2+) pump. *Mol Cell Endocrinol* **353**, 37–44.
- Ashida S, Orloff MS, Bebek G, Zhang L, Zheng P, Peehl DM & Eng C (2012). Integrated analysis reveals critical genomic regions in prostate tumor microenvironment associated with clinicopathologic phenotypes. *Clin Cancer Res* **18**, 1578–1587.
- Auffray C, Sieweke MH & Geissmann F (2009). Blood monocytes: development, heterogeneity, and relationship with dendritic cells. *Annu Rev Immunol* **27**, 669–692.
- Aytes A, Molleví DG, Martínez-Iniesta M, Nadal M, Vidal A, Morales A, Salazar R, Capellà G & Villanueva A (2012). Stromal interaction molecule 2 (STIM2) is frequently overexpressed in colorectal tumors and confers a tumor cell growth suppressor phenotype. *Mol Carcinog* **51**, 746–753.
- Babior BM (1984a). The Respiratory Burst of Phagocytes. *J Clin Invest* **73**, 599–601.
- Babior BM (1984b). Oxidants from phagocytes: agents of defense and destruction. *Blood* **64**, 959–966.
- Balch CM et al. (2009). Final version of 2009 AJCC melanoma staging and classification. *J Clin Oncol* **27**, 6199–6206.
- Bandyopadhyay BC, Pingle SC & Ahern GP (2011). Store-operated Ca²⁺ signaling in dendritic cells occurs independently of STIM1. *J Leukoc Biol* **89**, 57–62.
- Barnes KA, Samson SE & Grover AK (2000). Sarco/endoplasmic reticulum Ca²⁺-pump isoform SERCA3a is more resistant to superoxide damage than SERCA2b. *Mol Cell Biochem* **203**, 17–21.
- Barr VA, Bernot KM, Shaffer MH, Burkhardt JK & Samelson LE (2009). Formation of STIM and Orai complexes: puncta and distal caps. *Immunol Rev* **231**, 148–159.
- Beck B, Lehen'kyi V, Roudbaraki M, Flourakis M, Charveron M, Bordat P, Polakowska R, Prevarskaya N & Skryma R (2008). TRPC channels determine human keratinocyte differentiation: new insight into basal cell carcinoma. *Cell Calcium* **43**, 492–505.
- Bedard K & Krause K (2007). The NOX Family of ROS-Generating NADPH Oxidases : Physiology and Pathophysiology. *Physiol Rev* **245–313**.
- Bedogni B & Powell MB (2009). Hypoxia, melanocytes and melanoma - survival and tumor development in the permissive microenvironment of the skin. *Pigment Cell Melanoma Res* **22**, 166–174.
- Bedogni B, Welford SM, Cassarino DS, Nickoloff BJ, Giaccia AJ & Powell MB (2005). The hypoxic microenvironment of the skin contributes to Akt-mediated melanocyte transformation. *Cancer Cell* **8**, 443–454.
- Belousov V V, Fradkov AF, Lukyanov KA, Staroverov DB, Shakhbazov KS, Terskikh A V & Lukyanov S (2006). Genetically encoded fluorescent indicator for intracellular hydrogen peroxide. **3**, 281–286.

- El Benna J, Faust RP, Johnson JL & Babiorek BM (1996). Phosphorylation of the respiratory burst oxidase subunit p47^{phox} as determined by two-dimensional phosphopeptide mapping. Phosphorylation by protein kinase C, protein kinase A, and a mitogen-activated protein kinase. *J Biol Chem* **271**, 6374–6378.
- Berna-Erro A, Braun A, Kraft R, Kleinschnitz C, Schuhmann MK, Stegner D, Wulfsch T, Eilers J, Meuth SG, Stoll G & Nieswandt B (2009). STIM2 regulates capacitive Ca²⁺ entry in neurons and plays a key role in hypoxic neuronal cell death. *Sci Signal* **2**, ra67.
- Berridge MJ, Bootman MD & Lipp P (1998). Calcium—a life and death signal. *Nature* **395**, 645–648.
- Berridge MJ, Bootman MD & Roderick HL (2003). Calcium signalling: dynamics, homeostasis and remodelling. *Nat Rev Mol Cell Biol* **4**, 517–529.
- Biswas SK & Mantovani A (2010). Macrophage plasticity and interaction with lymphocyte subsets: cancer as a paradigm. *Nat Immunol* **11**, 889–896.
- Blandizzi C, Gionchetti P, Armuzzi A, Caporali R, Chimenti S, Cimaz R, Cimino L, Lapadula G, Lionetti P, Marchesoni A, Marcellusi A, Mennini FS, Salvarani C & Girolomoni G (n.d.). The role of tumour necrosis factor in the pathogenesis of immune-mediated diseases. *Int J Immunopathol Pharmacol* **27**, 1–10.
- Bogeski I, Kappl R, Kummerow C, Gulaboski R, Hoth M & Niemeyer BA (2011). Redox regulation of calcium ion channels: chemical and physiological aspects. *Cell Calcium* **50**, 407–423.
- Bogeski I, Kilch T & Niemeyer BA (2012). ROS and SOCE: recent advances and controversies in the regulation of STIM and Orai. *J Physiol* **590**, 4193–4200.
- Bogeski I, Kummerow C, Al-Ansary D, Schwarz EC, Koehler R, Kozai D, Takahashi N, Peinelt C, Griesemer D, Bozem M, Mori Y, Hoth M & Niemeyer BA (2010). Differential Redox Regulation of ORAI Ion Channels: A Mechanism to Tune Cellular Calcium Signaling. *Sci Signal* **3**, ra24–ra24.
- Bonner MY & Arbiser JL (2012). Targeting NADPH oxidases for the treatment of cancer and inflammation. *Cell Mol Life Sci* **69**, 2435–2442.
- Bourdon E & Blache D (2001). The importance of proteins in defense against oxidation. *Antioxid Redox Signal* **3**, 293–311.
- Bowen AR, Hanks AN, Allen SM, Alexander A, Diedrich MJ & Grossman D (2003). Apoptosis regulators and responses in human melanocytic and keratinocytic cells. *J Invest Dermatol* **120**, 48–55.
- Brandman O, Liou J, Park WS & Meyer T (2007). STIM2 is a feedback regulator that stabilizes basal cytosolic and endoplasmic reticulum Ca²⁺ levels. *Cell* **131**, 1327–1339.
- Brar SS, Kennedy TP, Sturrock AB, Huecksteadt TP, Quinn MT, Whorton AR & Hoidal JR (2002). An NAD(P)H oxidase regulates growth and transcription in melanoma cells. *Am J Physiol Cell Physiol* **282**, C1212–C1224.
- Brécharde S, Melchior C, Plançon S, Schenten V & Tschirhart EJ (2008). Store-operated Ca²⁺ channels formed by TRPC1, TRPC6 and Orai1 and non-store-operated channels formed by TRPC3 are involved in the regulation of NADPH oxidase in HL-60 granulocytes. *Cell Calcium* **44**, 492–506.

- Bréchar d S, Plançon S, Melchior C & Tschirhart EJ (2009). STIM1 but not STIM2 is an essential regulator of Ca²⁺ influx-mediated NADPH oxidase activity in neutrophil-like HL-60 cells. *Biochem Pharmacol* **78**, 504–513.
- Bréchar d S, Plançon S & Tschirhart EJ (2013). New insights into the regulation of neutrophil NADPH oxidase activity in the phagosome: a focus on the role of lipid and Ca(2+) signaling. *Antioxid Redox Signal* **18**, 661–676.
- Bréchar d S & Tschirhart EJ (2008). Regulation of superoxide production in neutrophils: role of calcium influx. *J Leukoc Biol* **84**, 1223–1237.
- Brüne B, Dehne N, Grossmann N, Jung M, Namgaladze D, Schmid T, von Knethen A & Weigert A (2013). Redox control of inflammation in macrophages. *Antioxid Redox Signal* **19**, 595–637.
- Bustin S a, Benes V, Garson J a, Hellemans J, Huggett J, Kubista M, Mueller R, Nolan T, Pfaffl MW, Shipley GL, Vandesompele J & Wittwer CT (2009). The MIQE guidelines: minimum information for publication of quantitative real-time PCR experiments. *Clin Chem* **55**, 611–622.
- Campbell DJ, Kim CH & Butcher EC (2003). Chemokines in the systemic organization of immunity. *Immunol Rev* **195**, 58–71.
- Capiod T, Shuba Y, Skryma R & Prevarskaya N (2007). Calcium signalling and cancer cell growth. *Subcell Biochem* **45**, 405–427.
- Carey TE, Takahashi T, Resnick LA, Oettgen HF & Old LJ (1976). Cell surface antigens of human malignant melanoma: mixed hemadsorption assays for humoral immunity to cultured autologous melanoma cells. *Proc Natl Acad Sci U S A* **73**, 3278–3282.
- Cargnello M & Roux PP (2011). Activation and function of the MAPKs and their substrates, the MAPK-activated protein kinases. *Microbiol Mol Biol Rev* **75**, 50–83.
- Carta S, Castellani P, Delfino L, Tassi S, Venè R & Rubartelli A (2009). DAMPs and inflammatory processes: the role of redox in the different outcomes. *J Leukoc Biol* **86**, 549–555.
- Castagna M, Takai Y, Kaibuchi K, Sano K, Kikkawa U & Nishizuka Y (1982). Direct activation of calcium-activated, phospholipid-dependent protein kinase by tumor-promoting phorbol esters. *J Biol Chem* **257**, 7847–7851.
- Cathcart MK (2004). Regulation of superoxide anion production by NADPH oxidase in monocytes/macrophages: contributions to atherosclerosis. *Arterioscler Thromb Vasc Biol* **24**, 23–28.
- Cheli Y, Ohanna M, Ballotti R & Bertolotto C (2010). Fifteen-year quest for microphthalmia-associated transcription factor target genes. *Pigment Cell Melanoma Res* **23**, 27–40.
- Chen C-L & Iijima M (2012). Myosin I: A new pip(3) effector in chemotaxis and phagocytosis. *Commun Integr Biol* **5**, 294–296.
- Chiarugi P (2005). PTPs versus PTKs: the redox side of the coin. *Free Radic Res* **39**, 353–364.
- Chomczynski P (1987). Single-Step Method of RNA Isolation by Acid Guanidinium Extraction. **159**, 156–159.

- Cifuentes-Pagano E, Meijles DN & Pagano PJ (2014). The quest for selective nox inhibitors and therapeutics: challenges, triumphs and pitfalls. *Antioxid Redox Signal* **20**, 2741–2754.
- Clapham DE (2007). Calcium signaling. *Cell* **131**, 1047–1058.
- Clark WH, Elder DE, Guerry D, Epstein MN, Greene MH & Van Horn M (1984). A study of tumor progression: the precursor lesions of superficial spreading and nodular melanoma. *Hum Pathol* **15**, 1147–1165.
- Collins SR & Meyer T (2011). Evolutionary origins of STIM1 and STIM2 within ancient Ca²⁺ signaling systems. *Trends Cell Biol* **21**, 202–211.
- Crabtree GR (1999). Generic signals and specific outcomes: signaling through Ca²⁺, calcineurin, and NF-AT. *Cell* **96**, 611–614.
- Dale DC, Boxer L & Liles WC (2008). The phagocytes: neutrophils and monocytes. *Blood* **112**, 935–945.
- Davies H et al. (2002). Mutations of the BRAF gene in human cancer. *Nature* **417**, 949–954.
- DeHaven WI, Smyth JT, Boyles RR & Putney JW (2007). Calcium inhibition and calcium potentiation of Orai1, Orai2, and Orai3 calcium release-activated calcium channels. *J Biol Chem* **282**, 17548–17556.
- Díez-Torre A, Andrade R, Eguizábal C, López E, Arluzea J, Silió M & Aréchaga J (2009). Reprogramming of melanoma cells by embryonic microenvironments. *Int J Dev Biol* **53**, 1563–1568.
- Dolmetsch RE, Lewis RS, Goodnow CC & Healy JI (1997). Differential activation of transcription factors induced by Ca²⁺ response amplitude and duration. *Nature* **386**, 855–858.
- Donato R, Cannon BR, Sorci G, Riuzzi F, Hsu K, Weber DJ & Geczy CL (2013). Functions of S100 proteins. *Curr Mol Med* **13**, 24–57.
- Dong J, Phelps RG, Qiao R, Yao S, Benard O, Ronai Z & Aaronson SA (2003). BRAF oncogenic mutations correlate with progression rather than initiation of human melanoma. *Cancer Res* **63**, 3883–3885.
- Dong Z, Saikumar P, Weinberg JM & Venkatachalam MA (2006). Calcium in cell injury and death. *Annu Rev Pathol* **1**, 405–434.
- Dröge W (2002). Free radicals in the physiological control of cell function. *Physiol Rev* **82**, 47–95.
- Eckert RL, Crish JF & Robinson NA (1997). The epidermal keratinocyte as a model for the study of gene regulation and cell differentiation. *Physiol Rev* **77**, 397–424.
- El-Benna J, Dang PM-C, Gougerot-Pocidalo MA, Marie JC & Braut-Boucher F (2009). p47phox, the phagocyte NADPH oxidase/NOX2 organizer: structure, phosphorylation and implication in diseases. *Exp Mol Med* **41**, 217–225.
- Elias P, Ahn S, Brown B, Crumrine D & Feingold KR (2002). Origin of the epidermal calcium gradient: regulation by barrier status and role of active vs passive mechanisms. *J Invest Dermatol* **119**, 1269–1274.

- Ercan E, Momburg F, Engel U, Temmerman K, Nickel W & Seedorf M (2009). A conserved, lipid-mediated sorting mechanism of yeast Ist2 and mammalian STIM proteins to the peripheral ER. *Traffic* **10**, 1802–1818.
- Eylenstein A, Schmidt S, Gu S, Yang W, Schmid E, Schmidt E-M, Alesutan I, Szteyn K, Regel I, Shumilina E & Lang F (2012). Transcription factor NF- κ B regulates expression of pore-forming Ca²⁺ channel unit, Orai1, and its activator, STIM1, to control Ca²⁺ entry and affect cellular functions. *J Biol Chem* **287**, 2719–2730.
- Ezeriņa D, Morgan B & Dick TP (2014). Imaging dynamic redox processes with genetically encoded probes. *J Mol Cell Cardiol*; DOI: 10.1016/j.yjmcc.2013.12.023.
- Faouzi M, Hague F, Potier M, Ahidouch A, Sevestre H & Ouadid-Ahidouch H (2011). Down-regulation of Orai3 arrests cell-cycle progression and induces apoptosis in breast cancer cells but not in normal breast epithelial cells. *J Cell Physiol* **226**, 542–551.
- Faust LR, el Benna J, Babior BM & Chanock SJ (1995). The phosphorylation targets of p47phox, a subunit of the respiratory burst oxidase. Functions of the individual target serines as evaluated by site-directed mutagenesis. *J Clin Invest* **96**, 1499–1505.
- Félix R, Crottès D, Delalande A, Fauconnier J, Lebranchu Y, Le Guennec J-Y & Velge-Roussel F (2013). The Orai-1 and STIM-1 Complex Controls Human Dendritic Cell Maturation. *PLoS One* **8**, e61595.
- Fenyo IM & Gafencu AV (2013). The involvement of the monocytes/macrophages in chronic inflammation associated with atherosclerosis. *Immunobiology* **218**, 1376–1384.
- Feske S (2010). CRAC channelopathies. *Pflugers Arch* **460**, 417–435.
- Feske S, Gwack Y, Prakriya M, Srikanth S, Puppel S-H, Tanasa B, Hogan PG, Lewis RS, Daly M & Rao A (2006). A mutation in Orai1 causes immune deficiency by abrogating CRAC channel function. *Nature* **441**, 179–185.
- Frischauf I, Muik M, Derler I, Bergsmann J, Fahrner M, Schindl R, Groschner K & Romanin C (2009). Molecular determinants of the coupling between STIM1 and Orai channels: differential activation of Orai1-3 channels by a STIM1 coiled-coil mutant. *J Biol Chem* **284**, 21696–21706.
- Galkina E & Ley K (2009). Immune and inflammatory mechanisms of atherosclerosis (*). *Annu Rev Immunol* **27**, 165–197.
- Gao Y, Hanley PJ, Rinné S, Zuzarte M & Daut J (2010). Calcium-activated K(+) channel (K(Ca)_{3.1}) activity during Ca(2+) store depletion and store-operated Ca(2+) entry in human macrophages. *Cell Calcium* **48**, 19–27.
- Garbe C, Eigentler TK, Keilholz U, Hauschild A & Kirkwood JM (2011). Systematic review of medical treatment in melanoma: current status and future prospects. *Oncologist* **16**, 5–24.
- Gebhardt C, Averbeck M, Viertel A, Kauer F, Saalbach A, Anderegg U & Simon JC (2007). Ultraviolet-B irradiation enhances melanoma cell motility via induction of autocrine interleukin 8 secretion. *Exp Dermatol* **16**, 636–643.
- Geissmann F, Manz MG, Jung S, Sieweke MH, Merad M & Ley K (2010). Development of monocytes, macrophages, and dendritic cells. *Science* **327**, 656–661.

- Gelderman KA, Hultqvist M, Holmberg J, Olofsson P & Holmdahl R (2006). T cell surface redox levels determine T cell reactivity and arthritis susceptibility. *Proc Natl Acad Sci U S A* **103**, 12831–12836.
- Gierut A, Perlman H & Pope RM (2010). Innate immunity and rheumatoid arthritis. *Rheum Dis Clin North Am* **36**, 271–296.
- Go Y-M & Jones DP (2008). Redox compartmentalization in eukaryotic cells. *Biochim Biophys Acta* **1780**, 1273–1290.
- Goodall J, Carreira S, Denat L, Kobi D, Davidson I, Nuciforo P, Sturm RA, Larue L & Goding CR (2008). Brn-2 represses microphthalmia-associated transcription factor expression and marks a distinct subpopulation of microphthalmia-associated transcription factor-negative melanoma cells. *Cancer Res* **68**, 7788–7794.
- Gordon S & Taylor PR (2005). Monocyte and macrophage heterogeneity. *Nat Rev Immunol* **5**, 953–964.
- Govindarajan B, Sligh JE, Vincent BJ, Li M, Canter JA, Nickoloff BJ, Rodenburg RJ, Smeitink JA, Oberley L, Zhang Y, Slingerland J, Arnold RS, Lambeth JD, Cohen C, Hilenski L, Griendling K, Martínez-Diez M, Cuezva JM & Arbiser JL (2007). Overexpression of Akt converts radial growth melanoma to vertical growth melanoma. *J Clin Invest* **117**, 719–729.
- Greene MH (1999). The genetics of hereditary melanoma and nevi. 1998 update. *Cancer* **86**, 2464–2477.
- Groitel B & Jakob U (2014). Thiol-based redox switches. *Biochim Biophys Acta* **1844**, 1335–1343.
- Grover AK, Samson SE & Misquitta CM (1997). Sarco(endo)plasmic reticulum Ca²⁺ pump isoform SERCA3 is more resistant than SERCA2b to peroxide. *Am J Physiol* **273**, C420–C425.
- Grupe M, Myers G, Penner R & Fleig A (2010). Activation of store-operated I(CRAC) by hydrogen peroxide. *Cell Calcium* **48**, 1–9.
- Grynkiewicz G, Poenie M & Tsien RY (1985). A new generation of Ca²⁺ indicators with greatly improved fluorescence properties. *J Biol Chem* **260**, 3440–3450.
- Guilliams M, Ginhoux F, Jakubzick C, Naik SH, Onai N, Schraml BU, Segura E, Tussiwand R & Yona S (2014). Dendritic cells, monocytes and macrophages: a unified nomenclature based on ontogeny. *Nat Rev Immunol* **14**, 571–578.
- Gutscher M, Pauleau A-L, Marty L, Brach T, Wabnitz GH, Samstag Y, Meyer AJ & Dick TP (2008). Real-time imaging of the intracellular glutathione redox potential. *Nat Methods* **5**, 553–559.
- Gwack Y, Srikanth S, Feske S, Cruz-Guilloty F, Oh-hora M, Neems DS, Hogan PG & Rao A (2007). Biochemical and functional characterization of Orai proteins. *J Biol Chem* **282**, 16232–16243.
- Gwack Y, Srikanth S, Oh-Hora M, Hogan PG, Lamperti ED, Yamashita M, Gelinas C, Neems DS, Sasaki Y, Feske S, Prakriya M, Rajewsky K & Rao A (2008). Hair loss and defective T- and B-cell function in mice lacking ORAI1. *Mol Cell Biol* **28**, 5209–5222.

- Hackam DJ, Rotstein OD, Zhang WJ, Demaurex N, Woodside M, Tsai O & Grinstein S (1997). Regulation of phagosomal acidification. Differential targeting of Na⁺/H⁺ exchangers, Na⁺/K⁺-ATPases, and vacuolar-type H⁺-atpases. *J Biol Chem* **272**, 29810–29820.
- Hadjigogos K (2003). The role of free radicals in the pathogenesis of rheumatoid arthritis. *Panminerva Med* **45**, 7–13.
- Hearing VJ (2005). Biogenesis of pigment granules: a sensitive way to regulate melanocyte function. *J Dermatol Sci* **37**, 3–14.
- Hennings H & Holbrook KA (1983). Calcium regulation of cell-cell contact and differentiation of epidermal cells in culture. An ultrastructural study. *Exp Cell Res* **143**, 127–142.
- Hilly M, Piétri-Rouxel F, Coquil JF, Guy M & Mauger JP (1993). Thiol reagents increase the affinity of the inositol 1,4,5-trisphosphate receptor. *J Biol Chem* **268**, 16488–16494.
- Hocker T & Tsao H (2007). Ultraviolet radiation and melanoma: a systematic review and analysis of reported sequence variants. *Hum Mutat* **28**, 578–588.
- Hoek KS, Eichhoff OM, Schlegel NC, Döbbeling U, Kobert N, Schaerer L, Hemmi S & Dummer R (2008). In vivo switching of human melanoma cells between proliferative and invasive states. *Cancer Res* **68**, 650–656.
- Hoek KS & Goding CR (2010). Cancer stem cells versus phenotype-switching in melanoma. *Pigment Cell Melanoma Res* **23**, 746–759.
- Hoek KS, Schlegel NC, Brafford P, Sucker A, Ugurel S, Kumar R, Weber BL, Nathanson KL, Phillips DJ, Herlyn M, Schadendorf D & Dummer R (2006). Metastatic potential of melanomas defined by specific gene expression profiles with no BRAF signature. *Pigment Cell Res* **19**, 290–302.
- Hogan PG, Lewis RS & Rao A (2010). Molecular basis of calcium signaling in lymphocytes: STIM and ORAI. *Annu Rev Immunol* **28**, 491–533.
- Holzmann C, Kilch T, Kappel S, Armbrüster A, Jung V, Stöckle M, Bogeski I, Schwarz EC & Peinelt C (2013). ICRAC controls the rapid androgen response in human primary prostate epithelial cells and is altered in prostate cancer. *Oncotarget* **4**, 2096–2107.
- Hoth M & Niemeyer BA (2013). The neglected CRAC proteins: Orai2, Orai3, and STIM2. *Curr Top Membr* **71**, 237–271.
- Hoth M & Penner R (1992). Depletion of intracellular calcium stores activates a calcium current in mast cells. *Nature*.
- Hou X, Pedi L, Diver MM & Long SB (2012). Crystal Structure of the Calcium Release-Activated Calcium Channel Orai. *Science*; DOI: 10.1126/science.1228757.
- Huggett J, Dheda K, Bustin S & Zumla A (2005). Real-time RT-PCR normalisation; strategies and considerations. *Genes Immun* **6**, 279–284.
- Hultqvist M, Olofsson P, Gelderman KA, Holmberg J & Holmdahl R (2006). A new arthritis therapy with oxidative burst inducers. *PLoS Med* **3**, e348.
- Hultqvist M, Olofsson P, Wallner FK & Holmdahl R (2014). Pharmacological Potential of NOX2 Agonists in Inflammatory Conditions. *Antioxid Redox Signal*; DOI: 10.1089/ars.2013.5788.

- Hultqvist M, Olsson LM, Gelderman K a & Holmdahl R (2009). The protective role of ROS in autoimmune disease. *Trends Immunol* **30**, 201–208.
- Hultqvist M, Sareila O, Vilhardt F, Norin U, Olsson LM, Olofsson P, Hellman U & Holmdahl R (2011). Positioning of a polymorphic quantitative trait nucleotide in the Ncf1 gene controlling oxidative burst response and arthritis severity in rats. *Antioxid Redox Signal* **14**, 2373–2383.
- Hwang S-Y & Putney JW (2012). Orai1-mediated calcium entry plays a critical role in osteoclast differentiation and function by regulating activation of the transcription factor NFATc1. *FASEB J* **26**, 1484–1492.
- Incalcaterra E, Accardi G, Balistreri CR, Caimi G, Candore G, Caruso M & Caruso C (2013). Pro-inflammatory genetic markers of atherosclerosis. *Curr Atheroscler Rep* **15**, 329.
- Ingersoll MA, Platt AM, Potteaux S & Randolph GJ (2011). Monocyte trafficking in acute and chronic inflammation. *Trends Immunol* **32**, 470–477.
- Ishii M, Shimizu S, Hara Y, Hagiwara T, Miyazaki A, Mori Y & Kiuchi Y (2006). Intracellular-produced hydroxyl radical mediates H₂O₂-induced Ca²⁺ influx and cell death in rat beta-cell line RIN-5F. *Cell Calcium* **39**, 487–494.
- Jacobs P, Bissonnette R & Guenther LC (2011). Socioeconomic burden of immune-mediated inflammatory diseases--focusing on work productivity and disability. *J Rheumatol Suppl* **88**, 55–61.
- Jankowski A, Scott CC & Grinstein S (2002). Determinants of the phagosomal pH in neutrophils. *J Biol Chem* **277**, 6059–6066.
- Jans R, Mottram L, Johnson DL, Brown AM, Sikkink S, Ross K & Reynolds NJ (2013). Lysophosphatidic acid promotes cell migration through STIM1- and Orai1-mediated Ca²⁺(i) mobilization and NFAT2 activation. *J Invest Dermatol* **133**, 793–802.
- Jaquet V, Scapozza L, Clark RA, Krause K & Lambeth JD (2009). NADPH Oxidases as Therapeutic Targets.
- Jin S-W, Zhang L, Lian Q-Q, Yao S-L, Wu P, Zhou X-Y, Xiong W & Ye D-Y (2006). Close functional coupling between Ca²⁺ release-activated Ca²⁺ channels and reactive oxygen species production in murine macrophages. *Mediators Inflamm* **2006**, 36192.
- Jing Y, Yang J, Wang Y, Li H, Chen Y, Hu Q, Shi G, Tang X & Yi J (2006). Alteration of subcellular redox equilibrium and the consequent oxidative modification of nuclear factor kappaB are critical for anticancer cytotoxicity by emodin, a reactive oxygen species-producing agent. *Free Radic Biol Med* **40**, 2183–2197.
- Johnson CM & Rodgers W (2008). Spatial Segregation of Phosphatidylinositol 4,5-Bisphosphate (PIP(2)) Signaling in Immune Cell Functions. *Immunol Endocr Metab Agents Med Chem* **8**, 349–357.
- Johnson JP (1999). Cell adhesion molecules in the development and progression of malignant melanoma. *Cancer Metastasis Rev* **18**, 345–357.
- Johnstone LS, Graham SJL & Dziadek MA (2010). STIM proteins: integrators of signalling pathways in development, differentiation and disease. *J Cell Mol Med* **14**, 1890–1903.

- Jones DP & Go Y-M (2010). Redox compartmentalization and cellular stress. *Diabetes Obes Metab* **12 Suppl 2**, 116–125.
- Judge AD, Sood V, Shaw JR, Fang D, McClintock K & MacLachlan I (2005). Sequence-dependent stimulation of the mammalian innate immune response by synthetic siRNA. *Nat Biotechnol* **23**, 457–462.
- Kar P, Bakowski D, Di Capite J, Nelson C & Parekh AB (2012). Different agonists recruit different stromal interaction molecule proteins to support cytoplasmic Ca²⁺ oscillations and gene expression. *Proc Natl Acad Sci U S A* **109**, 6969–6974.
- Kelkka T, Pizzolla A, Laurila JP, Friman T, Gustafsson R, Källberg E, Olsson O, Leanderson T, Rubin K, Salmi M, Jalkanen S & Holmdahl R (2013). Mice lacking NCF1 exhibit reduced growth of implanted melanoma and carcinoma tumors. *PLoS One* **8**, e84148.
- Kerkhoff C, Nacken W, Benedyk M, Dagher MC, Sopalla C & Doussiere J (2005). The arachidonic acid-binding protein S100A8/A9 promotes NADPH oxidase activation by interaction with p67phox and Rac-2. *FASEB J* **19**, 467–469.
- Kilch T, Alansary D, Peglow M, Dörr K, Rychkov G, Rieger H, Peinelt C & Niemeyer BA (2013). Mutations of the Ca²⁺-sensing stromal interaction molecule STIM1 regulate Ca²⁺ influx by altered oligomerization of STIM1 and by destabilization of the Ca²⁺ channel Orai1. *J Biol Chem* **288**, 1653–1664.
- Kolisek M, Beck A, Fleig A & Penner R (2005). Cyclic ADP-ribose and hydrogen peroxide synergize with ADP-ribose in the activation of TRPM2 channels. *Mol Cell* **18**, 61–69.
- Korczywska I (2014). Rheumatoid arthritis susceptibility genes: An overview. *World J Orthop* **5**, 544–549.
- Krause K-H (2004). Tissue distribution and putative physiological function of NOX family NADPH oxidases. *Jpn J Infect Dis* **57**, S28–S29.
- Lambeth JD (2004). NOX enzymes and the biology of reactive oxygen. *Nat Rev Immunol* **4**, 181–189.
- Landsman L, Bar-On L, Zerneck A, Kim K-W, Krauthgamer R, Shagdarsuren E, Lira SA, Weissman IL, Weber C & Jung S (2009). CX3CR1 is required for monocyte homeostasis and atherogenesis by promoting cell survival. *Blood* **113**, 963–972.
- Le Y, Murphy PM & Wang JM (2002). Formyl-peptide receptors revisited. *Trends Immunol* **23**, 541–548.
- Lee CF, Qiao M, Schröder K, Zhao Q & Asmis R (2010a). Nox4 is a novel inducible source of reactive oxygen species in monocytes and macrophages and mediates oxidized low density lipoprotein-induced macrophage death. *Circ Res* **106**, 1489–1497.
- Lee HJ, Wall B & Chen S (2008). G-protein-coupled receptors and melanoma. *Pigment Cell Melanoma Res* **21**, 415–428.
- Lee H-W, Choi H-J, Ha S-J, Lee K-T & Kwon Y-G (2013). Recruitment of monocytes/macrophages in different tumor microenvironments. *Biochim Biophys Acta* **1835**, 170–179.

- Lee HY, Kim SD, Shim JW, Kim HJ, Kwon JY, Kim J-M, Baek S-H, Park JS & Bae Y-S (2010b). Activation of human monocytes by a formyl peptide receptor 2-derived pepducin. *FEBS Lett* **584**, 4102–4108.
- Lee S (2014). Monocytes: a novel drug delivery system targeting atherosclerosis. *J Drug Target* **22**, 138–145.
- Levy C, Khaled M & Fisher DE (2006). MITF: master regulator of melanocyte development and melanoma oncogene. *Trends Mol Med* **12**, 406–414.
- Li Y-S, Wu P, Zhou X-Y, Chen J-G, Cai L, Wang F, Xu L-M, Zhang X-L, Chen Y, Liu S-J, Huang Y-P & Ye D-Y (2008). Formyl-peptide receptor like 1: a potent mediator of the Ca²⁺ release-activated Ca²⁺ current ICRAc. *Arch Biochem Biophys* **478**, 110–118.
- Li Z, Liu L, Deng Y, Ji W, Du W, Xu P, Chen L & Xu T (2011). Graded activation of CRAC channel by binding of different numbers of STIM1 to Orai1 subunits. *Cell Res* **21**, 305–315.
- Liou G-Y & Storz P (2010). Reactive oxygen species in cancer. *Free Radic Res* **44**, 479–496.
- Liou J, Kim ML, Heo W Do, Jones JT, Myers JW, Ferrell JE & Meyer T (2005). STIM is a Ca²⁺ sensor essential for Ca²⁺-store-depletion-triggered Ca²⁺ influx. *Curr Biol* **15**, 1235–1241.
- Lis A, Peinelt C, Beck A, Parvez S, Monteilh-Zoller M, Fleig A & Penner R (2007). CRACM1, CRACM2, and CRACM3 are store-operated Ca²⁺ channels with distinct functional properties. *Curr Biol* **17**, 794–800.
- Liu F, Gomez Garcia AM & Meyskens FL (2012). NADPH oxidase 1 overexpression enhances invasion via matrix metalloproteinase-2 and epithelial-mesenchymal transition in melanoma cells. *J Invest Dermatol* **132**, 2033–2041.
- Liu G-S, Wu J-C, Tsai H-E, Dusting GJ, Chan EC, Wu C-S & Tai M-H (2014). Proopiomelanocortin gene delivery induces apoptosis in melanoma through NADPH oxidase 4-mediated ROS generation. *Free Radic Biol Med*; DOI: 10.1016/j.freeradbiomed.2013.12.024.
- Livak KJ & Schmittgen TD (2001). Analysis of relative gene expression data using real-time quantitative PCR and the 2(-Delta Delta C(T)) Method. *Methods* **25**, 402–408.
- López E, Salido GM, Rosado J a & Berna-Erro A (2012). Unraveling STIM2 function. *J Physiol Biochem*; DOI: 10.1007/s13105-012-0163-1.
- Lukacs GL, Rotstein OD & Grinstein S (1990). Phagosomal acidification is mediated by a vacuolar-type H(+)-ATPase in murine macrophages. *J Biol Chem* **265**, 21099–21107.
- Luppi F, Longo AM, de Boer WI, Rabe KF & Hiemstra PS (2007). Interleukin-8 stimulates cell proliferation in non-small cell lung cancer through epidermal growth factor receptor transactivation. *Lung Cancer* **56**, 25–33.
- Lytton J, Westlin M & Hanley MR (1991). Thapsigargin inhibits the sarcoplasmic or endoplasmic reticulum Ca-ATPase family of calcium pumps. *J Biol Chem* **266**, 17067–17071.
- Mancarella S, Potireddy S, Wang Y, Gao H, Gandhirajan RK, Autieri M, Scalia R, Cheng Z, Wang H, Madesh M, Houser SR & Gill DL (2013). Targeted STIM deletion impairs calcium homeostasis, NFAT activation, and growth of smooth muscle. *FASEB J* **27**, 893–906.

- Manji SS, Parker NJ, Williams RT, van Stekelenburg L, Pearson RB, Dziadek M & Smith PJ (2000). STIM1: a novel phosphoprotein located at the cell surface. *Biochim Biophys Acta* **1481**, 147–155.
- Mantei A, Rutz S, Janke M, Kirchhoff D, Jung U, Patzel V, Vogel U, Rudel T, Andreou I, Weber M & Scheffold A (2008). siRNA stabilization prolongs gene knockdown in primary T lymphocytes. *Eur J Immunol* **38**, 2616–2625.
- Di Marco E, Gray SP, Chew P, Koulis C, Ziegler A, Szyndralewicz C, Touyz RM, Schmidt HHHW, Cooper ME, Slattery R & Jandeleit-Dahm KA (2014). Pharmacological inhibition of NOX reduces atherosclerotic lesions, vascular ROS and immune-inflammatory responses in diabetic Apoe (-/-) mice. *Diabetologia* **57**, 633–642.
- Marzuka-Alcalá A, Gabree MJ & Tsao H (2014). Melanoma susceptibility genes and risk assessment. *Methods Mol Biol* **1102**, 381–393.
- McAndrew D, Grice DM, Peters AA, Davis FM, Stewart T, Rice M, Smart CE, Brown MA, Kenny PA, Roberts-Thomson SJ & Monteith GR (2011). ORAI1-mediated calcium influx in lactation and in breast cancer. *Mol Cancer Ther* **10**, 448–460.
- Mercer JC, Dehaven WI, Smyth JT, Wedel B, Boyles RR, Bird GS & Putney JW (2006). Large store-operated calcium selective currents due to co-expression of Orai1 or Orai2 with the intracellular calcium sensor, Stim1. *J Biol Chem* **281**, 24979–24990.
- Migeotte I, Communi D & Parmentier M (2006). Formyl peptide receptors: a promiscuous subfamily of G protein-coupled receptors controlling immune responses. *Cytokine Growth Factor Rev* **17**, 501–519.
- Mignen O, Thompson JL & Shuttleworth TJ (2008a). Orai1 subunit stoichiometry of the mammalian CRAC channel pore. *J Physiol* **586**, 419–425.
- Mignen O, Thompson JL & Shuttleworth TJ (2008b). Both Orai1 and Orai3 are essential components of the arachidonate-regulated Ca²⁺-selective (ARC) channels. *J Physiol* **586**, 185–195.
- Mignen O, Thompson JL & Shuttleworth TJ (2009). The molecular architecture of the arachidonate-regulated Ca²⁺-selective ARC channel is a pentameric assembly of Orai1 and Orai3 subunits. *J Physiol* **587**, 4181–4197.
- Miller AJ & Mihm MC (2006). Melanoma. *N Engl J Med* **355**, 51–65.
- Missiaen L, Taylor CW & Berridge MJ (1991). Spontaneous calcium release from inositol trisphosphate-sensitive calcium stores. *Nature* **352**, 241–244.
- Monseil G, Ortonne N, Bagot M, Bensussan A & Dumaz N (2010). c-Kit mutants require hypoxia-inducible factor 1alpha to transform melanocytes. *Oncogene* **29**, 227–236.
- Monteith GR, Davis FM & Roberts-Thomson SJ (2012). Calcium channels and pumps in cancer: changes and consequences. *J Biol Chem* **287**, 31666–31673.
- Morgan MJ & Liu Z (2011). Crosstalk of reactive oxygen species and NF-κB signaling. *Cell Res* **21**, 103–115.
- Moser B, Wolf M, Walz A & Loetscher P (2004). Chemokines: multiple levels of leukocyte migration control. *Trends Immunol* **25**, 75–84.

- Motiani RK, Abdullaev IF & Trebak M (2010). A novel native store-operated calcium channel encoded by Orai3: selective requirement of Orai3 versus Orai1 in estrogen receptor-positive versus estrogen receptor-negative breast cancer cells. *J Biol Chem* **285**, 19173–19183.
- Motiani RK, Zhang X, Harmon KE, Keller RS, Matrougui K, Bennett JA & Trebak M (2013). Orai3 is an estrogen receptor α -regulated Ca^{2+} channel that promotes tumorigenesis. *FASEB J* **27**, 63–75.
- Murray PJ & Wynn T a (2011). Protective and pathogenic functions of macrophage subsets. *Nat Rev Immunol* **11**, 723–737.
- Nicholson LB, Raveney BJE & Munder M (2009). Monocyte dependent regulation of autoimmune inflammation. *Curr Mol Med* **9**, 23–29.
- Nordenfelt P & Tapper H (2011). Phagosome dynamics during phagocytosis by neutrophils. *J Leukoc Biol* **90**, 271–284.
- Numaga-Tomita T & Putney JW (2013). Role of STIM1- and Orai1-mediated Ca^{2+} entry in Ca^{2+} -induced epidermal keratinocyte differentiation. *J Cell Sci* **126**, 605–612.
- Nunes P, Cornut D, Bochet V, Hasler U, Oh-Hora M, Waldburger J-M & Demaurex N (2012). STIM1 Juxtaposes ER to Phagosomes, Generating Ca^{2+} Hotspots that Boost Phagocytosis. *Curr Biol* **22**, 1990–1997.
- Nunes P & Demaurex N (2010). The role of calcium signaling in phagocytosis. *J Leukoc Biol* **88**, 57–68.
- Nunes P & Demaurex N (2013). Redox regulation of Store Operated Ca^{2+} Entry. *Antioxid Redox Signal*; DOI: 10.1089/ars.2013.5615.
- Oh-Hora M, Yamashita M, Hogan PG, Sharma S, Lamperti E, Chung W, Prakriya M, Feske S & Rao A (2008). Dual functions for the endoplasmic reticulum calcium sensors STIM1 and STIM2 in T cell activation and tolerance. *Nat Immunol* **9**, 432–443.
- Olofsson P, Holmberg J, Tordsson J, Lu S, Akerström B & Holmdahl R (2003). Positional identification of Ncf1 as a gene that regulates arthritis severity in rats. *Nat Genet* **33**, 25–32.
- Olofsson P, Nerstedt A, Hultqvist M, Nilsson EC, Andersson S, Bergelin A & Holmdahl R (2007). Arthritis suppression by NADPH activation operates through an interferon-beta pathway. *BMC Biol* **5**, 19.
- Ozbalkan Z, Efe C, Cesur M, Ertek S, Nasiroglu N, Berneis K & Rizzo M (2010). An update on the relationships between rheumatoid arthritis and atherosclerosis. *Atherosclerosis* **212**, 377–382.
- Pahl HL (1999). Activators and target genes of Rel/NF-kappaB transcription factors. *Oncogene* **18**, 6853–6866.
- Pal R, Basu Thakur P, Li S, Minard C & Rodney GG (2013). Real-time imaging of NADPH oxidase activity in living cells using a novel fluorescent protein reporter. *PLoS One* **8**, e63989.
- Panaro MA, Acquafredda A, Sisto M, Lisi S, Maffione AB & Mitolo V (2006). Biological role of the N-formyl peptide receptors. *Immunopharmacol Immunotoxicol* **28**, 103–127.

- Pani G, Galeotti T & Chiarugi P (2010). Metastasis: cancer cell's escape from oxidative stress. *Cancer Metastasis Rev* **29**, 351–378.
- Parekh AB & Jr JWP (2005). Store-Operated Calcium Channels. 757–810.
- Parekh AB & Penner R (1995). Activation of store-operated calcium influx at resting InsP₃ levels by sensitization of the InsP₃ receptor in rat basophilic leukaemia cells. *J Physiol* **489** (Pt 2), 377–382.
- Partida-Sánchez S, Iribarren P, Moreno-García ME, Gao J-L, Murphy PM, Oppenheimer N, Wang JM & Lund FE (2004). Chemotaxis and calcium responses of phagocytes to formyl peptide receptor ligands is differentially regulated by cyclic ADP ribose. *J Immunol* **172**, 1896–1906.
- Parvez S, Beck A, Peinelt C, Soboloff J, Lis A, Monteilh-Zoller M, Gill DL, Fleig A & Penner R (2008). STIM2 protein mediates distinct store-dependent and store-independent modes of CRAC channel activation. *Fed Am Soc Exp Biol* **22**, 752–761.
- Pászty K, Antalffy G, Hegedüs L, Padányi R, Penheiter AR, Filoteo AG, Penniston JT & Enyedi A (2007). Cleavage of the plasma membrane Ca⁺-ATPase during apoptosis. *Ann N Y Acad Sci* **1099**, 440–450.
- De Paula D, Bentley MVLB & Mahato RI (2007). Hydrophobization and bioconjugation for enhanced siRNA delivery and targeting. *RNA* **13**, 431–456.
- Pearson G, Robinson F, Beers Gibson T, Xu BE, Karandikar M, Berman K & Cobb MH (2001). Mitogen-activated protein (MAP) kinase pathways: regulation and physiological functions. *Endocr Rev* **22**, 153–183.
- Peel SE, Liu B & Hall IP (2006). A key role for STIM1 in store operated calcium channel activation in airway smooth muscle. *Respir Res* **7**, 119.
- Peinelt C, Lis A, Beck A, Fleig A & Penner R (2008). 2-Aminoethoxydiphenyl borate directly facilitates and indirectly inhibits STIM1-dependent gating of CRAC channels. *J Physiol* **586**, 3061–3073.
- Penna A, Demuro A, Yeromin A V, Zhang SL, Safrina O, Parker I & Cahalan MD (2008). The CRAC channel consists of a tetramer formed by Stim-induced dimerization of Orai dimers. *Nature* **456**, 116–120.
- Pinner S, Jordan P, Sharrock K, Bazley L, Collinson L, Marais R, Bonvin E, Goding C & Sahai E (2009). Intravital imaging reveals transient changes in pigment production and Brn2 expression during metastatic melanoma dissemination. *Cancer Res* **69**, 7969–7977.
- Pizzolla A, Hultqvist M, Nilson B, Grimm MJ, Eneljung T, Jonsson I-M, Verdrengh M, Kelkka T, Gjertsson I, Segal BH & Holmdahl R (2012). Reactive oxygen species produced by the NADPH oxidase 2 complex in monocytes protect mice from bacterial infections. *J Immunol* **188**, 5003–5011.
- Poitras M, Bernier S, Servant M, Richard DE, Boulay G & Guillemette G (1993). The high affinity state of inositol 1,4,5-trisphosphate receptor is a functional state. *J Biol Chem* **268**, 24078–24082.
- Pollock PM, Harper UL, Hansen KS, Yudt LM, Stark M, Robbins CM, Moses TY, Hostetter G, Wagner U, Kakareka J, Salem G, Pohida T, Heenan P, Duray P, Kallioniemi O, Hayward

- NK, Trent JM & Meltzer PS (2003). High frequency of BRAF mutations in nevi. *Nat Genet* **33**, 19–20.
- Poole LB, Karplus PA & Claiborne A (2004). Protein sulfenic acids in redox signaling. *Annu Rev Pharmacol Toxicol* **44**, 325–347.
- Potier M, Gonzalez JC, Motiani RK, Abdullaev IF, Bisailon JM, Singer H a & Trebak M (2009). Evidence for STIM1- and Orai1-dependent store-operated calcium influx through ICRCAC in vascular smooth muscle cells: role in proliferation and migration. *FASEB J* **23**, 2425–2437.
- Prakriya M, Feske S, Gwack Y, Srikanth S, Rao A & Hogan PG (2006). Orai1 is an essential pore subunit of the CRAC channel. *Nature* **443**, 230–233.
- Prevarskaya N, Skryma R & Shuba Y (2011). Calcium in tumour metastasis: new roles for known actors. *Nat Rev Cancer* **11**, 609–618.
- Prins D, Groenendyk J, Touret N & Michalak M (2011). Modulation of STIM1 and capacitative Ca²⁺ entry by the endoplasmic reticulum luminal oxidoreductase ERp57. *EMBO Rep* **12**, 1182–1188.
- Qu B, Al-Ansary D, Kummerow C, Hoth M & Schwarz EC (2011). ORAI-mediated calcium influx in T cell proliferation, apoptosis and tolerance. *Cell Calcium* **50**, 261–269.
- Quevedo WC, Szabó G & Virks J (1969). Influence of age and UV on the populations of dopa-positive melanocytes in human skin. *J Invest Dermatol* **52**, 287–290.
- Raad H, Paclet M-H, Boussetta T, Krowiarski Y, Morel F, Quinn MT, Gougerot-Pocidallo M-A, Dang PM-C & El-Benna J (2009). Regulation of the phagocyte NADPH oxidase activity: phosphorylation of gp91phox/NOX2 by protein kinase C enhances its diaphorase activity and binding to Rac2, p67phox, and p47phox. *FASEB J* **23**, 1011–1022.
- Rao A (2009). Signaling to gene expression: calcium, calcineurin and NFAT. *Nat Immunol* **10**, 3–5.
- Rao A, Luo C & Hogan PG (1997). Transcription factors of the NFAT family: regulation and function. *Annu Rev Immunol* **15**, 707–747.
- Rees AJ (2010). Monocyte and macrophage biology: an overview. *Semin Nephrol* **30**, 216–233.
- Reth M (2002). Hydrogen peroxide as second messenger in lymphocyte activation. *Nat Immunol* **3**, 1129–1134.
- Robbins CS & Swirski FK (2010). The multiple roles of monocyte subsets in steady state and inflammation. *Cell Mol Life Sci* **67**, 2685–2693.
- Robinson LJ, Blair HC, Barnett JB, Zaidi M & Huang CL-H (2010). Regulation of bone turnover by calcium-regulated calcium channels. *Ann N Y Acad Sci* **1192**, 351–357.
- Roderick HL & Cook SJ (2008). Ca²⁺ signalling checkpoints in cancer: remodelling Ca²⁺ for cancer cell proliferation and survival. *Nat Rev Cancer* **8**, 361–375.
- Roesch A, Fukunaga-Kalabis M, Schmidt EC, Zabierowski SE, Brafford PA, Vultur A, Basu D, Gimotty P, Vogt T & Herlyn M (2010). A temporarily distinct subpopulation of slow-cycling melanoma cells is required for continuous tumor growth. *Cell* **141**, 583–594.

- Roos G & Messens J (2011). Protein sulfenic acid formation: from cellular damage to redox regulation. *Free Radic Biol Med* **51**, 314–326.
- Roos J, DiGregorio PJ, Yeromin A V, Ohlsen K, Lioudyno M, Zhang S, Safrina O, Kozak JA, Wagner SL, Cahalan MD, Veliçelebi G & Stauderman KA (2005). STIM1, an essential and conserved component of store-operated Ca²⁺ channel function. *J Cell Biol* **169**, 435–445.
- Ross K, Parker G, Whitaker M & Reynolds NJ (2008). Inhibition of calcium-independent phospholipase A impairs agonist-induced calcium entry in keratinocytes. *Br J Dermatol* **158**, 31–37.
- Ruano Y, Mollejo M, Ribalta T, Fiaño C, Camacho FI, Gómez E, de Lope AR, Hernández-Moneo J-L, Martínez P & Meléndez B (2006). Identification of novel candidate target genes in amplicons of Glioblastoma multiforme tumors detected by expression and CGH microarray profiling. *Mol Cancer* **5**, 39.
- Salzano M, Rusciano MR, Russo E, Bifulco M, Postiglione L & Vitale M (2012). Calcium/calmodulin-dependent protein kinase II (CaMKII) phosphorylates Raf-1 at serine 338 and mediates Ras-stimulated Raf-1 activation. *Cell Cycle* **11**, 2100–2106.
- Satyamoorthy K, DeJesus E, Linnenbach AJ, Kraj B, Kornreich DL, Rendle S, Elder DE & Herlyn M (1997). Melanoma cell lines from different stages of progression and their biological and molecular analyses. *Melanoma Res* **7 Suppl 2**, S35–S42.
- Saul S, Stanis H, Backes C, Schwarz EC & Hoth M (2013). How ORAI and TRP channels interfere with each other: interaction models and examples from the immune system and the skin. *Eur J Pharmacol*; DOI: 10.1016/j.ejphar.2013.10.071.
- Schindl R, Frischauf I, Bergsmann J, Muik M, Derler I, Lackner B, Groschner K & Romanin C (2009). Plasticity in Ca²⁺ selectivity of Orai1/Orai3 heteromeric channel. *Proc Natl Acad Sci U S A* **106**, 19623–19628.
- Schwarz EC, Qu B & Hoth M (2013). Calcium, cancer and killing: the role of calcium in killing cancer cells by cytotoxic T lymphocytes and natural killer cells. *Biochim Biophys Acta* **1833**, 1603–1611.
- Selvatici R, Falzarano S, Mollica A & Spisani S (2006). Signal transduction pathways triggered by selective formylpeptide analogues in human neutrophils. *Eur J Pharmacol* **534**, 1–11.
- Serbina N V, Jia T, Hohl TM & Pamer EG (2008). Monocyte-mediated defense against microbial pathogens. *Annu Rev Immunol* **26**, 421–452.
- Shaw PJ & Feske S (2012a). Regulation of lymphocyte function by ORAI and STIM proteins in infection and autoimmunity. *J Physiol* **590**, 4157–4167.
- Shaw PJ & Feske S (2012b). Physiological and pathophysiological functions of SOCE in the immune system. *Front Biosci (Elite Ed)* **4**, 2253–2268.
- Shaw PJ, Qu B, Hoth M & Feske S (2013). Molecular regulation of CRAC channels and their role in lymphocyte function. *Cell Mol Life Sci* **70**, 2637–2656.
- Shi C & Pamer EG (2011). Monocyte recruitment during infection and inflammation. *Nat Rev Immunol* **11**, 762–774.
- Singh S, Singh AP, Sharma B, Owen LB & Singh RK (2010). CXCL8 and its cognate receptors in melanoma progression and metastasis. *Futur Oncol* **6**, 1–9.

- Soboloff J, Rothberg BS, Madesh M & Gill DL (2012). STIM proteins: dynamic calcium signal transducers. *Nat Rev Mol Cell Biol* **13**, 549–565.
- Stanisz H, Saul S, Müller CSL, Kappl R, Niemeyer BA, Vogt T, Hoth M, Roesch A & Bogeski I (2014). Inverse regulation of melanoma growth and migration by Orai1/STIM2-dependent calcium entry. *Pigment Cell Melanoma Res*; DOI: 10.1111/pcmr.12222.
- Stanisz H, Stark A, Kilch T, Schwarz EC, Müller CSL, Peinelt C, Hoth M, Niemeyer B a, Vogt T & Bogeski I (2012). ORAI1 Ca(2+) channels control endothelin-1-induced mitogenesis and melanogenesis in primary human melanocytes. *J Invest Dermatol* **132**, 1443–1451.
- Stathopoulos PB & Ikura M (n.d.). Structural aspects of calcium-release activated calcium channel function. *Channels (Austin)* **7**, 344–353.
- Steinckwich N, Schenten V, Melchior C, Brécharde S & Tschirhart EJ (2011). An essential role of STIM1, Orai1, and S100A8-A9 proteins for Ca²⁺ signaling and FcγR-mediated phagosomal oxidative activity. *J Immunol* **186**, 2182–2191.
- Strehler EE & Treiman M (2004). Calcium pumps of plasma membrane and cell interior. *Curr Mol Med* **4**, 323–335.
- Sturgill-Koszycki S, Schlesinger PH, Chakraborty P, Haddix PL, Collins HL, Fok AK, Allen RD, Gluck SL, Heuser J & Russell DG (1994). Lack of acidification in Mycobacterium phagosomes produced by exclusion of the vesicular proton-ATPase. *Science* **263**, 678–681.
- Suttles J & Stout RD (2009). Macrophage CD40 signaling: a pivotal regulator of disease protection and pathogenesis. *Semin Immunol* **21**, 257–264.
- Tallone T, Turconi G, Soldati G, Pedrazzini G, Moccetti T & Vassalli G (2011). Heterogeneity of human monocytes: an optimized four-color flow cytometry protocol for analysis of monocyte subsets. *J Cardiovasc Transl Res* **4**, 211–219.
- Tavakoli S & Asmis R (2012). Reactive oxygen species and thiol redox signaling in the macrophage biology of atherosclerosis. *Antioxid Redox Signal* **17**, 1785–1795.
- Thiel M, Lis A & Penner R (2013). STIM2 drives Ca²⁺ oscillations through store-operated Ca²⁺ entry caused by mild store depletion. *J Physiol* **591**, 1433–1445.
- Thompson JL & Shuttleworth TJ (2013). How many Orai's does it take to make a CRAC channel? *Sci Rep* **3**, 1961.
- Topczewska JM, Postovit L-M, Margaryan N V, Sam A, Hess AR, Wheaton WW, Nickoloff BJ, Topczewski J & Hendrix MJC (2006). Embryonic and tumorigenic pathways converge via Nodal signaling: role in melanoma aggressiveness. *Nat Med* **12**, 925–932.
- Trachootham D, Lu W, Ogasawara M a, Nilsa R-DV & Huang P (2008). Redox regulation of cell survival. *Antioxid Redox Signal* **10**, 1343–1374.
- Trujillo JA, Croft NP, Dudek NL, Channappanavar R, Theodossis A, Webb AI, Dunstone MA, Illing PT, Butler NS, Fett C, Tscharke DC, Rossjohn J, Perlman S & Purcell AW (2014). The cellular redox environment alters antigen presentation. *J Biol Chem* **289**, 27979–27991.

- Ullevig S, Zhao Q, Lee CF, Seok Kim H, Zamora D & Asmis R (2012). NADPH oxidase 4 mediates monocyte priming and accelerated chemotaxis induced by metabolic stress. *Arterioscler Thromb Vasc Biol* **32**, 415–426.
- Valko M, Leibfritz D, Moncol J, Cronin MTD, Mazur M & Telser J (2007). Free radicals and antioxidants in normal physiological functions and human disease. *Int J Biochem Cell Biol* **39**, 44–84.
- Van der Veen BS, de Winther MPJ & Heeringa P (2009). Myeloperoxidase: molecular mechanisms of action and their relevance to human health and disease. *Antioxid Redox Signal* **11**, 2899–2937.
- Venkatakrisnan G, Salgia R & Groopman JE (2000). Chemokine receptors CXCR-1/2 activate mitogen-activated protein kinase via the epidermal growth factor receptor in ovarian cancer cells. *J Biol Chem* **275**, 6868–6875.
- Vig M, Beck A, Billingsley JM, Lis A, Parvez S, Peinelt C, Koomoa DL, Soboloff J, Gill DL, Fleig A, Kinet J-P & Penner R (2006a). CRACM1 multimers form the ion-selective pore of the CRAC channel. *Curr Biol* **16**, 2073–2079.
- Vig M, DeHaven WI, Bird GS, Billingsley JM, Wang H, Rao PE, Hutchings AB, Jouvin M-H, Putney JW & Kinet J-P (2008). Defective mast cell effector functions in mice lacking the CRACM1 pore subunit of store-operated calcium release-activated calcium channels. *Nat Immunol* **9**, 89–96.
- Vig M, Peinelt C, Beck a, Koomoa DL, Rabah D, Koblan-Huberson M, Kraft S, Turner H, Fleig a, Penner R & Kinet J-P (2006b). CRACM1 is a plasma membrane protein essential for store-operated Ca²⁺ entry. *Science* **312**, 1220–1223.
- Vignais P V (2002). The superoxide-generating NADPH oxidase: structural aspects and activation mechanism. *Cell Mol Life Sci* **59**, 1428–1459.
- Wang A-X & Qi X-Y (2013). Targeting RAS/RAF/MEK/ERK signaling in metastatic melanoma. *IUBMB Life* **65**, 748–758.
- Wang Y, Deng X, Zhou Y, Hendron E, Mancarella S, Ritchie MF, Tang XD, Baba Y, Kurosaki T, Mori Y, Soboloff J & Gill DL (2009). STIM protein coupling in the activation of Orai channels. *Proc Natl Acad Sci U S A* **106**, 7391–7396.
- Wang Y, Yang J & Yi J (2012). Redox sensing by proteins: oxidative modifications on cysteines and the consequent events. *Antioxid Redox Signal* **16**, 649–657.
- Waris G & Ahsan H (2006). Reactive oxygen species: role in the development of cancer and various chronic conditions. *J Carcinog* **5**, 14.
- Waugh DJJ & Wilson C (2008). The interleukin-8 pathway in cancer. *Clin Cancer Res* **14**, 6735–6741.
- Weber C, Belge KU, von Hundelshausen P, Draude G, Steppich B, Mack M, Frankenberger M, Weber KS & Ziegler-Heitbrock HW (2000). Differential chemokine receptor expression and function in human monocyte subpopulations. *J Leukoc Biol* **67**, 699–704.
- Weidenbusch M & Anders H-J (2012). Tissue microenvironments define and get reinforced by macrophage phenotypes in homeostasis or during inflammation, repair and fibrosis. *J Innate Immun* **4**, 463–477.

- Weyemi U, Redon CE, Parekh PR, Dupuy C & Bonner WM (2012). NADPH Oxidases NOXs and DUPXs As Putative Targets for Cancer Therapy. *Anticancer Agents Med Chem*. Available at: <http://www.ncbi.nlm.nih.gov/pubmed/22931418> [Accessed December 10, 2012].
- Whitehead KA, Dahlman JE, Langer RS & Anderson DG (2011). Silencing or stimulation? siRNA delivery and the immune system. *Annu Rev Chem Biomol Eng* **2**, 77–96.
- Williams RT, Manji SS, Parker NJ, Hancock MS, Van Stekelenburg L, Eid JP, Senior P V, Kazenwadel JS, Shandala T, Saint R, Smith PJ & Dziadek MA (2001). Identification and characterization of the STIM (stromal interaction molecule) gene family: coding for a novel class of transmembrane proteins. *Biochem J* **357**, 673–685.
- Winterbourn CC (2008). Reconciling the chemistry and biology of reactive oxygen species. *Nat Chem Biol* **4**, 278–286.
- Winterbourn CC (2013). The biological chemistry of hydrogen peroxide. *Methods Enzymol* **528**, 3–25.
- Winterbourn CC & Hampton MB (2008). Thiol chemistry and specificity in redox signaling. *Free Radic Biol Med* **45**, 549–561.
- Winterbourn CC, Hampton MB, Livesey JH & Kettle AJ (2006). Modeling the reactions of superoxide and myeloperoxidase in the neutrophil phagosome: implications for microbial killing. *J Biol Chem* **281**, 39860–39869.
- Winterbourn CC & Kettle AJ (2013). Redox reactions and microbial killing in the neutrophil phagosome. *Antioxid Redox Signal* **18**, 642–660.
- Wu S, Singh S, Varney ML, Kindle S & Singh RK (2012). Modulation of CXCL-8 expression in human melanoma cells regulates tumor growth, angiogenesis, invasion, and metastasis. *Cancer Med* **1**, 306–317.
- Wynn TA, Chawla A & Pollard JW (2013). Macrophage biology in development, homeostasis and disease. *Nature* **496**, 445–455.
- Xu KY, Zweier JL & Becker LC (1997). Hydroxyl radical inhibits sarcoplasmic reticulum Ca(2+)-ATPase function by direct attack on the ATP binding site. *Circ Res* **80**, 76–81.
- Yamaura M, Mitsushita J, Furuta S, Kiniwa Y, Ashida A, Goto Y, Shang WH, Kubodera M, Kato M, Takata M, Saida T & Kamata T (2009). NADPH oxidase 4 contributes to transformation phenotype of melanoma cells by regulating G2-M cell cycle progression. *Cancer Res* **69**, 2647–2654.
- Zhang SL, Yeromin A V, Zhang XH-F, Yu Y, Safrina O, Penna A, Roos J, Stauderman K a & Cahalan MD (2006). Genome-wide RNAi screen of Ca(2+) influx identifies genes that regulate Ca(2+) release-activated Ca(2+) channel activity. *Proc Natl Acad Sci U S A* **103**, 9357–9362.
- Zhang SL, Yu Y, Roos J, Kozak JA, Deerinck TJ, Ellisman MH, Stauderman K a & Cahalan MD (2005). STIM1 is a Ca2+ sensor that activates CRAC channels and migrates from the Ca2+ store to the plasma membrane. *Nature* **437**, 902–905.
- Zheng L, Stathopoulos PB, Li G-Y & Ikura M (2008). Biophysical characterization of the EF-hand and SAM domain containing Ca2+ sensory region of STIM1 and STIM2. *Biochem Biophys Res Commun* **369**, 240–246.

Zheng Y & Shen X (2005). H₂O₂ directly activates inositol 1,4,5-trisphosphate receptors in endothelial cells. *Redox Rep* **10**, 29–36.

Zhou Y, Lewis TL, Robinson LJ, Brundage KM, Schafer R, Martin KH, Blair HC, Soboloff J & Barnett JB (2011). The role of calcium release activated calcium channels in osteoclast differentiation. *J Cell Physiol* **226**, 1082–1089.

Ziegler-Heitbrock L, Ancuta P, Crowe S, Dalod M, Grau V, Hart DN, Leenen PJM, Liu Y-J, MacPherson G, Randolph GJ, Scherberich J, Schmitz J, Shortman K, Sozzani S, Strobl H, Zembala M, Austyn JM & Lutz MB (2010). Nomenclature of monocytes and dendritic cells in blood. *Blood* **116**, e74–e80.

Zweifach A & Lewis RS (1993). Mitogen-regulated Ca²⁺ current of T lymphocytes is activated by depletion of intracellular Ca²⁺ stores. *Proc Natl Acad Sci U S A* **90**, 6295–6299.

11 Register of Figures

Figure 1	Calcium homeostasis and signaling	17
Figure 2	The basics of redox-signaling – Sources and inter-conversion of ROS.....	21
Figure 3	Generation of reactive oxidants by cellular NADPH oxide systems	27
Figure 4	Schematic overview of the human skin and the comprising cell types	29
Figure 5	Melanoma Progression.....	30
Figure 6	Store-operated Calcium Entry (SOCE).....	36
Figure 7	Components and assembly of NADPH oxidase 2	38
Figure 8	Primary human monocytes and SK-MEL-5 and WM3734 melanoma cell lines....	50
Figure 9	Expression of Orai and STIM isoforms in primary human monocytes	68
Figure 10	Relative Orai3 expression levels.	69
Figure 11	Confirmation of RNAi induced down-regulation of Orai and STIM isoforms	70
Figure 12	Characterization of monocyte subset using flow cytometry	71
Figure 13	Activation and inhibition of SOCE in monocytes using two different stimuli.....	73
Figure 14	Contribution of single Orai and STIM isoforms to Store-operated Ca ²⁺	75
Figure 15	Contribution of Orai1 and STIM2 to Store-operated Ca ²⁺ Entry (SOCE) in	76
Figure 16	Dependency of superoxide production by primary human monocytes on SOCE ..	78
Figure 17	Preparatory experiments for fluorescence-based detection of H ₂ O ₂	79
Figure 18	Analysis of Ca ²⁺ - dependent ROS production by human monocytes.....	81
Figure 19	H ₂ O ₂ measurements to determine the contribution of the single CRAC	82
Figure 20	Quantification of H ₂ O ₂ measurements using AmplexUltraRed based on kinetics..	84
Figure 21	Inhibition of store-operated Ca ²⁺ entry in human monocytes by H ₂ O ₂	86
Figure 22	The role of Orai3 in modulating the redox-sensitivity of store-operated	87
Figure 23	Concurrence of Orai3 expression and redox-sensitivity of SOCE and	88
Figure 24	The role of Orai3 in Ca ²⁺ -dependent ROS production.....	89
Figure 25	Theoretical estimation and experimental determination of redox-sensitivity	91
Figure 26	Ca ²⁺ -dependency of melanoma proliferation.....	94
Figure 27	CRAC channel -dependent migration of the WM3734 melanoma cell line.	95
Figure 28	Expression analysis of phenotype markers in human melanoma cell line	96
Figure 29	IL-8 secretion by SK-MEL-5 melanoma cell line.....	97

Register of Figures

Figure 30	Monocyte survival in dependency of the Ca ²⁺ and redox environment.....	99
Figure 31	Interaction and binding within the assembly process of NADPH oxidase 2.....	105
Figure 32	Orai3 as modulator in the interdependency of SOCE and ROS production	108

12 Register of Tables and Equations

Table 1	Monocytes subsets in humans	25
Table 2	Surface markers used for classification of monocytes subsets.....	26
Table 3	Chemicals	43
Table 4	Kits and special laboratory equipment.....	45
Table 5	Devices and intended purpose	45
Table 6	Media and solutions for cell culture and experiments	46
Table 7	Multi-component buffers, solutions and media	47
Table 8	Activators and inhibitors of Ca ²⁺ and redox signaling pathways	49
Table 9	PCR conditions for quantitative real-time PCRs.....	53
Table 10	Primer sequences for quantitative RT-PCR of Orai and STIM.....	54
Table 11	Primer sequences for quantitative RT-PCR of NOX family members.....	55
Table 12	Antibodies and isotype controls used for flow cytometry.....	56
Table 13	Antibodies used for western blot	57
Table 14	Sequences of siRNAs used for specific gene knockdowns.....	59
Table 15	Sequences of non-targeting RNAs used as controls for specific gene knock-downs	60
Table 16	Experimental settings of CellTiterBlue Assays	64
Table 17	Parameters characterizing kinetics of H ₂ O ₂ production (presented in Figure 19) ..	84
Table 18	Parameters characterizing kinetics of H ₂ O ₂ production (presented in Figure 24) ..	90
Table 19	Ca ²⁺ concentration in RPMI medium supplemented with Ca ²⁺ chelator EGTA.....	93
Equation 1	RNA (ug/ml) = OD ₂₆₀ x 40 (Absorption coefficient) x Dilution factor.....	52
Equation 2	H ₂ O ₂ (nM) = (RFU/2.56) – 47.32	61
Equation 3	Calcium (nM) = Kd (Fura) x ((RFU-Rmin)/(Rmax-RFU)) x (sf2/sb2).....	62
Equation 4	Calcium (nM) = Kd (224nM) x ((RFU-0.183)/(5.736)) x 5.149.....	63
Equation 5	Calcium (nM) = Kd (224nM) x ((RFU-0.158)/(4.798)) x 6.421.....	63
Equation 6	Cell number = RFU/0.037	65
Equation 7	IL-8 (pg/ml) = ((Mean RLU – S0 (zero value of standard curve)) / 733.92.....	66
Equation 8	y = 63.59 ln(x) + 279.42.....	88

13 Publications

Manuscript in preparation:

A feedback loop between NADPH-oxidase 2 and Orai Ca²⁺ channels controls oxidative burst in human monocytes

Saul S, Conrad D, Kappl R, Diehler E, Tchernig T, Niemeyer BA, Bogeski I

Inverse regulation of melanoma growth and migration by Orai1/STIM2-dependent calcium entry.

Stanisz H*, **Saul S***, Müller CS, Kappl R, Niemeyer BA, Vogt T, Hoth M, Roesch A, Bogeski I.

Pigment Cell Melanoma Res. 2014 Jan 29. doi: 10.1111/pcmr.12222. [Epub ahead of print]

PMID:24472175

How ORAI and TRP channels interfere with each other: Interaction models and examples from the immune system and the skin.

Saul S, Stanisz H, Backes CS, Schwarz EC, Hoth M.

Eur J Pharmacol. 2013 Nov 28. pii: S0014-2999(13)00882-0. doi: 10.1016/j.ejphar.2013.10.071. [Epub ahead of print]

PMID:24291108

Hydroxylated derivatives of dimethoxy-1,4-benzoquinone as redox switchable earth-alkaline metal ligands and radical scavengers.

Gulaboski R*, Bogeski I*, Mirčeski V, **Saul S**, Pasieka B, Haeri HH, Stefova M, Stanoeva JP, Mitrev S, Hoth M, Kappl R.

Sci Rep. 2013; 3:1865. doi: 10.1038/srep01865.

PMID:23689559

* contributed equally

14 Curriculum Vitae

Personal Details

Name: Stephanie Saul
Address: Tilsiter Str.74, 66121 Saarbrücken, Germany
Phone: +49(0)163 - 7857982
Date/Place of Birth: 24th November 1984; Saarbrücken, Germany

Education and Training

10/2010 – 03/2014

Research Associate / PhD Student, Institut of Biophysics, Saarland University, Homburg (Saar)

Supervisors: Dr. I. Bogeski and Dr. B.A. Niemeyer

Research topic: Identification and characterization of calcium signalling pathways (store-operated calcium entry) in primary human monocytes and melanoma cell lines with focus on redox regulation of ion channels in immune cells and their role in melanoma progression.

10/2009 - 08/2010

Diploma Thesis, Department of Biophysics, Saarland University, Homburg (Saar), Germany

Title: *Redox regulation of leukocytes*

08/2008 – 09/2008

Internship, Oxford University, Oxford (UK)

Department of Physiology, Anatomy and Genetics; Dr. Robert Wilkins and Prof. Clive Ellory

10/2005 - 08/2010

Study of Biology (human- and molecular biology), Saarland University, Saarbrücken, Germany

Degree: Biologist (awarded, passed with distinction)

Majors: Physiology, Virology and Immunology and Structural Biology

09/2004 – 05/2005

Ausbildung zur Restaurantfachfrau (apprenticeship in hotel industry),

Baiersbronn, Germany (Finished ahead of time based on private motives)

06/2004

Abitur (german university entrance qualification), Wirtschaftswissenschaftliches Gymnasium, Saarbrücken, Germany